The beneficiation of rare earth element-bearing minerals

Adam Jordens

Department of Mining and Materials Engineering,

McGill University,

Montreal, Canada

A thesis submitted to McGill University in partial fulfillment of the requirements of the degree of Doctor of Philosophy

April 2016

Abstract

Rare earth elements (REE) comprise the fifteen elements of the lanthanide series as well as yttrium, and may be found in over 250 different minerals. These elements are required for many different applications such as high-strength permanent magnets, catalysts for petroleum refining, metal and glass additives and phosphors used in electronic displays. Contrary to their name, REE are abundant in the earth's crust, however deposits with economically extractable concentrations of these elements are much less common. The only REE bearing minerals (REM) that have been extracted on a commercial scale are bastnäsite, monazite, and xenotime. Increased demand for the different products manufactured from REE has resulted in a constriction of world supply from China, which currently produces the majority of the world's REE. Many new REE deposits are currently being developed to help meet the projections of future world demand, yet most of these developing deposits include REM for which there is limited processing knowledge. This thesis examines the separation techniques that are currently employed for REM beneficiation, identifies areas in need of further research, employs characterisation techniques to examine fundamental properties of certain REM, and then applies this knowledge to the beneficiation of the Nechalacho REE deposit in the Northwest Territories of Canada.

In order to build up the knowledge of the physicochemical properties of important REM, pure samples of minerals such as bastnäsite, allanite, fergusonite and zircon were acquired along with common gangue minerals in the Nechalacho deposit such as magnetite, hematite and quartz. The magnetic properties of each of these minerals was analysed as well as the surface chemistry of bastnäsite and allanite in the presence of different flotation reagents. Microflotation tests were used to confirm the results of the surface chemistry experiments. Subsequently, lab-scale separation experiments were conducted on a bulk sample from the Nechalacho deposit involving a series of gravity and magnetic separations. After analysing the results of these separations, a pre-concentration flowsheet was selected with the resultant product being used for

downstream flotation experiments. As the feed sample for flotation was concentrated in many REM, it provided an excellent opportunity for assessing flotation kinetics of these minerals in a multi-mineral system as well as investigating different reagent additions which may be applicable to the development of an industrial flotation process for this deposit.

The major findings from characterisation experiments include the verification of the paramagnetism of REM, the identification of hydroxamates as an ideal flotation reagent for the concentration of bastnäsite from silicate gangue as well as the finding that hydroxamates are not suitable for the flotation of allanite, a silicate REM. Additional work was undertaken to develop a means of floating allanite using alternative reagents such as dodecylamine and the addition of metal ion activators.

The concentration of REM from the Nechalacho deposit using physical separation was successfully achieved using a Knelson centrifugal gravity separator and a low intensity magnetic drum separator. High specific gravity REM were concentrated along with iron oxide minerals through the gravity separation stage with the iron oxide minerals largely removed through the subsequent magnetic separation step. The resultant product had a grade of 7.50 wt. % rare earth oxide (REO) and a REO recovery of 11.8 %. An additional finding from this work was that the concentration of the most valuable heavy REE is upgraded in the coarse size fractions after grinding to a P_{80} of 40 µm.

Subsequent ore flotation experiments using this material found that the kinetics of REM flotation from this deposit using hydroxamates are strongly dependent on mineral solubility as well as metal cation content. Additionally, the addition of lead cations to this system improves the flotation recovery of less floatable REMs such as allanite, and the staged addition of hydroxamates in flotation results in improved REM grade and recovery.

The implications of this research work includes an improved understanding of fundamental REM properties as well as multiple strategies for improving industrial process designs for the Nechalacho deposit. Implementing selective comminution strategies to upgrade the concentration of the most valuable REE could have a profound

effect on any future process by providing a simple means of beneficiation as well as minimizing energy losses in overgrinding. Two different flotation reagent strategies have been investigated with different outcomes. The staged addition of hydroxamate targets REM with rapid flotation kinetics whereas the addition of lead ions is able to improve the recovery of REM with slower flotation kinetics. These reagent schemes may have applications in different stages of an industrial flotation process.

Résumé

Les éléments des terres rares (ETR) comprennent les quinze éléments de la série des lanthanide ainsi que l'yttrium. Ces éléments se retrouve dans plus des 250 minéraux et sont requis dans plusieurs applications technologiques telles les puissants aimants permanents, les catalyseurs pétrochimiques, les additifs pour le métal et le verre ainsi que les luminophores dans les affichages électroniques.

Contrairement à leur nom, les ETR sont abondant dans la croute terrestre. Cependant, il y a peu de dépôt ayant des concentrations économiquement exploitables. Les seuls minéraux contenant des ETR ayant été exploité à l'échelle commerciale sont la bastnaésite, la monazite et le xénotime. La demande croissante pour les différents produits fabriqués à partir des ETR à un effet de contrainte sur la production provenant de la Chine, pays qui produit actuellement la majorité des ETR de la planète. Plusieurs nouveaux dépôt d'ETR sont en développement afin de remplir les projections de la demande mondiale. Par contre, la plupart des ces dépôts contiennent des ETR pour lesquels il n'existe pas de technologies d'extraction connues. Cette thèse examine donc les techniques de séparation actuellement utilisées dans la purification des ETR, elle identifie les domaines où il y a un manque de connaissance, elle emploie différentes techniques de caractérisation des propriétés fondamentales de certains ETR et finalement elle applique cette connaissance à la purification des ETR provenant du dépôt Nechalacho au Territoires du Nord-Ouest.

Afin d'améliorer la connaissance des propriétés physicochimiques des minéraux importants contenant des ETR (METR), des échantillons purs de minéraux tels la bastnaésite, l'allanite, la fergusonite et le zircon ont été obtenus ainsi que des échantillons de gangue commune dans le dépôt Nechalacho tels que la magnétite, l'hématite et le quartz. Les propriétés magnétiques de chaque minéraux ont été analysés de même que la chimie de surface de la bastnaésite et de l'allanite en présence de réactifs de flottation. Des tests de microflottation ont permis de confirmer les résultats des analyses de la chimie de surface.

Ensuite, des expériences de séparation gravimétrique et magnétique en laboratoires ont été conduites sur un échantillon en vrac provenant du dépôt Nechalacho. Après l'analyse des résultats de la séparation, un schéma de procédé de pré-concentration a été choisi et le produit de ce schéma a été utilisé pour des expériences de flottation. L'alimentation des tests de flottation étant un concentré de METR, la cinétique de flottation a été analysée de même que l'effet de différents réactifs potentiellement applicable au développement d'un procédé industriel spécifique à ce dépôt.

Le découverte majeur de la phase de caractérisation inclus la vérification du paramagnétisme des METR, l'identification des hydroxamates comme réactifs idéaux pour la séparation de la bastnaésite des gangues silicates, de même que la démonstration que les hydroxamates ne peuvent être utilisés pour la flottation de l'allanite, un METR de la famille des silicates. Des travaux supplémentaires ont été réalisés afin de valider la flottabilité de l'allanite avec l'utilisation de réactifs tel que du dodécylamine et l'addition d'ions métallique activateurs.

La séparation physique des METR provenant du dépôt Nechalacho a été réalisée avec succès par l'utilisation d'un séparateur centrifuge Knelson et d'un séparateur à tambour magnétique à faible intensité. Les METR ayant une densité relative élevée ainsi que les minéraux d'oxydes ferreux ont été concentrés lors de l'étape de séparation gravimétrique pour ensuite retirer les oxydes ferreux par la séparation magnétique. Le concentré produit a une teneur en oxydes de terres rares (OTR) de 7.50 % (par masse) avec une récupération de 11.8 %. Un autre découverte de ce travail est que les ETR ayant la plus grande valeur économique sont concentrés dans la fraction grossière après un broyage à 80 % passant (P80) 40 µm.

Des expériences de flottation de ce produit avec l'utilisation de réactifs hydroxamates ont permis d'établir que la cinétique de flottation des METR de ce dépôt est fortement influencée par la solubilité des minéraux présents ainsi que par la concentration de cations métalliques dans la solution.

L’addition de cations de plomb à ce système a amélioré la récupération des METR les moins propices à la flottation tels l’allanite. Quand à elle, l’addition par étape d’hydroxamates lors de la flottation améliore la teneur du concentré et la récupération des METR.

L’implication de ces travaux de recherches inclus l’amélioration de la compréhension des propriétés fondamentales des METR ainsi que des multiples stratégies d’amélioration du procédés de traitement du dépôt Nechalacho. L’implantation d’une comminution sélective améliorant la teneur des ETR ayant la plus grande valeur économique pourrait avoir un impact important en considérant l’augmentation de teneur qu’elle pourrait fournir ainsi que la réduction des pertes d’énergie dues à un surbroyage.

Finalement, deux réactifs de flottation on été testés, chacun fournissant un résultats différents. L’addition par étape d’hydroxamate cible les METR avec un flottabilité rapide alors que l’addition d’ions de plomb améliore la récupération de METR avec une flottabilité plus lentes. Cette recette de réactifs pourrait avoir plusieurs applications dans différentes étapes du procédé de flottation industriel.

Acknowledgements

I consider myself tremendously fortunate to have spent the last four years under the supervision of Professor Kristian E. Waters as a member of the McGill mineral processing group. The encouragement, instruction and opportunities I have been afforded have enabled me to grow personally and professionally throughout my graduate studies. I am incredibly appreciative of the time spent reviewing this thesis as well as the numerous papers we have published. I have also benefited from the significant trust he has placed in me, to direct my own research as well as to contribute to the direction of other research taking place within our group. I will always look back on my decision to come to McGill for doctoral studies as one of the best decisions of my life.

Thanks are also due to other senior members of the research group including Ray Langlois, Professor Jim Finch and Frank Rosenblum, for allowing me to lean on their considerable experience and expertise in confronting the challenges inherent in every PhD project. The time and effort saved thanks to these discussions has been a major factor in the completion of this thesis.

I have had the pleasure during my studies of collaborating with multiple experts outside of McGill who have been exceedingly generous with their expertise and equipment including Dr. Tassos Grammatikopoulos (QEMSCAN), Professor Neil Rowson (magnetic separations), Dr. Richard Sheridan (VSM) and Professor Brian Hart. I am especially thankful for the many fruitful discussions and collaborations I have had with Dr. Grammatikopoulos.

I have been privileged during my studies to work with many talented junior members of the research group who have provided assistance in completing numerous repetitive experiments. I would like to acknowledge Juan Helal, Xiangzhou Ding, Ying Ping Cheng, Olga Kuzmina, Sheelah McCarthy and Chris Marion for their help. Chris in particular has been, and will continue to be, a great asset in furthering the research work on rare earth minerals.

Within the McGill community I have benefited greatly from working with experts such as Dr. Patrick Boyle, Ranjan Roy, Dr. Sriraman Rajagopalan and Monique Riendeau. Professor Raynald Gauvin, Hendrix Demers and Chaoyi Teng are also acknowledged for their assistance with scanning electron microscopy. Additionally, Barbara Hanley deserves a special thanks for the tireless work she contributes to the department and each and every graduate student.

The mineral processing research group at McGill University is also deserving of special acknowledgement. The impact of working alongside such knowledgeable and passionate colleagues cannot be understated. In particular I would like to thank Dr. Wei Zhang, Dr. Jarrett Quinn, Dr. Miguel Maldonado, Marc Nassif, Nalini Singh, Dr. Amir Nazari, Dr. Yue Hua Tan, Darryel Boucher, Pengbo Chu, Joshua Sovechles, Dr. Ozan Kokkilic and Dr. Mayeli Alvarez.

Avalon Rare Metals is acknowledged for providing the bulk of the funding for this research program. The research work has been positively impacted over the years by conversations with Ian London, Dr. Bill Mercer and Dave Marsh. I am also very grateful to the McGill Engineering Doctoral Award (MEDA) program for providing me with three years of doctoral funding as well as the Natural Sciences and Engineering Research Council of Canada (NSERC) for providing me with both Masters and Doctoral level awards during the course of my studies.

I also thank my family for the love and support afforded me over the last four years and throughout my life. I am where I am today as a direct result of you.

Finally, and most importantly, I am grateful to Jess for suggesting I return to school with her in Montreal. The love, support and encouragement you've given me have played an integral role in the completion of this thesis.

"Life begins at the end of your comfort zone."

- Ogden Nash

Table of Contents

List of Figures

List of Tables

Nomenclature

d_a, d_b	μm	Particle diameter
dB/dx	T m^{-1}	Magnetic flux gradient
F_g	N	Force due to gravity
F_G	N	Centrifugal force
F_x	N	Magnetic force felt by a particle in the x-direction
F_m	N	Magnetic force
g	m s^{-2}	Acceleration due to Earth's gravity
G		Ratio of centrifugal force to the force due to Earth's gravity
H	A m^{-1}	Applied magnetic field strength
$HREE$		Heavy rare earth elements
HTR		High tension roll
k	min^{-1}	First-order flotation rate constant
K_m	min^{-1}	Modified flotation rate constant
W_{adh}	J	Work of adhesion
$LREE$		Light rare earth elements
M_{sat}	A m^{-1}	Saturation magnetisation
n		Exponent in free-settling ratio
QEMSCAN		Quantitative evaluation of minerals by scanning electron microscopy

r	m	Radius of the particle trajectory
R	%	Mineral Recovery
R_{max}	%	Ultimate Mineral Recovery
REE		Rare earth elements
REM		Rare earth mineral
REO		Rare earth oxide
SEM		Scanning electron microscope
t	min	Time
V	m^3	Particle volume
VSM		Vibrating sample magnetometer

QEMSCAN Definitions

Free	Particles with > 95 % of surface area belonging to the mineral of interest
Liberated	Particles with > 80 % and < 95 % of surface area belonging to the mineral of interest

Greek Letters

θ	°	Contact angle
θ_1	°	Angle of Frantz separator perpendicular to particle flow
θ_2	°	Angle of Frantz separator parallel to particle flow
$\gamma_{s/a}$	$J\ m^{-2}$	Solid-air interfacial energy
$\gamma_{w/a}$	$J\ m^{-2}$	Water-air interfacial energy

$\gamma_{s/w}$	J m^{-2}	Solid-water interfacial energy
ρ_a, ρ_b	g cm^{-3}	Mineral density
ρ_f	g cm^{-3}	Fluid density
χ_p		Particle volume magnetic susceptibility
χ_m		Fluid medium volume magnetic susceptibility
χ_{para}		Magnetic susceptibility of the paramagnetic component
Ω	m s^{-1}	Tangential velocity

Key Minerals of Nechalacho Deposit

Allanite	$(REE,Ca)_2(Al,Fe^{2+},Fe^{3+})_3(SiO_4)_3(OH)$
Bastnäsite	$(REE)CO_3F$
Columbite	$FeNb_2O_6$
Fergusonite	$(REE)NbO_4$
Hematite	Fe_2O_3
K-Feldspar	$KAlSi_3O_8$
Magnetite	Fe_3O_4
Monazite	$(REE,Th)PO_4$
Plagioclase	$(Na,Ca)AlSi_3O_8$
Quartz	SiO_2
Synchysite	$Ca(REE)(CO_3)_2F$
Zircon	$(Zr,REE)SiO_4$

1. Introduction

1.1 Rare earth elements

The term “rare earth elements” (REE) refers to the fifteen metallic elements of the lanthanide series, coupled with the chemically similar yttrium, and occasionally scandium (Gupta & Krishnamurthy, 1992). These elements are typically split into two sub-groups, the cerium sub-group of “light” rare earth elements (LREE) which includes lanthanum to europium and the yttrium sub-group of “heavy” rare earth elements (HREE) which include the remaining lanthanides, gadolinium to lutetium, as well as yttrium (Gupta & Krishnamurthy, 1992; Trifonov, 1963). Scandium, when it is classified as a rare earth element, is actually not included in either the LREE or HREE classifications (Gupta & Krishnamurthy, 1992). Multiple grouping configurations have been used in the past, typically when classifying these elements based on varying chemical criteria. However, from the standpoint of REE mineral (REM) exploitation, the sub-groupings listed above are sufficient (Schoeller & Powell, 1955).

1.1.1 Applications of REE

The demand for REE has spiked in recent years due to their increasing usage in numerous high-technology applications, including high strength permanent magnets, phosphors for electronic displays, applications in a variety of renewable energy technologies, and as alloying agents in metals (Crow, 2011; Meyer & Bras, 2011; Preinfalk & Morteani, 1986). Each of these applications requires specific REE (the lanthanides are not all interchangeable) as can be seen in Table 1.1. Combining the differing levels of demand for each REE with the crustal abundance variations described above, it can be seen that the task of ensuring a stable mineral supply of these elements presents significant challenges (Meyer & Bras, 2011). For example, magnet and phosphor manufacturers require terbium (Tb) and europium (Eu), two of the least abundant REEs, and will therefore be more affected by REE supply issues than a manufacturer of petroleum refining catalysts requiring lanthanum (La) and cerium (Ce), which are an order of magnitude more abundant.

Table 1.1 - Rare earth element requirements by application. Adapted from (Long *et al.*, 2010)

REE Applications	La (%)	Ce (%)	Pr (%)	Nd (%)	Sm (%)	Eu (%)	Gd (%)	Tb (%)	Dy (%)	Y (%)	Other (%)
Magnets			23.4	69.4			2.0	0.2	5.0		
Battery Alloys	50.0	33.4	3.3	10.0	3.3						
Metal Alloys	26.0	52.0	5.5	16.5							
Auto Catalysts	5.0	90.0	2.0	3.0							
Petroleum Refining	90.0	10.0									
Polishing Compounds	31.5	65.0	3.5								
Glass Additives	24.0	66.0	1.0	3.0						2.0	4.0
Phosphors	8.5	11.0				4.9	1.8	4.6		69.2	
Ceramics	17.0	12.0	6.0	12.0						53.0	
Other	19.0	39.0	4.0	15.0	2.0		1.0			19.0	

Percentages are estimates of the total REE content required in a given application

1.1.2 Oddo-Harkins Rule

In spite of their name, and aside from promethium, which does not exist naturally in a stable form, the abundance of REE in the earth's crust is actually significantly higher than other commonly exploited elements, including the platinum group elements and mercury (Gupta & Krishnamurthy, 1992; Trifonov, 1963). The crustal abundance of the individual REE is shown in Figure 1.2. As a comparison, the crustal abundance of gold and silver are 5×10^{-7} wt. % and 1×10^{-5} wt. % respectively (Trifonov, 1963). The difficulty in REM exploitation is that the REM are not commonly found in economic concentrations (Gupta & Krishnamurthy, 2005; Vijayan *et al.*, 1989). REE are never found as pure metals, instead they are found in a variety of minerals including silicates, oxides, carbonates, phosphates and halides (Levy, 1924; Vijayan *et al.*, 1989). There are more than 250 REM that have been discovered to date, many containing very low concentrations of REE varying from 10 to 300 ppm (Chi *et al.*, 2001; Gupta & Krishnamurthy, 2005; Vijayan *et al.*, 1989; Zhang & Edwards, 2012).

The challenge of the REE supply due to the scarcity of mineral deposits is aggravated by the fact that the elements are never found in an equal or even predictable distribution (Gupta & Krishnamurthy, 1992). The REE crustal abundance, as depicted in Figure 1.1, also demonstrates the Oddo-Harkin's rule, which states that elements with even atomic numbers are significantly more prevalent in the earth's crust than their neighbours in the periodic table (Parak, 1973; Trifonov, 1963). The availability of HREE is even further impacted by the fact that the REE distributions of the two most commonly extracted REM,

bastnäsite and monazite, exhibit lower percentages of the elements samarium to lutetium than would be expected based on the abundance data from Figure 1.1 (Gupta & Krishnamurthy, 1992).

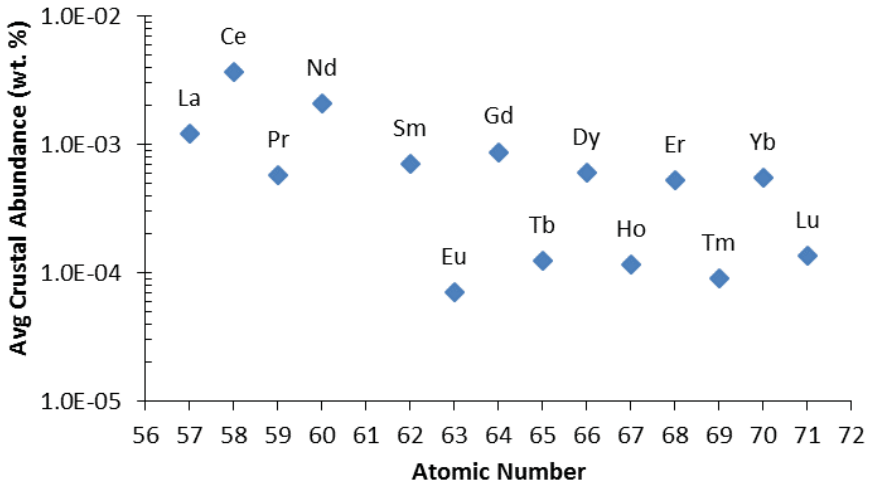

Figure 1.1 - Crustal abundance of lanthanide elements. Adapted from Trifonov (1963)

1.1.3 The Balance Problem

The relatively high abundance of both Ce and La causes problems to the economics of REM projects as an increase in the supply of the most valuable elements such as Eu and Dy would also increase the supply of other REE for which there may be significantly less demand (Golev *et al.*, 2014). Some of the 16 REE are inherently more valuable (high value REE = Pr, Nd, Eu, Dy, Gd, Tb, Er and Y [as determined by Dec. 3, 2015 market prices]) due to their unique properties and for a few of these elements, in particular Eu and Dy, there exists no substitute capable of delivering comparable performance (Graedel *et al.*, 2013). It is important to note when discussing market prices that REE concentrations are often discussed in terms of rare earth oxide (REO) concentrations. Concentrations are presented this way due to the conventions of geology, however the actual REM are almost universally more complicated than simple metal oxides. This classification of the most valuable REE is consistent with other work which has identified the most critical REEs as Nd, Eu, Tb, Dy, Y and Er (Seredin, 2010).This challenge is best

illustrated by considering two elements in two different time periods, the supply and demand of Eu in the 1960s and the projected supply and demand of Dy in 2050.

In the first scenario of the 1960s, Eu was the most important REE due to its use in red phosphors with the bulk of the world's Eu supply at this time coming from the mine at Mountain Pass, USA (Binnemans *et al.*, 2013b). For every ton of Eu_2O_3 extracted from bastnäsite (the chief REM at Mountain Pass) 300 tons of La_2O_3 and 450 tons of CeO_2 were produced, resulting in a significant excess (Binnemans *et al.*, 2013b). The impact of such an overproduction on the economics of a mining project is significant as the production costs of the mine can only be distributed over the products (metals or minerals) for which there is a viable market.

In the projected scenario of 2050 total worldwide demand for Dy has been estimated at approximately 8390 tons with 25 % of this demand coming solely from wind power generation (Elshkaki & Graedel, 2014). This demand cannot be met by the Mountain Pass mine (no Dy present in bastnäsite), and if it were met by the Bayan Obo (China) mine the La:Dy and Ce:Dy production ratios would be 225:1 and 467:1 respectively (Elshkaki & Graedel, 2014). Similarly for the Mount Weld (Australia) mine the La:Dy and Ce:Dy ratios are 127:1 and 238:1 respectively (Elshkaki & Graedel, 2014).

While the market for La has been reported to be relatively balanced at the moment, there are certain REE (Ce, Ho, Tm, Yb, Lu) for which no substantial demand exists (Binnemans *et al.*, 2013b; Elshkaki & Graedel, 2014; Seredin, 2010). In order to address this balance problem there are three possible solutions (Binnemans *et al.*, 2013a; Carlston, 2014; Golev *et al.*, 2014):

- Stockpile the excess REE produced to remove them from the world market
- Increased focus on recycling of critical REE-rich waste streams
- Development of new applications for excess REE (*e.g.* use of Ce for water treatment to remove phosphorous)

1.1.4 Factors affecting REE prices

There are approximately one hundred million tons of proven REO reserves globally, scattered across more than 30 countries (Chen, 2011). At one point approximately 97 % of the world's supply originated in China and the most recent data from 2015 indicates that it is still producing up to 85 % of world supply (Gambogi, 2015; Pitts, 2011). Increased development in China prompted the Chinese government, beginning in 2010, to limit yearly export quotas to approximately 35,000 tons of REO, while non-Chinese yearly demand was expected to reach 80,000 tons by the year 2015 (Chen, 2011; Chi *et al.*, 2001). This constriction of supply has created a situation where many new REM deposits outside of China have become very economically attractive (Chen, 2011). One of the more advanced deposits is the Nechalacho deposit located in the Northwest Territories of Canada which contains multiple REM including zircon, bastnäsite, fergusonite, allanite and monazite (Cox *et al.*, 2011). This development of many new rare earth mining projects has brought to light the distinctive mining and processing challenges facing these deposits (Chen, 2011).

The more unique issues facing potential REE producers include (Delaney, 2010):

- a limited availability of technical expertise (outside of China),
- the issues associated with the radioactive wastes produced as by-product of REE extraction
- the high degree of capital outlay associated with new REE plants (conventional plant costs are close to one billion dollars)
- the lack of a predictable and readily available market price (REE are sold on contract, as per industrial minerals)
- the very short time period during which a new REE mine must start-up to ensure sufficient demand for its products
- the inconsistent demand levels for individual REE (Section 1.1.4)

The supply of REE continues to be an increasingly important worldwide concern as China, the world's chief REE supplier, continues to restrict its REE exports (Tien, 2013). This

has important consequences for all downstream consumers of technologies requiring REE as inputs, such as high-strength permanent magnets and phosphors for electronic displays (Massari & Ruberti, 2013). The change in supply and demand equilibrium has increased research into new means of meeting these demands including recycling (Anand *et al.*, 2011; Binnemans *et al.*, 2013a; Darcy *et al.*, 2013; Golev *et al.*, 2014; Li *et al.*, 2009; Lister *et al.*, 2014; Meyer & Bras, 2011; Resende & Morais, 2015), scavenging of available REE-rich waste streams (Yu *et al.*, 2014), improved efficiency of REE extraction processes (Abreu & Morais, 2014; Amer *et al.*, 2013; Xie *et al.*, 2014), development of new REM deposits (Tu *et al.*, 2015; Yang *et al.*, 2015) and even seeking alternatives to REE use entirely (Massari & Ruberti, 2013). While the projections of future REE demand are robust, the level of demand (and therefore price) varies from element to element (Golev *et al.*, 2014; Massari & Ruberti, 2013).

1.1.5 REE Beneficiation

The beneficiation of REM is a subject which requires a great deal of investigation to fill the knowledge gaps surrounding developing REM projects. A number of books exist that present detailed information on the life-cycle of REE from world-wide mineral occurrences through to their numerous end-use applications (Browning, 1908; Eyring, 1964; Ginzburg, 1963; Gupta & Krishnamurthy, 2005; Levy, 1924; Schoeller & Powell, 1955; Trifonov, 1963). Similarly, there are numerous peer-reviewed articles on REE mineralogy as well as the hydrometallurgical processing of REE concentrates (Alex *et al.*, 1998; Bau, 1991; Gromet, 1983; Ring *et al.*, 1993; Schnetzler & Philpotts, 1970; Uda *et al.*, 2000). A common feature amongst these sources is their lack of detailed descriptions of the beneficiation processes required to concentrate REM. The reasons for this gap are most likely three-fold (Abeidu, 1972; Cheng *et al.*, 1994; Cuthbertson, 1952; Fuerstenau *et al.*, 1982; Gupta & Krishnamurthy, 1992; Luo & Chen, 1984; Pavez & Peres, 1994; Pradip, 1981):

- There are only three major REM that are currently exploited commercially (bastnäsite, monazite, and xenotime) excluding ion-adsorbed clays, which currently undergo little or no beneficiation

- The economically viable occurrences of two of these three minerals (monazite and xenotime) are typically in heavy mineral sand deposits, for which the beneficiation processes are well-developed and require little or no comminution
- The third REM (bastnäsite) has been economically extracted on a large scale in only one non-Chinese location worldwide (Mountain Pass, USA)

A recent review of Chinese REM processing schemes by Zhang & Edwards (2012) demonstrates that even when peer-reviewed publications from China are added to the literature body on REM beneficiation, opportunities still exist for timely, meaningful research. Recently announced quota restrictions for Chinese REE exports, coupled with increasing demand for these elements, have resulted in REE prices that justify developing a number of new REE deposits (Chen, 2011; Meyer & Bras, 2011). Given the nature of the deposits under development, the existing knowledge base of REM beneficiation must be increased (Chen, 2011).

1.2 Thesis Objectives

The goal of this thesis was to investigate the surface and bulk properties of multiple REM which control their separation behaviour and then to employ this information in the design of an effective process for concentrating the REM from the Nechalacho deposit. Many of the minerals in question have effectively no established knowledge base in mineral processing literature. As such, a decision was made early on in the research program to focus initial experiments on:

- Establishing baseline information regarding individual mineral properties

Subsequent efforts in the research program had two objectives:

- Quantify mineral separation behaviour in more complex, multi-phase separation systems including gravity, magnetic and froth flotation separations

- Develop processing routes which could be applied to the Nechalacho ore on an industrial scale

While this thesis presents significant progress on all of these objectives it should be noted that successful development of this deposit will require a great deal of additional research on single mineral systems as well as real ore samples. Additionally, the limits in scope of this thesis must be acknowledged, in that the impacts of the proposed processes in terms of downstream hydrometallurgical operations and associated environmental considerations are not generally discussed.

1.3 Thesis Structure

This thesis is presented as a traditional monograph thesis consisting of 8 Chapters and 1 Appendix. The outline of the individual chapters is as follows:

Chapter 1: Introduction

Important background information on rare earth elements is provided. This is required to properly understand the research motivations behind this thesis. An overview of thesis objectives and thesis structure are also provided.

Chapter 2: Mineral Processing Background

Background information for readers unfamiliar with mineral processing is provided. The theories of different separation techniques discussed in this thesis are explained along with a discussion of the operating principles of various pieces of lab-scale separation equipment.

Chapter 3: Review of the beneficiation of rare earth element-bearing minerals

The current knowledge base for the beneficiation of REM is reviewed for individual minerals. The literature is also examined from the standpoint of different beneficiation techniques. Finally the knowledge gaps and areas with significant research needs are identified.

Chapter 4: Experimental Methods

A detailed description of the experimental procedures used throughout this research.

Chapter 5: Properties of Single Minerals

The results of characterisation and separation experiments used to determine the properties of the selected constituent minerals of the Nechalacho deposit are presented. This information is discussed in terms of its implications for the beneficiation of this deposit.

Chapter 6: Physical Separation

A pre-concentration flowsheet of gravity and magnetic separations applied to an ore sample from the Nechalacho deposit is described. The results are characterised using a range of analytical tools and the optimal process is selected to provide a high grade product for downstream froth flotation experiments.

Chapter 7: Froth Flotation

An investigation into the flotation characteristics of the Nechalacho ore is presented with experiments conducted on the pre-concentrated sample produced from physical separation experiments. The flotation testwork is used to determine fundamental flotation behaviour of the various REM such as recoveries and kinetics. Different reagent combinations are proposed for possible use at different stages of an industrial flotation process.

Chapter 8: Conclusions, Contributions and Future Work

This chapter details the major conclusions of the thesis, highlights contributions to original knowledge and suggests areas in need of further research.

Appendix: Published work not included in this thesis

Two published manuscripts containing the results of preliminary experimental work during the course of this thesis are included here. Much of this information was excluded from the body of the thesis to minimize repetition and improve overall readability.

2. Mineral Processing Background

2.1 Introduction

This thesis deals with the application of established mineral processing separation techniques to beneficiate rare earth minerals (REM), a newly important class of minerals with a very limited existing knowledge base. As such, it was deemed appropriate to introduce the fundamentals of the separation techniques themselves, as well as the operating principles of the equipment used in this work, prior to chapters containing a literature review of REM beneficiation and subsequent experimental work. This chapter deals primarily with theoretical aspects of mineral processing separation techniques, including gravity separation, magnetic separation, electrostatic separation and froth flotation. These separation processes are discussed here to ensure that any reader unfamiliar with mineral processing can follow the discussion regarding the current state of the art of REM beneficiation detailed in Chapter 3. Chapter 4 then explains the laboratory-scale processes that were employed throughout this thesis.

2.2 Gravity Separation

2.2.1 Gravity Separation Theory

Gravity separations exploit differences in the specific gravity of minerals to achieve separation. Gravity separation in general may be regarded as a form of particle classification, where the settling velocity of a given particle in a fluid medium is determined by the interaction of various forces. In mineral processing applications these forces are primarily gravity, buoyancy and fluid drag; thus the equilibrium between these three forces can be resolved for different flow regimes (or the corresponding particle sizes): Stokes' law for fine (< 50 μm) particles; and Newton's law for coarse (> 500 μm) particles (Wills & Finch, 2016). From these laws it is then possible to derive a free-settling ratio to indicate the ratio of particle size at which two particles of differing specific gravities will have the same settling velocity defined as (Wills & Finch, 2016):

$$\frac{d_a}{d_b} = \left(\frac{\rho_b - \rho_f}{\rho_a - \rho_f}\right)^n \tag{2.1}$$

where d_a and d_b correspond to the particle diameters of mineral a and mineral b respectively; ρ_a, ρ_b, and ρ_f correspond to the densities of mineral a, mineral b and the fluid respectively. The exponent n varies from 0.5 to 1 depending on the flow regime (Stokes' law versus Newton's law). As equation 2.1 is derived from a force balance including fluid drag, the effect of changes in fluid viscosity with increased slurry density must be considered (Wills & Finch, 2016). When the solids concentration increases above approximately 15 vol. %, particle settling is increasingly controlled by hindered-settling mechanisms such as particle-particle interactions and increases in fluid viscosity and slurry density (Wills & Finch, 2016). The net difference between hindered-settling and free-settling is that hindered-settling regimes increase the value of the ratio in Equation 2.1 (provided that $\rho_b > \rho_a$) relative to the free-settling situation, thereby minimizing the effect of particle size on settling velocity. This is why many gravity separators operate at high solids concentrations to maximize separation by specific gravity and not particle size.

As particle size decreases, the exponent n in Equation 2.1 decreases as well, such that the free-settling ratio decreases in magnitude and selective separations based only on specific gravity become much more difficult. One means of counteracting this limitation is by enhancing the gravitational force felt by the particles through the use of centrifugal separators. These separators operate such that the force of gravity (F_g) felt by a particle settling in a fluid is replaced by the force due to centrifugal acceleration (F_G). These separators may be described in part by the ratio of the centrifugal force felt by the particle to the force acting on the particle due to Earth's gravity:

$$G = \frac{F_G}{F_g} = \frac{\Omega^2}{g\,r} \tag{2.2}$$

where Ω is the tangential velocity of the particle, g is the acceleration due to Earth's gravity and r is the radius of the particle trajectory. Modern centrifugal separators are able to produce G ratios (Equation 2.2) of up to 300, which can dramatically increase the settling velocities felt by small particles.

Various separators are utilized to allow fine, high specific gravity material to separate from coarse, lower specific gravity particles (Falconer, 2003). Two commonly used separators that will be discussed in this chapter are spiral separators and centrifugal gravity concentrators.

2.2.2 Spiral Separators

In a spiral separator, a mineral slurry flows along an inclined helical path where centrifugal and gravitational forces act to bring the densest particles towards the central column of the separator where they form the concentrate (Falconer, 2003). Spiral separators afford improvements over other gravity concentrators such as cone separators and jigs as the increased force felt by the particle, in conjunction with a lower slurry density, can achieve higher upgrade ratios and an improved treatment of fines (Falconer, 2003). Within the spiral trough there are two distinct zones; an inner zone near the column which acts to control concentrate grade and an outer zone that handles the bulk of the slurry flow and must allow heavy particles to settle to the spiral surface so that they can migrate towards the concentrate (Holland-Batt & Holtham, 1991).

2.2.3 Centrifugal Gravity Separators

The most common and successful type of gravity separator used for fine particle sizes is a centrifugal gravity concentrator (Falconer, 2003). Centrifugal gravity separators are employed for very fine particle sizes as they are able to increase the force on a particle to many times that of gravity (Section 2.2.1). These separators operate by the introduction of a mineral slurry into a rapidly rotating bowl, which generates a centrifugal acceleration on the particles that is much greater than that of the Earth's gravity and therefore decreases the lower size limit for effective gravity separation (Falconer, 2003). The high settling velocities experienced by the particles trap high specific gravity material against the sides of the bowl to become the gravity concentrate while lower specific gravity material is carried along with the flowing fluid to report to the gravity tailings (Falconer, 2003). These concentrators are operated in a semi-continuous mode where the accumulated concentrate is periodically removed by washing (Fullam & Grewal, 2001).

2.2.3.1 Knelson Concentrator

One of the most common centrifugal separators is the Knelson Concentrator (Figure 2.1), which employs an inclined bowl lined with collecting ridges where the heavy (specific gravity > 4) value mineral is collected (Ferron *et al.*, 1991; Fullam & Grewal, 2001). The bowl's sides are lined with ridges to trap dense particles. These ridges contain perforations through which fluidizing water is pumped in order to fluidize the material collecting in the ridges and allow for the exchange of low specific gravity material (which may have initially reported to the concentrate) with high specific gravity material (Fullam & Grewal, 2001; Knelson, 1992). The fluidising water also ensures that unintentional entrapment of low specific gravity particles into the concentrate phase is minimized (Fullam & Grewal, 2001). The Knelson Concentrator is able to produce a G-ratio (Equation 2.2) of up to 60 (Fullam & Grewal, 2001).

The Knelson Concentrator works very well for applications where the desired high specific gravity mineral is present in very low concentrations (ppm) but runs into operational difficulties processing ores with higher contents (typically > 1%) of high specific gravity material as the concentrate accumulates very rapidly (Fullam & Grewal, 2001). If the accumulated gravity concentrate is not flushed promptly the selectivity of the separation will suffer significantly (Fullam & Grewal, 2001; Knelson, 1992). An additional limitation to the Knelson Concentrator is that the efficiency of the concentration step decreases with feed fineness (Laplante, 1993). Laplante (1993) suggested that for the specific case of gold particles, the poor performance of the Knelson concentrator in treating fine feeds (< 75 μm) is more likely attributable to the shape of the fine gold particles rather than their size.

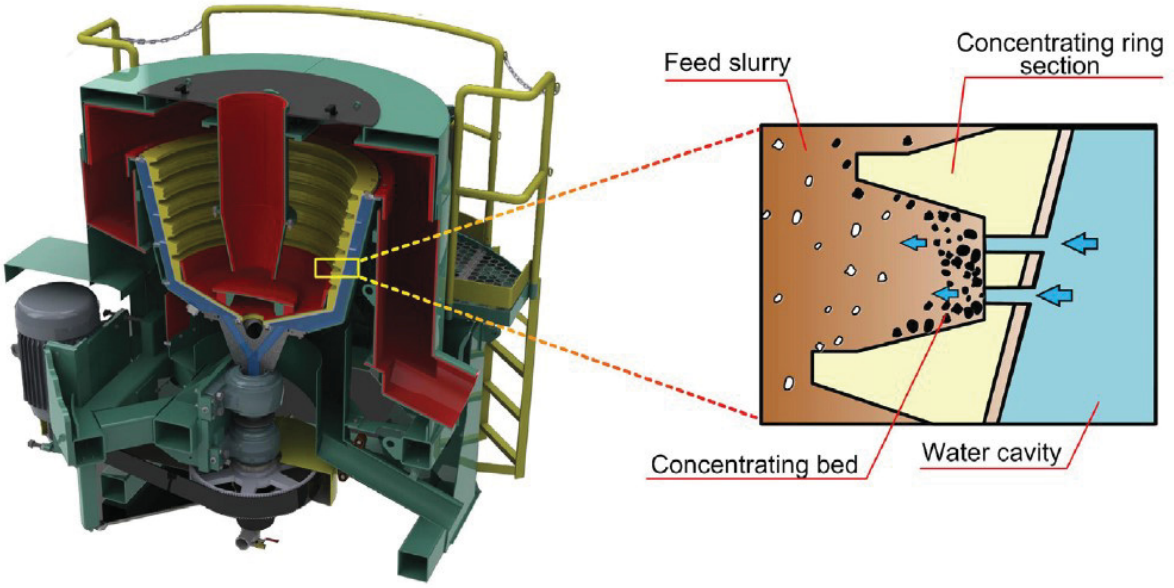

Figure 2.1 – Cut view of the Knelson Concentrator along with schematic diagram of the collection riffle after Wills & Finch (2016)

2.2.3.2 Falcon Concentrator

The Falcon Ultra-Fine (UF) Concentrator was designed specifically to process very fine particle sizes. It lacks the fluidizing water used in other centrifugal concentrators; instead relying on the geometry of the bowl walls to retain the high specific gravity material (Lins *et al.*, 1992). This design changes the mechanism of high specific gravity particle collection as there is no opportunity for particle exchange once a particle has been deposited on the wall of the spinning bowl (Kroll-Rabotin *et al.*, 2011). Laplante *et al.* (1994) showed that there are three steps in a Falcon concentrator separation: initial non-selective deposition of material on the concentrate bed along the bowl wall, selective concentration until the concentrate bed is saturated; and finally, minimal recovery as the concentrate bed is unable to accept additional particles. It can be seen from these three phases of material recovery that it is crucial to ensure that the concentrator is stopped at suitable time intervals to maximize the separator's efficiency by not operating with a fully-loaded bowl.

2.3 Magnetic Separation

2.3.1 Magnetism in Mineral Processing

Magnetic separation of minerals is based on different behaviours of mineral particles when exposed to an applied magnetic field. The magnetic response of a material to an applied magnetic field is due to the presence of unpaired electrons which induce magnetic dipoles in the material. These magnetic dipoles possess individual magnetic moments and the alignment of these magnetic moments with an applied magnetic field will produce a resultant magnetic force on the material when these moments are aligned by an externally applied magnetic field. The magnetisation of a material is a measure of the density of magnetic dipoles induced in the material.

In mineral processing terminology there are three distinct behaviours that a mineral particle may exhibit: ferromagnetic and paramagnetic mineral particles will both be attracted along the lines of an applied magnetic field; whereas a diamagnetic mineral particle will be repelled along the magnetic field lines. The main difference in ferromagnetic and paramagnetic minerals is that a ferromagnetic material is able to much more rapidly align its magnetic moments such that the magnetisation (and consequently the magnetic force felt by the particles) is much higher at lower applied magnetic field strengths. An excellent introduction to magnetism in materials and other associated concepts can be found in the work of Jiles (1990).

The magnetic recovery in a magnetic separator is dependent on the applied magnetic field strength, the magnetic field gradient and the magnetic susceptibility of the mineral particles and accompanying fluid medium as can be seen in Equation 2.3 (Oberteuffer, 1974):

$$F_x = V(\chi_p - \chi_m) H \frac{dB}{dx} \tag{2.3}$$

In this equation F_x is the magnetic force felt by a particle [N], V is the particle volume [m^3], χ_p is the dimensionless volume magnetic susceptibility of the particle, χ_m is the volume magnetic susceptibility of the fluid medium, H is the applied magnetic field strength [A/m] and dB/dx is the magnetic flux gradient [T/m = N/Am^2] (Oberteuffer, 1974; Svoboda &

Fujita, 2003). The magnetic force on a particle in a magnetic separator may be controlled by varying the magnetic susceptibility of the particle/medium, the applied magnetic field or the magnetic field gradient. Another important conclusion from Equation 2.3 is that high applied magnetic field strengths will exert no magnetic force without an accompanying field gradient. Thus, many magnetic separators are designed to maximise gradient in addition to having very high applied magnetic fields.

The size range at which magnetic separation is effective depends on which of the three main forces on a particle (gravitational, magnetic and fluid drag) is dominant at a particular size (Oberteuffer, 1974). The fluid drag forces on a particle are proportional to the radius, r, while the magnetic force on a particle can be shown for an idealized system to be proportional to r^2 (although for the general case the magnetic force is a function of the particle volume as seen in Equation 2.3) (Oberteuffer, 1974). Similarly the force due to gravity can be shown to scale with r^3 so that for particles of very small radius the fluid drag forces are dominant while for a much larger particle radius gravitational forces are the most significant forces on a particle (Oberteuffer, 1974). The particle radius at which magnetic separation may be effective has been determined to be approximately 5 μm up to 1 mm (Oberteuffer, 1974) however the recovery of increasingly fine magnetic material (down to even nano-scale particles) is an area of active research (Chen *et al.*, 2012; Ebner *et al.*, 1997; Menzel *et al.*, 2012; Roy, 2011).

It is not possible to fully explain the intricacies of magnetic separation in this section, interested readers are encouraged to consult the work of Oberteuffer (1974), Svoboda & Fujita (2003) as well as Wills & Finch (2016). Prior to applying magnetic separation to a given mineral system, it is necessary that the magnetic properties of the individual minerals be known. For many minerals, this information is available in literature but it may also be determined empirically using a variety of characterisation techniques. Once the magnetic properties of the minerals are known then the variables controlling magnetic separation (applied magnetic field, magnetic field gradient, particle size *etc.*) may be tailored to the required separation.

2.3.2 Vibrating Sample Magnetometer

As stated in Section 2.3.1 all minerals may be classified (for simplicity) into three categories of magnetic behaviour. The specific behaviour of a single mineral may be analysed by looking at the magnetisation of the material as a function of applied magnetic field. One method of obtaining this information is by using a vibrating sample magnetometer (VSM) which suspends a small quantity of mineral from an oscillating rod (Foner, 1959). The material is then subjected to a series of uniform magnetic fields of varying strength and the changes in magnetisation within the material are measured by a series of detection coils (Foner, 1956). The direct measurement output of the VSM is the magnetic moment of the sample, which is converted to magnetisation by dividing by the volume of the sample.

An example of typical diamagnetic, paramagnetic and ferromagnetic behaviour may be seen in Figure 2.2. A diamagnetic material, due to its unaligned magnetic dipoles, will be repelled along the lines of an applied magnetic field and as such it will exhibit a slightly negative linear variation of magnetisation with increasing applied magnetic field as shown in Figure 2.2 (Jiles, 1990; Waters *et al.*, 2007). On the same graph a paramagnetic material will show a positive linear increase in magnetisation as higher applied magnetic field strengths will cause more of the magnetic dipoles present in the material to align (Waters *et al.*, 2007). A ferromagnetic material will rapidly increase in magnetisation at relatively low applied magnetic field strengths until it reaches its saturation magnetisation (M_s) at which point increased applied magnetic field strength will have a minimal effect on magnetisation (see Figure 2.2) (Waters *et al.*, 2007). The explanation for this rapid increase is that magnetic dipoles in a ferromagnetic material are able to interact with one another to form magnetic domains which then allow for rapid alignment of the magnetic dipoles at relatively low magnetic field strengths (Jiles, 1990). The plateau in magnetisation that occurs at a ferromagnetic material's saturation magnetisation is due to the fact that once the majority of the magnetic domains in a material are aligned there is a very limited ability for any further dipole alignment to occur (Jiles, 1990). The saturation magnetisation is characteristic of a given ferromagnetic material and may be

used to determine the ferromagnetic fraction of a binary mixture of para- and ferromagnetic materials (Waters *et al.*, 2007).

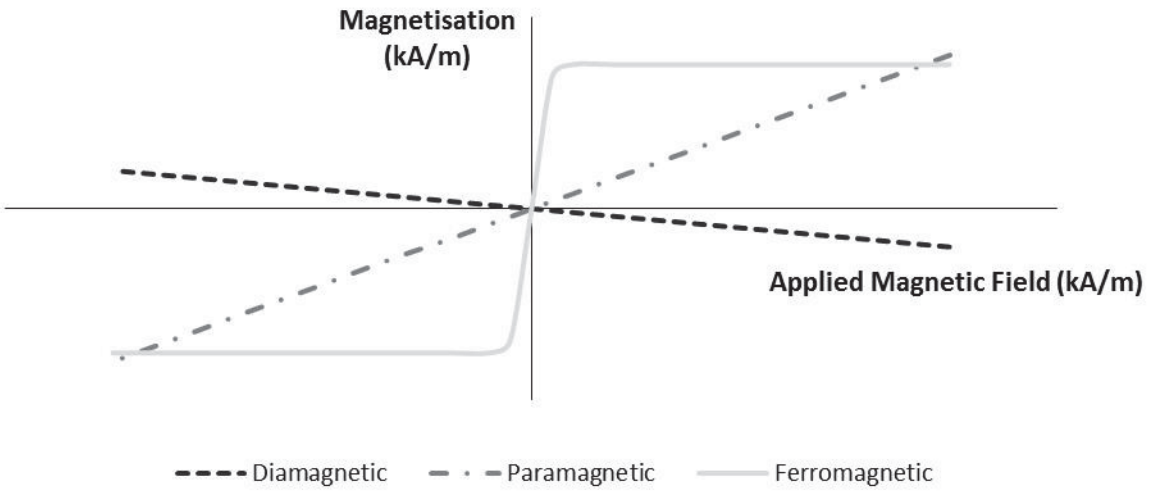

Figure 2.2 - Typical VSM results for diamagnetic, paramagnetic and ferromagnetic material

2.3.2.1 Honda-Owen Analysis

In the case of a binary mixture of a paramagnetic and a ferromagnetic material the trend of magnetisation as a function of applied magnetic field strength will be a combination of both materials (as shown in Figure 2.3) (Waters *et al.*, 2007). If the slope (or susceptibility) of the linearly sloped portion of the binary mixture trend is extracted and plotted as a function of the inverse applied magnetic field (Figure 2.4) it is possible to identify the paramagnetic material's volume susceptibility from the intercept of this graph (Waters *et al.*, 2007; Yang *et al.*, 2009). The slope of the graph in Figure 2.4 is then equivalent to the fraction of the mixture taken up by the ferromagnetic material multiplied by the saturation magnetisation of the given ferromagnetic material (Waters *et al.*, 2007; Yang *et al.*, 2009). This technique may allow the estimation of the concentration of the ferromagnetic component in a binary mixture (Male, 1980) or it may allow the determination of the susceptibility of the paramagnetic component, by removing the effects of any ferromagnetic impurities (Yang *et al.*, 2009).

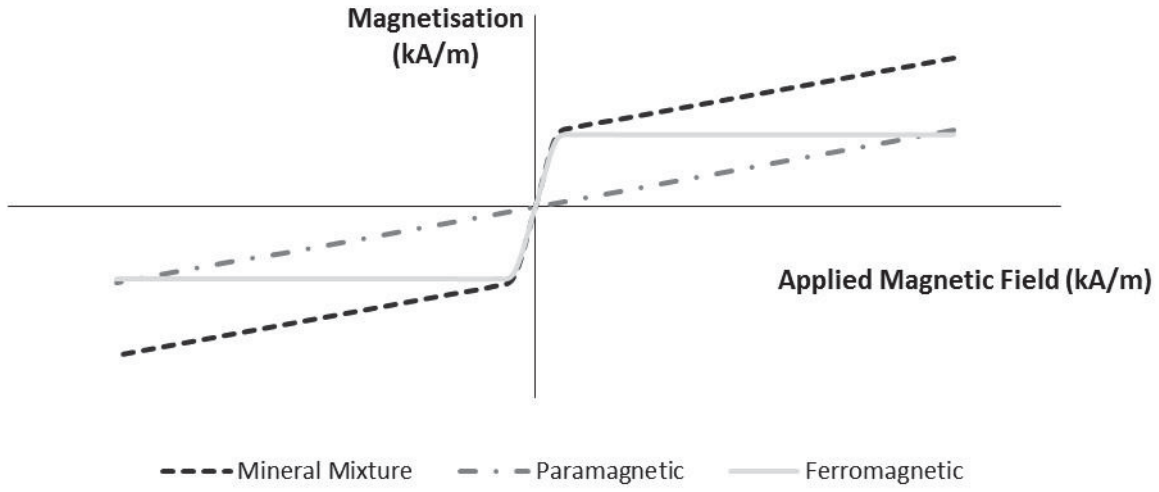

Figure 2.3 - VSM results for a binary mixture of paramagnetic and ferromagnetic mineral along with the extracted individual paramagnetic and ferromagnetic trends (from Honda-Owen plot)

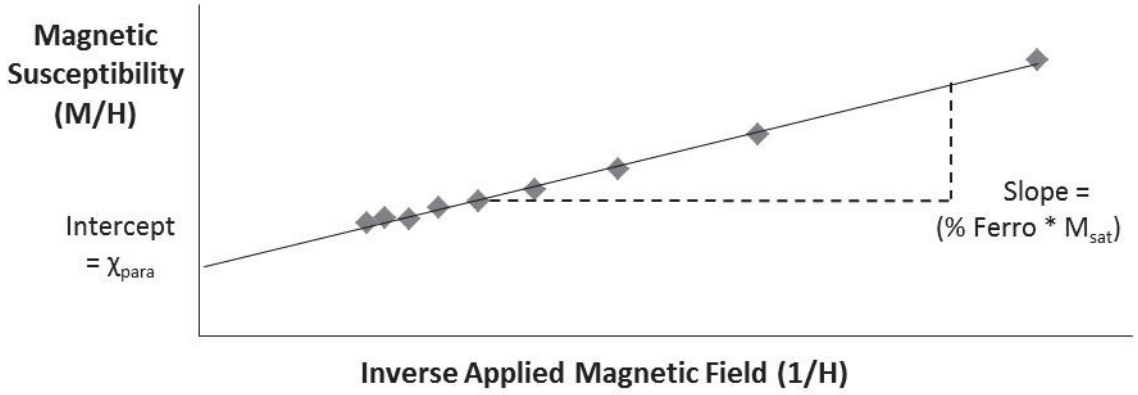

Figure 2.4 - Honda-Owen plot to determine paramagnetic and ferromagnetic components of a binary mixture

2.3.3 Frantz Isodynamic Separator

A very useful lab-scale magnetic separator is the Frantz Isodynamic Separator (Frantz, USA) shown in Figure 2.5. This separator operates by using an electromagnetic coil to generate a magnetic force to oppose the force of gravity on mineral particles as they pass through the separator on an inclined path (described by θ_1 and θ_2 in Figure 2.5). The Frantz is designed to provide a constant magnetic force along its length (hence

isodynamic) provided the magnetic susceptibility and orientation of the particle remain constant (McAndrew, 1957). If the attractive magnetic force is dominant the particle reports to the right chute in Figure 2.5 and if the magnetic force is insufficient to overcome gravity, the particle reports to the left chute. In this way the Frantz may be used to achieve separations for a wide range of minerals by tuning the magnetic force (varying the current passing through the electromagnetic coil) as well as the gravitational force (varying θ_1 and θ_2).

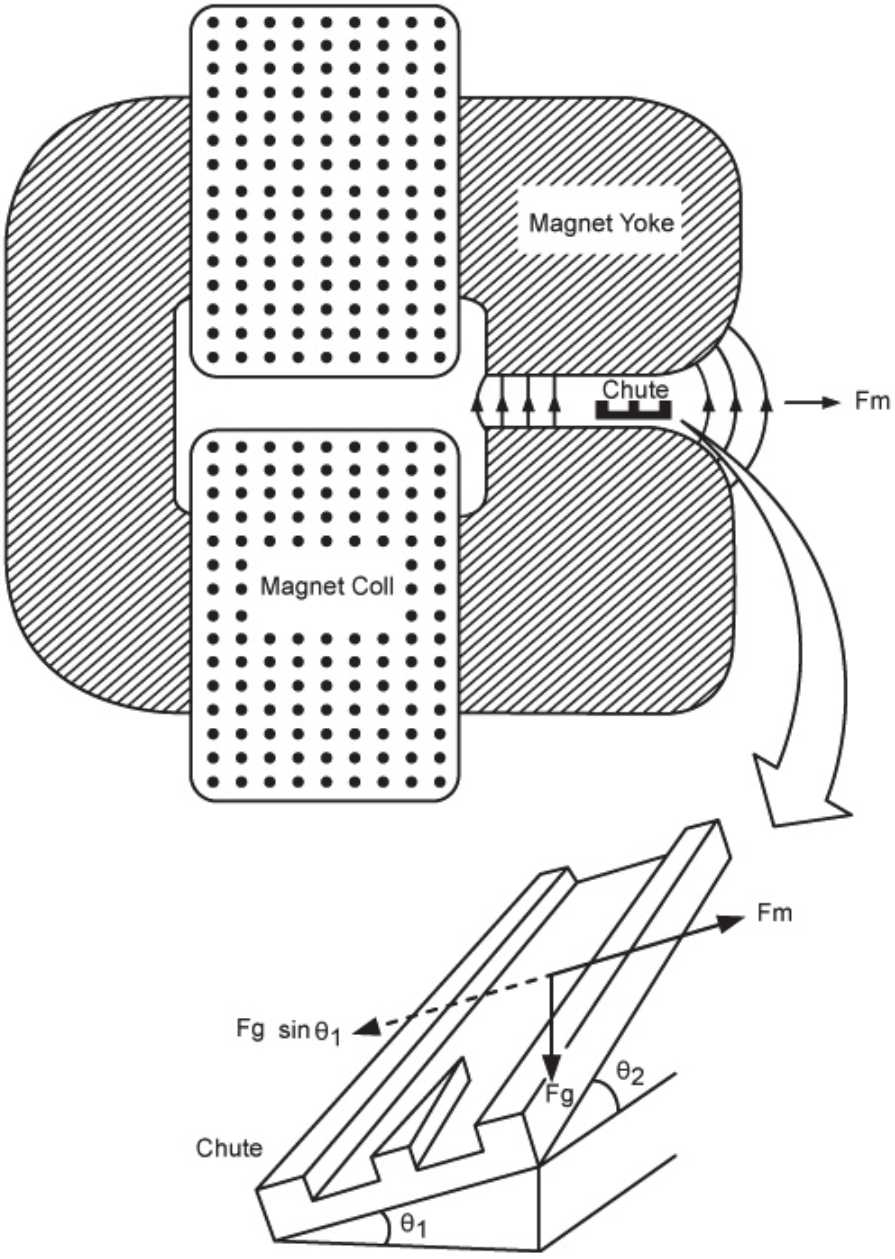

Figure 2.5 - Diagram of the Frantz isodynamic magnetic separator after Wills & Finch (2016)

2.3.4 Low Intensity Drum Separator

Minerals with relatively high magnetic susceptibility at low applied magnetic field strength may be concentrated using a low intensity (< 0.3 T) field (Murariu & Svoboda, 2003). One of the primary separators used in low intensity magnetic separation is a wet drum magnetic separator as can be seen in Figure 2.6. This separator contains permanent

magnets in the body of the drum (held in a fixed position) surrounded by an external rotating shell. As a mineral slurry is fed to the separator, mineral particles which experience a net attractive force (that is a magnetic attractive force which exceeds the forces of gravity and fluid drag) will be pinned to the rotating drum surface until they pass out of the magnetic field and are released, reporting to the concentrate launder in Figure 2.6. Mineral particles which are not held by the drum surface will report with the bulk of the slurry water to the tailings outlet. This separator is typically used to concentrate ferromagnetic minerals, such as magnetite, due to their strong magnetic response (high magnetic susceptibility at low applied field strength).

In any mineral separation, the influence of particle size must be considered to avoid the unintended loss of valuable minerals to the tailings. In the wet drum separator this loss occurs as fine, strongly magnetic mineral particles, which do not experience a sufficiently strong magnetic attraction to counteract the large influence of fluid drag. One potential solution to this problem is to replace the permanent magnets within the drum with magnets of stronger field strength (*i.e.* rare earth-based magnets replacing ferritic magnets). In this way it is possible to increase the attractive force felt by the strongly magnetic mineral particles and therefore improve their recovery to the concentrate. An optimized low intensity magnetic separation circuit will often include both rougher and cleaner separations and should always begin initially at the lowest applied magnetic field strength to avoid entrainment of non-magnetic gangue or potential clogging of the separator itself.

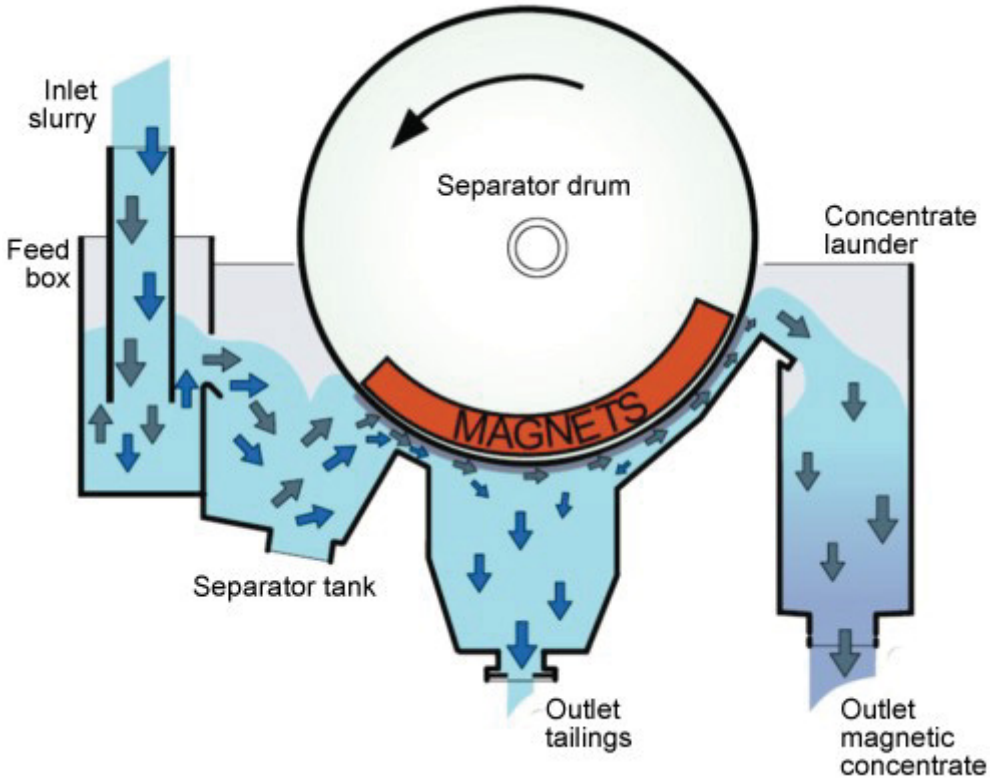

Figure 2.6 - Diagram of a wet drum magnetic separator after Wills & Finch (2016)

2.3.5 Wet High Intensity Magnetic Separation

For minerals with a lower magnetic susceptibility at low applied magnetic field strengths (usually paramagnetic minerals) it is necessary to increase both the magnetic field strength of the separator as well as the magnetic field gradient of the separator. A classic example of this is the wet high intensity magnetic separator (WHIMS) which passes a mineral slurry through a high intensity magnetic field generated by an electromagnet (Figure 2.7). The separation chamber to which the slurry is fed contains a matrix constructed from a ferromagnetic material, such as steel, to concentrate the applied magnetic field and provide a high number of points of very high gradient to increase the capture of weakly magnetic mineral particles. Examples of three different types of matrix material may be seen in Figure 2.8. In this separator, mineral particles for which the attractive magnetic force overcomes the forces of fluid drag and gravity will remain attached to the matrix with non-magnetic mineral particles passing through the separation chamber.

Certain lab-scale WHIMS use a variety of different matrix materials, in conjunction with a variable intensity electromagnet to tune the separation conditions (gradient and applied magnetic field strength) for a given mineral slurry. In this way separation may be achieved for a wide range of mineral mixtures provided they have sufficiently different magnetic properties. Similar to the discussion in Section 2.3.4, care must be taken to pass material through such a separator only after all strongly magnetic material has first been removed, in order to avoid separator blockage. Additionally, if multiple separations from the same mineral stream are desired, it is important to progress from the lowest magnetic field strength (targeting the minerals with the strongest magnetic response) to the highest magnetic field strength to avoid entrainment of weaker magnetic particles (or even non-magnetic particles) into the magnetic concentrate.

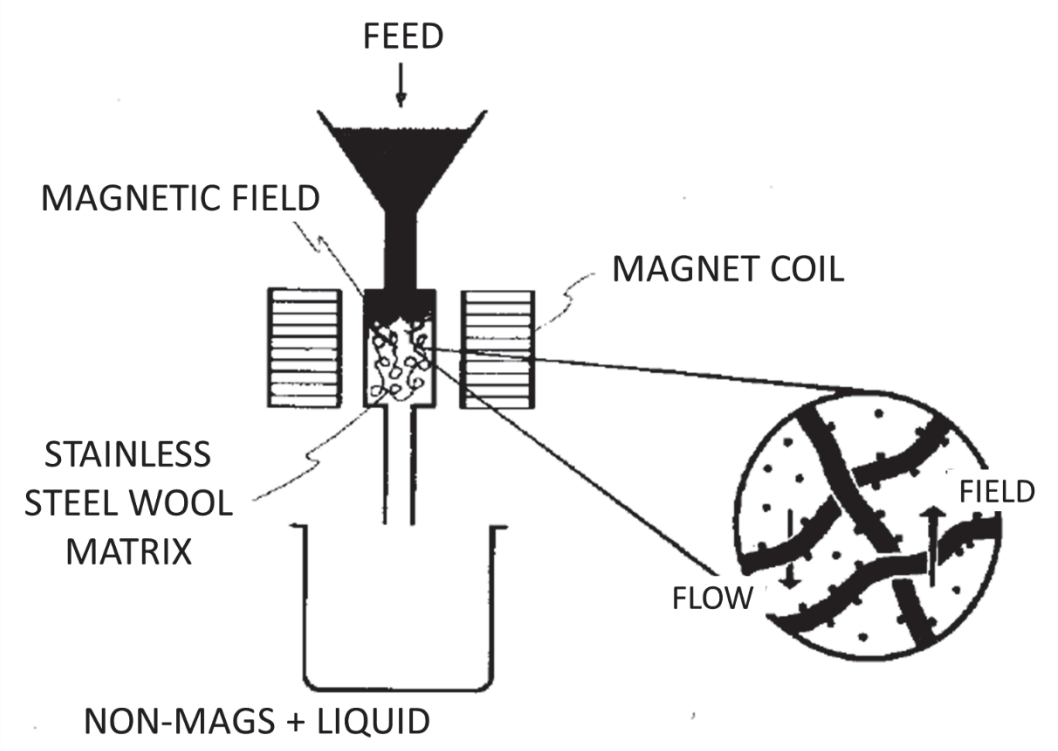

Figure 2.7 - Schematic of a wet high intensity magnetic separator adapted from (Oberteuffer, 1974)

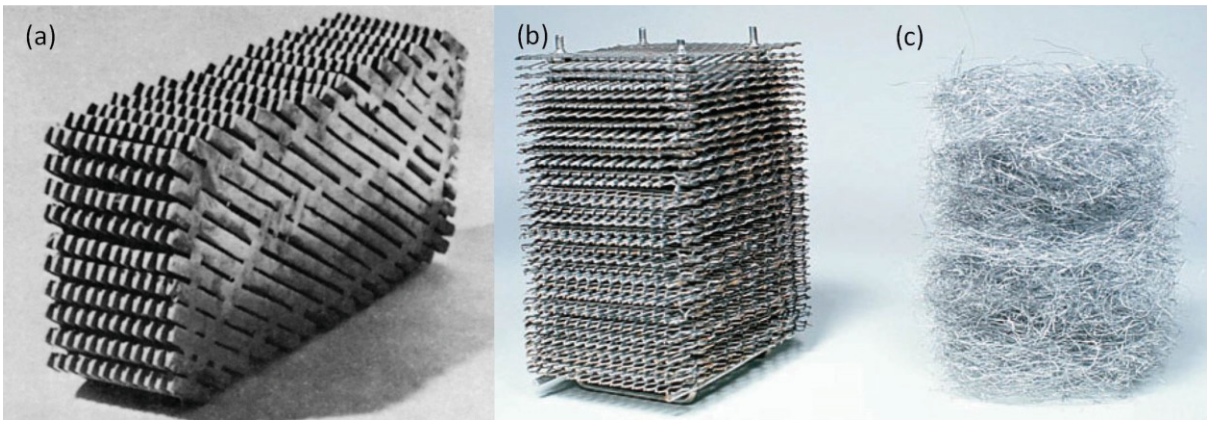

Figure 2.8 - Ferromagnetic WHIMS matrix materials: (a) Grid assembly of stainless steel bars, (b) Expanded stainless steel matrix used for coarse particle capture, (c) Stainless steel wool used for fine particle capture after Wills & Finch (2016)

2.4 Electrostatic Separation

Electrostatic separation relies on the differences in mineral conductivity, a surface property, in order to separate minerals. While this technique is limited in mineral processing applications because of feed requirements (low feed moisture, inability to treat very fine particle sizes) it is used in the concentration of monazite and xenotime, REM, from beach sand deposits. The most common electrostatic separator is the high-tension roll (HTR) separator, the operation of which is shown in Figure 2.9. In this separator a dry feed of particles is fed to the top of a rotating earthed roll. As the particles move forward along the roll they pass through a spray discharge ionizing electrode which imparts a surface charge to the minerals. As the mineral particles move past the ionizing electrode's field, strongly conductive minerals will quickly lose this charge to the earthed roll while weaker conducting minerals will maintain this charge and remain pinned to the roll. The rotational velocity of the roll throws the strongly conductive minerals from the roll while the pinned, weakly conducting minerals are removed from the roll mechanically by a brush. This separator typically produces distinct streams of particles which are then separated by a splitter and collected in different bins. Readers interested in more information on electrical separation of mineral are advised to consult reviews by Kelly & Spottiswood (1989c, 1989a, 1989b) as well as Wills & Finch (2016).

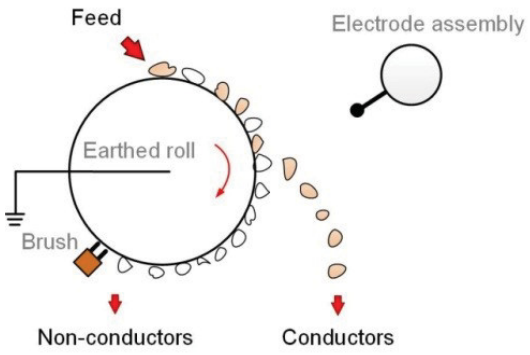

Figure 2.9 – Diagram of operation of a HTR separator after Wills & Finch (2016)

2.5 Froth Flotation

2.5.1 Froth flotation theory

Froth flotation is a mineral separation technique involving the interaction of a mineral slurry with ascending air bubbles. When a mineral with a hydrophobic surface contacts an air bubble it may attach to the air bubble and rise to the surface of the flotation cell to become part of the froth phase. The froth phase overflows (in laboratory systems this is often accomplished by skimming) at regular intervals so that the hydrophobic mineral particles become the concentrate from the flotation process. Minerals with hydrophilic surfaces will not attach to the ascending air bubbles and therefore remain in suspension (in the pulp). After a given particle collection time (based on cell volumes and slurry flow rates in continuous systems) all material remaining in the pulp of the flotation cell reports to the tailings of the flotation process. A schematic of the flotation process may be seen in Figure 2.10.

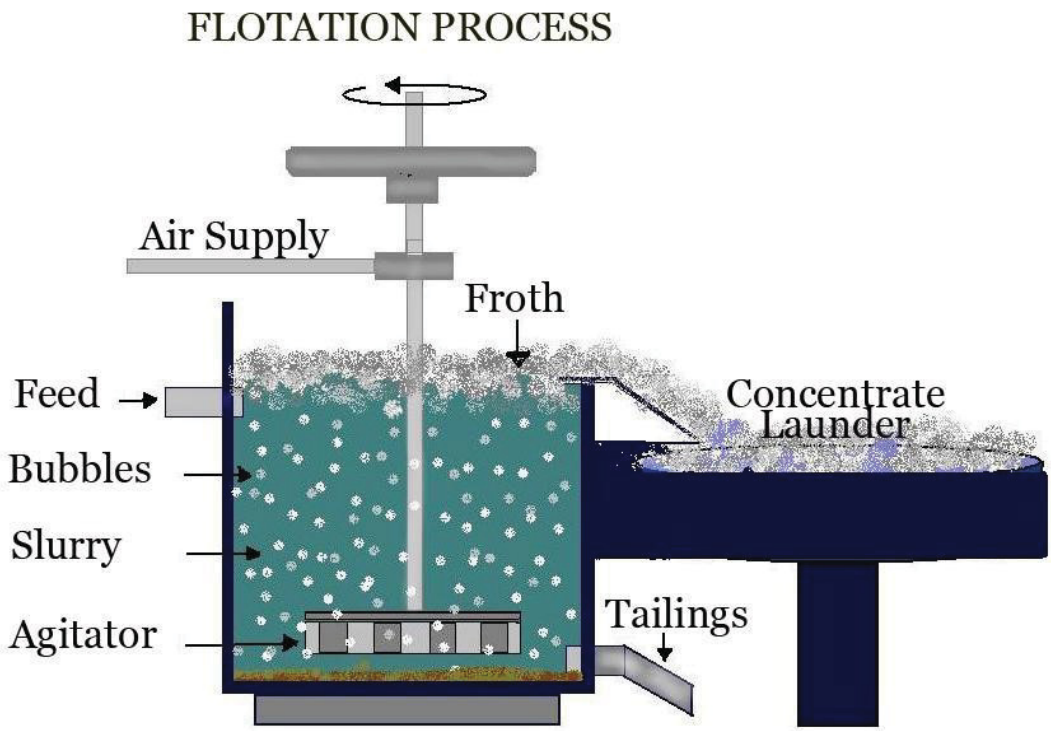

Figure 2.10 - Schematic of the froth flotation process for a mineral slurry after Michaud (2013)

The froth flotation process is extremely complex and successful applications of froth flotation must be based on an understanding of the aqueous and surface chemistry involved, as well as the physics of the three phase system present in a flotation cell. Only flotation concepts relevant to this thesis are discussed here, but there is a large body of literature available on these subjects. Interested readers are advised to read widely. Two excellent starting points in flotation literature are Fuerstenau *et al.* (2007) and Wills & Finch (2016).

2.5.1.1 Mineral hydrophobicity

The interaction between a solid mineral particle and an air bubble in a flotation cell is often considered from the standpoint of the interfacial energies of each of the surfaces present. These include the solid-air interface ($\gamma_{s/a}$), the water-air interface ($\gamma_{w/a}$), and the solid-water interface ($\gamma_{s/w}$) as shown in Figure 2.11. It is possible to define a force equilibrium at the point of three phase (solid, air and water) contact point (Equation 2.4) as well as a work of adhesion (W_{adh}) which is the energy required to pull apart the interface between

the solid particle and the air bubble (Equation 2.5) (Wills & Finch, 2016). The angle, θ, in Figure 2.11 and Equation 2.5 is the contact angle between the mineral particle and the air bubble. Combining Equations 2.4 and 2.5 yields an equation for the work of adhesion which depends only on the interfacial energy of the water-air interface and the contact angle. The contact angle provides an indication of the hydrophobicity of the mineral and therefore mineral surfaces which are more inherently hydrophobic (higher contact angle in water) will have a greater work of adhesion. These particles will then be expected to more readily attach to an ascending air bubble in a flotation cell. There are additional factors at play in the physics of bubble-particle attachment which are not discussed here; interested readers should consult Wills & Finch (2016) for a more detailed explanation.

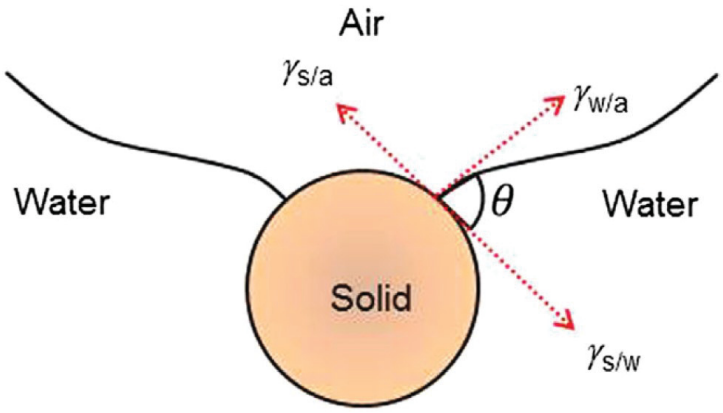

Figure 2.11 – Schematic of contact angle between mineral surface and air bubble in flotation after Wills & Finch (2016)

$$\gamma_{s/a} = \gamma_{s/w} + \gamma_{w/a} \cos\theta \quad (2.4)$$

$$W_{adh} = \gamma_{w/a} + \gamma_{s/w} - \gamma_{s/a} \quad (2.5)$$

$$W_{adh} = \gamma_{w/a}(1 - \cos\theta) \quad (2.6)$$

2.5.1.2 Flotation Kinetics

The recovery of a given mineral in flotation as a function of time is often described by the first order flotation rate equation (Arbiter *et al.*, 1985):

$$R = R_{max}(1 - e^{-kt}) \quad (2.7)$$

Where t is flotation time (min), k is the flotation rate constant (min^{-1}) and R_{max} is the maximum recovery achievable at t=∞. Comparison of flotation rate constants for different minerals is commonly used as a predictor for the possibility of a separation of two floatable components based on the kinetic rate of flotation recovery. An alternative method is to employ the modified flotation rate constant as proposed by Xu (1998):

$$K_m = R_{max} \times \mathrm{k} \tag{2.8}$$

Where K_m is the modified flotation rate constant. Since it accounts for both the maximum recovery and the rate of recovery, it is more reflective of true selectivity in a flotation system. Thus, a selectivity index, SI, can be defined by dividing the modified rate constants of two different minerals (Xu, 1998):

$$SI = \frac{K_{m_1}}{K_{m_2}} \tag{2.9}$$

The higher the SI, the higher the possibility of separation of the two minerals in a multiple stage flotation process.

2.5.2 Surface Chemistry in Flotation

Most minerals are not sufficiently hydrophobic to allow for their collection directly through froth flotation; surfactants must be added to the system to achieve the desired results. These surfactants may be separated into multiple different classes: frothers act to preserve the flotation bubble size as well as stabilize the froth phase, collectors interact with mineral surfaces to render them sufficiently hydrohphobic to enable attachment to air bubbles, depressants act in opposition to collectors such that they attach to mineral surfaces to render them more hydrophilic; activators may be considered as intermediate reagents which are added to render a mineral surface more amenable to adsorbing another reagent (most often collectors).

Solid particles in an aqueous suspension will develop a surface charge due to various factors such as surface group ionisation, preferential dissolution of ions, ion adsorption to the surface and isomorphous substitution in the mineral lattice (Riley, 2005). A charged surface will attract a layer of counter ions immediately adjacent to the surface as well as

a second, more diffuse, layer of counter ions. Together these layers are called the diffuse double layer and result in a decreasing electrochemical potential as a function of distance from the particle surface (Chander & Hogg, 1984). In the study of surface properties, the electrical double layer governs the adsorption of various flotation reagents, which in turn directly affect the flotation response of a given mineral (Fuerstenau & Pradip, 2005; Pradip, 1981). A common means of investigating the chemical characteristics of a mineral surface is zeta potential measurements of mineral particles.

2.5.2.1 Zeta Potential

As the surface charge of a particle suspension can be quite difficult to measure directly it is possible to define a plane of shear at which the counter ions are sufficiently attracted to the particle surface that they will move with the particle when the particle is set in motion. As there is a decreasing electrochemical potential as a function of distance from the particle surface, the potential at the plane of shear has a distinct value which is referred to as the zeta potential. This concept is illustrated schematically in Figure 2.12. For an excellent introduction to the concept of zeta potentials and their application to mineral flotation interested readers should consult Riley (2005) and Fuerstenau & Pradip (2005).

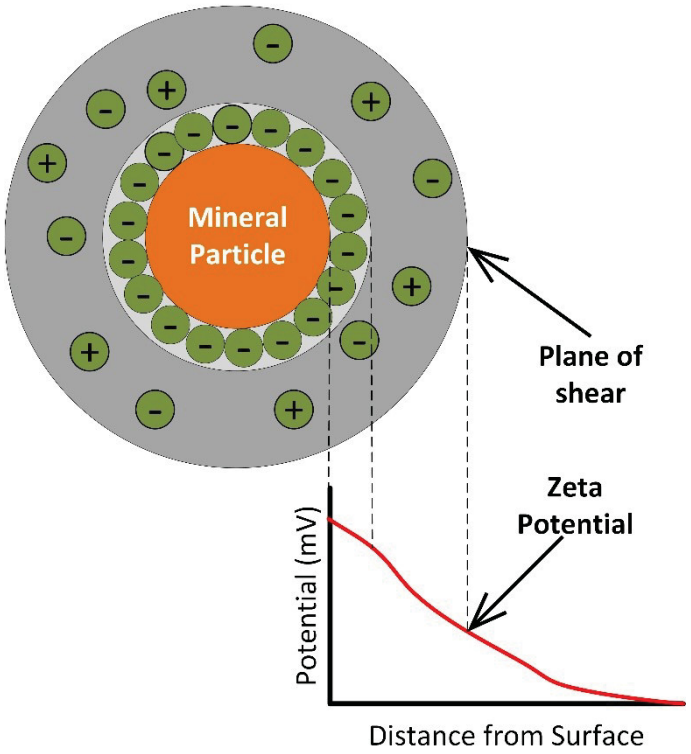

Figure 2.12 - Diffuse double layer about a mineral particle with corresponding electrochemical potential

For mineral surfaces in flotation, a very important property that can be used to characterize the electrical double layer is the isoelectric point (IEP); which is the pH value at which the zeta potential is zero (Pope & Sutton, 1973). The IEP can be used to predict the sign of the charge on a mineral surface in a given pH region (Pope & Sutton, 1973). Understanding the zeta potential of a mineral, and the IEP, combined with a knowledge of a collector's ionization behaviour at various pH levels in aqueous conditions allows one to predict the mechanism of collector adsorption on the mineral surface (Cheng *et al.*, 1993; Pope & Sutton, 1973). The variation of this parameter in the presence of various flotation reagents is important in understanding flotation as the IEP of different minerals in an ore can help select flotation conditions which allow minerals to be effectively separated (Cheng, 2000; Cheng *et al.*, 1994; Fuerstenau *et al.*, 1992; Pradip, 1981). Work by Kosmulski (2001b, 2001a, 2002, 2004, 2006, 2009) and Parks (1965) provides IEP data for many common minerals, and Fuerstenau & Pradip (2005) presents a good overview of how zeta potential data of oxide/silicate minerals may be related to flotation.

2.5.3 Laboratory Equipment

2.5.3.1 Denver Flotation Cell

One of the most common lab-scale flotation cells in mineral processing labs is the Denver flotation cell (Figure 2.13). This cell simulates conventional industrial-scale mechanical flotation cells. The Denver cell is mechanically driven and may be operated in either self-aspirated or forced air modes. Air in this cell is introduced through the hollow standpipe which also contains the impeller shaft. Both the air input and the impeller speed may be modulated (in the case of the self-aspirated mode the impeller speed is used to control the air flow). In this style of mechanical flotation cell, the incoming air mass is sheared by the impeller to produce fine bubbles (Do, 2003). These cells have been extensively characterized for their hydrodynamics, interested readers should consult the following sources: Arbiter *et al.* (1976); Girgin *et al.* (2006); Harris (1974); Harris & Mensah-Biney (1977).

Figure 2.13 - Denver D12 lab-scale flotation cell after Wills & Finch (2016)

2.5.3.2 Microflotation Column

For the purposes of small-scale (microflotation) flotation research several different experimental setups have been used, including modifications of a Hallimond tube and the Partridge-Smith design (Feasby, 1966; Fuerstenau *et al.*, 1957; Matis *et al.*, 1991; Ozkan & Yekeler, 2003; Partridge & Smith, 1971). Common benefits of small-scale flotation experiments in all of these cases are low reagent and mineral requirements, easily manipulated flotation parameters and repeatability. The chief advantage of the Partridge-Smith design is that the volume of the flotation cell and required mineral mass are both very low. These features make the Partridge-Smith design especially suited to single mineral flotation experiments and it is this type of microflotation column that has been used throughout the experimental work presented in this thesis. An image and schematic diagram of this microflotation column may be seen in Figure 2.14.

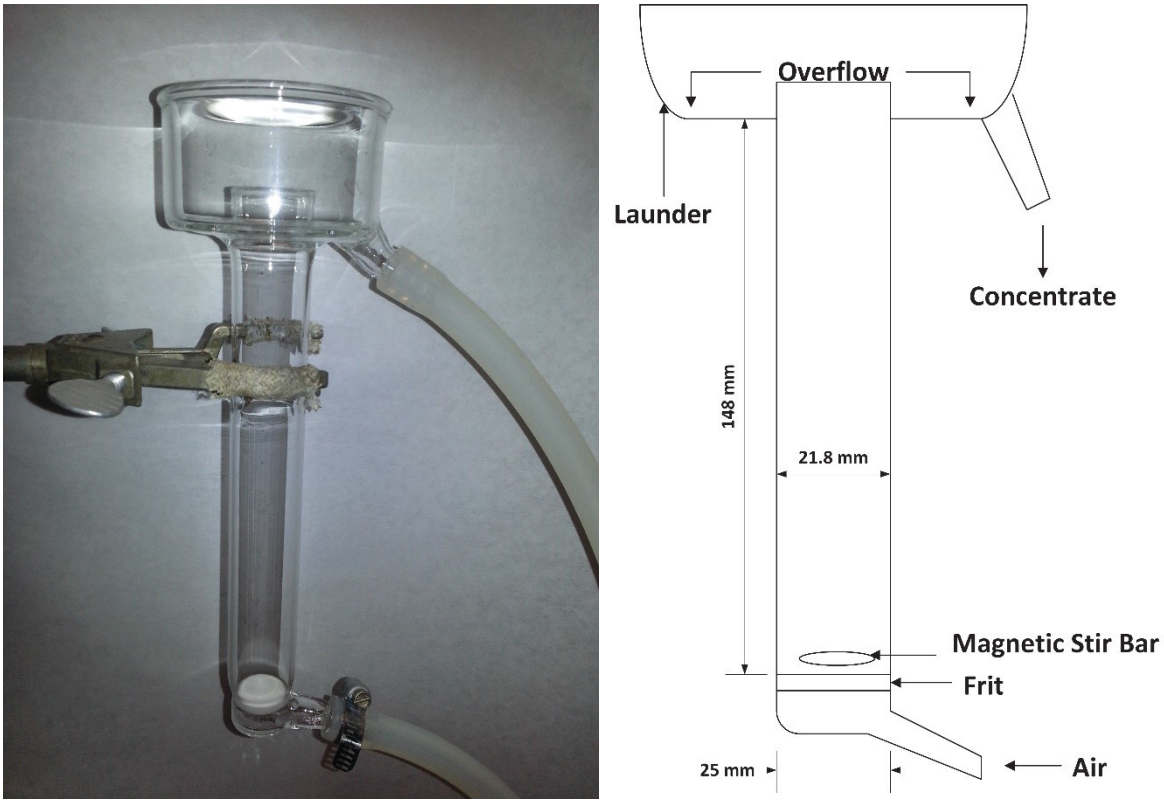

Figure 2.14 - Image and schematic of a modified Partridge-Smith microflotation cell

2.5.3.3 Zeta Potential Measurements

Zeta potential may be measured by multiple different methods including electrokinetics and electroacoustics. Electrokinetic techniques are based on the relationship between the motion of the particle or fluid, and the electric field in a suspension. Sedimentation potential and streaming potential approaches measure the electric field generated by the motion of charged particles and the electrolyte solution respectively (Riley, 2005). In electrophoretic and electroosmotic techniques the motion of charged particles and the electrolyte solution respectively, are measured under the influence of an applied electric field (Riley, 2005).

In the electrophoretic zeta potential analyser used in this work, laser scattering is used to measure the velocity of particles in an electrolyte solution when an electric field is applied to the solution (Riley, 2005). The zeta potential may then be calculated from the velocity of the particles, the applied electric field and the viscosity and permittivity of the background electrolyte (Riley, 2005).

The second apparatus used is an electroacoustic zeta potential analyzer which applies an electrical field to an aqueous solution containing the mineral of interest. The main advantage of this method over electrophoretic methods is that it can be applied to solutions with higher concentrations that are not optically transparent (Riley, 2005). The electrical field causes the particles to oscillate along the field lines so that tiny acoustic dipoles are generated, resulting in an acoustic signal (Hunter, 1998). This acoustic signal may then be converted to the zeta potential of the particles provided the particle concentration, diameter and density are known (Hunter, 1998). The zeta potential analyser is equipped with an automatic titration unit allowing for zeta potential determination over a range of pH levels or chemical additions. For further information on the uses of electroacoustics in measuring zeta potential see the reviews by Hunter (1998) and Greenwood (2003).

2.6 Conclusions

This chapter details the fundamentals of the mineral processing techniques used throughout this thesis. An overview of various separation techniques was given including

gravity, magnetic and flotation separations as well as several measurement techniques used to investigate the bulk and surface properties governing mineral separation behaviour in these separations. Finally, the operating principles of the main lab-scale separation and measurement equipment used in this thesis were introduced.

3. Review of the Beneficiation of Rare Earth Element-Bearing Minerals

3.1 Introduction

This chapter explores the current literature on the beneficiation of rare earth element-bearing minerals (REM). Areas examined include the minerals processed, the unit operations employed, some processes currently utilized at the major rare earth mines and processing plants and finally, areas necessitating further research.

3.2 Currently exploited minerals

Today, over 250 REM have been discovered, but much of the actual REE supply comes from only a handful of sources (Bulatovic, 2010; Chi *et al.*, 2001; Gupta & Krishnamurthy, 2005). REM can be differentiated into multiple groups based on their REE content. These minerals may be identified as cerium or yttrium type minerals based on whether the distribution of the lanthanides in the mineral is part of the previously (Chapter 1, Section 1.1) described “light” or “heavy” rare earth sub-groups (Cesbron, 1986; Trifonov, 1963). The cerium group of REM includes bastnäsite and monazite, and the yttrium group includes xenotime; these three being the most commonly extracted REM (Bulatovic, 2010; Gupta & Krishnamurthy, 2005). Similarly, they may be complex minerals, with a REE distribution that includes all of the lanthanides, or selective minerals, with REE distributions that only include a portion of the lanthanides (Ferron *et al.*, 1991).

The trivalent REE cations have coordination numbers between 6 and 11 with larger coordination numbers (8-11) corresponding to the larger rare earth cations of the LREE and smaller coordination numbers (6-8) for the smaller HREE cations (Kanazawa & Kamitani, 2006; Miyawaki & Nakai, 1993). This is important as the REE with smaller coordination numbers are more likely to be present in oxides such as silicates, resulting in a higher concentration of HREE in these minerals, whereas carbonates are more likely to have increased concentrations of LREE (due to their higher coordination numbers) (Kanazawa & Kamitani, 2006).

Table 3.1 contains examples of REM with different coordination numbers. The REM may also be classified according to their crystal structures with the most comprehensive review to date of REM crystal structures found in Miyawaki & Nakai (1993). This system of classification (summarized in Table 3.2) is based on the shape and linkage of the anionic groups found in REM. It is interesting to note that the two most widely exploited minerals, bastnäsite and monazite, represent the two crystal structures with isolated anionic groups whereas silicate minerals predominantly contain linked anionic groups. These different structures have potential implications on downstream processes as they are likely to produce varied distributions of exposed ions on the surfaces of freshly fractured minerals.

Table 3.1 - Examples of REM for various coordination numbers. Adapted from (Miyawaki & Nakai, 1993)

Coordination Number	Mineral Name
6	Eudialyte, Agrellite
7	Britholite (Ce), Apatite, Mosandrite
8	Monazite, Gadolinite (Y), Rhabdophane (Ce), Allanite, Fergusonite
9	Britholite (Y), Britholite (Ce), Steenstrupine (Ce)
10	Lanthanite, Ancylite (Ce)
11	Bastnäsite, Fluocerite (Ce)

Table 3.2 - Classification of REM on the basis of crystal structure. Adapted from (Miyawaki & Nakai, 1993)

RE Crystal Structures	Anionic Group Shape	Linked/Isolated	Mineral Class	Example
Class 1	Triangular	Isolated	Carbonates	Bastnäsite
Class 2a	Tetrahedral	Isolated	Phosphates	Monazite
Class 2b	Tetrahedral	Linked	Silicates	Eudialyte
Class 3	Tetrahedral + Octahedral	Linked	Aluminosilicates, Titanosilicates	Allanite
Class 4	Octahedral	Linked	Complex Oxides (Ti, Nb, V)	Fergusonite
Class 5	None	N/A	Fluorides, Simple Oxides	Fluocerite

A listing of some common REM, along with chemical formulas, specific gravities, magnetic characteristics, contents of rare earth oxide (REO), uranium and thorium of these minerals (where this information is known) is shown in Table 3.3 to Table 3.7. In

these tables bastnäsite, monazite and xenotime are highlighted as they are the three commonly extracted REM. Table 3.8 gives examples of the REE distributions found in major deposits of these minerals, as well as the REE distribution of the ion-adsorbed clay deposits of China.

Historically, monazite was the principal source of REE until the discovery of the Bayan Obo mine in China. With the development of this mine as well as the Mountain Pass mine in the United States, bastnäsite has become the world's primary source of REE (Gupta & Krishnamurthy, 2005). As the Mountain Pass mine has only recently resumed operations (with ongoing doubts to the mines long term viability), the majority of the world's REE are currently produced from Chinese sources (Pitts, 2011).

Table 3.3 - Carbonate REM. Adapted from (Anthony *et al.*, 2001; Long *et al.*, 2010; Rosenblum & Brownfield, 1999)

Mineral Name	Chemical Formula	Density (g/cm^3)	Magnetic Properties	Weight Percent		
Carbonates			Para/Diamagnetic?	REO	ThO_2	UO_2
Ancylite (Ce)	$Sr(Ce,La)(CO_3)_2OH{\cdot}H_2O$	3.82-4.30	n/a	46-53	0-0.4	0.1
Ancylite (La)	$Sr(La,Ce)(CO_3)_2OH{\cdot}H_2O$	3.69	n/a	46-53	0-0.4	0.1
Bastnäsite (Ce)	**$(Ce,La)(CO_3)F$**	**4.90-5.20**	**Paramagnetic**	**70-74**	**0-0.3**	**0.09**
Bastnäsite (La)	**$(La,Ce)(CO_3)F$**	**n/a**	**Paramagnetic**	**70-74**	**0-0.3**	**0.09**
Bastnäsite (Y)	**$Y(CO_3)F$**	**3.90-4.00**	**Paramagnetic**	**70-74**	**0-0.3**	**0.09**
Calcio-ancylite (Ce)	$(Ca,Sr)Ce_3(CO_3)_4(OH)_3{\cdot}H_2O$	3.95	n/a	60	-	-
Calcio-ancylite (Nd)	$Ca(Nd,Ce,Gd,Y)_3(CO_3)_4(OH)_3{\cdot}H_2O$	4.02	n/a	60	-	-
Doverite	$YCaF(CO_3)_2$	3.90	n/a	-	-	-
Parisite (Ce)	$Ca(Ce,La)_2(CO_3)_3F_2$	4.33	Paramagnetic	59	0-0.5	0-0.3
Parisite (Nd)	$Ca(Nd,Ce)_2(CO_3)_3F_2$	4.20-4.50	Paramagnetic	-	-	-
Synchysite (Ce)	$Ca(Ce,La)(CO_3)_2F$	3.90	n/a	49-52	1.6	-
Synchysite (Nd)	$Ca(Nd,La)(CO_3)_2F$	4.14 (calc)	n/a	-	-	-
Synchysite (Y) (doverite)	$Ca(Y,Ce)(CO_3)_2F$	3.90	n/a	-	-	-

Table 3.4 - Halide REM. Adapted from (Anthony *et al.*, 2001; Long *et al.*, 2010; Rosenblum & Brownfield, 1999)

Mineral Name	Chemical Formula	Density (g/cm^3)	Magnetic Properties	Weight Percent		
Halides			Para/Diamagnetic?	REO	ThO_2	UO_2
Fluocerite (Ce)	$(Ce,La)F_3$	5.93	Paramagnetic	-	-	-
Fluocerite (La)	$(La,Ce)F_3$	5.93	Paramagnetic	-	-	-
Fluorite	$(Ca,REE)F_2$	3.18-3.56	Diamagnetic	-	-	-
Gagarinite (Y)	$NaCaY(F,Cl)_6$	4.11-4.29	n/a	-	-	-
Pyrochlore	$(Ca,Na,REE)_2Nb_2O_6(OH,F)$	4.45-4.90	Paramagnetic	-	-	-
Yttrofluorite	$(Ca,Y)F_2$	n/a	n/a	-	-	-

Table 3.5 - Oxide REM. Adapted from (Anthony *et al.*, 2001; Long *et al.*, 2010; Rosenblum & Brownfield, 1999)

Mineral Name	Chemical Formula	Density (g/cm^3)	Magnetic Properties	Weight Percent		
Oxides			Para/Diamagnetic?	REO	ThO_2	UO_2
Anatase	$(Ti,REE)O_2$	3.79-3.97	Diamagnetic	-	-	-
Brannerite	$(U,Ca,Y,Ce)(Ti,Fe)_2O_6$	4.20-5.43	Paramagnetic	-	-	-
Cerianite (Ce)	$(Ce^{4+},Th)O_2$	7.20 (syn)	n/a	-	-	-
Euxenite (Y)	$(Y,Ca,Ce,U,Th)(Nb,Ta,Ti)_2O_6$	5.30-5.90	Paramagnetic	-	-	-
Fergusonite (Ce)	$(Ce,La,Y)NbO_4$	5.45-5.48	Paramagnetic	-	-	-
Fergusonite (Nd)	$(Nd,Ce)(Nb,Ti)O_4$	n/a	Paramagnetic	-	-	-
Fergusonite (Y)	$YNbO_4$	5.60-5.80	Paramagnetic	-	-	-
Loparite (Ce)	$(Ce,Na,Ca)(Ti,Nb)O_3$	4.60-4.89	n/a	-	-	-
Perovskite	$(Ca, REE)TiO_3$	3.98-4.26	Diamagnetic	<37	0-2	0-0.05
Samarskite	$(REE,Fe^{2+},Fe^{3+},U,Th,Ca)(Nb,Ta,Ti)O_4$	5.00-5.69	Paramagnetic	-	-	-
Uraninite	$(U,Th,Ce)O_2$	10.63-10.95	Paramagnetic	-	-	-

Table 3.6 - Phosphate REM. Adapted from (Anthony *et al.*, 2001; Long *et al.*, 2010; Rosenblum & Brownfield, 1999)

Mineral Name	Chemical Formula	Density (g/cm^3)	Magnetic Properties	Weight Percent		
Phosphates			Para/Diamagnetic?	REO	ThO_2	UO_2
Britholite (Ce)	$(Ce,Ca)_5(SiO_4,PO_4)_3(OH,F)$	4.20-4.69	Paramagnetic	56	1.5	-
Britholite (Y)	$(Y,Ca)_5(SiO_4,PO_4)_3(OH,F)$	4.35	Paramagnetic	56	1.5	-
Brockite	$(Ca,Th,Ce)(PO_4)\cdot H_2O$	3.9	n/a	-	-	-
Chevkinite (Ce)	$(Ca,Ce,Th)_4(Fe^{2+},Mg)_2(Ti,Fe_{3+})_3Si_4O_{22}$	4.53-4.67	Paramagnetic	-	-	-
Churchite (Y)	$YPO_4\cdot H_2O$	3.26	n/a	-	-	-
Crandallite	$CaAl_3(PO_4)_2(OH)_5\cdot H_2O$	2.78-3.04	n/a	-	-	-
Florencite (Ce)	$CeAl_3(PO_4)_2(OH)_6$	3.45-3.54	n/a	-	1.4	-
Florencite (La)	$(La,Ce)Al_3(PO_4)_2(OH)_6$	3.52	n/a	-	1.4	-
Florencite (La)	$(Nd,Ce)Al_3(PO_4)_2(OH)_6$	3.70 (calc)	n/a	-	1.4	-
Fluorapatite	$(Ca,Ce)_5(PO_4)_3F$	3.10-3.25	n/a	-	-	-
Gorceixite	$(Ba,REE)Al_3[(PO_4)_2(OH)_5]\cdot H_2O$	3.04-3.19	Diamagnetic	-	-	-
Goyazite	$SrAl_3(PO_4)_2(OH)_5\cdot H_2O$	3.26	Diamagnetic	-	-	-
Monazite (Ce)	**$(Ce,La,Nd,Th)PO_4$**	**4.98-5.43**	**Paramagnetic**	**35-71**	**0-20**	**0-16**
Monazite (La)	**$(La,Ce,Nd,Th)PO_4$**	**5.17-5.27**	**Paramagnetic**	**35-71**	**0-20**	**0-16**
Monazite (Nd)	**$(Nd,Ce,La,Th)PO_4$**	**5.43 (calc)**	**Paramagnetic**	**35-71**	**0-20**	**0-16**
Rhabdophane (Ce)	$(Ce,La)PO_4\cdot H_2O$	3.77-4.01	n/a	-	-	-
Rhabdophane (La)	(La,Ce)PO4·H2O	4.4	n/a	-	-	-
Rhabdophane (Nd)	(Nd,Ce,La)PO4·H2O	4.79 (calc)	n/a	-	-	-
Vitusite (Ce)	$Na_3(Ce,La,Nd)(PO_4)_2$	3.60-3.70	n/a	-	-	-
Xenotime (Y)	**YPO_4**	**4.40-5.10**	**Paramagnetic**	**52-67**	**-**	**0-5**

Table 3.7 - Silicate REM. Adapted from (Anthony *et al.*, 2001; Long *et al.*, 2010; Rosenblum & Brownfield, 1999)

Mineral Name	Chemical Formula	Density (g/cm^3)	Magnetic Properties	Weight Percent		
Silicates			Para/Diamagnetic?	REO	ThO_2	UO_2
Allanite (Ce)	$(Ce,Ca,Y)_2(Al,Fe^{2+},Fe^{3+})_3(SiO_4)_3(OH)$	3.50-4.20	Paramagnetic	3-51	0-3	-
Allanite (Y)	$(Y,Ce,Ca)_2(Al,Fe^{3+})_3(SiO_4)_3(OH)$	n/a	Paramagnetic	3-51	0-3	-
Cerite (Ce)	$Ce_9Fe^{3+}(SiO_2)_6[(SiO_3)(OH)](OH)_3$	4.75	Paramagnetic	-	-	-
Cheralite (Ce)	$(Ca,Ce,Th)(P,Si)O_4$	5.28	n/a	-	<30	-
Eudialyte	$Na_4(Ca,Ce)_2(Fe^{2+},Mn^{2+},Y)ZrSi_8O_{22}(OH,Cl)_2$	2.74-3.10	n/a	1-10	-	-
Gadolinite (Ce)	$(Ce,La,Nd,Y)_2Fe^{2+}Be_2Si_2O_{10}$	4.2	Paramagnetic	-	-	-
Gadolinite (Y)	$Y_2Fe^{2+}Be_2Si_2O_{10}$	4.36-4.77	Paramagnetic	-	-	-
Gerenite (Y)	$(Ca,Na)_2(Y,REE)_3Si_6O_{18}\cdot 2H_2O$	n/a	n/a	-	-	-
Hingganite (Ce)	$(Ce,Y)_2Be_2Si_2O_8(OH)_2$	4.82 (calc)	n/a	-	-	-
Hingganite (Y)	$(Y,Yb,Er)_2Be_2Si_2O_8(OH)_2$	4.42-4.57	n/a	-	-	-
Hingganite (Yb)	$(Yb,Y)_2Be_2Si_2O_8(OH)_2$	4.83 (calc)	n/a	-	-	-
Iimoriite (Y)	$Y_2(SiO_4)(CO_3)$	4.47	n/a	-	-	-
Kainosite (Y)	$Ca_2(Y,Ce)_2Si_4O_{12}(CO_3)\cdot H_2O$	3.52	n/a	-	-	-
Rinkite (rinkolite)	$(Ca,Ce)_4Na(Na,Ca)_2Ti(Si_2O_7)_2F_2(O,F)_2$	3.18-3.44	n/a	-	-	-
Sphene (titanite)	$(Ca,REE)TiSiO_5$	3.48-3.60	Paramagnetic	<3	-	-
Steenstrupine (Ce)	$Na_{14}Ce_6Mn_2Fe_2(Zr,Th)(Si_6O_{18})_2(PO_4)_7\cdot 3H_2O$	3.38-3.47	n/a	-	-	-
Thalenite (Y)	$Y_3Si_3O_{10}(F,OH)$	4.16-4.41	n/a	-	-	-
Thorite	$(Th,U)SiO_4$	6.63-7.20	Paramagnetic	<3	-	10-16
Zircon	$(Zr,REE)SiO_4$	4.60-470	Diamagnetic	-	0.1-0.8	-

Table 3.8 - REE Distribution of major REM deposits. Adapted from (Chen, 2011; Long *et al.*, 2010)

Element	Bastnäsite	Bastnäsite	Monazite	Xenotime	High Y REE Clay	Low Y REE Clay
	Mountain Pass	Bayan Obo	Green Cove	Lehat	Longnan	Xunwu
	USA	China	Spring	Malaysia	China	China
La (%)	**33.8**	**23.0**	**17.5**	1.2	1.8	**43.3**
Ce (%)	**49.6**	**50.0**	**43.7**	**3.1**	0.4	2.4
Pr (%)	**4.1**	**6.2**	**5.0**	0.5	0.7	**7.1**
Nd (%)	**11.2**	**18.5**	**17.5**	1.6	**3.0**	**30.2**
Sm (%)	0.9	0.8	**4.9**	1.1	**2.8**	**3.9**
Eu (%)	0.1	0.2	0.2	Trace	0.1	**0.5**
Gd (%)	0.2	0.7	**6.0**	**3.5**	**6.9**	**4.2**
Tb (%)	-	0.1	0.3	0.9	**1.3**	Trace
Dy (%)	-	0.1	0.9	**8.3**	**7.5**	Trace
Ho (%)	-	Trace	0.1	**2.0**	**1.6**	Trace
Er (%)	-	Trace	Trace	**6.4**	**4.9**	Trace
Tm (%)	-	Trace	Trace	**1.1**	**0.7**	Trace
Yb (%)	-	Trace	0.1	**6.8**	**2.5**	0.3
Lu (%)	Trace	Trace	Trace	**1.0**	0.4	0.1
Y (%)	0.1	Trace	2.5	**61.0**	**65.0**	8.0

Bolded values indicate that a certain mineral deposit is a major source of the given element.

3.2.1 Bastnäsite

Bastnäsite is a fluorocarbonate mineral with a REO content of approximately 70% that is primarily Ce, La, Pr and Nd (~97.95% of total REO) (Bulatovic, 2010; Gupta & Krishnamurthy, 1992; Gupta & Krishnamurthy, 2005; Ozbayoglu & Atalay, 2000; Pradip & Fuerstenau, 2013). Bastnäsite would be considered a selective, cerium type mineral although these classifications are not absolute due to the interchangeable nature of the lanthanide elements (Cesbron, 1986; Ferron *et al.*, 1991; Trifonov, 1963). Within the last fifty years bastnäsite has replaced monazite as the chief mineral source of REE (Ozbayoglu & Atalay, 2000). This is primarily due to the discovery and development of the world's largest REE mine, the Bayan Obo mine in China, and the Mountain Pass mine in the United States (Gupta & Krishnamurthy, 2005). It is interesting to note that Bayan Obo, which accounted for 45% of the world's REE production in 2005, was initially developed as an iron ore mine in 1927 (it is also China's largest iron ore mine with almost 1.5 billion tonnes of reserves) and did not begin REE production until decades later (Gupta & Krishnamurthy, 2005; Wu, 2008). This major source of REE is in fact the tailings of the iron ore processing scheme at this mine (Zhang & Edwards, 2012). The separation process for bastnäsite ores may employ numerous operations including gravity and magnetic concentration, however the two deposits mentioned here rely primarily on flotation using a fatty-acid or hydroxamate-based collector system (Chi *et al.*, 2001; Fuerstenau *et al.*, 1982; Luo & Chen, 1984).

3.2.2 Monazite

Monazite is a phosphate mineral with a REE content of approximately 70% REO that is, similar to bastnäsite, primarily Ce, La, Pr and Nd (varies by deposit between 83.55% and 94.5% of total REO) and would consequently be considered a selective, cerium type mineral (Cesbron, 1986; Ferron *et al.*, 1991; Gupta & Krishnamurthy, 1992; Gupta & Krishnamurthy, 2005; Trifonov, 1963). Unlike bastnäsite, monazite also includes 4-12 wt. % thorium and a variable amount of uranium (values are typically small but have been reported to be as high as 14 wt. %) (Gramaccioli & Segalstad, 1978; Gupta & Krishnamurthy, 2005). Monazite is found throughout the world in placer deposits, beach sands and is also a component of the Bayan Obo deposit (Gupta & Krishnamurthy, 2005).

The most important deposits for monazite extraction are the beach sands, which are typically concentrated by initial high-capacity gravity separation steps, to take advantage of the high specific gravity (monazite has a specific gravity greater than 5, while the typical gangue minerals in these deposits have specific gravities less than 3.5), followed by additional gravity, magnetic, electrostatic and occasionally flotation separation steps (Bulatovic & Willett, 1991; Ferron *et al.*, 1991; Houot *et al.*, 1991; Neiheisel, 1962; Zhang & Edwards, 2012).

3.2.3 Xenotime

Xenotime is a yttrium phosphate mineral with a REO content of approximately 67% with Ce, La, Pr, Nd contents that are much less than monazite or bastnäsite (~8.4%) (Gupta & Krishnamurthy, 1992; Gupta & Krishnamurthy, 2005). Xenotime is typically found alongside monazite in concentrations of 0.5-5.0% of that of monazite (Cesbron, 1986; Ferron *et al.*, 1991; Gupta & Krishnamurthy, 2005; Trifonov, 1963). Xenotime is important, in spite of its rarity, as it is a major source of HREE along with the Chinese ion-adsorbed REE-bearing clays (Cheng *et al.*, 1994; Chi *et al.*, 2001). Xenotime is typically a by-product of monazite processing and as such, its processing follows a similar path to that of monazite (Cheng *et al.*, 1994; Ferron *et al.*, 1991). A limited amount of research into xenotime beneficiation has focused on its separation from monazite using flotation and magnetic separation (Cheng, 2000; Cheng *et al.*, 1993; Cheng *et al.*, 1994; Ito *et al.*, 1991).

3.2.4 Ion-Adsorbed Clays

Ion-adsorbed clays are a very important source of heavy REE (up to 60% of REO content in these clays comes from yttrium group elements) with these elements occurring as REE ions (Zhang & Edwards, 2012). Due to their nature, these clays require little to no physical beneficiation, being processed directly using hydrometallurgical methods. These will not be discussed in this thesis, but further information can be found in Chi *et al.* (2001).

3.2.5 Other REM

As can be seen in Table 3.3 to Table 3.7, there are numerous minerals that contain REE, many of which have been exploited to varying degrees of success. However, these are

typically small-scale, unique operations for which it is difficult to obtain data, and even more difficult to determine general separation characteristics. A limited discussion of such minerals is included in Sections 3.3.1, 3.3.2 and 3.3.4.4.

3.3 Beneficiation Unit Operations

The principle separation processes employed in the beneficiation of REM include gravity separation, magnetic separation, electrostatic separation and froth flotation. These processes are here examined as they have been applied to REM.

3.3.1 Gravity Separation

REM are good candidates for gravity separation as they have relatively large specific gravities (4-7) and are typically associated with gangue material (primarily silicates) that is significantly less dense (Ferron *et al.*, 1991). The most commonly utilized application of gravity separation is in monazite beneficiation from heavy mineral sands. Beach sand material is typically initially concentrated using a cone concentrator to produce a heavy mineral pre-concentrate (20-30% heavy minerals) before a more selective gravity separation step, often employing a spiral concentrator, is used to achieve concentrations of 80-90% heavy minerals (Gupta & Krishnamurthy, 1992). At this point, a series of magnetic, electrostatic and further gravity separation operations must be applied, according to each individual deposit's mineralogy (Ferron *et al.*, 1991).

An example of a flowsheet designed to concentrate monazite from Egyptian beach sands containing approximately 30 wt. % valuable heavy minerals can be seen in Figure 3.1 (Moustafa & Abdelfattah, 2010). In this flowsheet, low specific gravity gangue is discarded by wet gravity concentration (the authors employed a Wifley shaking table for this purpose), then low intensity magnetic separation is used to discard any ferromagnetic minerals without removing paramagnetic monazite (Moustafa & Abdelfattah, 2010). The non-magnetic stream that remains contains most of the valuable monazite, zircon and rutile as well as a portion of the gangue minerals which were not removed in the first two steps. A series of gravity, magnetic and electrostatic separations are then applied to exploit the different properties of the monazite, zircon and rutile minerals and produce the final concentrate streams. Rutile is removed as it reports to the conductor fraction after

electrostatic separation (monazite and zircon are non-conductive) and then diamagnetic zircon may be removed from the paramagnetic monazite using further magnetic separation (Moustafa & Abdelfattah, 2010).

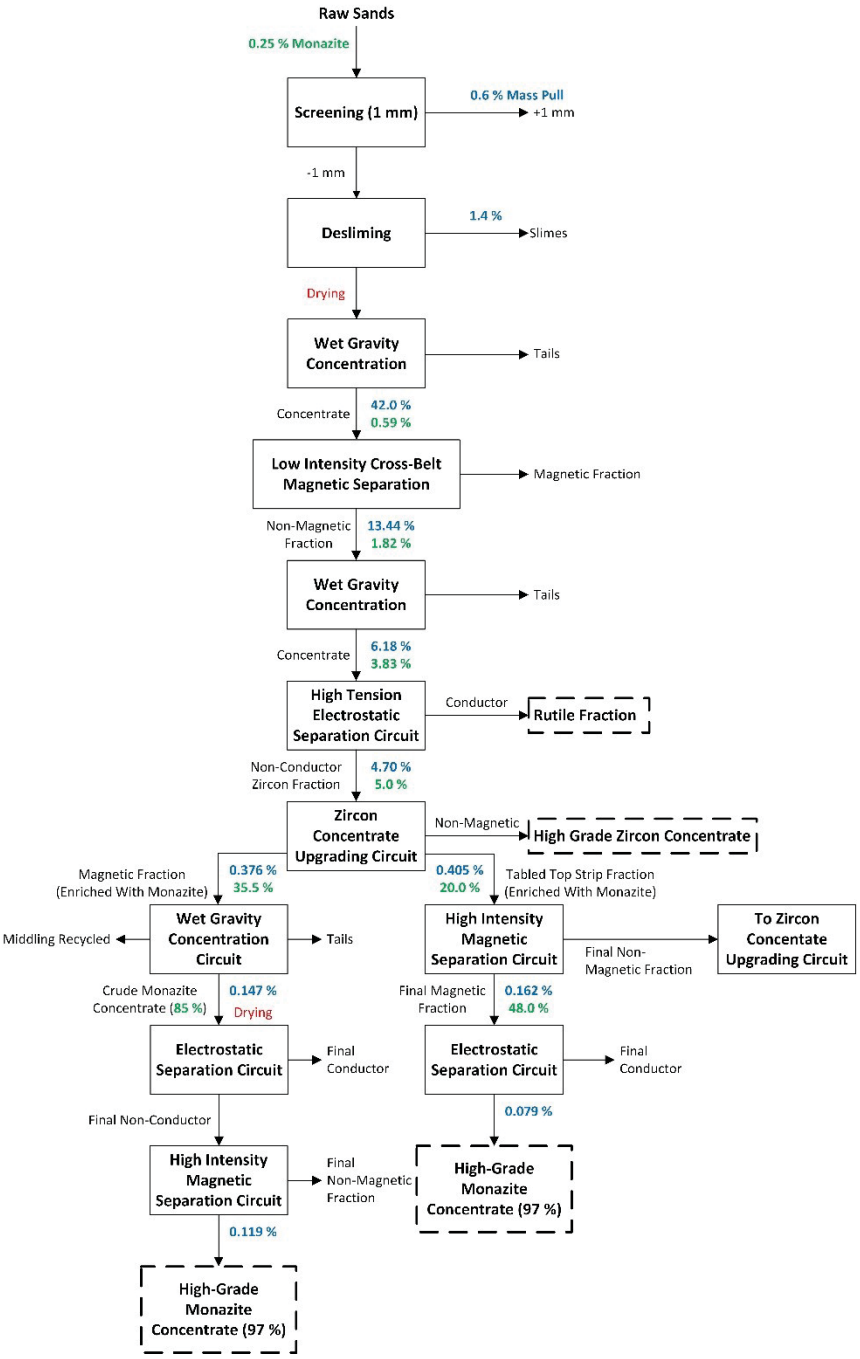

Figure 3.1 - Flowsheet for concentrating monazite from Egyptian beach sand. For each stream, the first and second percentages represent total weight recovery and monazite grade respectively. Adapted from (Moustafa & Abdelfattah, 2010)

In addition to the processing of beach sands, gravity separation (shaking tables, spiral concentrators, and conical separators) is used in combination with froth flotation at many REM processing operations throughout China (Chi *et al.*, 2001). An example of this is at Bayan Obo, where gravity separation has been employed between the rougher and cleaner flotation circuits to efficiently separate monazite and bastnäsite from the iron-bearing and silicate gangue material (Chi *et al.*, 2001; Luo & Chen, 1984). Some challenges associated with gravity separation of the Bayan Obo ore are that gangue minerals (*e.g.* barite) have similar specific gravities to the desired REM and report to the concentrate stream. In addition, gravity separation is ineffective at separating very fine particles resulting in large losses of REE (Ming, 1993). Some separation of very fine particles can be achieved for minerals with very large differences in specific gravity, such as gold from silicate gangue, by employing centrifugal gravity separators such as the Knelson, Falcon and Mozley Multi-Gravity Separators (Falconer, 2003; Gee *et al.*, 2005). Most of these fine particle separators are designed for semi-continuous operation where the valuable dense material is present in low concentrations (< 0.1 wt. %) which may limit their suitability to REM separation (Fullam & Grewal, 2001). The ongoing development of centrifugal separators capable of continuous operation (*e.g.* the Knelson CVD) may address this issue as the manufacturers claim to be able to process feed materials with valuable heavy mineral contents of up to 50 wt. % (Fullam & Grewal, 2001).

Outside of China, lab-scale gravity separations have been successfully completed on Turkish and Australian deposits with very fine-grained mineralisations (Guy *et al.*, 2000; Ozbayoglu & Atalay, 2000). In both of these cases, one of the key findings was that the REM were concentrated into the very fine (< 5 μm) particle size range (Guy *et al.*, 2000; Ozbayoglu & Atalay, 2000). This was dealt with by either modifying the grinding steps to prevent excess fine generation or by employing a Multi-Gravity Separator, specifically designed to recover ultrafine particles via gravity separation (Guy *et al.*, 2000; Ozbayoglu & Atalay, 2000). The modified grinding procedure employed an attrition scrubbing step prior to further grinding to produce a product that was 100% -300 μm (the size which was identified as the maximum limit for downstream flotation), while reducing the slime losses to the -5 μm size fraction by an average of 7.8% (Guy *et al.*, 2000). The results from Guy

et al. (2000) can be seen in Figure 3.2. The importance of adequately liberating REM without excessive fine production has also been shown by Fangji & Xinglan (2003), who employed screening and secondary grinding steps after gravity and magnetic separations at a mine in Maoniuping, China to produce a bastnäsite flotation concentrate with a grade of 62% REO and a recovery of 80-85%. Recently, Dehaine & Filippov (2014) demonstrated the ability of a Falcon Concentrator to concentrate light REM from a waste stream produced during kaolin production.

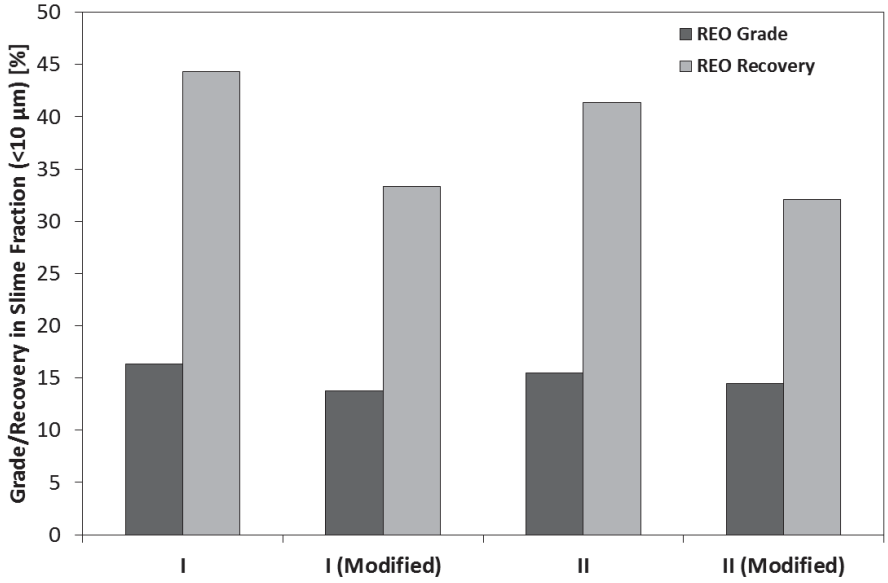

Figure 3.2 - Changes in REO slime losses with modified grinding procedure. Adapted from (Guy *et al.*, 2000)

A final interesting application of gravity separation to REM concentration is the use of roasting operations prior to gravity separation as outlined in a 1956 patent (Kasey, 1956). The idea presented involved roasting a rare earth carbonate ore at temperatures in excess of 1000 °C to convert the carbonates into oxides, thereby increasing the mineral density and susceptibility to gravity separation (Kasey, 1956). The process included an industrial application involving quenching the roasted ore particles from high temperatures; a process that would likely significantly decrease the energy required for crushing and grinding operations as detailed by Fitzgibbon (1990) in their research into

thermally assisted liberation. To the best of the author's knowledge, this process was never successfully applied on an industrial or pilot scale.

3.3.2 Magnetic Separation

Magnetic separation techniques are a common separation step in REM beneficiation to eliminate highly magnetic gangue, or to concentrate the desired paramagnetic REM such as monazite or xenotime (Gupta & Krishnamurthy, 1992). As explained previously, REE generally have a series of electrons occupying a shielded 4*f* sub-shell and these electrons will typically have magnetic moments which do not cancel out, resulting in a material with some degree of magnetism (Spedding, 1975). The magnetic susceptibilities of individual REE have been calculated by Ito *et al.* (1991) and used to predict REM magnetic susceptibilities based on their chemical compositions. This work focused on the magnetic susceptibilities of the most common M^{3+} lanthanide ions and did not investigate any changes in magnetic behaviour for different oxidation states of these elements. The results of these calculations indicated that the elements from gadolinium to erbium had the highest magnetic susceptibilities of all the lanthanides, and the higher concentrations of Gd, Dy and Er ions present in xenotime explained its threefold increase in magnetic susceptibility when compared with monazite (Ito *et al.*, 1991). These results are consistent with other references which confirm that the most strongly paramagnetic REE ions are Gd, Tb, Dy, Ho and Er (Spedding & Daane, 1961; Topp, 1965).

Along with gravity separation, magnetic separators are instrumental to monazite beneficiation from beach sands. They are used to eliminate strongly magnetic minerals such as magnetite prior to more selective separation steps, and are also used to separate paramagnetic monazite from diamagnetic heavy mineral gangue material such as zircon and rutile (Ferron *et al.*, 1991; Tran, 1991; Zhang & Edwards, 2012). Xenotime, a paramagnetic mineral which is more susceptible to magnetic separation than monazite, may be isolated using these techniques, however for fine grain sizes (> 100 μm), flotation is the preferred means of separation (Rosenblum & Brownfield, 1999; Zhang & Edwards, 2012).

Magnetic separators are used in the beneficiation of Chinese bastnäsite REE ores to eliminate Fe-bearing gangue minerals prior to REE-specific separation steps, and as a cleaning step for flotation feeds and concentrates (Chi *et al.*, 2001; Zhang & Edwards, 2012). In the case of China's second biggest REE deposit, the Sichuan Maoniuping REE deposit, magnetic separation has been combined successfully with gravity separation to achieve a bastnäsite recovery greater than 55% without the need for flotation (Chi *et al.*, 2001).

Test work has been conducted on an Australian REE deposit to examine the possibility of magnetically separating ground ore after being subjected to a roasting operation (Chan, 1992). Roasting temperatures from 400 °C up to 1000 °C were tested, however no benefit to the response to magnetic separation of the ore was observed (Chan, 1992). In another series of experiments, similar to those described in the gravity separation section of this Chapter (Section 3.3.1), the effect of feed size on the magnetic separation of a REM ore was investigated (Gao & Chen, 2010). The results of this work showed that when the feed (with a Sc grade of 48.9 g/t) had a particle size of 80% -74 µm the recovery and grade of the scandium and REE concentrate were optimized, yielding a Sc grade of 314.89 g/t with a recovery of 77.53 % (Gao & Chen, 2010).

Loparite is an oxide REM similar to perovskite, found extensively in Russia's Kola Peninsula where almost 6500 tons of REO are extracted annually (Hedrick *et al.*, 1997). This mineral occurs alongside gangue such as aegirine, feldspar, nepheline and ramsayite and is concentrated via a combination of gravity and magnetic separation techniques (Hedrick *et al.*, 1997). Several other REM (including eudialyte, apatite and synchysite (Y)) are extracted in this region; the REE composition of these minerals can be seen in Table 3.9 (Hedrick *et al.*, 1997).

Table 3.9 - REE Distribution in REM from Eastern Europe. Adapted from (Hedrick *et al.*, 1997)

Element	Loparite Revda Russia	Eudialyte Revda Russia	Apatite Khibiny Russia	Synchysite (Y) Kutessaisk Kazakstan
La (%)	**25.0**	**15.2**	**24.0**	**14.0**
Ce (%)	**50.5**	**29.7**	**52.0**	**26.0**
Pr (%)	**5.0**	**2.9**	**5.5**	**2.7**
Nd (%)	**15.0**	**12.7**	**14.0**	**9.8**
Sm (%)	0.7	**3.4**	**2.5**	**3.5**
Eu (%)	0.1	**1.3**	0.5	0.1
(Gd (%)	0.6	**3.0**	**1.4**	**3.5**
Tb (%)	-	**2.8**	0.2	**0.7**
Dy (%)	0.6	**4.3**	0.3	**4.3**
Ho (%)	0.7	**2.9**	0.1	**0.8**
Er (%)	0.8	**2.1**	0.2	**3.8**
Tm (%)	0.1	-	0.1	0.3
Yb (%)	0.2	**1.6**	0.1	**1.2**
Lu (%)	0.2	0.3	0.1	0.3
Y (%)	1.3	**21.4**	1.5	**29.0**

Bolded values indicate that a certain mineral deposit contains a significant concentration of the given element

An interesting study was recently undertaken by Raslan (2009) in which a heavy mineral occurrence with a significant (approximately 1.5 wt. %) occurrence of samarskite (Y) was subjected to lab-scale separations. This work used sieving, desliming, gravity separation (using a shaking table) and magnetic separation to produce a samarskite (Y) concentrate according to the following procedure (Raslan, 2009):

- A feed consisting of samarskite (Y), columbite, zircon, magnetite, garnet, goethite, ilmenite, hematite and mica was deslimed and then sieved to 100% passing 1 mm
- The sieved material was sized and the resultant size fractions were individually fed to a gravity shaking table
- The heavy fractions were then subjected to two magnetic separation steps; the first to remove magnetite and the second high intensity step to produce a non-magnetic concentrate containing predominantly samarskite (Y) and zircon

On a lab-scale, these researchers were able to produce a non-magnetic samarskite (Y) concentrate comprised of 73.8 wt. % samarskite (Raslan, 2009).

3.3.3 Electrostatic Separation

Electrostatic separation is a dry beneficiation technique that exploits the differences in conductivity between different minerals to achieve separation (Higashiyama & Asano, 2007; Kelly & Spottiswood, 1989c, a, b). Electrostatic separation techniques are typically only used when alternative processing techniques will not suffice, as the comminution steps in mineral processing flowsheets are generally wet processes and the energy requirements to drive off all moisture prior to electrostatic separation can be significant (Kelly & Spottiswood, 1989c). In the context of REM processing, the typical use of electrostatic separation is in the separation of monazite and xenotime from gangue minerals with similar specific gravity and magnetic properties (Ferron *et al.*, 1991; Zhang & Edwards, 2012). A specific example of this is when xenotime, which is more strongly paramagnetic than monazite, is concentrated with ilmenite after magnetic separation of heavy mineral sands (Gupta & Krishnamurthy, 1992). In this case the only means by which xenotime may be removed from the ilmenite is by electrostatic separation, as ilmenite is conductive but xenotime is not (Gupta & Krishnamurthy, 1992).

Electrostatic separation is a valuable technique for heavy mineral sand beneficiation, and the successful application of this process to separate ultrafine (< 37 μm) coal particles may present an opportunity to treat the fines produced in many currently operating mineral processing circuits that account for significant REE losses (Higashiyama & Asano, 2007). Unfortunately, all electrostatic separation techniques (high tension roll, electrostatic plate-type, triboelectric *etc.*) have the operating limitation that the feed material must be completely dry (Higashiyama & Asano, 2007). Aside from the heavy mineral sand deposits, almost all other discovered REE deposits (aside from the ion-adsorbed clays in southern China) require some form of comminution prior to separation and these grinding operations are heavily reliant on a slurried feed. The energy costs associated with completely drying a ground ore prior to an electrostatic separation step

are likely to be far too cost-prohibitive for such a process to be applied on an industrial scale.

3.3.4 Froth Flotation

Froth flotation is commonly applied to the beneficiation of rare earth ores due to the fact that it is possible to process a wide range of fine particle sizes, and the process can be tailored to the unique mineralogy of a given deposit. An illustration of this is the Bayan Obo REM deposit, with its complex inter-related mineralogy and a mineral grain sizes varying from 10-74 μm, which would render it impossible to process were it not for flotation (Zhang & Edwards, 2012).

The area of froth flotation of REM has seen a relatively large amount of research compared to other beneficiation techniques, typically using hydroxamate-based collector systems. The research has primarily focused on bastnäsite and monazite, in terms of their surface properties as they relate to flotation response, as well as industrial scale flotation experiments in plants such as Mountain Pass and Bayan Obo.

3.3.4.1 Surface chemistry

In the study of surface characteristics, the electrical double layer governs the adsorption of various flotation reagents, which in turn directly affect the flotation response of a given mineral (Chapter 2, Section 2.4.2). The IEP values for bastnäsite and monazite reported in literature vary greatly, with ranges from pH 1.1-9.0 for monazite and pH 4.6-9.5 for bastnäsite (Cheng, 2000; Houot *et al.*, 1991). Bastnäsite samples from Mountain Pass, USA have reported IEP values of 4.6 to 9.3, synthetic bastnäsite has an IEP of 9.5, bastnäsite from various Chinese sources has been reported as having an IEP from 7.0 to 8.0 and a bastnäsite sample from Pocos de Caldas (Brazil) has a reported IEP of 4.9 (Houot *et al.*, 1991; Luo & Chen, 1984; Pavez *et al.*, 1996; Pradip, 1981; Ren *et al.*, 1997; Ren *et al.*, 2000; Smith & Shonnard, 1986; Zhang *et al.*, 2013). Recent examinations of bastnäsite samples from Zagi Mountain (Pakistan) and Mountain Pass (USA) have determined the IEP of bastnäsite to be pH 8.1 and 9.3 respectively (Herrera-Urbina *et al.*, 2013; Zhang *et al.*, 2013).

The variation in reported IEPs for bastnäsite is shown graphically in Figure 3.3 along with the origin of the different bastnäsite samples. This figure illustrates that for even the most well reported source of bastnäsite (Mountain Pass, USA) there is a significant variation in reported isoelectric points. Measurements for other minerals are usually quite repeatable (In_2O_3 and CuO have reported IEP values of 7.0-7.7 and 8.5-9.7 respectively) (Kosmulski, 2001). The large discrepancies in the IEP for bastnäsite are likely due to variations in potential determining ions (those ions that can interact with both the mineral surface and the aqueous phase in forming the electrical double layer), mineral composition and the structure of the mineral surfaces as well as differences in the technique used to determine the IEP (Cheng, 2000). Errors associated with sample storage and the presence of impurities in pure mineral samples, or the indifferent electrolytes, used in the measurement of the IEP could account for the observed discrepancy; yet, a review of many of the published procedures used during these investigations suggests that the observed variations in IEP are likely due to sample variability and not experimental error (Abeidu, 1972; Cheng, 2000; Cheng *et al.*, 1994; Luo & Chen, 1984; Pavez *et al.*, 1996; Pradip, 1981)

Herrera-Urbina *et al.* (2013) have computed the solution equilibria of the bastnäsite-H_2O system as shown in Table 3.10. It can be seen from the variety of species present in this system that the factors affecting the zeta potential and surface charge of bastnäsite are much more complex than those of a more traditional insoluble oxide mineral where H^+ and OH^- are typically the major potential determining ions (Herrera-Urbina *et al.*, 2013).

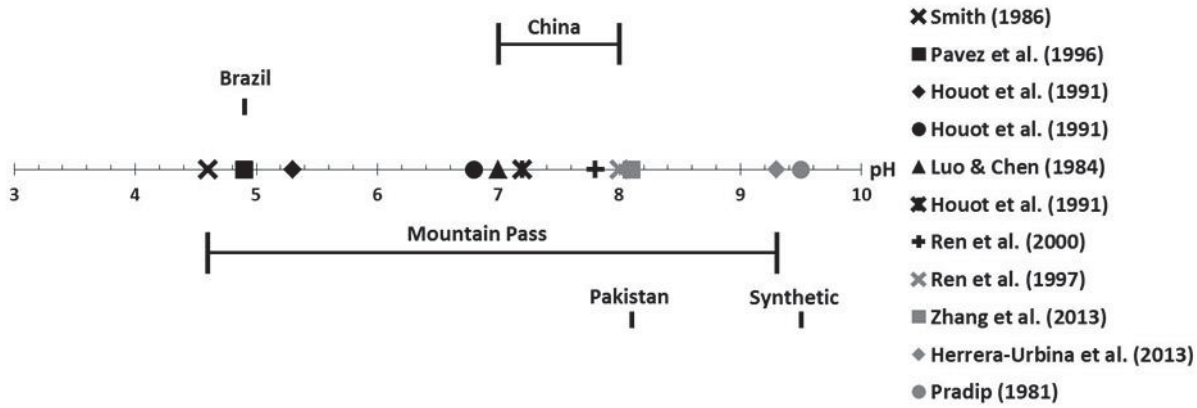

Figure 3.3 - Reported isoelectric points of bastnäsite with author and sample origin

Table 3.10 - Speciation of bastnäsite in aqueous solution (0.05 wt. %) adapted from (Herrera-Urbina *et al.*, 2013)

pH range	Solid phases present
<5.2	CeF
5.22-5.74	$CeFCO_3$, CeF_3
5.74-8.55	$CeFCO_3$
8.56-10.12	$CeFCO_3$, $Ce(OH)_3$
>10.2	$Ce(OH)_3$

3.3.4.2 Bastnäsite Flotation

The primary mineral on which REM flotation knowledge is based is the semi-soluble mineral bastnäsite which may be floated using fatty acids or hydroxamate collectors at pH 9 (Pradip, 1981). Flotation is used to beneficiate bastnäsite in many locations, including Mountain Pass and Bayan Obo (Zhang & Edwards, 2012). Common collectors used for bastnäsite flotation include variations of hydroxamates, fatty acids, dicarboxylic acids and organic phosphoric acids (Ferron *et al.*, 1991; Jun *et al.*, 2003). Typical depressants used in these situations include sodium silicate, sodium hexafluorosilicate, lignin sulfonate and sodium carbonate (Houot *et al.*, 1991).

Bastnäsite often has similar physical and chemical properties to the gangue minerals present and therefore requires highly selective and effective flotation reagents (Bulatovic, 2010; Jun *et al.*, 2003). Since the 1960's, the effectiveness of collectors containing hydroxamate, phosphoric acid ester and carboxylic acid functional groups have been studied in REM flotation (Bulatovic, 2010; Jun *et al.*, 2003; Zhang & Edwards, 2012). These specific classes of collectors are all considered oxhydryl collectors as their functional groups consist of an oxygen anion and a double-bonded oxygen to which a metal cation will bind (Bulatovic, 2007). The key differences between carboxylic acids, hydroxamates and phosphoric acid esters is the atom to which the oxygen atoms are attached (carbon, nitrogen and phosphorous respectively) (Bulatovic, 2007).

3.3.4.2.1 Carboxylic Acids

Carboxylic (or fatty) acids are the least selective of all collectors used in REM flotation however they are widely used in non-sulphide mineral flotation thanks to their low cost and ease of availability (Bulatovic, 2007). Another reason for their frequent use in flotation is that sodium oleate is one of the most extensively researched flotation collectors (Bulatovic, 2007). Fatty acids are commonly used in the flotation of bastnäsite, however they require the addition of high concentrations of depressants and elevated temperatures (as shown in Figure 3.4), in order to achieve acceptable selectivity (Bulatovic, 2010; Jianzhong *et al.*, 2007; Pradip, 1981). A common depressant for REM flotation is sodium silicate which has been reported as having a weak affinity for REM at low dosage but a much higher affinity for silicate gangue minerals (Houot *et al.*, 1991). The adsorption mechanism of anionic fatty acids onto bastnäsite mineral surfaces is believed to be chemical in nature as the oleate anion has been shown to adsorb onto the mineral surface at pH values where the zeta potential of the mineral is negative (Pavez *et al.*, 1996; Pavez & Peres, 1993).

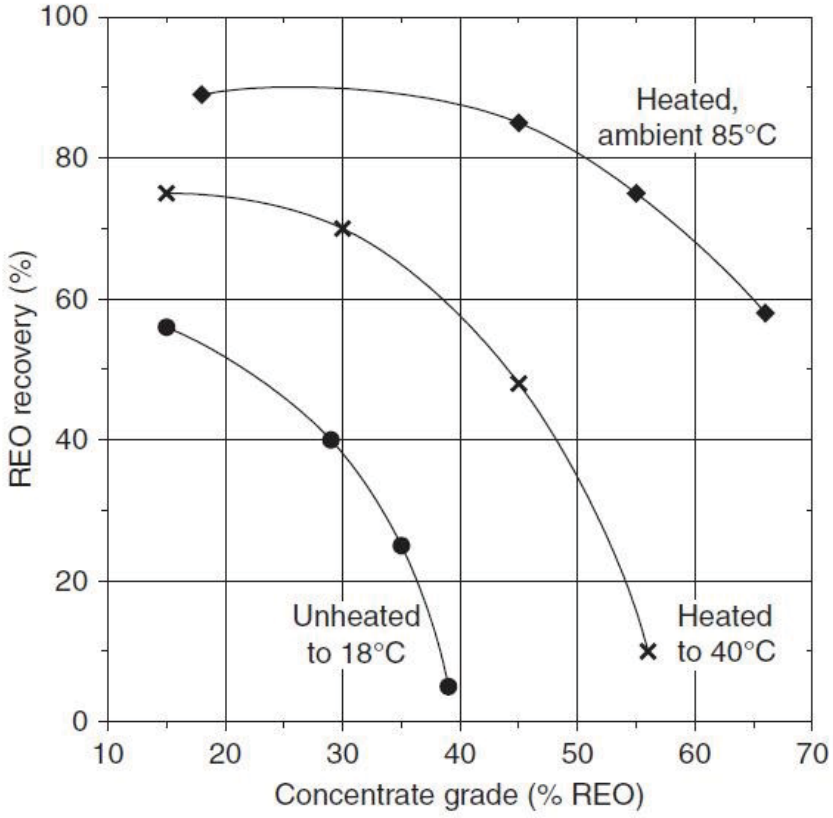

Figure 3.4 - Effect of temperature on bastnäsite flotation using a fatty acid collector. After (Bulatovic, 2010)

To improve upon the performance of fatty acid flotation, researchers have utilized phosphoric acids (Houot *et al.*, 1991; Jun *et al.*, 2003), hydroxamic acids (Fangji *et al.*, 1989; Fuerstenau & Pradip, 1991; Houot *et al.*, 1991; Jianzhong *et al.*, 2007; Jun *et al.*, 2003), petroleum sulfonate (Morrice & Wong, 1983) and a patented collector emulsion consisting of: secondary amine-modified sulphonated fatty acid, high rosin containing tall oil fatty acid, anionic petroleum sulfonate and high molecular weight primary amine (Bulatovic, 1988). These alternative flotation schemes focus on minimizing reagent usage and eliminating costly processing steps including the heating of flotation pulps (such as Mountain Pass) prior to flotation (Bulatovic, 1988; Fuerstenau & Pradip, 1991). Hydroxamic acid collectors have been shown to be preferable to phosphorous-based collectors (phosphoric/phosphonic acids) for carbonate flotation, as maintaining the pH at

the acidic levels required for the successful application of phosphorous-based collectors can prove difficult for this type of mineral (Ni *et al.*, 2012).

3.3.4.2.2 Hydroxamic Acids

The theory of hydroxamate collection and specificity for REM is often explained by means of the large stability constants of metal cation-hydroxamate complex formation (Fuerstenau, 2005). While the formation of highly stable REE-hydroxamate complexes has been well documented (Agrawal & Kapoor, 1977; Fuerstenau, 2005) the collection mechanism in flotation has also been linked to mineral solubility (Assis *et al.*, 1996). Successful flotation using hydroxamates is also believed to require the presence of both dissociated and undissociated forms of the molecule, such that most successful hydroxamate flotation schemes adjust the pH to a value near the pK_a of the reagent (Fuerstenau, 2005).

Hydroxamates are much more selective than fatty acids based on differences in the stability of the complexes that the two collector groups will form with metal cations (Nagaraj, 1988). The lower stability of hydroxamate-metal complexes and corresponding increased selectivity is partially due to the substitution of a nitrogen atom for the carbon atom to which one of the oxygen atoms of the collector functional group are bound (Nagaraj, 1988). As nitrogen is more electronegative than carbon it will have a greater influence on the electron density of the oxygen atom so that the singly bonded oxygen atom in hydroxamates is a weaker electron donor and less available to interact with metal cations (Nagaraj, 1988). The stabilities of hydroxamates with various metal cations are represented visually by the stability constants for acetohydroxamate in Figure 3.5. This information indicates that the preferred cations for hydroxamate complex formation include highly charged cations such as Fe^{3+}, Al^{3+}, Cu^{2+} and Pb^{2+} (Fuerstenau, 2005; Nagaraj, 1988). RE metal cations are the next most stable class of hydroxamate-metal complexes which helps these collectors attach to and float REM without significant attachment to many gangue minerals (Nagaraj, 1988).

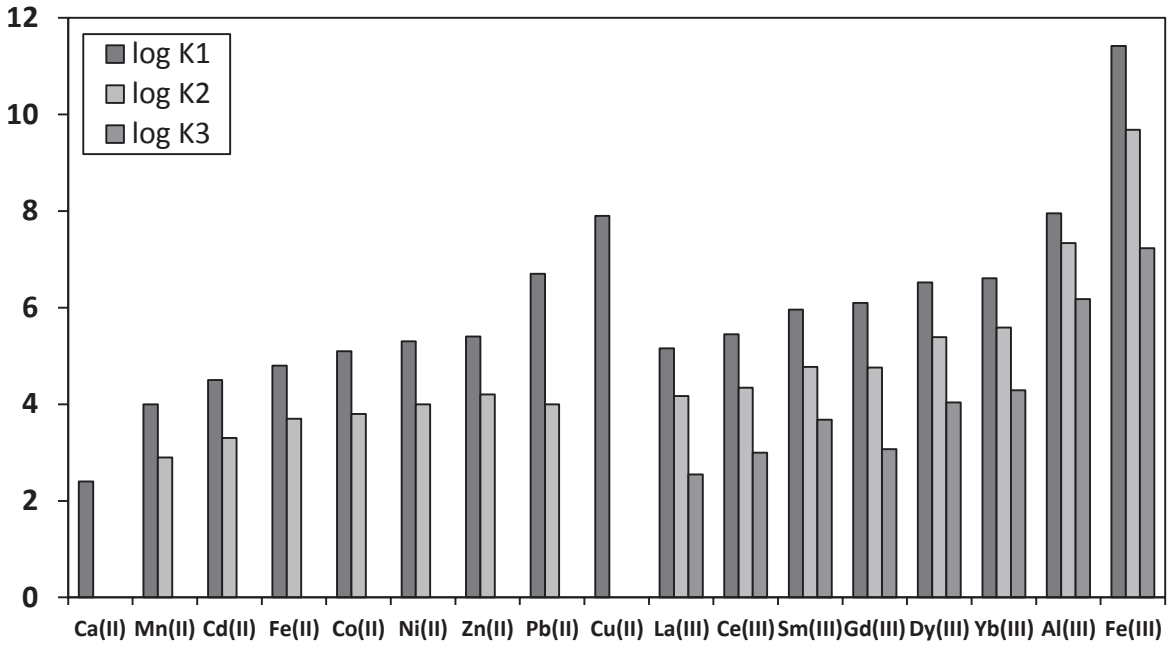

Figure 3.5 - Stability constants of metal acetohydroxamates at 20 °C in $NaNO_3$, adapted from (Fuerstenau, 2005)

Bastnäsite presents an ideal candidate for hydroxamate flotation as it has a high RE content as well as a relatively high degree of solubility. This mineral solubilizes in aqueous suspension with many resultant species (depending on pH), including the positively charged Ce^{3+}, $Ce(OH)^{2+}$, $Ce(OH)_2^{+}$, CeF^{2+}, CeF_2^{+}, $CeCO_3^{+}$, $CeHCO_3^{+}$; as well as the anionic F^-, HCO_3^-, CO_3^{2-} and $Ce(CO_3)_2^-$ (see also Table 3.10). While the required ions for hydroxamate adsorption have not been definitively identified for the bastnäsite system, Assis *et al.* (1996) showed a distinct correlation between mineral solubility and flotation recovery using hydroxamates.

The currently accepted mechanism of hydroxamate surface adsorption involves hydrolysis of a dissolved metal cation, the formation of a hydroxyl complex in solution and then adsorption of this complex at the mineral surface (Assis *et al.*, 1996; Fuerstenau, 2005). As this adsorption process relies on the dissolution of some cations from the mineral surface, Assis *et al.* (1996) suggested that the adsorption kinetics may simply be a function of mineral solubility such that the most soluble mineral will have the fastest kinetics of collector adsorption. Results from cassiterite flotation experiments using alkyl

hydroxamate collectors support this hypothesis as Sreenivas & Padmanabhan (2002) showed that increasing conditioning time prior to microflotation dramatically increased the recovery of this insoluble mineral. Fuerstenau (2005) also noted that at a pH of approximately 9, a portion of the hydroxamic acid molecules ionize so that the hydroxamate ion is present alongside the hydroxamic acid molecule. This condition leads to, in some mineral systems, multilayer adsorption of hydroxamate on the mineral surface and significantly improved flotation (Fuerstenau, 2005).

Hydroxamic acids may exist in one of two different forms, hydroxyamide or hydroxyoxime, as seen in Figure 3.6, but only the hydroxyamide form is able to form chelates with metal cations (Pradip & Fuerstenau, 1983). The adsorption of a chelating collector (N-hydroxyl phthalicimide) at the bastnäsite surface is shown schematically in Figure 3.7 (Ren, 1993). An additional benefit of the hydroxamic acids is that they are believed to interact with REE cations in solution to form hydroxylated REE ions, which then adsorb onto the mineral surface, acting as additional activation sites (Cheng *et al.*, 1993). The enhanced selectivity of a hydroxamic acid (alkyl hydroxamate) in comparison to fatty acids (tall oil) at Mountain Pass has been explained by the fact that alkyl hydroxamate is more likely to form chelates with the REE ions in bastnäsite than the calcium and barium ions present on the mineral surfaces of calcite and barite (Jianzhong *et al.*, 2007; Pavez *et al.*, 1996; Pradip, 1981; Pradip & Fuerstenau, 1983). The effectiveness of hydroxamic acids at the Bayan Obo mine has been shown to be affected by water hardness and decreasing pH, as Ca^{2+} and Mg^{2+} ions can consume large amounts of the collector, and excess hydrogen ions prevent the formation of the chelated compounds (Fangji *et al.*, 1989).

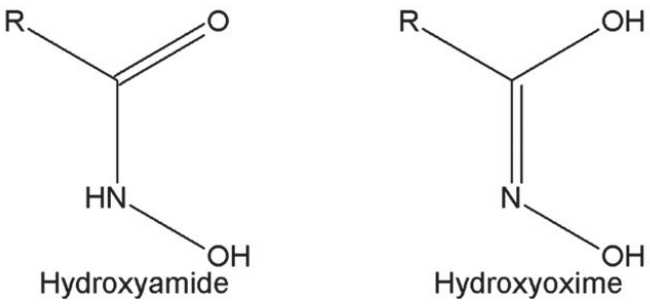

Figure 3.6 - The two tautomeric forms of hydroxamic acid. Adapted from (Pradip & Fuerstenau, 1983)

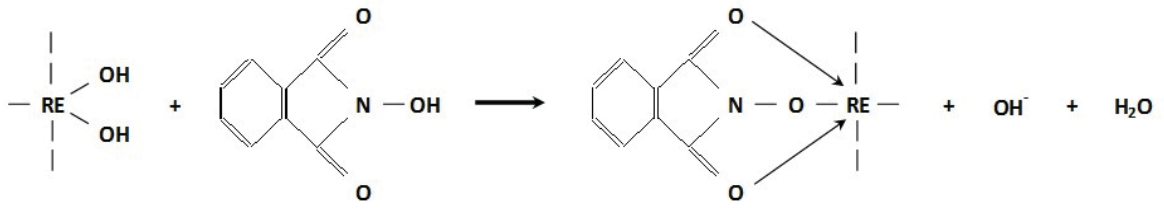

Figure 3.7 - Schematic of chelation reaction between bastnäsite surface and N-hydroxyl phthalicimide. After (Ren, 1993)

Hydroxamates have only recently become a viable industrial option as flotation chemical manufacturers have developed more cost effective methods of production (Gorken *et al.*, 2005). Some additional challenges to the use of hydroxamates include differences in structure between hydroxamate manufacturers, carbon chain length (hydroxamates with a hydrocarbon chain containing more than 9 carbon atoms have been shown in some cases to lead to a reduced flotation performance), the nature of the hydrophobic group attached to the hydroxamate functional group, chemical stability during long storage periods and difficulties in processing ores containing a large volume of slimes (Bulatovic, 2007; Chowdhury & Antolasic, 2012; Gorken *et al.*, 2005).

The key process step (explained in greater detail in Section 3.3.4.2.5) in the beneficiation of the Mountain Pass ore is the heated flotation of bastnäsite from calcite and barite using a fatty acid collector system (Fuerstenau & Pradip, 1991; Pradip, 1981). The Bayan Obo REE deposit, in contrast, is actually a very large iron ore deposit with a relatively small quantity of REM present amongst the iron mineralization (Gupta & Krishnamurthy, 1992). Numerous processing schemes have been described for this deposit; the common elements for many of these flowsheets involve a non-selective flotation of REE and similar gangue minerals from the iron-bearing minerals followed by a more selective flotation step to beneficiate the REO concentrate (Chi *et al.*, 2001; Luo & Chen, 1984; Zhang & Edwards, 2012). According to Luo & Chen (1984), the non-selective flotation step can be completed using a fatty acid, but this poses problems downstream. This is because the fatty acid, a portion of which will chemically adsorb to the surface of gangue minerals, must be removed from adsorption sites, to be replaced by a more selective collector such as hydroxamic acid to facilitate the selective flotation of the REE (Luo & Chen, 1984).

For Chinese bastnäsite ores, a naphthyl hydroxamic acid collector, known as H_{205}, has been widely used to produce REO concentrates with grades of 50% REO or more (Jianzhong *et al.*, 2007; Zhang & Edwards, 2012). The H_{205} collector is preferable over cycloalkyl hydroxamic acids as it is less costly, requires fewer depressants, and the non-polar naphthyl group present in the H_{205} collector molecule is more stable and has more carbon atoms than the cycloalkyl group (Yan, 1991). The use of H_{205} does have some drawbacks as its frothing abilities are not as good as cycloalkyl hydroxamic acid (in practice the frother used for H_{205} flotation contains 5-6% cycloalkyl hydroxamic acid) and the high dosage of H_{205} required to successfully float REM reduces the selectivity of this reagent (Yan, 1991). The H_{205} flotation process is still quite expensive, and further research into phosphoric acids and modified hydroxamic acids is ongoing to develop collectors that minimize reagent costs whilst achieving acceptable REO concentrate grades (Jianzhong *et al.*, 2007; Jun *et al.*, 2003; Ren, 1993; Ren *et al.*, 1997). An example of this is the L_{102} hydroxamic acid collector which is an improvement over H_{205} as it requires a lower dosage, resulting in decreased reagent costs, and can achieve comparable results with only one rougher and one cleaner flotation stage (Fangji *et al.*, 2002).

3.3.4.2.3 Phosphoric Acids

Phosphoric acid esters are another type of anionic collector in which two oxygen atoms will form a complex with the metal cation on the mineral surface (Rao, 2004). These compounds will form complexes with transition metals and alkaline earths and have been used in the flotation of tin (cassiterite), iron and chromium (chromite), titanium (perovskite, ilmenite and rutile), tungsten (wolframite), phosphates (apatite) as well as REM such as bastnäsite (Bulatovic & Wyslouzil, 1999; Guney *et al.*, 1999; Jun *et al.*, 2003; Rao, 2004; Samson *et al.*, 2013; Srinivas *et al.*, 2004). Similar to the hydroxamate collector class the substitution of a phosphorous atom as the binding site for oxygen atoms has an impact on the electron donor capacity of the oxygen atoms (Nagaraj, 1988). In contrast to hydroxamates the phosphorous atom is actually less electronegative than carbon or nitrogen so that the oxygen electrons are more available for complex formation with metal cations (Nagaraj, 1988). Phosphoric acids may be used successfully in either acidic or

basic conditions (depending on the mineral class to be floated) and typically require modifications or combinations with depressants to achieve selective flotation (Bulatovic, 2007; Bulatovic & Wyslouzil, 1999; Nagaraj, 1988). For bastnäsite, reported uses of phosphorous-based collectors have ranged from pH 4 to pH 10 (Zhang & Edwards, 2012). In the case of the Nechalacho REE deposit, recent work by Chehreh Chelgani *et al.* (2013) has shown that the presence of a phosphoric acid based collector appears to be directly responsible for the collection of REM particles in froth flotation.

3.3.4.2.4 Depressants

Choices for depressants are invariably influenced by the composition of the ore deposit and the major gangue minerals present in the flotation feed. There are several depressants that have been extensively researched in established REM flotation processes. At Mountain Pass, lignin sulfonate is added as a depressant to suppress the calcite and barite gangue minerals, however it also affects bastnäsite to a certain degree (Houot *et al.*, 1991; Morrice & Wong, 1983). Sodium carbonate is used extensively in bastnäsite flotation to control the supply of carbonate anions which affect both the pH of flotation and the surface properties of bastnäsite and related gangue minerals (CO_3^- is a potential-determining ion for these minerals) (Fuerstenau & Pradip, 1991; Houot *et al.*, 1991). Smith & Shonnard (1986) showed that the addition of sodium carbonate preferentially increased the magnitude of the negative surface charge on both calcite and barite while leaving bastnäsite unaffected. However, other research has shown that with elevated sodium carbonate additions (≥1 mM) the surfaces of both calcite and barite are positive at pH 9 while bastnäsite has a negative surface charge (Fuerstenau & Pradip, 1991; Pradip, 1981). This effect helps the negatively charged lignin sulfonate molecule to achieve its depressant effects by adsorbing onto the positively charged surfaces of barite, allowing fatty acid molecules to adsorb in greater quantities to the surface of the bastnäsite mineral (Fuerstenau & Pradip, 1991; Pradip, 1981). The same research also noted that the selective nature of lignin sulfonate is not affected by the elevated temperatures at which flotation takes place in the Mountain Pass process (Fuerstenau & Pradip, 1991; Pradip, 1981).

Sodium fluoride and sodium hexafluorosilicate have also been used by different researchers as generic depressants for barite and calcite gangue in the Mountain Pass system (Houot *et al.*, 1991; Morrice & Wong, 1983; Pradip, 1981). At Bayan Obo, sodium silicate is used to depress iron-bearing and silicate minerals, which are not present in the Mountain Pass ore (Houot *et al.*, 1991; Luo & Chen, 1984). Taikang & Yingnan (1980) identified hydroxamic acid and sodium silicate as the two most important reagents for successful flotation of the Bayan Obo ores; the sodium silicate addition was large enough (25 kg/t) to depress the flotation of all minerals, and then a small amount of hydroxamic acid was added to selectively float only the REM. This very large requirement for sodium silicate has been addressed by Jun (1992) who showed that a combination of sodium silicate and either alum or carboxymethyl cellulose (CMC) reduced the dosage required to achieve an efficient depression of gangue minerals in Chinese REM flotation. Sodium metaphosphate has been shown to be an effective depressant of calcite gangue at slightly alkaline pH and in the presence of a hydroxamic acid collector (Ni *et al.*, 2012). Sodium hexafluorosilicate has also been used at Bayan Obo to depress fluorite, calcite and barite minerals as well as to act as an activator for REM (Luo & Chen, 1984; Taikang & Yingnan, 1980). Fangji *et al.* (1989) showed that the popular H_{205} collector does not require the addition of sodium hexafluorosilicate to achieve an effective beneficiation of REM at Bayan Obo, which is significant as sodium hexafluorosilicate is an environmental pollutant as well as a hazard for plant workers (Jun, 1989; Yan, 1991). The elimination of sodium hexafluorosilicate in the work of Fangji *et al.* (1989) was not explained in detail but the authors did state that the RE^{3+} cation was able to form more stable chelates with the H_{205} collector than other metallic cations such as Ca^{2+}, Mg^{2+}, Fe^{3+} and Ba^{2+}; this property was exploited, in conjunction with long mixing times, to desorb the H_{205} collector from the gangue minerals and increase the REE grade of the concentrate. Recently Cui *et al.* (2012) investigated the interaction of hydroxamates with bastnäsite and other RE oxides and confirmed that hydroxamates will form chelates with calcite and barite gangue minerals when REM are not present. However, when REM are present, preferential adsorption of hydroxamate collectors onto REM surfaces (due to the more highly charged RE^{3+} cations) is still expected (Cui *et al.*, 2012; Pradip & Fuerstenau, 1983).

In the case of the collector emulsion proposed by Bulatovic (1988), additional suggested gangue depressants include: citric acid and oxalic acid (for quartz, dolomite, calcite, and barite gangue), and alkali metal hydrogen sulphides (for fluorite, albite and mica gangue). The effective use of metal salts such as aluminium and lead in flotation are heavily dependent upon the collector system, as they have been used in some instances as bastnäsite activators, as depressants for both monazite and bastnäsite at elevated pH, and in one case as a selective depressant of monazite in the presence of bastnäsite (Houot *et al.*, 1991; Ren *et al.*, 2000).

While flotation has proven to be a very useful technique for the separation of bastnäsite, it is important to note that a process employing only flotation will most likely underachieve compared to one that employs multiple (different) unit operations. Fangji & Xinglan (2003) have shown that a properly designed bastnäsite beneficiation process employing sizing, gravity, magnetic and flotation separation steps can outperform alternative bastnäsite separation processes at other plants such as: Mountain Pass (flotation at elevated temperatures); Weishan (flotation using hydroxamic acid); and Dalucao (magnetic and gravity separation). Specifically, their process at the Maoniuping plant was able to achieve similar grades (62-70% REO) to the best performing plants (Weishan produces a concentrate with a grade of 69.55% REO) while achieving recoveries that were significantly higher than the best performer amongst the other plants (85-92% REO recovery at Maoniuping versus 78.11% at Dalucao) (Fangji & Xinglan, 2003).

3.3.4.2.5 Effect of Temperature

The effect of elevated temperatures on flotation has been explained (for the Mountain Pass orebody) by the increased solubility of fatty acids (and other collector molecules) with increasing temperature, increased solubility of cations present on the mineral surface, and preferentially enhanced collector adsorption on the bastnäsite surface relative to gangue minerals (Pradip, 1981). The effect of temperature on bastnäsite flotation selectivity is due to a significant increase in the rate of collector adsorption onto bastnäsite relative to gangue such as calcite and barite (Pradip, 1981). This increase in bastnäsite collector adsorption with temperature may be due to the fact that for the

Mountain Pass ore, process conditions (*i.e.* pH) are such that only bastnäsite is able to make the transition from a physical adsorption to chemical adsorption mechanism (and hence an overall increase in collector adsorption) with increasing temperature, as shown in Figure 3.8 (Houot *et al.*, 1991; Pavez *et al.*, 1996; Pradip, 1981). It is possible that, in a mechanism slightly different to the one shown in Figure 3.8, the interaction of calcite and fatty acid collector molecules at the conditioning temperature used in Mountain Pass would fall into one of the regimes where collector adsorption is actually decreased with increased temperature. Pradip (1981) observed that the grade of the bastnäsite concentrate decreased (without any decrease in the recovery of bastnäsite) as temperature was increased above an optimum temperature of 75°C. This finding suggests that at temperatures above 75°C, gangue minerals adsorb greater amounts of collector, thereby reducing the grade of the bastnäsite concentrate (Pradip, 1981). Pradip (1981) did not conduct enough experiments to conclusively determine the exact mechanisms behind the effect of temperature in this flotation system. In a later study Pradip & Fuerstenau (1985) were able to calculate the free energies of adsorption of hydroxamate onto bastnäsite, barite and calcite surfaces as a function of temperature. Their results showed that the adsorption of hydroxamate onto the bastnäsite surface was thermodynamically favoured over calcite and barite at all temperatures investigated as can be seen in Figure 3.9 (Fuerstenau, 2005; Pradip & Fuerstenau, 1985). Interestingly, as the temperature increases, the difference between the free energies of adsorption of bastnäsite and calcite and bastnäsite and barite increased (Fuerstenau, 2005; Pradip & Fuerstenau, 1985). While this study examined the effect of temperature on hydroxamate adsorption, it is possible that the improved performance of sodium oleate flotation at Mountain Pass with increased temperature could be explained in a similar manner. With the re-opening of the Mountain Pass mine, the influence of temperature on the flotation of bastnäsite merits further investigation.

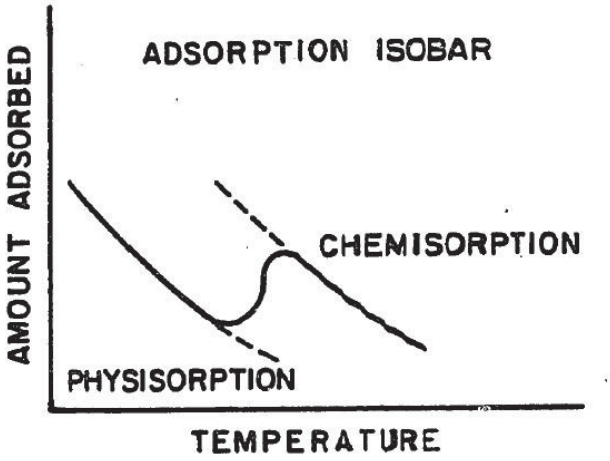

Figure 3.8 - Adsorption isobar of adsorption amount versus temperature showing transition region between physical adsorption and chemical adsorption. After (Pradip, 1981)

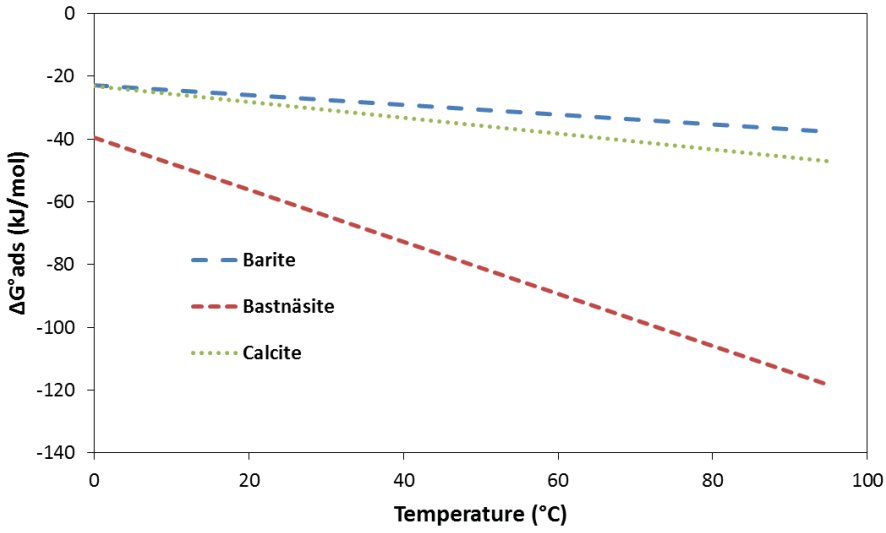

Figure 3.9 - Gibbs free energy of adsorption of potassium octyl hydroxamate onto bastnäsite, calcite and barite as a function of temperature. Adapted from (Fuerstenau, 2005)

3.3.4.3 Monazite Flotation

The flotation process of monazite is different to that of bastnäsite due to the different mineralogy of the deposits, as well as the lack of research sources dealing with the same deposit (unlike the Bayan Obo and Mountain Pass processes). Gangue minerals associated with monazite can include ilmenite, rutile, quartz, and zircon; typically requiring

slightly different flotation reagents to bastnäsite ores to achieve a reasonable separation (Pavez & Peres, 1993, 1994).

Monazite behaves in a similar manner to bastnäsite in terms of collectors used (fatty acids and hydroxamates) as the monazite surface will contain many of the same REE cations present on the bastnäsite surface (Luo & Chen, 1984). The adsorption mechanism of both fatty acids and hydroxamates onto a monazite mineral surface is believed to be chemical in nature, similar to bastnäsite minerals, and the increased bastnäsite selectivity of these collectors with increasing temperature applies similarly to monazite flotation (Houot *et al.*, 1991; Pavez *et al.*, 1996; Pavez & Peres, 1993).

Two of the typical monazite gangue minerals, zircon and rutile, require a depressant in order for selective flotation to be possible (Pavez & Peres, 1994). Common depressants used for this purpose include sodium silicate (also used in bastnäsite flotation), sodium sulphide and sodium oxalate (Abeidu, 1972; Houot *et al.*, 1991; Pavez & Peres, 1993, 1994). The depressing action of both sodium sulphide and sodium oxalate has been proposed to be in part due to a selective activation of monazite (Abeidu, 1972; Bulatovic, 2010; Zakharov *et al.*, 1967). The available literature on sodium sulphide and sodium oxalate employs reagent nomenclature (gangue activators referred to as depressants) that is not in accordance with generally accepted flotation terminology. To ensure their work is accurately represented, the original authors' terminology will be used when describing these two reagents.

Sodium sulphide has been reported to have both an activating and depressing effect on zircon, dependent on dosage. For small additions (10 mg/L) Zakharov *et al.* (1967) showed that sodium sulphide activated zircon, pyrochlore and monazite minerals. However, as the dosage increased (up to 37.5 mg/L) pyrochlore and zircon were depressed, with the monazite flotation unchanged (Zakharov *et al.*, 1967). Sodium sulphide depression of zircon has been explained by the adsorption of SH^- and S^{2-} ions to the mineral surface, and the subsequent unavailability of the metal cations on the mineral surface, reducing the potential sites for collector adsorption (Zakharov *et al.*, 1967). The activation of monazite was explained by the large oxidizing power of REE

cations on the monazite surface which oxidize the SH^- ions and allow fatty acid collector molecules to adsorb onto the monazite surface (Zakharov *et al.*, 1967). An alternative explanation, for the flotation response of this mineral system in the presence of sodium sulphide is the selective desorption of sodium oleate from zircon and pyrochlore surfaces, with an accompanying incomplete desorption from monazite surfaces (Pol'kin *et al.*, 1967). A third alternative explanation of the mechanism of activation of monazite by sodium sulphide is explained via Equations 3.1-3.5 (Abeidu, 1972):

$$:::CeOH + SH^- = :::CeSH + OH^- \quad (pH\sim8) \quad (3.1)$$

$$:::CeSH + OL^- = :::CeSHOL^- \quad (pH\sim8) \quad (3.2)$$

$$:::CeO^- + OLH = :::CeO.HOL^- \quad (pH\sim8) \quad (3.3)$$

$$:::PO_4^- + SH^- = :::SH^+ + PO_4^{3-} \quad (pH\sim8) \quad (3.4)$$

$$:::SH^+ + OL^- = :::SH.OL \quad (pH\sim8) \quad (3.5)$$

These equations describe the activation of the REE cations (Ce^{3+}) and phosphate anions by sulphide ions and then the subsequent binding of the oleic acid collector (OL). According to Abeidu (1972), the only probable mechanism for monazite activation by sodium sulphide is shown by Equations 3.4 and 3.5, and the effective depression of zircon minerals by sodium sulphide can then be explained by the inability of silicon ions on the zircon surface to bind or react with the sulphide ions. While there is no consensus on the mechanism of monazite interaction with sodium sulphide, it is clear that sodium sulphide can be effectively used to float monazite from zircon.

Sodium oxalate has been discussed as both a depressant and activator of monazite flotation, but the prevalent opinion appears to be that sodium oxalate activates monazite when combined with a sulfonate collector (Bulatovic, 2010; Houot *et al.*, 1991). The importance of conditioning time when using sodium oxalate as a depressant agent for monazite gangue can be seen in Figure 3.10 (Bulatovic, 2010).

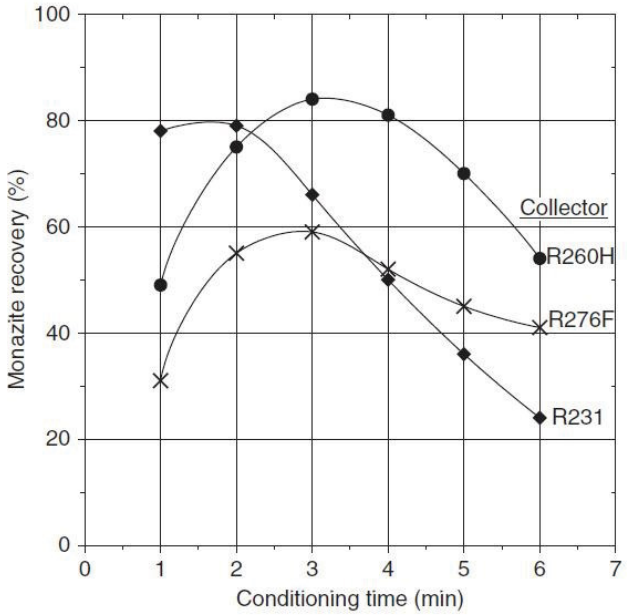

Figure 3.10 - Effect of conditioning time with sodium oxalate on lab-scale monazite recovery using various sulfonate collectors. Reproduced with permission from (Bulatovic, 2010)

Other important depressants of monazite are starches, which have been used with a variety of collectors including: sulfonates (Houot *et al.*, 1991), cationic amines (Cuthbertson, 1952), phosphoric acid esters (Ferron *et al.*, 1991; Houot *et al.*, 1991) and a unique collector emulsion (different from the patented collector emulsion used for bastnäsite flotation) of a fatty acid, an emulsifier, a phosphonic acid derivative and optional oil/amine additions (Bulatovic & Willett, 1991). Most of these collector systems have not been extensively applied in industrial settings due to the lack of any significant monazite deposits (on the scale of Mountain Pass or Bayan Obo) that require the use of flotation as a separation method.

3.3.4.4 Flotation of other REM

Apart from monazite and bastnäsite, there is very little research available on the flotation of REM such as xenotime and even less for some of the newer complex ore deposits such as Mount Weld in Australia.

The surface characteristics of xenotime have been studied by Cheng (2000), with the reviewed literature values of the point of zero charge (the point at which the concentration

of positively charged ionic species is equal to the concentration of negatively charged ionic species on the mineral surface) for this mineral exhibiting a wide range of values, similar to the point of zero charge (PZC) results obtained for bastnäsite and monazite. This work also confirmed the variation in chemical composition of both monazite and xenotime minerals from surface to bulk, and concluded that this is a likely cause for the wide variation in reported values for the PZC and IEP values of these minerals (Cheng, 2000). Another study of monazite and xenotime mineral flotation, with a sodium oleate collector, concluded that sodium fluoride additions altered the bubble attachment times as a function of temperature (Cross & Miller, 1989). With sodium fluoride additions in excess of the concentration needed for surface precipitation, bubble attachment times decreased with increasing temperature, but with insufficient sodium fluoride additions, bubble attachment times were actually shown to increase (Cross & Miller, 1989). This finding illustrates the importance of determining the optimum concentration of flotation reagents, in addition to the correct type of reagents, for the recovery of a REM.

Another novel REE flotation process involved completely depressing monazite and an unspecified yttrium-bearing mineral using phosphoric acid at acidic pH, and an organic depressant to achieve a separation through reverse flotation. The naturally hydrophobic gangue (albite, chlorites and aegirine) floated without the need for collector addition (Ferron *et al.*, 1991).

Disregarding Bayan Obo and Mountain Pass, the published literature on flotation as a means of REE concentration is limited. In the 1960's a process for flotation of monazite and steenstrupine was investigated for the large Kvanefjeld REE deposit in Greenland (which only in 2012 began to move towards full-scale development) using sodium oleate as a collector and sodium silicate as a depressant (Sorensen & Lundgaard, 1966). This study also explored the use of lanthanum ions as an activator for the REM, with limited success. Lanthanum ion uptake was correlated directly with flotation recovery of monazite and steenstrupine, however excess lanthanum ion additions were found to increase the flotation recoveries of the gangue (arfvedsonite and aegirine) (Sorensen & Lundgaard, 1966).

Apatite, as can be seen in Table 3.6 and Table 3.9, can occur in forms that make it another potential source of REE. Some examples of REE-rich apatite deposits include: Kola and Kovdor in Russia, Palfos in South Africa as well as sedimentary deposits in Jordan and Morocco (Jorjani & Bagherieh, 2007). A study by Jorjani & Bagherieh (2007) has recently identified a significant source of REEs in the apatite-containing tailings of the Chadormalu iron ore concentrator in Iran. Apatites are an important mineral for the phosphate industry, and the flotation of this class of mineral is well-established using fatty acid collector systems (Lu *et al.*, 1998). Due to the similar chemical nature of common gangue minerals such as calcite and fluorite, fatty acids such as sodium oleate will preferentially adsorb onto these gangue minerals instead of apatite (Lu *et al.*, 1998). Apatite from the Kola Peninsula in Russia has been successfully recovered via flotation using a tall oil collector and sodium silicate as a gangue depressant (Houot, 1982). After six flotation stages (one rougher, two scavenger and three cleaner stages), the resultant concentrate grade was 94.8% apatite with a 94% phosphate recovery (Houot, 1982).

The other major REE deposit that is actively being developed is in Mount Weld in Australia where the complex mineralogy of the deposit is distinct from currently operating REE mines (Chan, 1992). Some of the REM comprising the Mount Weld ore body include: monazite, cheralite, cerianite, florencite, and small quantities of rhabdophane (Chan, 1992). Goethite, apatite, crandalite, dolomite, cryptomelane and jacobsite are present as gangue (Chan, 1992). Two flotation schemes have been proposed for this ore body. The first, by Chan (1992), describes a blended collector emulsion (separate from previously mentioned collector emulsions) of fatty acid, with an emulsifier such as a secondary amino modified sulfonated fatty acid and an oil as froth stabilizer, with sodium sulphide, sodium silicate and a starch as depressants. This work also mentions the possibility of utilizing an amine collector, provided suitable depressants could be developed, as being advantageous due to the ease with which an amine could be removed from mineral surfaces after flotation (Chan, 1992). The second method, by Guy *et al.* (2000), employs a fatty acid collector with sodium sulphide, starch and sodium silicate as the depressants. As the Mount Weld deposit has only recently been brought to full-scale production, there is currently no available data to determine which flotation scheme has been adopted and

how it is performing. A comparison between these two reagent schemes shows that the primary path of innovation for new flotation processes for REE ores has thus far involved developing new collectors, whilst depressant schemes remain relatively untouched.

One of the most advanced REE mining development projects in Canada is the Nechalacho deposit in the Northwest Territories (owned by Avalon Rare Metals) with the majority of its REE located in the minerals zircon, allanite, monazite, columbite, bastnäsite and fergusonite (Cox *et al.*, 2011). While zircon contains the majority of the REE in the deposit, allanite, a RE-silicate, contains the second highest amount of REE in the deposit at 12.3 % (Cox *et al.*, 2011). In contrast to the traditionally exploited REE carbonate mineral bastnäsite, the REE content of allanite is much lower and the REE distribution in allanite is significantly weighted towards the heavy REE (Gd to Lu) due to differences in mineral structure (Kanazawa & Kamitani, 2006). These differences are inherently linked to mineral structure and are not specific to this deposit. For the reasons mentioned above the successful recovery of allanite is therefore a major determinant to the successful exploitation of this deposit. As silicate minerals are inherently less soluble than carbonate minerals the recovery of allanite by froth flotation must overcome the dual obstacles of a lower RE content and lower solubility than bastnäsite.

3.4 The Future of REE Processing

REE mine development is expanding at a rapid pace in light of increasing global demand for these elements in high-technology applications and the quotas being placed on Chinese exports of REE (Chen, 2011). In 1989, the annual production capacity of world REE mines was approximately 50,000 tonnes, and in 2011 the annual production capacity from non-Chinese sources in 2015 was expected to be close to 170,000 tonnes (Chen, 2011; O'Driscoll, 1991). In reality, the development of non-Chinese REE mines has proved incredibly challenging, for a variety of technical and economic reasons, and total world-wide production in 2015 was only 110,000 tonnes (95,000 tonnes from China) (Gambogi, 2015). Nevertheless, many non-Chinese REE deposits continue to progress towards full-scale production (Argus, 2015).

The increase in production outside of China is being welcomed by the Chinese government as serious challenges in the mature Chinese REE industry have recently come to light (China, 2012). China produces the majority of the global REE supply, however this supply comes from a reserve base that is only 23% of the known global reserves (Chen, 2011; China, 2012). Note that the 23% figure for China's proportion of the world REE reserve base is significantly lower than those reported (50.0% of 2012 world REE reserves, 42.3% of 2015 world REE reserves) in the widely cited USGS Mineral Commodity Surveys ((Cordier, 2011, 2012; Gambogi, 2015; Hedrick, 2009, 2010). The reserve values reported by Chinese sources are reported here as the USGS data does not appear to include a large number of developing Canadian and Australian deposits that have been delineated as REE resources (Simandl, 2012). Since NI 43-101 and JORC reporting requirements are quite stringent in Canada and Australia many of these resources may be classifiable as reserves in other jurisdictions (Simandl, 2012). These resources would then be expected to increase the worldwide total REE reserve base and therefore decrease the Chinese proportion of world reserves (Simandl, 2012). The inevitable depletion of this resource base (the ratio of Chinese ion-absorbed clay reserves, a major source of HREE, to the amount of this material extracted each year has reportedly fallen from 50:1 to 15:1 in the last twenty years), combined with new environmental regulations led to the creation of a quota system to limit REE exports (China, 2012). While these quotas have recently been removed, Chinese dominance of the REE industry persists.

This new growth in global REE capacity may outstrip demand, but it will surely result in multiple new REE producers being established. The means of evaluating these deposits is challenging as there is no single market for REE. One means of evaluating the deposits is to look at the % of the REEs in the deposit which are critical REEs (as defined in Section 1.1.4) as well as the outlook coefficient in Equation 3.6 defined by Seredin (2010) as:

$$REE\ Outlook\ Coefficient = \frac{\frac{(Nd+Eu+Tb+Dy+Er+Y)}{Total\ REE}}{\frac{(Ce+Ho+Tm+Yb+Lu)}{Total\ REE}} \quad (3.6)$$

where all REE contents are expressed as a percentage of the deposit. Such a plot is presented in Figure 3.11 for the most advanced REE projects outside of China. This plot illustrates the vast differences between REE deposits and highlights some promising, very high grade (in terms of the most important REEs) deposits. It can be seen from Figure 3.11 that the two major non-Chinese REE mines fall very low on this measure of high value REE content. There is clearly a second criterion for a successful REE deposit which is predicated on the total amount of REEs present (and by extension mine life). Figure 3.12 attempts to illustrate this by presenting the same deposits from Figure 3.11 on a plot of value REE (as defined in Section 1.1.4) versus the total REE content of the deposit. It can be seen from this figure that the operating mines now fall near the optimum in terms of value REE content and total REE content, indicating the economic opportunity presented by these two mines.

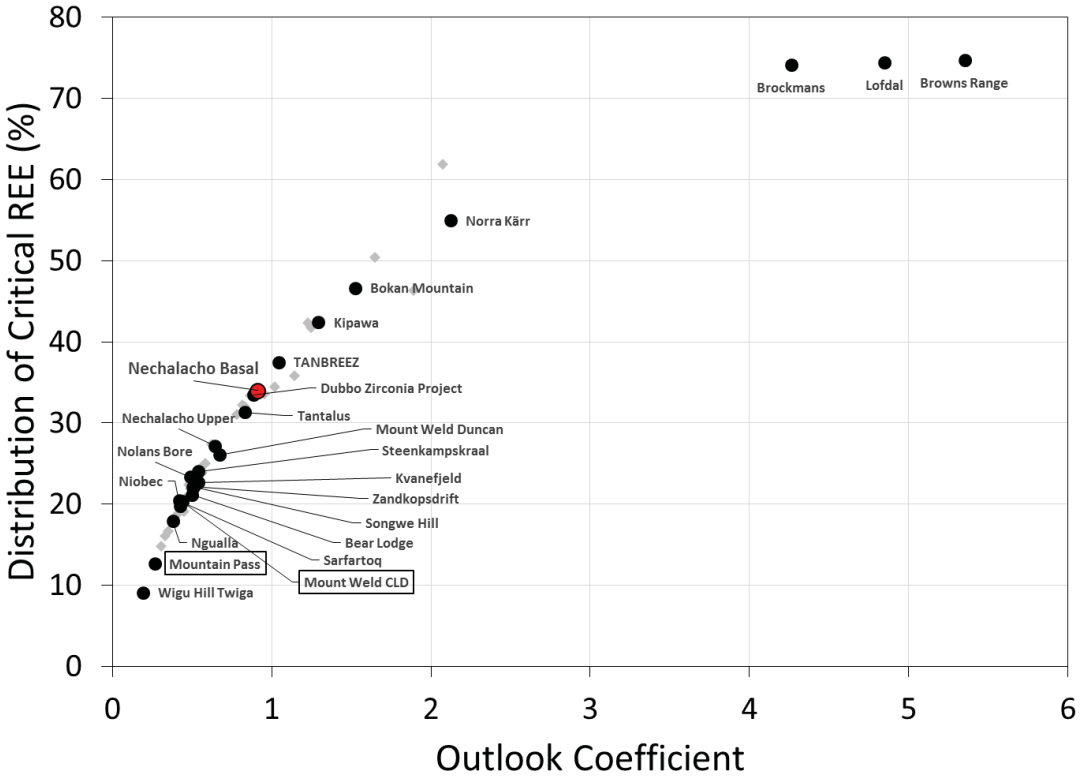

Figure 3.11 - Plot of the distribution of critical REE content (as a % of total REE) versus REE outlook coefficient for 58 advanced non-Chinese REE projects. Labeled deposits indicate the most advanced projects (as determined by Argus Media). Boxed labels indicate currently producing mines. Data from (Research, 2015)

One of the most advanced non-operating major deposits is the Nechalacho deposit in the Northwest Territories (Canada) shown in Figure 3.11 and Figure 3.12 as a red circle. This deposit is attractive both for its absolute REE content as well as the high concentration of important heavy REEs. The beneficiation of this deposit will involve minerals and ore compositions that have never been successfully processed and a great deal of industrial and academic research is required to bridge this knowledge gap. Common minerals, such as sulphides, have been investigated extensively and there are numerous published works on aspects such as interaction with collectors, effects of depressants, magnetic properties *etc.* This knowledge base does not exist for many of the REM in this deposit and is essential for the successful processing of these minerals. All of the separation techniques described above need to be investigated in this context, with a dual focus on the behaviour of individual REM as well as overall REE oxide concentration from ores. The most important of these techniques will likely prove to be flotation as additional reagents and processing conditions are developed and explored.

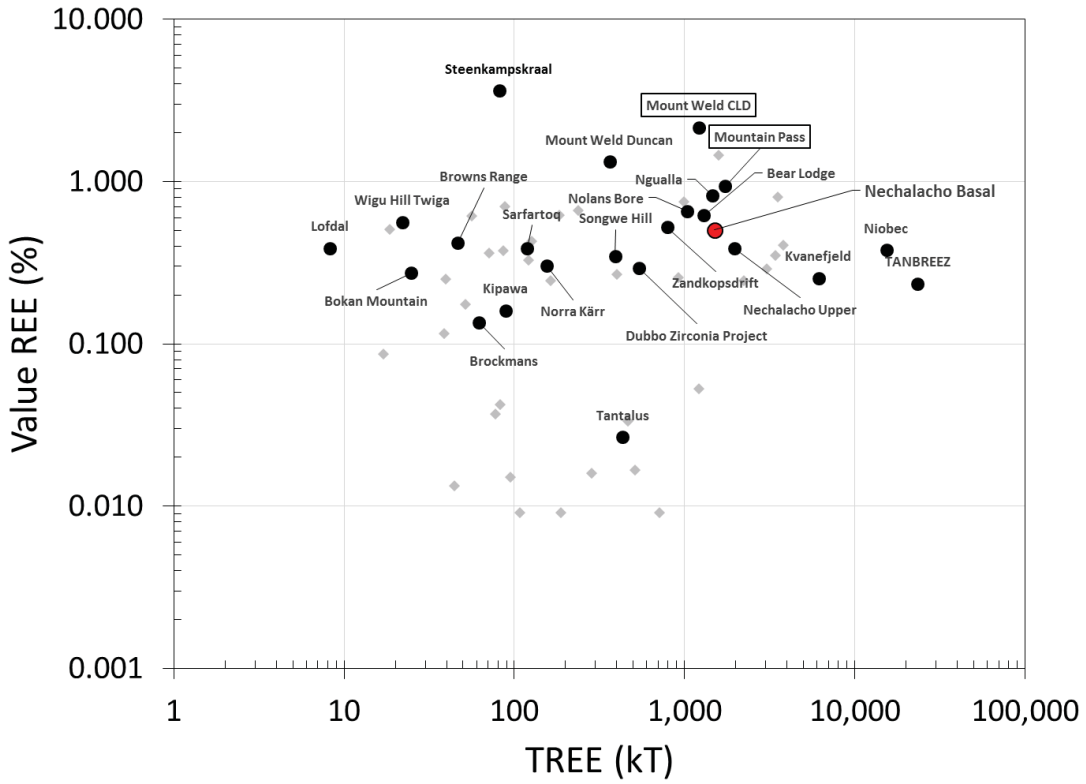

Figure 3.12 - Plot of the distribution of value REE (as a % of the deposit) versus absolute REE content for 58 advanced non-Chinese REE projects. Labelled deposits indicate the most advanced projects (as determined by Argus Media). Boxed labels indicate currently producing mines. Data from (Research, 2015)

3.5 Conclusions

The separation of REM may be fully described using only a handful of mineral developments worldwide, though growing commercial demand for the elements of the lanthanide series has greatly increased the opportunities for the development of new REM deposits with novel mineralogy, as well as the research required to effectively separate these minerals. The existing literature on the physical beneficiation of REM is mainly focused on the two major REM deposits, Bayan Obo and Mountain Pass, with a small amount of research material available on other minor REM. A considerable amount of rare earth research has been reported in Chinese journals, however, efforts at translating this information have revealed that many of these articles lack the requisite background information (proper chemical names of collector molecules, detailed descriptions of processes etc.) to provide any significant insights into the development of

separation processes for alternative REM. Each REM, no matter how widely investigated, presents significant opportunities for future research.

3.5.1 Bastnäsite

Bastnäsite processing is accomplished using gravity and magnetic separation steps prior to flotation. Some post-flotation processing may occur in the form of additional gravity and magnetic separations steps but the most important separation process for this mineral is froth flotation. The two most widely explored collector systems are fatty acids and hydroxamates. Reviewing the literature on bastnäsite separation leads to the conclusion that a great deal of research is still required for the concentration of this mineral.

- Basic research findings for this mineral such as reported IEP values do not generally agree with one another. Further studies may be able to achieve more reproducible results or propose explanations for the reported differences.
- Chinese researchers have developed a series of alternate reagents to be used in the flotation of the various Chinese bastnäsite deposits yet it seems likely that a great many of the existing processes could benefit greatly from additional work to optimize the flotation process and maximize the utilization of these resources.
- At Mountain Pass, fatty acid and hydroxamate flotation are the principle techniques that have been explored, but with the advances in flotation research, as well as the development of many new flotation reagents since the mine was closed, this deposit will certainly require more research into beneficiation techniques to successfully restart production.
- Many developing REE deposits are finding that their REE mineralogy includes bastnäsite in addition to other REM. These new bastnäsite deposits will require a great deal of future studies to develop beneficiation processes tailored to their varied deposit characteristics.

3.5.2 Monazite/Xenotime

Monazite and xenotime processing is well established from beach sands via a combination of gravity, magnetic and electrostatic separations tailored to the composition

of an individual deposit. The flotation of monazite however has not been widely explored. This subject area will become increasingly important as alternate sources of monazite are found in new REE deposits. These deposits may require significantly different beneficiation processes and these needs will drive future research work regarding this mineral. Monazite's physico-chemical characteristics will need to be confirmed and the flotation knowledge base for monazite should also be expanded.

3.5.3 Other REM

This chapter has presented data on a wide variety of REM, however only some are found in deposits of economic significance. Some examples of these include eudialyte, synchysite, samarskite, allanite, zircon, steenstrupine, cheralite, rhabdophane, apatite, florencite, fergusonite, loparite, perovskite, cerianite, and pyrochlore. A few of these minerals, such as zircon, apatite and pyrochlore, are extracted for other constituent elements like Zr, P and Nb. As such, the beneficiation of these minerals for REE extraction may be able to borrow extensively from the established processes for these minerals. For the rest, there is essentially no published research available. These minerals present the most attractive opportunity for research into REM as any investigation into the characteristics and behaviours of these minerals, in the context of mineral beneficiation, will present a significant advance in REM processing knowledge.

For many of the REM that are present in newly developing deposits there is effectively no peer-reviewed knowledge base to rely on when designing a new REM beneficiation process. As the REM processing industry grows to accommodate expanding demand, this knowledge deficit will have to be addressed.

4. Experimental Methods

4.1 Introduction

This chapter details the methodologies used throughout the experimental program on which this thesis is based. Descriptions of the theoretical basis of different characterisation and separation technologies may be found in Chapter 2.

4.2 Materials

4.2.1 Minerals

Pure mineral samples examined in this thesis were obtained from Gregory, Bottley and Lloyd (UK), Daubois (Canada) and Excalibur Minerals (USA). Allanite and bastnäsite (originating from Madagascar) were purchased from Gregory, Bottley and Lloyd (UK), quartz was purchased from Daubois (Canada) and a second sample of bastnäsite (originating from the Birthday Vein, Mountain Pass Mine) was purchased from Excalibur Minerals (USA).

4.2.2 Ore

The raw ore used in the bulk of this work originated from the Nechalacho deposit (Avalon Rare Metals, Inc.) located in the Northwest Territories, Canada. This deposit has 183.4 million tonnes of inferred resources at a grade of 1.27 % total rare earth oxide (TREO) (Ciuculescu *et al.*, 2013), and contains a variety of REE minerals (REM) with very fine-grained mineralization (approximately 10–20 μm). There is also a significant amount of iron present in the deposit in the form of iron oxides and columbite.

Two distinct samples were received to conduct preliminary experiments (Batch 1) as well as a final flowsheet evaluation (Batch 2). The major minerals present in the deposit are listed in Table 4.1 by batch. Most of the REM present in this deposit have high specific gravities (relative to gangue minerals such as quartz and feldspar) and some degree of paramagnetic behaviour. The most important REM in this deposit is zircon as it has been reported to host over 65% of all REE in the deposit due to the unique geological processes at work in this deposit (Cox *et al.*, 2011). This REE-bearing zircon is unique to this deposit as zircon will not conventionally contain economic concentrations of REE. The major gangue minerals are quartz, feldspars, biotite and iron oxides.

Table 4.1 - Mineralogy of the Nechalacho REE deposit for two different batches

Mineral Name	Composition (wt. %)	
	Batch 1	*Batch 2*
Columbite(Fe)	0.5	0.4
Fergusonite	0.3	0.2
Bastnasite	1.3	0.9
Synchysite	0.2	0.5
Allanite	0.1	0.6
Monazite	0.2	0.5
Other REE	0.0	0.0
Zircon	4.1	7.1
Apatite	0.2	0.0
Quartz	35.1	20.9
Plagioclase	10.5	18.6
K-Feldspar	20.5	21.8
Biotite	9.6	13.2
Muscovite	0.0	0.0
Clays	0.4	0.2
Chlorite	0.0	0.1
Amphibole	0.8	0.5
Other Silicates	0.0	0.1
Calcite	1.9	0.6
Dolomite	1.8	
Ankerite	3.7	2.9
Other Carbonates	0.0	0.3
Fluorite	0.3	0.5
Fe-Oxides	8.3	9.5
Sulphides	0.2	
Other Oxides		0.1
Other	0.1	0.2

4.2.3 Reagents

Sodium silicate, potassium chloride, ferric chloride hexahydrate, ferrous chloride tetrahydrate and lead chloride used in this work were obtained from Fisher Scientific (Canada); benzohydroxamic acid was purchased from Alfa Aesar (USA); and F150 (a polypropylene glycol-based frother) was obtained from Flottec (USA). Sodium oleate, dodecylamine and methyl isobutyl carbinol (MIBC) were purchased from Sigma-Aldrich, Flotinor SM15 (mixture of phosphoric acid esters) was obtained from Clariant (USA). All reagents were used as supplied.

Sodium hydroxide and hydrochloric acid (Fisher Scientific, Canada) were used for pH modification in all work diluted to 0.1 – 1 M. Stock solutions of benzohydroxamic acid and sodium oleate were prepared by dissolving the respective solids in deionized water to form aqueous solutions whereas dodecylamine was dissolved in acetic acid at a 4:1 molar ratio of acetic acid:dodecylamine before being diluted with deionized water. SM15 and sodium silicate were used as provided by the manufacturer in liquid form.

4.3 Characterisation techniques

4.3.1 X-Ray diffraction

The presence and relative amounts of various minerals was verified using X-Ray Diffraction (XRD). XRD analyses were conducted using two Bruker D8 Discovery X-Ray Diffractometers equipped with a copper and cobalt x-ray generating source respectively. The resultant diffraction patterns were processed using Xpert High Score software (PANalytical) to identify peaks and relate them to selected mineral phases present in the Nechalacho ore, as well as individual mineral samples.

4.3.2 Quantitative evaluation of minerals by scanning electron microscopy (QEMSCAN)

All samples analysed by QEMSCAN in this study were prepared as polished sections and analyzed at the Advanced Mineralogy Facility at SGS Canada (Lakefield, Canada). QEMSCAN is an EVO 430 automated scanning electron microscope equipped with four light-element energy-dispersive X-ray spectrometers and iDiscover software capable of processing the data and images. QEMSCAN operates with a 25 kV accelerating voltage and a 5 nA beam current. The QEMSCAN measures, and the iDiscover software processes, data from every pixel across a sample with a pixel size defined based on the scope of the analysis. The software assigns each pixel a mineral name based on 1,000 counts of energy dispersive X-ray spectral data and backscatter electron intensities.

If the minerals or constituent phases comprising the sample are chemically distinct, QEMSCAN is capable of reliably discriminating and quantifying minerals. Magnetite and hematite are grouped together and referred to as Fe-oxides. Distinction between the two minerals when needed was conducted by optical mineralogy and X-ray diffraction (XRD) analysis. The mineral definitions were validated and refined to fit the particular samples.

A reference mineral list was developed using XRD (primarily to define the major minerals), a scanning electron microscope (SEM) equipped with an energy dispersive spectrometer, and electron probe micro analysis (EPMA).

Coarse samples (> 300 µm) were analyzed with the Field Image method. Chemical spectra were collected at a set interval within the field of view. Data acquisition from the polished sections was conducted at a 6-20 µm pixel size. The typical diameter of a polished section was 30 mm.

The Particle Mineral Analysis (PMA) method was used for finer size samples (< 300 µm). PMA is a two-dimensional mapping analysis aimed at resolving liberation and locking characteristics of a generic set of particles. A pre-defined number of particles were mapped at a 3-6 µm pixel size.

REM in QEMSCAN were identified based on their major REE. For example, monazite is defined as $(Ce,La,Nd)PO_4$. It should be noted that the QEMSCAN technique does not quantify the exact chemistry of the minerals, *e.g.*, Y in zircon or Eu in REM that occur in trace amounts. Mineral chemistry is exclusively defined by EPMA and adjusted in the software accordingly for additional calculations.

4.3.3 Electron Probe Micro Analysis

The compositions of the REM in this work were determined (to develop the QEMSCAN mineral definitions) using the wavelength-dispersive spectrometer (WDS) mode on the JEOL JXA-8900L electron microprobe at McGill University (Grammatikopoulos *et al.*, 2013).

4.3.4 Inductively coupled plasma mass spectrometry (ICP-MS)

The REE content of selected samples was determined by inductively coupled plasma mass spectrometry (ICP-MS). Due to difficulties in digesting silicate minerals in the deposit, sodium peroxide was mixed with 0.1 g of sample and then heated to form a homogeneous melt. This melt was then digested in hydrochloric acid followed by ICP-MS analysis. All digestion and ICP-MS analysis in this work was conducted by SGS Canada

(Lakefield, Canada). For data validation purposes, calculated assays from QEMSCAN measurements were compared to chemical assays obtained from ICP-MS.

4.3.5 Scanning Electron Microscopy (SEM)

For the final gravity and magnetic separations representative samples of each product, as well as the feed, were analysed with a cold field emission SEM Hitachi SU-8230 (Hitachi High-Technologies, Canada) equipped with an XFlash 6|60 SDD (Bruker Nano GmbH, Germany) energy-dispersive X-ray spectrometer. The X-ray maps were acquired at an accelerating voltage of 15 kV with a beam current of 4 nA for one hour with a count rate of 19.3 kcps (~5% dead time). The element intensity maps were obtained with the quick deconvolution feature of the Esprit software (Bruker Nano GmbH, Germany) and qualitative phase maps were calculated with the *f*-ratio intensity method (Horny *et al.*, 2010) using a custom Python script.

4.3.6 Vibrating sample magnetometer

The vibrating sample magnetometer (VSM) measurements in this work were conducted using a LakeShore 7300 series VSM. All mineral samples, with the exception of two zircon crystals which were analysed intact, were pulverized in a T100 ring and disc pulveriser (Siebtechnik, Germany) prior to VSM measurements. To conduct the measurements 50-100 mg of powdered sample was placed into the cylindrical VSM sample holder (for the case of zircon, a single crystal was suspended from the sample holder) and attached to the end of an oscillating rod. The sample is positioned such that it sits in the middle of 4 pick-up coils and a hall probe. The rod is then oscillated about this central point as a magnetic field is applied to the sample to create a full hysteresis loop between +2 T and -2 T with measurements taken every 0.1 T. The data output of the VSM consists of measured magnetic moment as a function of magnetic induction. Measurements were also conducted on the empty sample holder such that any magnetic contribution of the sample holder may be subtracted from the sample data. The measured magnetic moment data (as a function of magnetic field) was converted into magnetisation by dividing by the sample volume (determined using theoretical mineral densities). The magnetic induction

values are converted into magnetic field strength by dividing by the constant of permeability of free space, $4\pi \times 10^{-7}$ V s / A m.

Samples of fergusonite, bastnäsite, allanite and two different types of zircon were analysed in the VSM to experimentally determine the magnetic behaviour of these minerals prior to any attempts to concentrate the REM present in the Nechalacho deposit. Samples of several of the gangue minerals (including quartz, hematite and magnetite) found in the Nechalacho deposit were also examined.

The VSM was also used to measure products of gravity and magnetic separation to assess the distribution of magnetic phases through these separation steps.

4.4 Sample preparation

4.4.1 Mineral purification

4.4.1.1 Mineral composition analysis

The allanite and bastnäsite (from Madagascar) obtained for this work were analysed using QEMSCAN to determine their respective mineralogical compositions. Allanite was found to be the primary component of the allanite sample (65 % pure) with major gangue minerals identified as calcite, quartz and other silicates, and pyrite. The bastnäsite from Madagascar was already pure (> 95 % bastnäsite) and was therefore used as obtained. Measurements of chemical composition were also conducted on the allanite and bastnäsite sample as-received using ICP-MS.

4.4.1.2 Allanite

Based on the magnetic properties of the gangue minerals found in the allanite sample a Frantz Isodynamic Separator (Frantz, USA) was used to separate the various mineral phases based on their magnetic properties. The sample was stage pulverized to a top size of 106 µm and then wet screened to remove all particles less than 25 µm. The resultant 25-106 µm fraction was then passed through the Isodynamic Separator (at a forward slope of 30° and side slope of 15°) to remove unwanted ferromagnetic and diamagnetic minerals. The allanite sample was processed at 0.1 A (~0.2 T) and then at 1.7 A (~2.1 T) to produce three fractions: 0.1 A Mag, 1.7 A Mag and Non-Mag. The Non-

Mag fraction was processed twice at 1.7 A to ensure maximum rejection of diamagnetic material. As the QEMSCAN results do not distinguish between different forms of iron oxide (*i.e.* magnetite and hematite) the 0.1 A Mag fraction was further separated using a weak hand magnet to remove any strongly ferromagnetic material. The most ferromagnetic material was classified as the Mag 1 fraction and the remaining material was classified as the Mag 2 fraction. The 1.7 A Mag fraction was reprocessed at 0.3 A (~0.45 T) to further remove strongly magnetic material with the remaining material classified as Potential Allanite. In order to determine the success of these purification steps X-ray diffraction (XRD) was employed The XRD results for the different separated streams may be seen in Figure 4.1 along with the only available reference diffraction patterns for allanite.

Figure 4.1 shows that the Mag 1 product was found to contain two ferromagnetic phases, magnetite and pyrrhotite (QEMSCAN results had also shown ~0.1 % sulphide content in the sample). The Mag 2 product displayed peaks associated with hematite. Based on the results shown in Figure 4.1 it was assumed that the concentration of allanite was successful as the primary peak for the potential allanite product of the Frantz separation corresponded perfectly to the primary peak for all available patterns for allanite. The other two peaks appear to correspond to the hematite peaks identified for the Mag 2 product. These peaks were considered less important as QEMSCAN results (Section 4.4.1.1) indicated that the total concentration of iron oxides in the as-received sample were less than 1 %. As allanite may exist in a wide variety of compositions it is likely that the allanite investigated in this work does not match up exactly with the composition of either of the two reference allanite samples whose diffraction patterns are shown in Figure 4.1.

The resultant purified allanite was then wet screened at 38 μm to produce a 38-106 μm fraction for microflotation tests. For certain microflotation experiments this sample was further screened at 53 μm to produce a narrow size fraction. The purified allanite was wet ground in a Pulverisette 6 planetary monomill (Fritsch, Germany) to produce a fine size fraction (d_{50} = 5.6 μm) for zeta potential measurements. Particle size (d_{50}) was determined using a LA-920 particle size analyser (Horiba, USA).

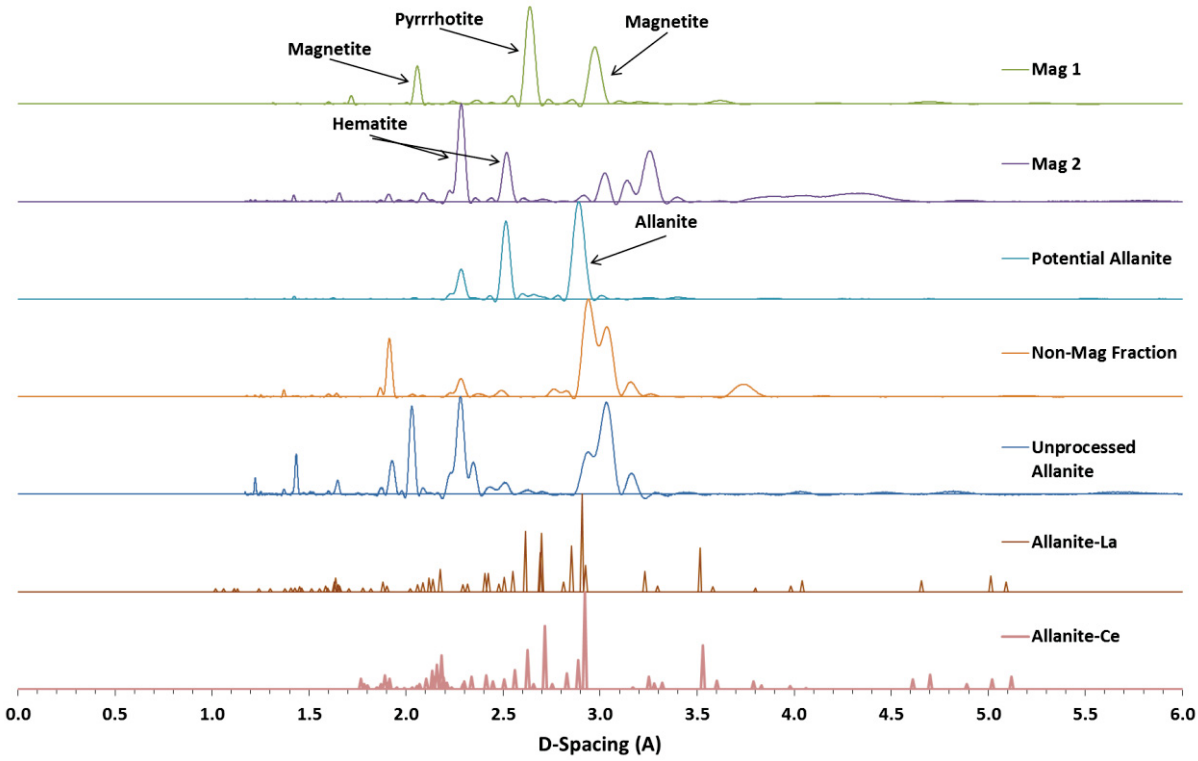

Figure 4.1 – X-ray diffraction patterns for products of allanite separation along with reference patterns for Allanite-La and Allanite-Ce. All diffraction peaks have been normalized to the maximum peak intensity for each pattern.

4.4.1.3 Bastnäsite

The bastnäsite sample from Mountain Pass was not as pure as the sample from Madagascar and as such required a significant amount of purification using magnetic and gravity separation.

Both samples of bastnäsite were stage pulverized to produce a 38-106 µm size fraction and a 20-106 µm fraction for the samples from Madagascar and Mountain Pass respectively. The Mountain Pass bastnäsite required purification using a series of gravity and magnetic separations steps. For these purposes a Mozley MKII Laboratory Separator (Mozley, UK) and Frantz Isodynamic Separator (Frantz, USA) were employed. In order to simplify purification the Mountain Pass bastnäsite sample was screened into four narrow size fractions (20-38 µm, 38-53 µm, 53-75 µm, and 75-106 µm).

From literature the major gangue minerals in the Mountain Pass deposit are barite, calcite and quartz (Pradip, 1981). The relevant data on these minerals is shown in Table 4.2. From this information it can be seen that gravity separation should readily concentrate both barite and bastnäsite which can then be separated using a magnetic separation step. The purification steps employed to isolate the bastnäsite from the other Mountain Pass minerals involved passing each size fraction through a series of magnetic separation steps on a Frantz Isodynamic Separator at increasing magnetic field strengths (with the non-magnetic fraction of each separation step reprocessed at higher field strength).

Table 4.2 – Major minerals in the Mountain Pass bastnäsite sample including information on magnetic properties and specific gravity (Anthony *et al.*, 2001; Liley *et al.*, 1997; Pradip, 1981; Rosenblum & Brownfield, 1999)

Mineral	Magnetic Properties	Specific Gravity
Barite	Diamagnetic	4.5
Bastnäsite	Paramagnetic	4.9-5.2
Calcite	Diamagnetic	2.7
Quartz	Diamagnetic	2.7

The Frantz separator was operated with a 15° side slope and a forward slope that varied from 30° to 40° (increased for fractions of lower particle size in order to enhance particle flow down the separator). As bastnäsite has been reported as having a relatively small magnetic susceptibility (Chapter 5, Table 5.1) it was found that a bastnäsite enriched fraction was produced only at the maximum magnetic field strength of 2.1 T. This bastnäsite enriched fraction was then processed on a flat Mozley shaking table operated at 90 rpm with a 3.5” stroke and approximately 3 L/min of wash water. After the table step, the heavy fraction was assumed to contain primarily bastnäsite and barite and was therefore processed once more through the Frantz separator at a magnetic field strength of 2.1 T to remove as much of the remaining barite as possible. The success of these purification steps was determined using XRD.

Figure 4.2 shows XRD patterns for the 53-75 µm fraction of the products of the shaking table (Heavy/Light) as well as after subsequent magnetic processing of the heavy fraction (Heavy+Frantz). From these results one can observe that the XRD pattern of the final product of purification (Heavy+Frantz) exhibits all the characteristic peaks of bastnäsite,

and also corresponds very well with the measured pattern of the bastnäsite sample from Madagascar. It is therefore reasonable to assume that the purified Mountain Pass sample is of comparable purity to the sample from Madagascar. Figure 4.3 shows the XRD patterns for the final purified Mountain Pass bastnäsite product for each particle size range. The XRD patterns of the 20-38 µm and the 75-106 µm fractions exhibit the peaks of bastnäsite along with the major peaks of the gangue minerals in the Mountain Pass deposit such as quartz, calcite and barite. This demonstrates that the lower limit for effective separation of the Mountain Pass sample is 38 µm and above 75 µm the purification is not possible. This may be potentially due to incomplete liberation, although the work of Pradip (1981) reported the Mountain Pass flotation circuit to operate at a k_{80} of 150 µm.

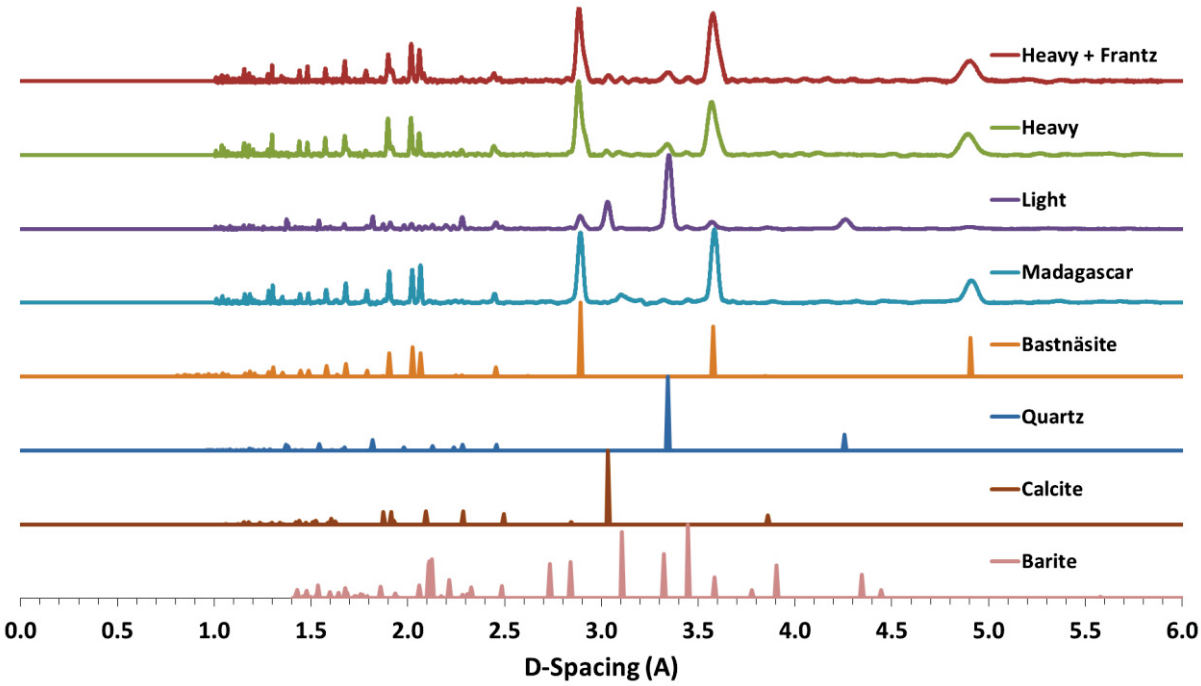

Figure 4.2 – XRD patterns of the products (53-75 µm) of Mountain Pass bastnäsite shaking table purification (Heavy/Light) as well as from subsequent magnetic separation (Heavy + Frantz). Reference patterns are provided from literature for all major minerals from the Mountain Pass deposit as well as the measured pattern of the bastnäsite sample from Madagascar. All diffraction peaks have been normalized to the maximum peak intensity for each pattern

Bastnäsite used in zeta potential investigations was ground wet using a Pulverisette 6 planetary monomill (Fritsch, Germany) to produce very fine particle sizes (bastnäsite

Madagascar d_{50} = 2.0 µm, bastnäsite Mountain Pass d_{50} = 1.9 µm,). Particle size was determined using a LA-920 particle size analyser (Horiba, USA).

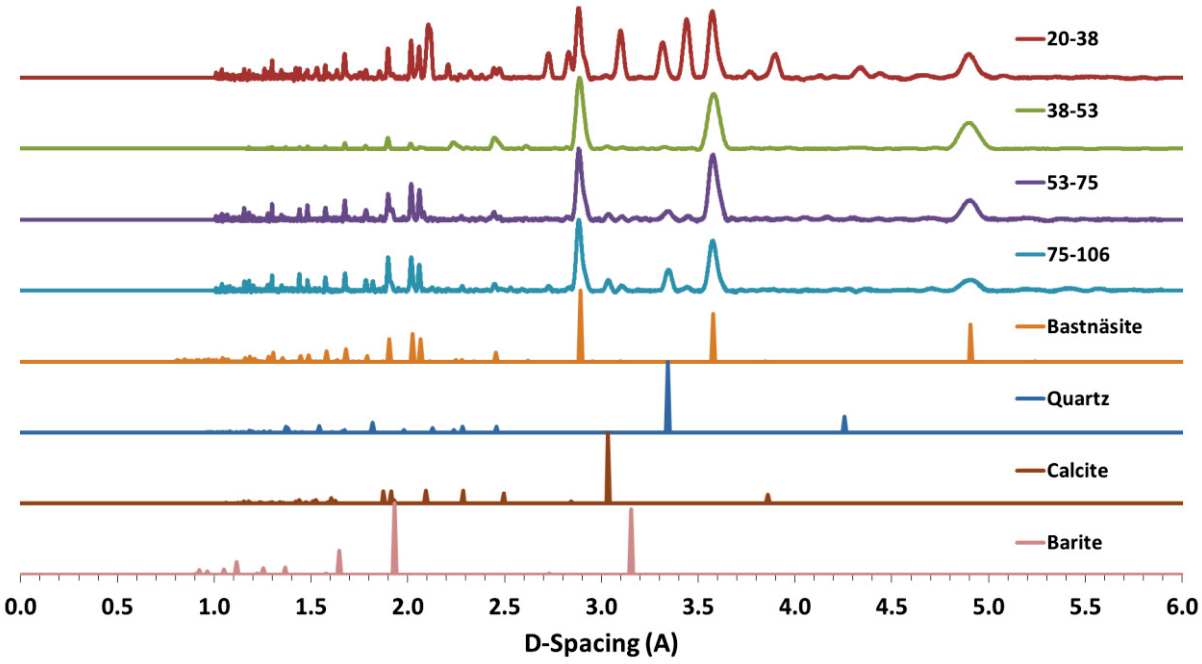

Figure 4.3 – XRD patterns of the purified Mountain Pass bastnäsite samples of various size ranges. Reference patterns are provided for all major minerals from the Mountain Pass deposit. All diffraction peaks have been normalized to the maximum peak intensity for each pattern

4.4.1.4 Quartz

Quartz was ground in a rod mill and then screened (wet and dry) to obtain a -106 +38 µm fraction for microflotation testing. A portion of the quartz was further screened to produce a narrowly sized -53 +38 µm microflotation fraction. For zeta potential analysis the quartz was wet ground in a Pulverisette 6 planetary monomill (Fritsch, Germany) to produce a fine fraction (d_{50} = 5.3 µm for quartz/allanite experiments, d_{50} = 2.9 µm for quartz/bastnäsite experiments) for zeta potentials. Particle size was determined using a LA-920 particle size analyser (Horiba).

4.4.2 Ore preparation

4.4.2.1 Feed for initial pre-concentration

The first batch of ore (Batch 1) was initially crushed to a top size of 850 µm using a jaw and cone crusher. After crushing, a portion of the ore was stage pulverized for 4.5 min in 1 kg batches in a T100 ring and disc pulveriser (Siebtechnik, Germany) to a P_{80} of 53 µm to be fed to the Knelson Concentrator; a second portion of the ore was ground dry for 15 min in a rod mill before being stage pulverized to a P_{80} of 44 µm and fed to the Falcon Concentrator. The different comminution steps were chosen to maximize mineral liberation without compromising gravity concentrator effectiveness, while also avoiding the overproduction of excessively fine (< 5 µm) material.

Experimental results obtained using the Batch 1 sample are shown in the publications included in the Appendix

4.4.2.2 Feed for final flowsheet

The second batch of ore, with an initial top size of 3.36 mm, was supplied in 2 kg bags, which were subsequently riffled and recombined to ensure representative samples for further processing. For Batch 2 flowsheet experiments, a 192 kg sample of ore was ground dry in 13 kg batches in a laboratory rod mill (custom built 29 cm x 60 cm with rotation speed of 46 rpm) for 30 min, followed by dry grinding in 3.25 kg batches in a laboratory F.C. Bond Bico ball mill (Bico, USA) for 65 min. The resultant product had a P_{80} of 40 µm. For mineralogical analysis a representative sample of the milled feed was wet screened at 20 µm (with 58 wt. % passing 20 µm) and both resultant size fractions were sent for analysis to determine the bulk mineralogy and REE chemical composition.

4.5 Gravity separations

4.5.1 Knelson Concentrator

The Knelson Concentrator used in this thesis was a lab-scale model (KC MD3) obtained from FLSmidth Knelson (Canada).

4.5.1.1 Initial pre-concentration

Initial pre-concentration of the ore was conducted using the Knelson Concentrator operated at a material flow rate of 300 - 400 g/min. The slurrying water flow rate varied from 2.3 to 2.9 L/min, the fluidizing water flow rate varied from 6 to 9 L/min and the operating water pressure was 2.5 - 3 psi. During operation the concentrator was stopped every four minutes to remove the accumulated concentrate.

4.5.1.2 Final flowsheet

For the final gravity separation experiments the Knelson Concentrator was operated on an 8 kg batch basis with a feed rate of 200 g/min. The Knelson was stopped every 4 minutes to remove the accumulated concentrate from the bowl (which was subsequently dried), while the tailings stream was accumulated in an intermediate 20 gallon drum. The fluidizing water to the Knelson Concentrator was set at 6 L/min with slurrying water set at approximately 2 L/min.

The Knelson Concentrator was operated at 58% of the maximum motor speed (equivalent to a centrifugal acceleration of 40 times Earth's gravitational acceleration) The Knelson Concentrator rotation speed was deliberately set at a low level to provide a lower centrifugal acceleration due to the relatively small differences in specific gravity of the value and gangue minerals in the ore. It is well established that increased gravitational acceleration will provide an enhanced settling velocity. However, Luttrell *et al.* (1995) showed that for material with SG values of 4.8 and 2.5 (very similar to the value and gangue minerals, respectively, in the Nechalacho deposit) the curves of settling velocity versus particle size are significantly higher in magnitude at elevated centrifugal accelerations, especially for larger particle sizes. As the Knelson in this work is expected to concentrate any coarse particles remaining in the feed after grinding, it is important to choose a low value of centrifugal acceleration in this system. In this way, the settling velocities experienced by coarser particle sizes of low SG are not so elevated that the conditions for selective concentration of higher SG particles are eliminated.

Throughout the gravity separation flowsheet processes, at least 1 sample was taken from each stream for every 8 kg processed. The flowsheet corresponding to these operating conditions may be seen in Figure 4.4.

4.5.2 Falcon Concentrator

The Falcon Concentrator used in this thesis was a lab-scale model (SB-6A) equipped with an ultra-fine bowl and obtained from Sepro Mineral Systems, Canada.

4.5.2.1 Initial pre-concentration

The ultrafine bowl was used in the Falcon Concentrator as it is designed especially for concentrating high specific gravity fines, is smooth-walled and has no fluidizing water. The slurrying water flow rate during operation was 4.7 L/min and the mass flow rate was approximately 400 g/min. During operation, the Falcon Concentrator was stopped every four minutes to remove the accumulated concentrate.

4.5.2.2 Final flowsheet

For the final flowsheet experiments, the Falcon Concentrator was operated at 1,550 rpm (equivalent to a centrifugal acceleration of 130 times Earth's gravitational acceleration). This was chosen due to the use of a different bowl geometry (Ultra-Fine), the lack of fluidizing water and the assumption that the feed to the Falcon would contain no significant concentration of very coarse particles. The flowsheet corresponding to these operating conditions may be seen in Figure 4.4.

Once sufficient tailings from the Knelson were accumulated (*i.e.* the intermediate drum was approximately half full), the tailings slurry was mixed and then pumped to the Falcon Concentrator which was operated in a batch basis with 30 minute intervals between concentrate removals. The longer batch time for the Falcon was chosen due to the expected decrease in high specific gravity mineral content in the Knelson gravity tailings. Additionally, the mechanism of particle capture in the Falcon ultrafine bowl is different than that of the Knelson in that the concentrate capacity is significantly higher than the limited volume in the riffles of the Knelson bowl.

4.6 Magnetic separations

4.6.1 Dry Variable Intensity Magnetic Separator (DVIMS)

During the final gravity and magnetic flowsheet experiments the feed to the dry magnetic drum separator consisted of the oversize material (+300 µm) from the Knelson gravity concentrate. This material was removed due to particle size limitations of the wet drum magnetic separator. The oversize material was split into 4 different size fractions (300-425 µm, 425-600 µm, 600-1180 µm, 1180-1700 µm) and then each size fraction was passed through a series of drum magnetic separations at different magnetic field strengths (0.5, 1.0, 1.5 and 2.0 T). At each field strength the material was passed through a rougher and cleaner separation with scavenger stages for both rougher and cleaner non-magnetic products. The flowsheet corresponding to these operating conditions may be seen in Figure 4.5.

4.6.2 Wet High Intensity Magnetic Separator (WHIMS)

Wet high intensity magnetic separation (WHIMS) was conducted using a laboratory scale wet variable intensity magnetic separator (BoxMag Rapid, UK). The feed to the wet high intensity magnetic separation stage consisted of the non-magnetic product from medium intensity wet drum magnetic separation of both the Knelson and Falcon gravity concentrates respectively. The wet high intensity magnetic separation was conducted by slurrying a 50 g representative sample with 250 mL of water and then passing the resultant slurry through the magnetic matrix at increasing applied magnetic field strengths (0.1, 0.4. 0.7 and 0.9 T). After every separation stage the non-magnetic fraction was reprocessed at an increased magnetic field strength, while the magnetic material trapped in the matrix of the separator was removed as the magnetic concentrate. The flowsheet corresponding to these operating conditions may be seen in Figure 4.6.

4.6.3 Low Intensity Drum Magnetic Separator

Low intensity magnetic separation was conducted using a lab-scale model WD(20) wet drum permanent magnetic separator (Carpco Inc., USA) with the ability to modulate the magnetic field intensity by switching the iron-based (low intensity; 0.03 T at drum surface) permanent magnets to rare earth (medium intensity; 0.3 T at drum surface) permanent

magnets. The magnetic drum separator was fed with the concentrates from both the Knelson and the Falcon (each concentrate was fed separately). Due to the presence of coarse particles the Knelson gravity concentrate was screened at 300 μm with only the undersize fed to the magnetic separator. Each gravity concentrate was initially fed to the low intensity separator to remove strongly ferromagnetic iron oxide minerals followed by a medium intensity magnetic separation stage to target any remaining iron oxide minerals as well as strongly paramagnetic REM. Solid flow rates to the wet drum magnetic separator varied from 100-300 g/min with slurrying water added at a rate of 1.2-2.2 L/min. Wash water was applied to the drum at a rate of 0.4-0.8 L/min to minimize entrainment of non-magnetic material.

Due to the very high concentration of strongly magnetic iron oxide minerals (and consequently very high magnetic mass pull) in the Knelson gravity concentrate, this magnetic product was reprocessed through the low intensity wet drum magnetic separator prior to medium intensity magnetic separation. The flowsheet corresponding to these operating conditions may be seen in Figure 4.4.

4.7 Surface chemistry techniques

4.7.1 Electrophoretic zeta potential

Electrophoretic zeta potential measurements in this thesis were carried out using a ZetaPlus analyser (Brookhaven Instruments, USA). To prepare suspensions for measurement, mineral particles were suspended in 200 mL solutions at a solids concentration of 0.08 wt. %. Before each measurement the mineral particle suspensions were allowed to equilibrate for a minimum of 30 min. Zeta potential measurements were carried out from pH 3 to pH 10, the largest range possible with this equipment. At each new pH level the suspension was allowed to equilibrate for at least 5 min. Similarly the suspension was allowed to condition for a minimum of 5 minutes after each addition of collector. In order to avoid zeta potential hysteresis, different suspensions were made for titrations from natural pH to the acidic and basic regions respectively.

For measurements without activating ions, the background electrolyte used was 10^{-3} M KCl with an identical molar concentration of metal cations maintained for measurements

with ferric and ferrous chloride as well as lead chloride (*i.e.* 10^{-3} M for $FeCl_2$, $FeCl_3$ and $PbCl_2$). In the case of measurements with both activator and collector the mineral particles were first suspended in 100 mL of the metal chloride solution at a concentration of 2 x 10^{-3} M for 30 min before adding 100 mL of benzohydroxamic acid at a concentration of 1.17 x 10^{-3} M and conditioning for an additional 30 min. This resulted in a final concentration in the mineral suspension of 10^{-3} M metal cations and 5.83 x 10^{-4} M benzohydroxamic acid.

4.7.2 Electroacoustic zeta potential

Electroacoustic zeta potential measurements were conducted using a FieldESA (PartikelAnalytik, Germany) equipped with an automatic titration unit and a small volume (~80 mL) cell. To prepare samples for electroacoustic measurements the appropriate amount of material was suspended in 60 mL of 10^{-3} M KCl to yield a 5 wt. % suspension, and then sonicated for 30 s using a UP400S ultrasonic processor (Hielscher, Germany) to ensure complete particle dispersion. The suspension was then transferred to the electroacoustic cell and allowed to condition until both pH and zeta potential stabilized. After this point (approximately 1 h) a pH titration was conducted in steps of 0.25 pH units to pH 10 and then back to pH 3. An interval of 300 s prior to zeta potential measurement at each pH allowed the suspension to equilibrate. In the case of reagent additions the reagent in question was added with the aid of the automatic titration unit in set intervals with a delay of 300 s before each zeta potential measurement. After the full reagent addition was complete, a pH titration was then carried out on the mineral suspension. For electroacoustic measurements in the presence of benzohydroxamic acid, a stock solution of benzohydroxamic acid was prepared at a concentration of 1.6 g/L and this solution was titrated into the mineral suspension in steps of 0.5 mL up to a total addition of 10.5 mL (1.73 x 10^{-3} M).

4.8 Froth flotation separations

4.8.1 Modified Partridge-Smith microflotation cell

4.8.1.1 Single mineral

Microflotation tests were conducted using a 65 mL modified Partridge-Smith flotation column (Partridge & Smith, 1971). The outer diameter of the microflotation column is 25 mm with an inner diameter of 21.8 mm. This column employs a magnetic stir bar located on top of a fine porous frit (pore size < 5 μm) through which air was passed at a flow rate of 36 mL/min. Material transported into the froth phase during the test overflows the top of the cell and was collected in the launder that encircles the top of the column. Prior to flotation, 1 g of mineral per test was conditioned in 40 mL of solution (distilled water + collector) for 5 minutes under constant agitation. The resultant suspension was then transferred to the flotation column using 20 mL of distilled water. The initial water level of each test was set to the same level using distilled water. After the air was connected, two drops of 20 mg/mL frother were added to ensure the frother concentration was in excess of the critical coalescence concentration (CCC). The CCC defines the concentration of frother needed to fully prevent bubble coalescence as first discussed by Cho & Laskowski (2001). Frothers used included MIBC (a relatively weak frother) and F150 (a strong frother) (Cappuccitti & Finch, 2008). The CCC_{95} (an alternative measure for the critical coalescence concentration) values for MIBC and F150 are 11.2 and 6 ppm respectively (Zhang *et al.*, 2012). Papers by Cho & Laskowski (2001) and Zhang *et al.* (2012) offer a good summary of the critical coalescence concentration concept as well as CCC_{95} values for various frothers. Froth collection was performed for 1 min (with the exception of microflotation rate experiments) per test, beginning with the initial appearance of air bubbles in the cell. A schematic view of the microflotation cell, along with an image of the cell, may be seen in Chapter 2 (Figure 2.14).

4.8.1.2 Single mineral with activators

For microflotation experiments with activators, conditioning was conducted by suspending 1 g of mineral (38-53 μm) in 40 mL of metal chloride solution for 5 min under constant agitation, and then transferring this suspension to the microflotation cell. The concentration of iron chloride was selected so that the molar concentration of Fe cations

per unit surface area calculated from average particle sizes (allanite = 3.53 x 10^{-3} M_{Fe}/m^2, quartz = 3.73 x 10^{-3} M_{Fe}/m^2) was kept constant. The concentration of lead chloride added was kept constant on a molar basis resulting in different molar concentrations of Pb cations per unit surface area (allanite = 1.50 x 10^{-4} M_{Pb}/m^2, quartz = 9.94 x 10^{-5} M_{Pb}/m^2). This was calculated using the measured d_{50} particle sizes of the mineral samples used for electrophoretic measurements as well as an assumed d_{50} of 45 µm for the 38-53 µm fraction used in microflotation.

In the case of flotation with both metal chloride and benzohydroxamic acid, 1 g of mineral particles were conditioned in 20 mL of metal chloride solution (at twice the concentration used for flotation with metal chloride only) for 5 min followed by an addition of 20 mL of benzohydroxamic acid solution and another 5 min conditioning period. The concentration of benzohydroxamic acid used was 2000 g/ton of mineral.

4.8.1.3 Mixed mineral

In the case of mixed mineral microflotation 0.5 g of quartz and 0.5 g of bastnäsite were mixed to create a binary mixture of 1 g. All other conditions related to microflotation were kept consistent with single mineral microflotation experiments.

4.8.1.4 Ore

Microflotation tests of the ore were conducted on gravity concentrates (Knelson and Falcon) produced from the Nechalacho deposit as detailed in Section 4.5. As both Knelson and Falcon concentrates contain elevated concentrations of iron oxide minerals (magnetite and hematite) a magnetic separation was necessary in order to prevent any accumulation of strongly magnetic gangue minerals onto the magnetic stir bar used in the microflotation experiments. This magnetic separation was accomplished by passing a hand magnet (field strength of ~0.5 T) through a suspension of the gravity concentrate and washing the magnetic product several times in tap water to remove any accumulated fines or non-ferromagnetic material. The remainder of each gravity concentrate was used as the feed to the microflotation experiments. All other parameters related to the operation of the microflotation cell were identical to single mineral experiments including the amount (1 g) of mineral used.

4.8.2 Lab-scale Denver flotation cell

Final flowsheet flotation tests were carried out using a 1.5 L Denver D12 lab-scale flotation cell operated at 1200 rpm with a constant air flow rate of 5.6 L/min. For each flotation test 200 g of the high grade (REM-enriched) feed were mixed with tap water in the cell, with the water level adjusted to the constant 1.2 L level line immediately prior to turning on the air. The suspension was allowed to condition for 1 min after the addition of collector (5 kg/ton benzohydroxamic acid) and pH adjustment. All flotation tests were carried out at an initial pH of 9 with 2 drops of F150 (calculated to be in excess of the CCC_{95} value) added to the cell. Concentrate collection was carried out for 5 min before reconditioning and 7 min after reconditioning. A total of 7 concentrates were collected at 0.5, 1, 2, 5, 5.5, 6 and 12 min cumulative time with the pulp level re-adjusted to approximately 1.2 L after each concentrate. The reconditioning stage consisted of 2 min of conditioning with different reagent additions depending on the test. For every test the pH was readjusted to 9 and a single drop of F150 was added.

The three different reconditioning stages investigated were: no further addition of collector, the addition of a further 5 kg/ton (relative to the initial feed mass) of benzohydroxamic acid, and the addition of 500 g/ton (relative to the intial feed mass) of $PbCl_2$ followed by 5 kg/ton of benzohydroxamic acid. In the case of the dual addition of lead and benzohydroxamic acid, the suspension was allowed to condition for 1 min with the lead followed by 1 min with the benzohydroxamic acid.

For each test fresh solutions of benzohydroxamic acid and lead chloride were prepared by dissolving the 1 g and 0.1 g respectively in approximately 150 mL of deionized water to form aqueous solutions. The lead chloride solution was adjusted to pH 9 prior to adding it to the cell. The flowsheet corresponding to these operating conditions may be seen in Figure 4.7.

4.9 Flowsheets

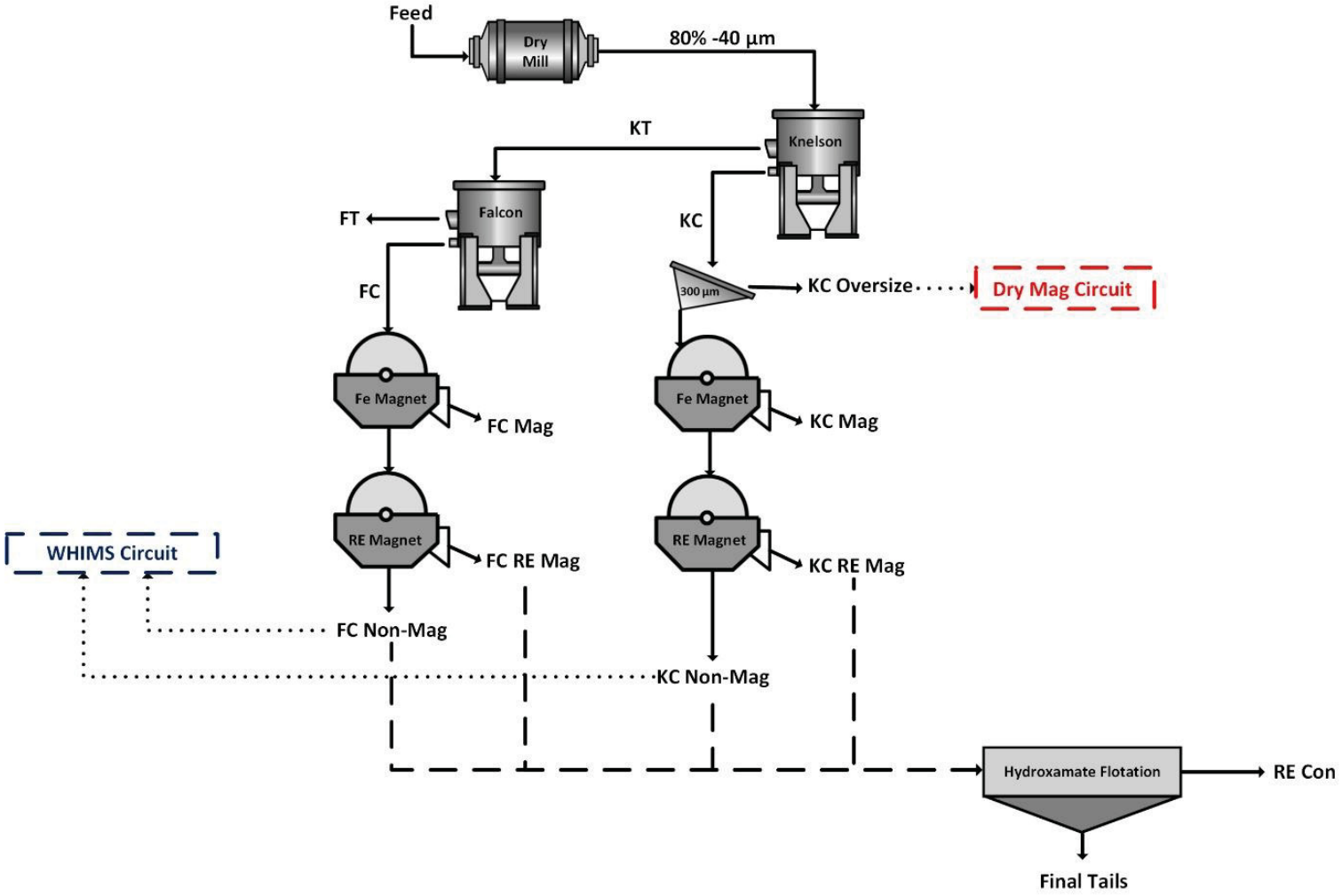

Figure 4.4 – Final flowsheet of gravity and magnetic separations to pre-concentrate rare earth minerals

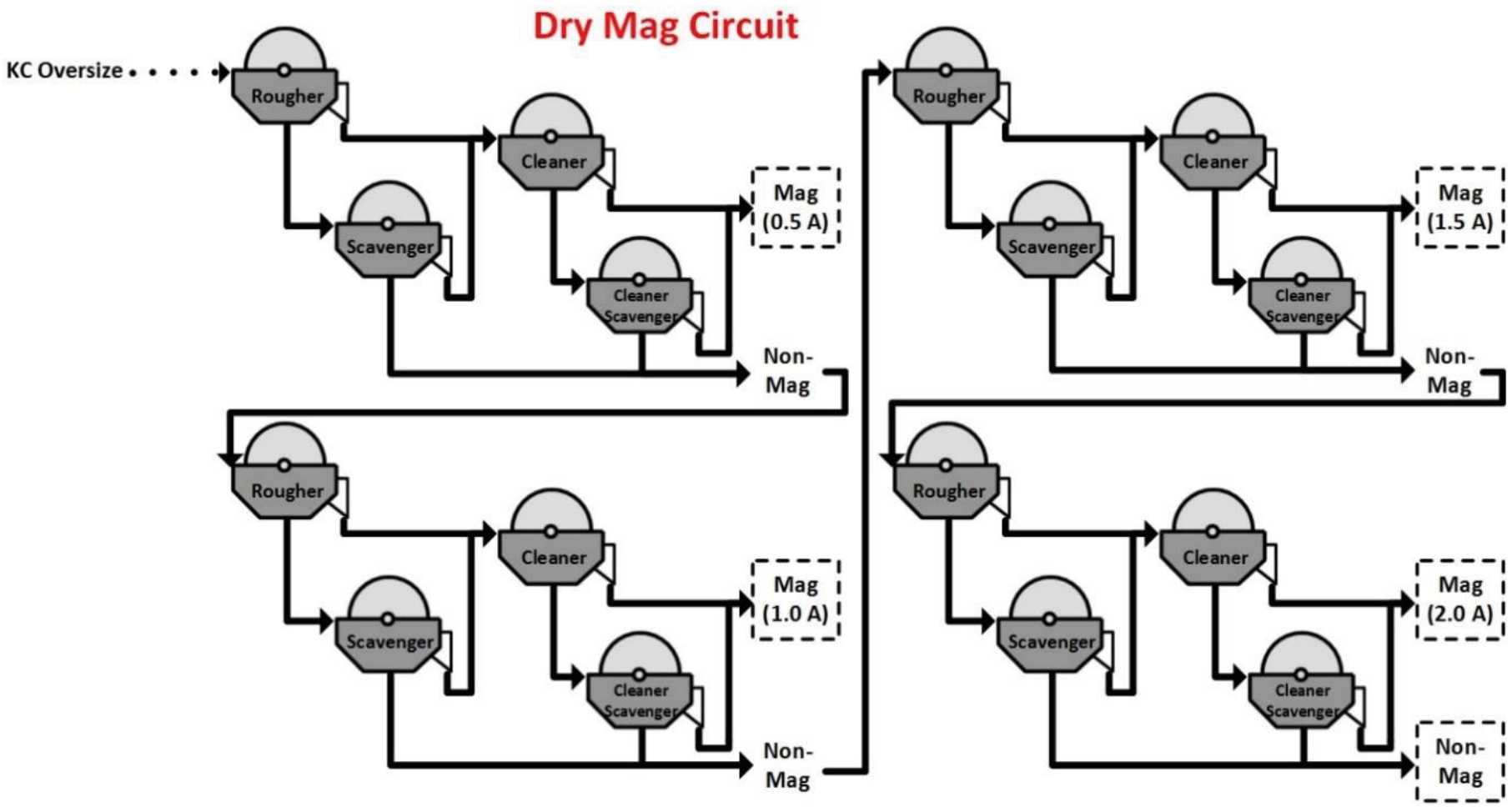

Figure 4.5 – Dry magnetic separation flowsheet applied to oversize (> 300 µm) material from the final flowsheet Knelson gravity concentrate

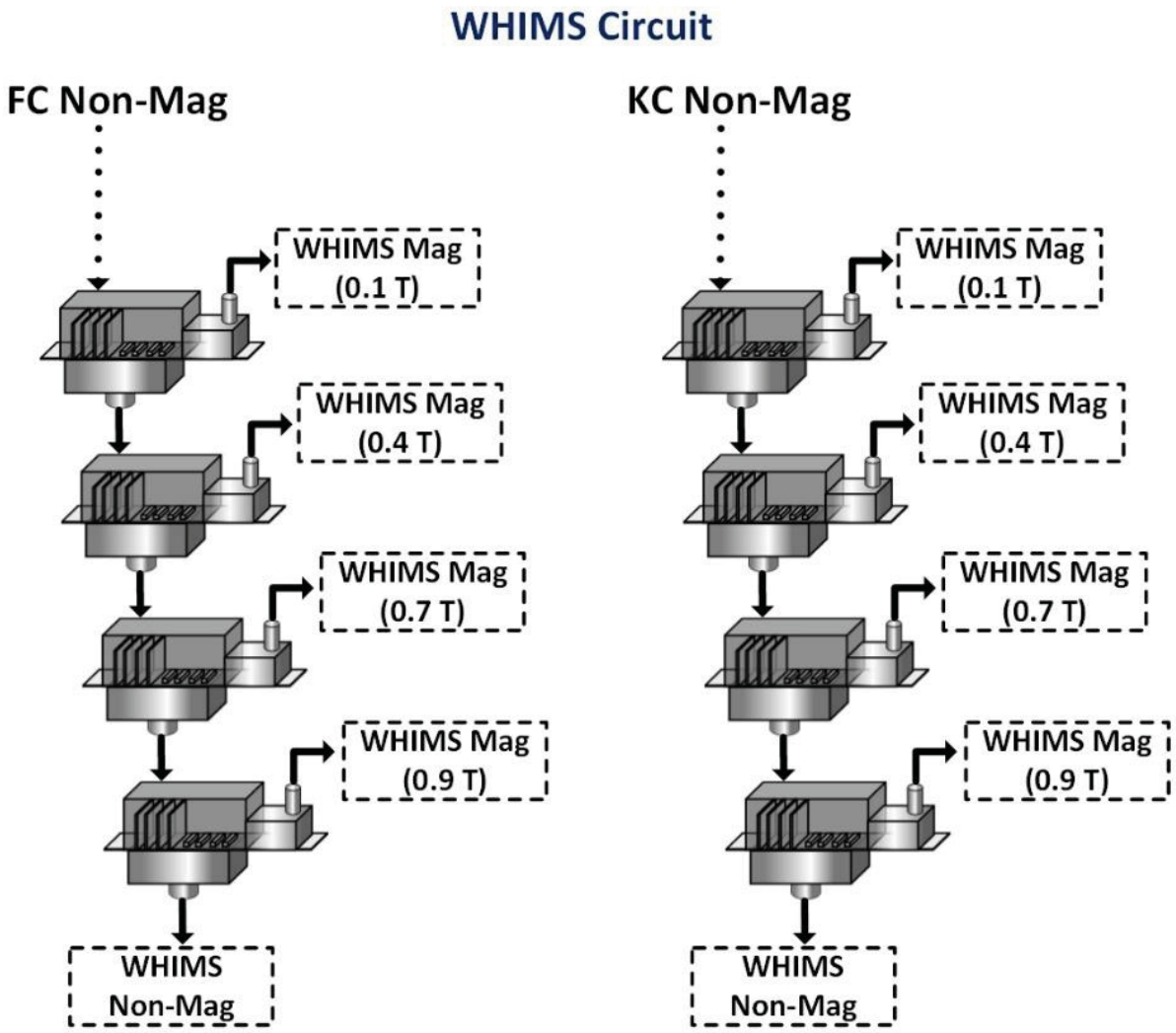

Figure 4.6 – Flowsheet of wet variable intensity magnetic separations applied to gravity tailings produced from final physical separations flowsheet

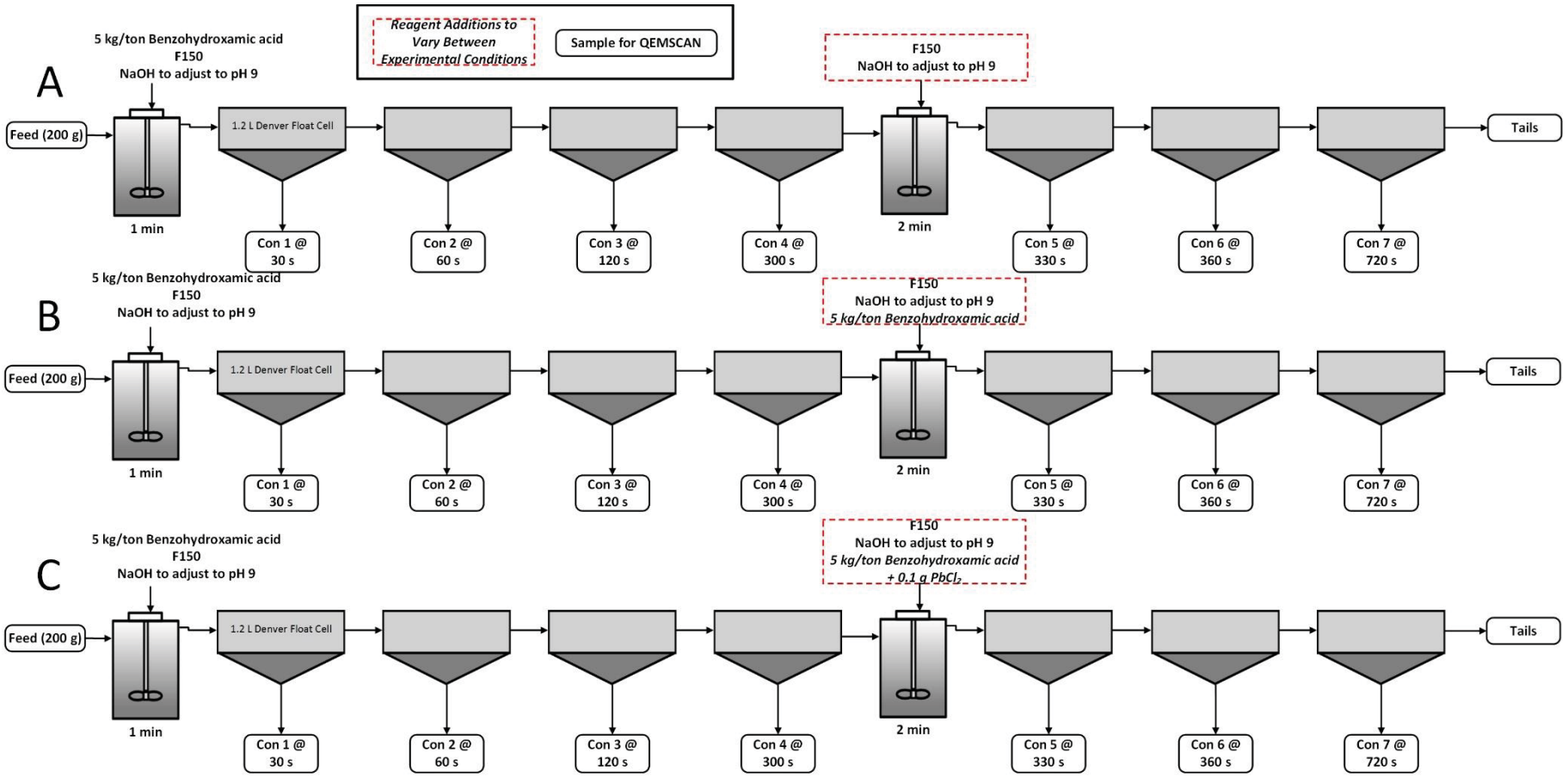

Figure 4.7 – Schematic of flotation conditions for final flotation experiments

4.10 Conclusions

This chapter has detailed the experimental conditions employed throughout this thesis along with the corresponding flowsheets where appropriate. Readers interested in the operating principles and theory of a given separation or characterisation technique should consult Chapter 2.

5. Properties of Single Minerals

5.1 Introduction

This chapter presents the results of investigations into the properties of single minerals found in the Nechalacho deposit. These minerals are investigated from the standpoint of their magnetic properties, surface chemistry and microflotation response. The findings presented here are used to inform the flowsheet design applied to the Nechalacho deposit in Chapters 6 and 7.

5.2 Vibrating sample magnetometer measurements

The magnetisation as a function of magnetic field strength for selected pure minerals representing gangue minerals from the Nechalacho deposit (magnetite, hematite and quartz) can be seen in Figure 5.1. As expected, magnetite (Fe_3O_4) exhibits a clear ferromagnetic tendency with a large saturation magnetisation value while hematite exhibits a slight ferromagnetic tendency with a much smaller saturation magnetisation. While magnetite is in fact ferrimagnetic (with magnetic moments of unequal magnitude aligned in an antiparallel orientation such that the material experiences a net magnetic moment) its magnetic response in the VSM can, for mineral processing purposes, be considered to be identical to that of a ferromagnetic material (Jakubovics, 1994). Two different samples of quartz were analysed with both exhibiting an unexpected ferromagnetic behaviour. This is likely due to the presence of ferromagnetic impurities originating from the quartz crystals or introduced during pulverising. In order to remove the effect of the ferromagnetic impurity on the quartz 2 trend the quartz data was analysed using a Honda-Owen plot. In order for this analysis to be valid the quartz must be assumed to be present in a binary mixture with the ferromagnetic impurity. The resultant diamagnetic and ferromagnetic trends can be seen in Figure 5.2. The resolved diamagnetic trend of the quartz sample has a slope (susceptibility) of -7.25×10^{-6}, which is within the expected range for a diamagnetic material (Jiles, 1990).

The VSM results for bastnäsite and fergusonite can be seen in Figure 5.3. Both of these minerals are reported in literature to be paramagnetic and it can be seen that the general trends for both minerals are also linear, paramagnetic trends. The fergusonite sample

was not completely pure and as such the trend appears to indicate that there may be a competing diamagnetic mineral present as well in the sample that was analysed. No prior work has reported the susceptibilities of these two minerals however there is reported empirical evidence to suggest that fergusonite is more strongly paramagnetic than bastnäsite (Rosenblum & Brownfield, 1999).

The VSM results for two different zircon samples, from two different localities, can also be seen in Figure 5.3. The zircons, similar to the quartz samples, exhibit a slight ferromagnetic trend. Assuming a binary mixture of ferromagnetic impurity and zircon mineral allows the determination of the zircon's magnetic susceptibility from a Honda-Owen plot. The results of this analysis can be seen in Figure 5.4 and Figure 5.5. The zircon crystals from Brazil and Sri Lanka, after removing the ferromagnetic aspect from each VSM trend, exhibit magnetic susceptibilities of 2.50×10^{-6} and 7.04×10^{-7} respectively. This indicates that both zircons are slightly paramagnetic. This is in disagreement with the generally reported data on the magnetic behaviour of zircon (Moustafa & Abdelfattah, 2010; Rosenblum & Brownfield, 1999) although zircon may also have different magnetic properties dependent on its composition (Raslan, 2009).

As the zircons analysed were single crystals there was no possibility of a ferromagnetic impurity being introduced during pulverising or any other sample preparation. Therefore, the ferromagnetic and paramagnetic tendencies measured must be due to the presence of magnetic elements within the crystal lattices of the two zircon minerals. Given the significant concentration of REE within the crystal structure of zircon from the Nechalacho deposit it seems likely that the magnetic behaviour of the REE-bearing zircon would also be non-diamagnetic as many of the REE have significant paramagnetic properties due to their unpaired electrons (Ito *et al.*, 1991).

The VSM results for allanite appear to indicate both ferromagnetic behaviour and paramagnetic behaviour (as can be seen in Figure 5.6), therefore a Honda-Owen analysis was conducted on the allanite data. The resolved ferromagnetic and paramagnetic components of the allanite trend are also shown in Figure 5.6. As allanite has been reported to be paramagnetic, the underlying assumption in the Honda-Owen analysis is

that there is a ferromagnetic impurity present along with allanite (Rosenblum & Brownfield, 1999). The calculated magnetic susceptibility of the paramagnetic component (5.15×10^{-4}) corresponds to published data, which indicate that allanite is more strongly paramagnetic than bastnäsite and has a similar magnetic susceptibility to fergusonite (Rosenblum & Brownfield, 1999). A summary of all VSM findings may be seen in Table 5.1.

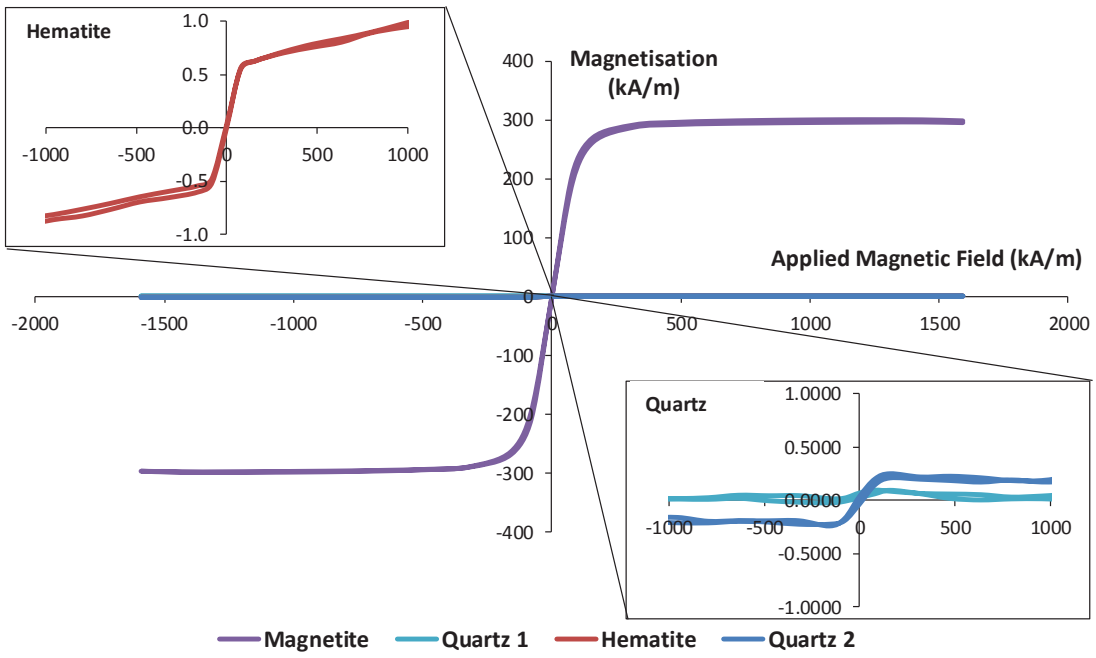

Figure 5.1 – VSM results for magnetite, hematite and quartz

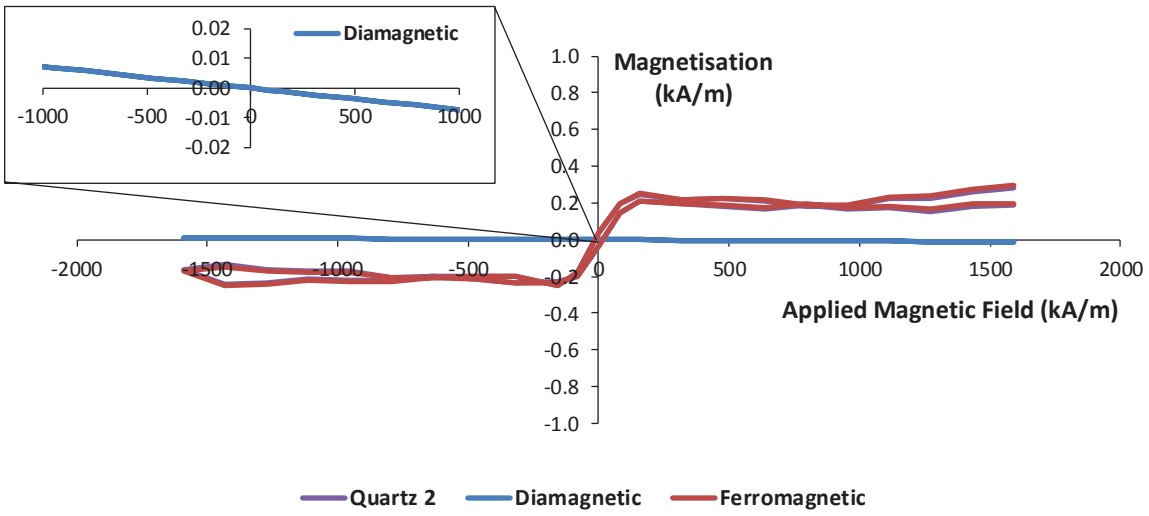

Figure 5.2 – VSM results for quartz using diamagnetic and ferromagnetic trends calculated via Honda-Owen analysis

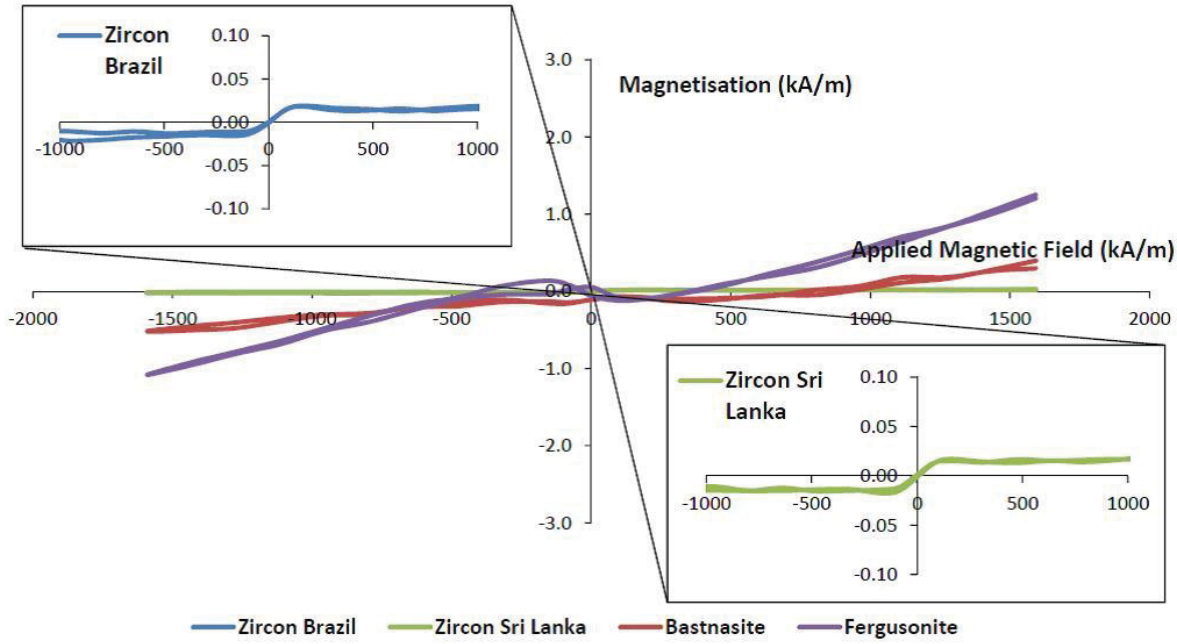

Figure 5.3 – VSM results for zircon, bastnäsite and fergusonite

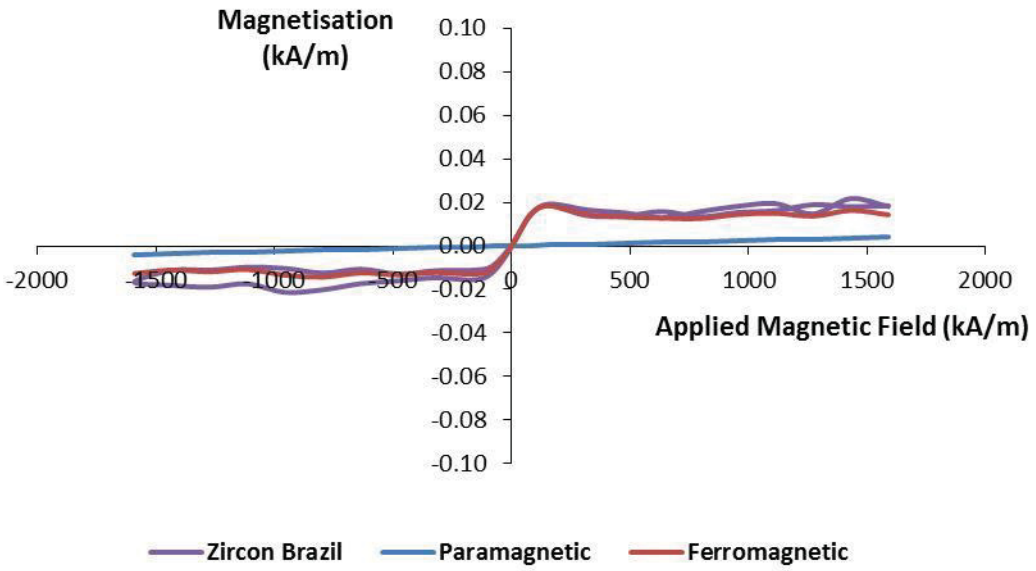

Figure 5.4 – VSM results for zircon (Brazil) including paramagnetic and ferromagnetic trends calculated via Honda-Owen analysis

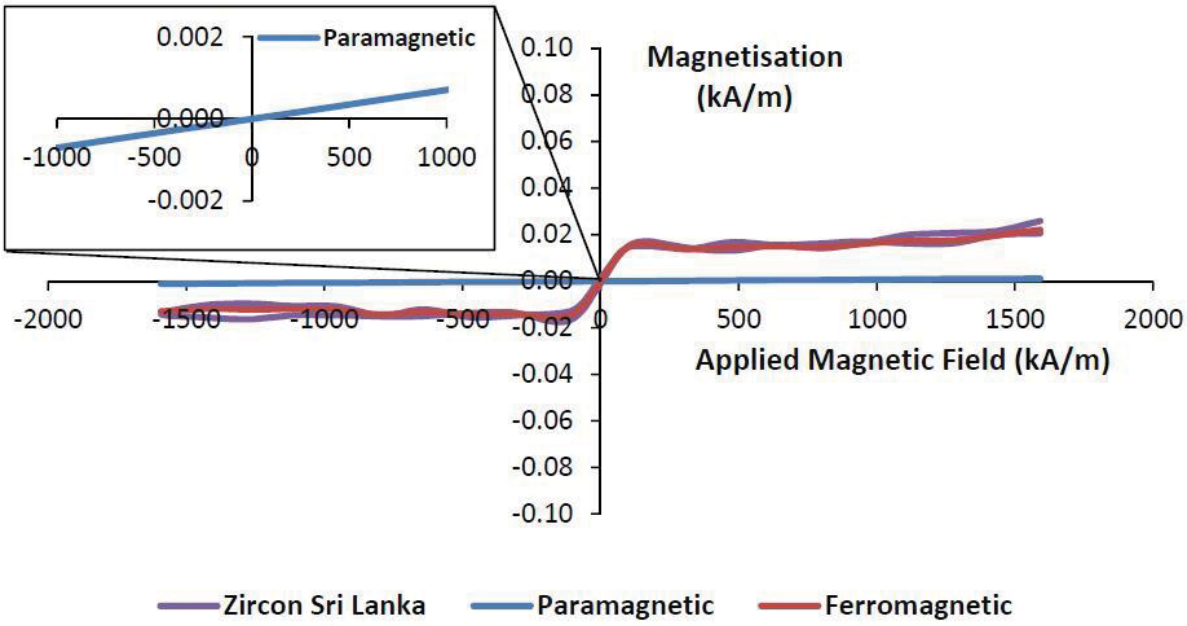

Figure 5.5 – VSM results for zircon (Sri Lanka) including paramagnetic and ferromagnetic trends calculated via Honda-Owen analysis

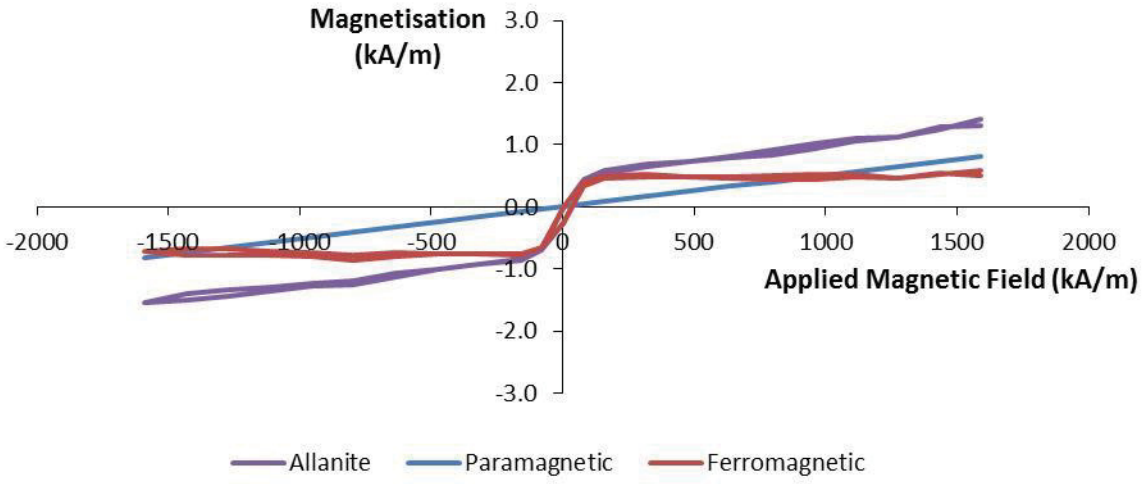

Figure 5.6 – VSM results for allanite including paramagnetic and ferromagnetic trends calculated via Honda-Owen analysis

Table 5.1 – Summary of VSM results for single minerals

Mineral	Magnetic Properties	Magnetic Susceptibility	Saturation Magnetisation (kA/m)
Magnetite	Ferrimagnetic		291
Hematite*	Para/Ferromagnetic	4.06×10^{-4}	0.1
Silica	Diamagnetic	-7.25×10^{-6}	
Bastnäsite	Paramagnetic	2.12×10^{-4}	
Allanite	Paramagnetic	4.63×10^{-4}	
Fergusonite	Paramagnetic	6.01×10^{-4}	
Zircon (Brazil)	Paramagnetic	2.50×10^{-6}	
Zircon (Sri Lanka)	Paramagnetic	2.77×10^{-6}	

*Note that hematite may have both paramagnetic and ferromagnetic behaviour (Lin, 1959). Values shown for hematite were calculated from a Honda-Owen plot for this mineral

5.3 REM chemistry

The primary REE minerals (REM) chosen for surface chemistry and microflotation experiments were bastnäsite and allanite. These minerals were chosen as they are major REE-bearing minerals in the Nechalacho deposit and were available in large enough quantities for complete surface chemical and microflotation investigations. Allanite and bastnäsite are examples of heavy REE and light REE minerals due to their different mineral structures and coordination numbers (as discussed in Chapter 3). A representative sample of each mineral was analysed for REE content with the results

shown in Figure 5.7 (on a REO basis). It can be seen in this figure that while the total REO content of allanite is significantly lower than that of bastnäsite, the concentration of high value heavy REE such as Dy and Y are actually higher in the allanite sample. This is an important consideration in the beneficiation of REM, efforts should be placed on concentrating the minerals containing high levels of heavy REE as these are the elements which will drive a project's economics.

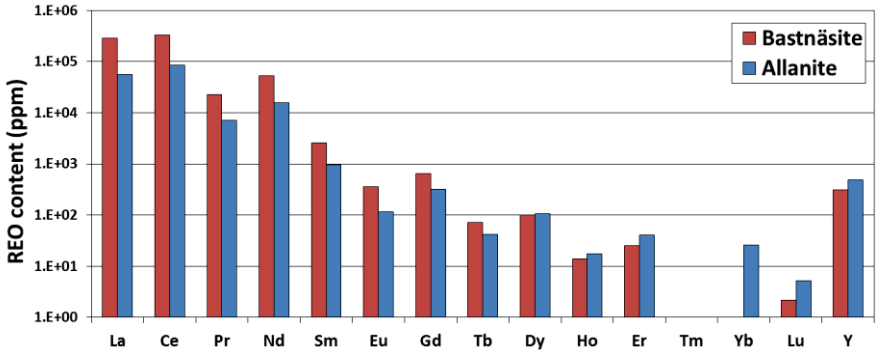

Figure 5.7 - REO composition of bastnäsite and allanite used in this work

5.4 Zeta potentials

The traditional means of displaying zeta potential data consists of conducting multiple measurements at each discrete pH level investigated, averaging these measurements, and then representing the zeta potential of the mineral as a set of discrete data points (often with accompanying error bars). In this work, the trends of all minerals and reagent combinations were fit to third-order polynomials (appropriate for the behaviour observed in the systems investigated in this work) with accompanying 95 % confidence intervals calculated using a commercial statistical software package (Stata 13, StataCorp). This was done in order to provide an indication of error for each dataset while maintaining sufficient visual simplicity in the resultant graphs. This technique was first employed for zeta potential data in Marion *et al.* (2015) and the approach used in this work is very similar. A detailed explanation of the statistical approach used is available in Marion *et al.* (2015) and a representative dataset from electrophoretic zeta potential investigations of bastnäsite is shown in Figure 5.8. It can be seen that the averages for each discrete pH level fall approximately within the calculated confidence intervals. The bulk of the actual

data points fall outside the confidence intervals, but are captured within the calculated prediction limits. These prediction limits indicate the accuracy interval for the prediction of a future zeta potential measurement using the fitted third-order polynomial (Marion *et al.*, 2015). As the purpose of zeta potential measurements in this work is the comparison of different mineral-reagent systems and not the precise determination of system zeta potentials, the inclusion of only the confidence intervals in the zeta potential graphs was considered appropriate.

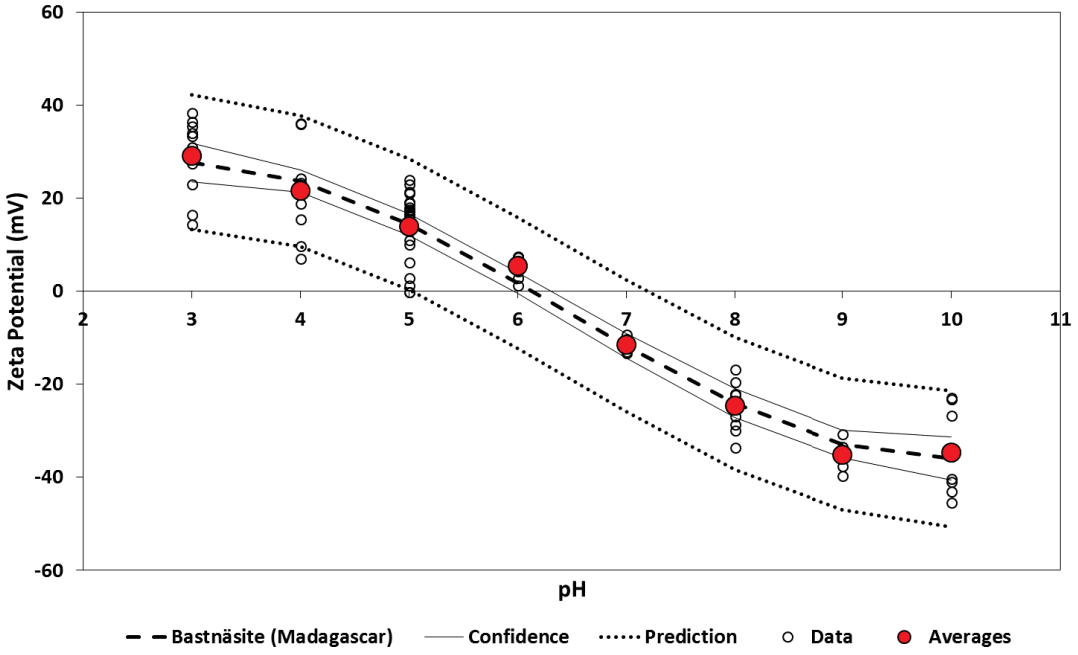

Figure 5.8 – Zeta potential as a function of pH for bastnäsite (Madagascar) determined electrophoretically with accompanying averaged data, fitted third order polynomial trendline, 95 % confidence intervals and 95 % prediction limits

When determining zeta potential electroacoustically an automatic titration unit is generally used, resulting in repeat tests measuring zeta potentials at slightly dissimilar pH levels. One approach to presenting this data would be to average all zeta potential measurements for a certain pH interval (*i.e.* 0.5 pH units). In this work it was decided to instead use the third-order polynomial technique described earlier for electrophoretic measurements. An example of the resultant polynomial with calculated confidence and prediction intervals can be seen in Figure 5.9. Similar to Figure 5.8 it can be seen that the

bulk of the measured values exceed the 95 % confidence intervals however it is also visually apparent that the fitted polynomial represents the approximate averaged behaviour of this system.

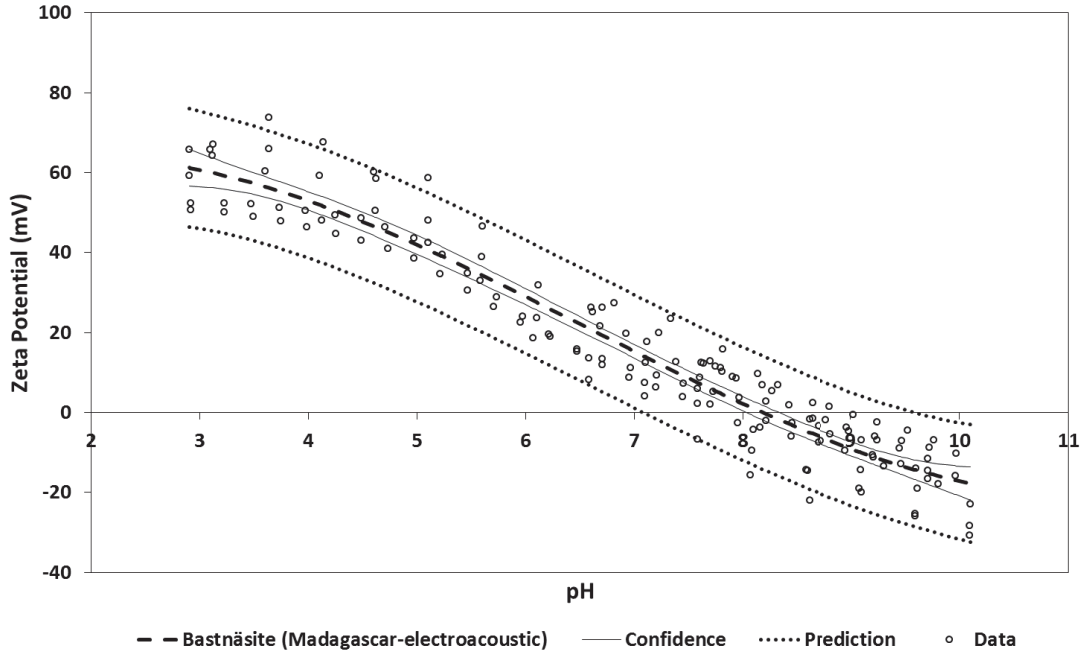

Figure 5.9 – Zeta potential as a function of pH for bastnäsite (Madagascar) determined electroacoustically with accompanying fitted third order polynomial trendline, 95 % confidence intervals and 95 % prediction limits

5.4.1 Electrophoretic zeta potentials

5.4.1.1 Single minerals

The zeta potentials for selected pure minerals representing the minerals from the Nechalacho deposit may be seen in Figure 5.10. It can be seen that the minerals from the deposit have a variety of isoelectric points (IEPs): approximately 6.5 for bastnäsite; 4 for allanite; 3.5 for the zircon sample from Sri Lanka; and no IEP observed across the pH range tested for the zircon sample from Brazil, as well as quartz. As there was insufficient sample available for more than an initial zeta potential investigation, no further experiments were possible with the zircon samples.

The single mineral zeta potential results in Figure 5.10 display the expected negative zeta potential trend for quartz over this pH range (Deju & Bhappu, 1967; Fuerstenau, 1956;

Kosmulski, 2001; Li & De Bruyn, 1966). The zeta potential results for bastnäsite indicate an IEP at pH 6.2 (Madagascar) and at pH 6.4 (Mountain Pass) for this mineral which is well within the range of IEP values reported in literature as discussed earlier in Chapter 3. The close alignment of these isoelectric points would appear to indicate that mineral origin plays a smaller role in observed bastnäsite IEP variations than the measurement technique employed. The data for allanite indicates an isoelectric point for this mineral at pH 4. This finding is consistent with work by Deju & Bhappu (1967) who showed that silicate minerals with higher O:Si ratios (2:1 for quartz, ~4:1 for allanite) will have an IEP shifted to a higher pH. The speculated explanation for this behaviour is that silicate minerals with higher O:Si ratios will have higher H^+ surface adsorption. The zeta potential trends of both allanite and quartz minerals look very similar (with the allanite shifted upwards) suggesting that perhaps the sorosilicate structure of allanite is very similar in surface behaviour to that of quartz. The O:Si ratio in zircon is also approximately 4:1, similar to allanite. The zeta potential trend of one of the zircon samples (Sri Lanka) is shifted relative to quartz whereas the zeta potential trend of the other zircon sample (Brazil) is similar to quartz.

In this Chapter the properties of value minerals such as bastnäsite and allanite are compared to quartz, a common silicate gangue mineral. These comparisons are made in order to predict separability in mixed mineral systems.

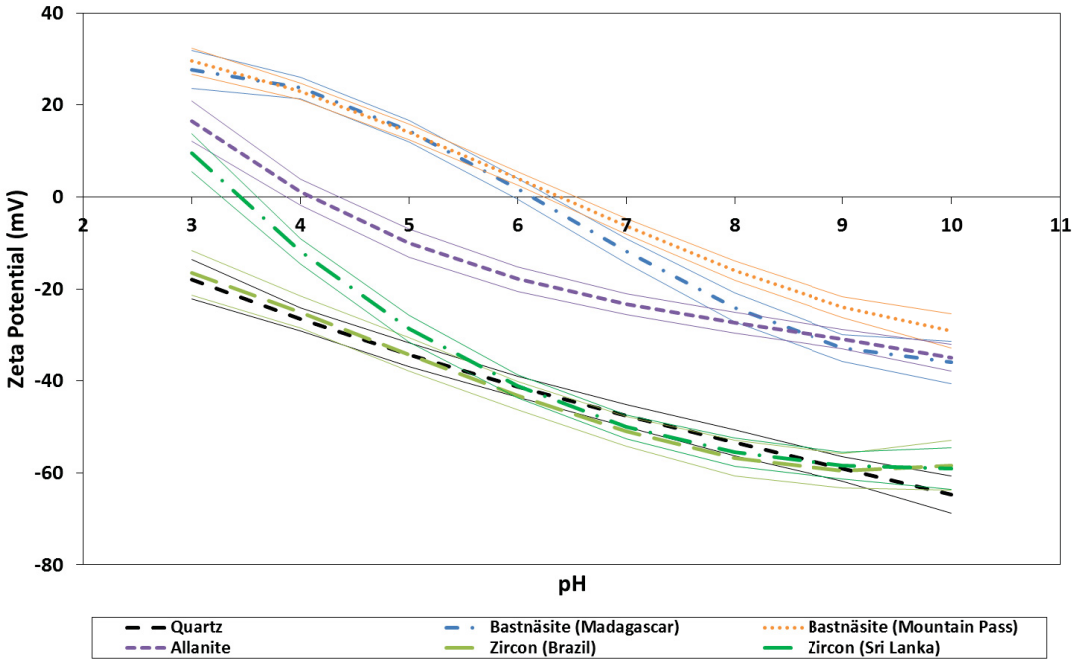

Figure 5.10 - Zeta potential as a function of pH for pure minerals. Confidence interval lines represent 95 % confidence about a third order polynomial trendline

5.4.1.2 Bastnäsite and quartz

The zeta potential results for bastnäsite (Madagascar and Mountain Pass) and quartz with various flotation reagents may be seen in Figure 5.11 to Figure 5.14. Figure 5.11 to Figure 5.13 include the single mineral trends as well as zeta potential data for these three minerals in the presence of different flotation collectors (benzohydroxamic acid, sodium oleate and Flotinor SM15 respectively). The collector concentration used in these zeta potential experiments was determined empirically by adding increasing amounts until the deviation (or lack thereof) in zeta potential was satisfactorily established. The molar concentration for Flotinor SM15 was not calculated as the molar mass of Flotinor SM15 was not provided by the manufacturer.

The zeta potential data in Figure 5.11 of bastnäsite and benzohydroxamic acid indicates adsorption across the entire pH range investigated, particularly from pH 5 to pH 10, and a corresponding shift in the IEP to a higher pH for both bastnäsite samples. These results correspond well with previous work on a Brazilian bastnäsite sample using potassium octyl hydroxamate in that the greatest deviation between the zeta potential of the pure

mineral from that of the mineral in the presence of hydroxamate was observed in the pH range of approximately pH 5 to pH 10 (Pavez *et al.*, 1996). It is surprising, however, that an anionic collector such as benzohydroxamic acid causes a positive shift in the zeta potential of the bastnäsite surface as the work of Pavez *et al.* (1996) has shown that octyl hydroxamate adsorption causes the bastnäsite surface to become more negative. The finding reported here with benzohydroxamic acid is also in contradiction to the observed effect of octyl hydroxamate on other oxide mineral surfaces where the presence of octyl hydroxamate results in a more negative zeta potential (Fuerstenau & Pradip, 2005). A possible explanation for the increased positive surface charge of bastnäsite in the presence of benzohydroxamic acid may be the adsorption of positively charged REE metal-hydroxamate complexes produced from the reaction of the undissociated hydroxamic acid molecule and hydrolysed REE cations in the bulk solution as outlined in Chapter 3.

As the pK_a of benzohydroxamic acid is between pH 8 and pH 9, the undissociated form of benzohydroxamic acid must exist in some proportion across the entire pH range investigated (Agrawal & Tandon, 1972; Shrivastava & Ghosh, 2007; Steinberg & Swidler, 1965). At elevated pH (*i.e.* pH > pK_a) the increased presence of the hydroxamate anion may explain the decrease in benzohydroxamic acid adsorption at pH 10, suggested by the results in Figure 5.11. This is in agreement with literature explanations for the sharp decrease in mineral flotation observed in systems employing a potassium octyl hydroxamate collector at pH values significantly greater than the reagent's pK_a. Fuerstenau (2005) suggested that multilayers of hydroxamate adsorption occur at the pK_a of the hydroxamic acid as the hydroxamate anion adsorbs alongside the neutral molecule, however, if the pH greatly exceeds the pK_a, electrostatic repulsion between the mineral surface and the hydroxamate anion will prevent successful flotation (Fuerstenau & Pradip, 2005). Further investigation is required to understand the differences between octyl hydroxamic acid (the hydroxamate most often used in literature) and benzohydroxamic acid which may account for the different effects of their adsorption on the bastnäsite surface. The zeta potential data for quartz and hydroxamate indicates a lack of adsorption

which is consistent with previously published work by Hope *et al.* (2010) who were able to show that hydroxamate will not interact with a quartz surface.

The zeta potential data from Figure 5.12 of bastnäsite in the presence of sodium oleate indicates that there is a significant adsorption of sodium oleate onto the bastnäsite surface across the entire pH range. This is evident from the large change in zeta potential relative to the trend for bastnäsite without collectors. As sodium oleate is an anionic collector the mechanism of adsorption onto the bastnäsite surface at pH > ~6.3 (the IEP of bastnäsite) must be chemical in nature (chemisorption) as at alkaline pH the bastnäsite surface is negatively charged and should electrostatically repel anions. For the pH range from 3 to 6.3 it is not possible from zeta potential data alone to predict the mechanism of collector adsorption. In acidic conditions the bastnäsite surface will be positively charged resulting in electrostatic attraction for the sodium oleate anion. Given the relatively constant value of the zeta potential in the presence of sodium oleate over the pH range investigated, it seems likely that at pH < 6.3 the adsorption mechanism is a mixture of both physical (*i.e.* electrostatic or physisorption) and chemical mechanisms. The interaction of sodium oleate and quartz appears to be negligible as there is minimal change in the zeta potential of quartz when in the presence of sodium oleate. This finding is consistent with other published literature that has shown that quartz will only float with a sodium oleate collector when an activator such as Ca^{2+} is also present (Fuerstenau & Elgillani, 1967).

The zeta potential data of Flotinor SM15 and bastnäsite in Figure 5.13 indicates a significant adsorption across all pH ranges as the anionic phosphoric acid ester results in a significantly more negative zeta potential compared to the bastnäsite without collector. Similarly to the bastnäsite and sodium oleate, the adsorption of SM15 onto the bastnäsite surface is likely to be chemisorption over the alkaline pH range (pH > 6.3) and a mixture of both physisorption and chemisorption in the acidic pH range (pH < 6.3). For the quartz-SM15 system the zeta potential data indicates that there is adsorption of the SM15 collector to the quartz surface across the entire pH range. As the zeta potential of quartz is negative from pH 3 to pH 10 the adsorption of this collector to the quartz surface must

occur by chemisorption as the anionic SM15 would be electrostatically repelled by the negatively charged quartz surface.

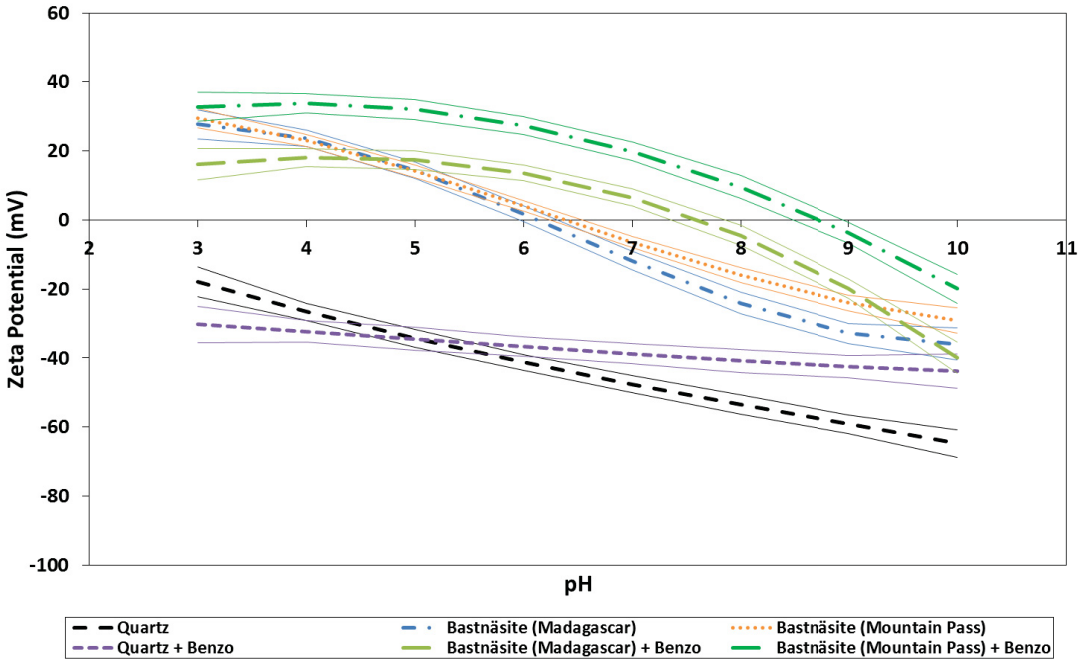

Figure 5.11 – Zeta potential as a function of pH for bastnäsite (Madagascar and Mountain Pass) and quartz without collector and in the presence of 5.83 x 10^{-4} M benzohydroxamic acid (Benzo). Confidence interval lines represent 95 % confidence about a third order polynomial trendline

The zeta potentials of quartz and bastnäsite in the presence of sodium silicate are shown in Figure 5.14. Sodium silicate is a common depressant for silicate minerals in REM flotation as discussed in Chapter 3. The concentration of 10^{-2} M was chosen to ensure that the concentration would be high enough to observe adsorption onto the bastnäsite surface. The zeta potential data from Figure 5.14 indicate that for both quartz and bastnäsite, the presence of sodium silicate shifted the zeta potential of these minerals to a more negative state. While sodium silicate may exist in a colloidal state under certain conditions, zeta potential measurements of sodium silicate in this system at the same concentration, but without mineral particles, showed a zeta potential of zero across the pH range investigated, indicating that no colloidal sodium silicate particles were present (data not shown). While the dissociation of sodium silicate in aqueous environments is poorly understood, the observed shift in zeta potential is a clear indicator of adsorption to

both quartz and bastnäsite surfaces in agreement with literature (Houot *et al.*, 1991; Mishra, 1982).

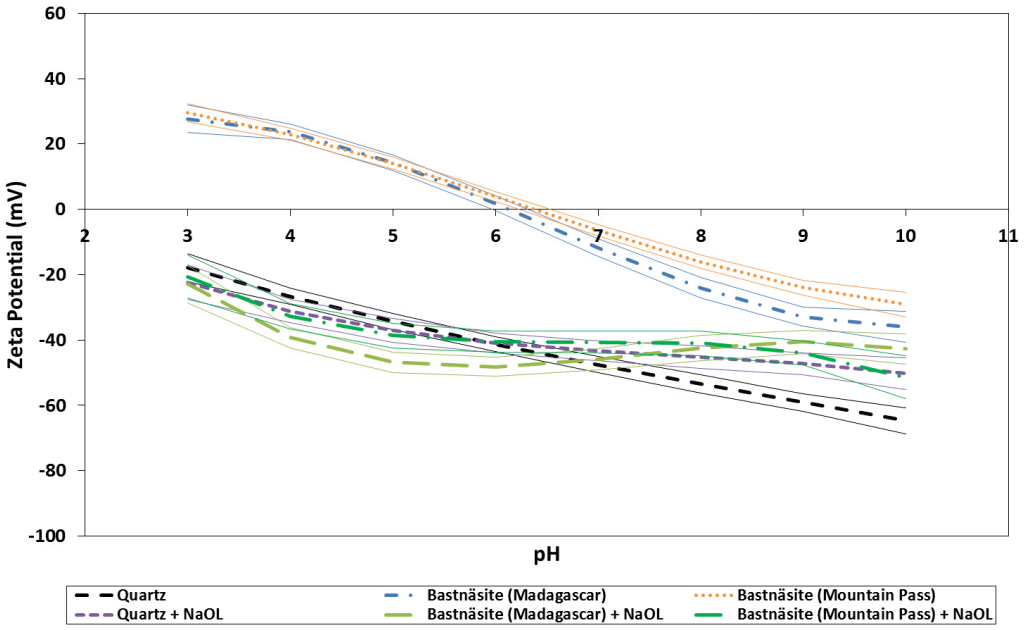

Figure 5.12 – Zeta potential as a function of pH for bastnäsite (Madagascar and Mountain Pass) and quartz without collector and in the presence of 2.62 x 10^{-4} M sodium oleate (NaOL). Confidence interval lines represent 95 % confidence about a third order polynomial trendline

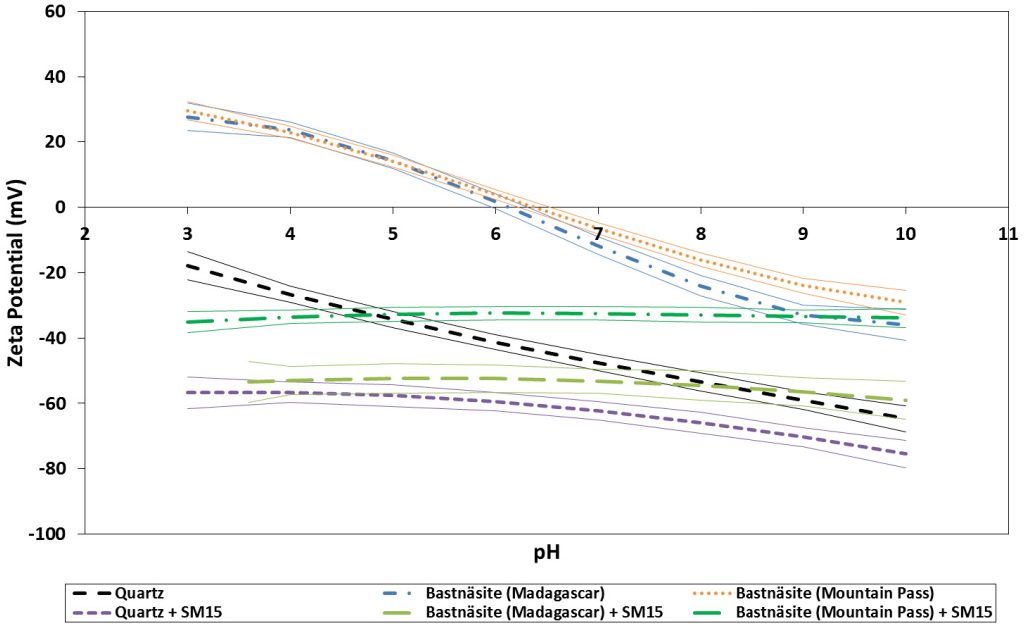

Figure 5.13 - Zeta potential as a function of pH for bastnäsite (Madagascar and Mountain Pass) and quartz without collector and in the presence of 0.08 g/L phosphoric acid ester (Flotinor SM15). Confidence interval lines represent 95 % confidence about a third order polynomial trendline

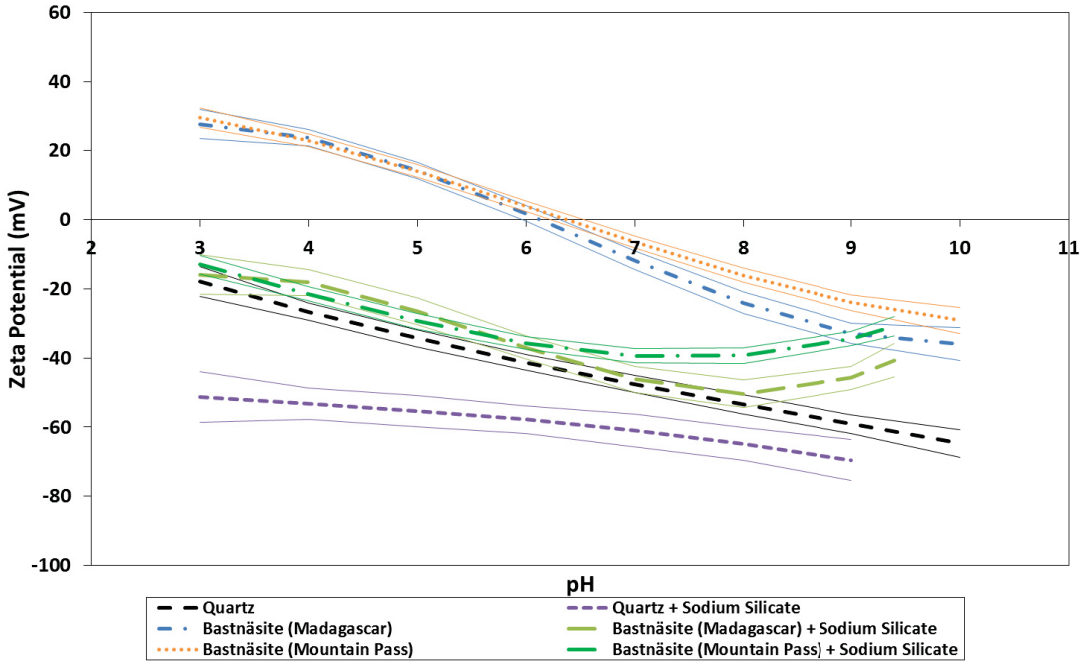

Figure 5.14 - Zeta potential as a function of pH for bastnäsite (Madagascar and Mountain Pass) and quartz without reagents and in the presence of 10^{-2} M sodium silicate. Confidence interval lines represent 95 % confidence about a third order polynomial trendline

5.4.1.3 Allanite and quartz

The zeta potential trends of allanite and quartz (Figure 5.10) indicate that a separation of these two minerals will be quite difficult using a collector whose adsorption mechanism relies purely on electrostatic attractive forces. As both allanite and quartz are negatively charged from pH 4 to pH 10 the only range where the mineral surfaces have opposing charges is at pH < 4. Acidic flotation is generally not preferred in industrial applications due to high reagent (*i.e.* pH modifier) requirements, the possibility of mineral dissolution and workplace safety concerns.

The zeta potential of these two minerals in the presence of four different collectors (benzohydroxamic acid, sodium oleate, dodecylamine and Flotinor SM15) is shown in Figure 5.15 to Figure 5.18. Concentrations used were determined empirically by adding increasing amounts of collector until the deviation (or lack thereof) in zeta potential was successfully established. The zeta potential of quartz in the presence of benzohydroamic acid, sodium oleate and Flotinor SM15 was discussed in Section 5.4.1.2 with only Flotinor

SM15 showing any interaction with quartz. The zeta potential of quartz in the presence of dodecylamine (Figure 5.18) indicates that significant adsorption occurs over a pH range of 5-10. This is in agreement with reported literature, as dodecylamine is a common cationic collector used in the flotation of quartz (Smith & Scott, 1990). The mechanism of dodecylamine adsorption has been reported as occurring by adsorption of individual dodecylamine molecules onto the surface of quartz at relatively low pH (pH > 2-3), resulting in some degree of hydrophobicity (Smith & Scott, 1990). At higher pH values the solubility limit of the dodecylamine is exceeded (Smith & Scott, 1990). This results in precipitation of the amine onto the quartz surface and consequently a significant increase in flotation recovery (Smith & Scott, 1990). This is a likely explanation for the observed zeta potential of quartz in the presence of dodecylamine as shown in Figure 5.18.

The zeta potential trend for allanite in the presence of benzohydroxamic acid (Figure 5.15) indicates very little interaction with the allanite surface except for at low pH (pH < 5), which is surprising as hydroxamates are widely reported to be very strong collectors of REM (Luo & Chen, 1984; Pradip & Fuerstenau, 1983). Sodium oleate (Figure 5.16) appears to adsorb on to the allanite surface as the zeta potential of the mineral in the presence of this collector is more negative across the whole pH range. As sodium oleate is an anionic collector it appears that this collector is able to overcome the inherent electrostatic repulsion with the allanite surface and chemically adsorb. This is consistent with the interaction of sodium oleate with REM surfaces where the mechanism of adsorption has been reported as chemisorption (Pavez *et al.*, 1996). The interaction of Flotinor SM15 with allanite (Figure 5.17) appears similar to that of quartz, with the zeta potential shifted to a more negative value across the entire pH range. This likely indicates chemisorption to the allanite surface, potentially by a similar mechanism to adsorption onto the quartz surface. The zeta potential data for dodecylamine and allanite (Figure 5.18) is also similar to quartz, indicating adsorption of dodecylamine to the allanite surface when the allanite surface is negatively charged (pH 4 to pH 10). This would appear to suggest that a possible route of adsorption for the cationic dodecylamine is physical adsorption (physisorption) to the allanite surface through electrostatic interactions.

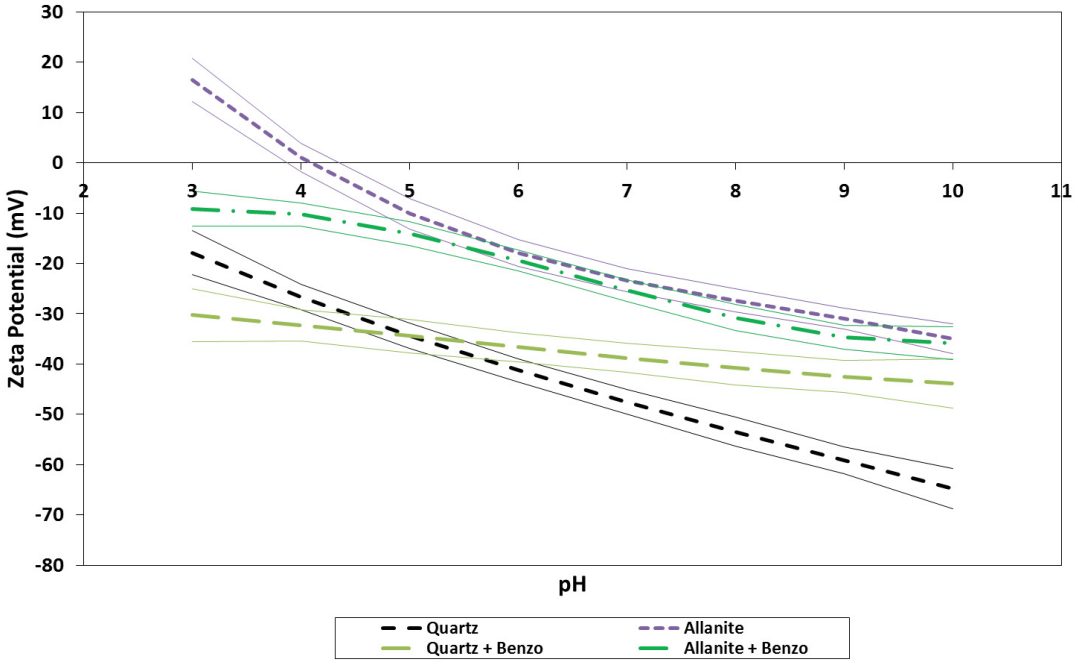

Figure 5.15 - Zeta potential as a function of pH for allanite and quartz without collector and in the presence of 5.83 x 10^{-4} M benzohydroxamic acid (Benzo). Confidence interval lines represent 95 % confidence about a third order polynomial trendline

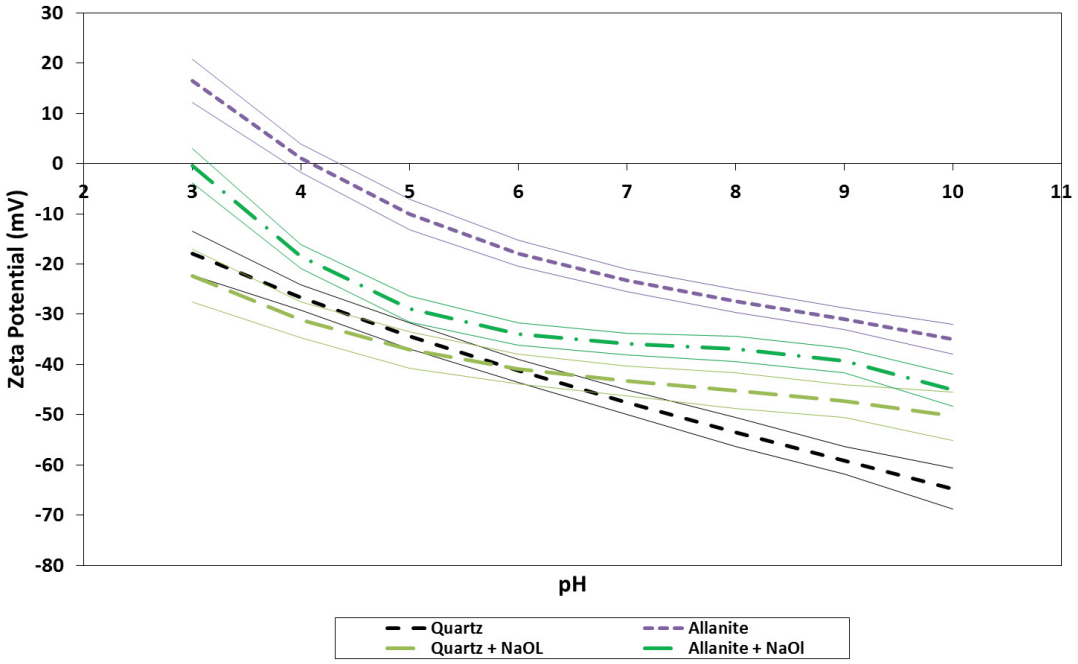

Figure 5.16 - Zeta potential as a function of pH for allanite and quartz without collector and in the presence of 2.62 x 10^{-4} M sodium oleate (NaOL). Confidence interval lines represent 95 % confidence about a third order polynomial trendline

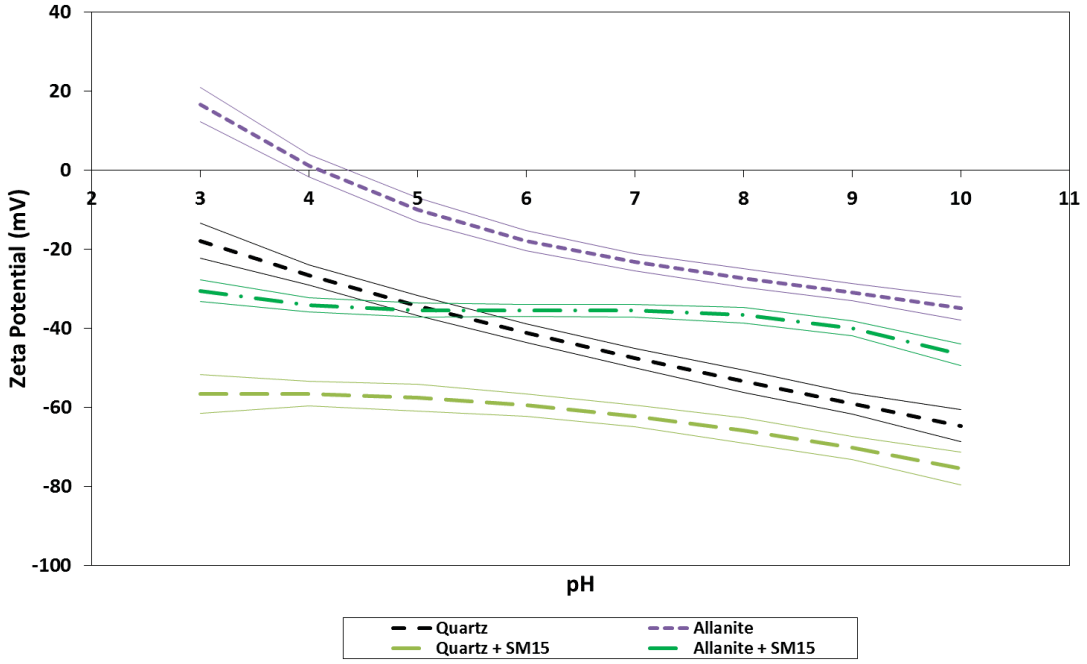

Figure 5.17 - Zeta potential as a function of pH for allanite and quartz without collector and in the presence of 0.08 g/L phosphoric acid ester (Flotinor SM15). Confidence interval lines represent 95 % confidence about a third order polynomial trendline

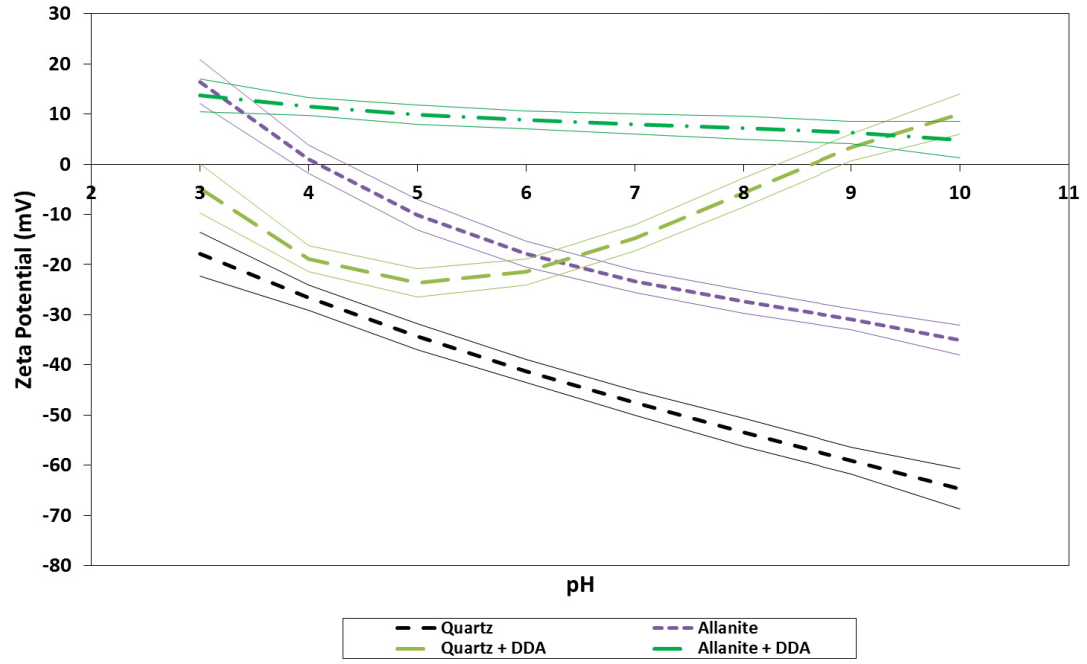

Figure 5.18 - Zeta potential as a function of pH for allanite and quartz without collector and in the presence of 4.32 x 10^{-4} M dodecylamine (DDA). Confidence interval lines represent 95 % confidence about a third order polynomial trendline

5.4.2 Electroacoustic zeta potentials

Due to the inherent solubility of the bastnäsite mineral, the zeta potential of this mineral was investigated via the electroacoustic technique. As this technique measures zeta potential from an acoustic signal rather than optically, it is possible to measure much more concentrated suspensions. Due to limited mineral quantities it was not possible to investigate allanite in a similar manner.

Figure 5.19 shows the results of electroacoustic determination of the zeta potential of one of the bastnäsite samples (Madagascar) and quartz in the presence of an indifferent electrolyte (10^{-3} M KCl) and in the presence of 1.74 x 10^{-3} M benzohydroxamic acid. As these measurements were conducted at higher solids content (5 wt. %) than the electrophoretic measurements, an increased benzohydroxamic acid concentration was used. The results in Figure 5.19 show an IEP for bastnäsite of 8.1 which is significantly shifted from the IEP determined electrophoretically (Figure 5.10). As the primary difference between the two techniques is the solids concentration it seems likely that mineral dissolution and the resultant differences in potential determining ion content in the bulk may explain the observed inconsistency in IEPs. This shift in the IEP to a higher pH as solids content increases has also been observed by Nosrati *et al.* (2011) in measuring dispersions of muscovite. The proposed mechanism for the shift in IEP in their system was the increased importance of leached metal cations in affecting the zeta potential of a suspension of higher solids content (Nosrati *et al.*, 2011). This further reinforces the importance of the measurement technique in determining the IEP of this mineral. The electroacoustic results of bastnäsite and benzohydroxamic acid shows a shift in the IEP to a more alkaline region similar to the shift observed in Figure 5.11. Additionally, both the electrophoretic and electroacoustic results show a positive shift in the value of the zeta potential across a similar range (approximately pH 5 to pH 10). These electroacoustic results for bastnäsite suggests that while the IEP may differ widely for this mineral dependent on the measurement technique employed, the general trends observed with flotation collectors are consistent regardless of measurement technique.

The electroacoustic results for quartz show the expected zeta potential trend for quartz that corresponds well with the results in Figure 5.11. While the trend in Figure 5.19 for quartz and benzohydroxamic acid is shifted upwards across the entire pH range this may potentially be due to compression of the electrical double layer, and not adsorption, due to the increase in electrolyte concentration from the benzohydroxamic acid addition.

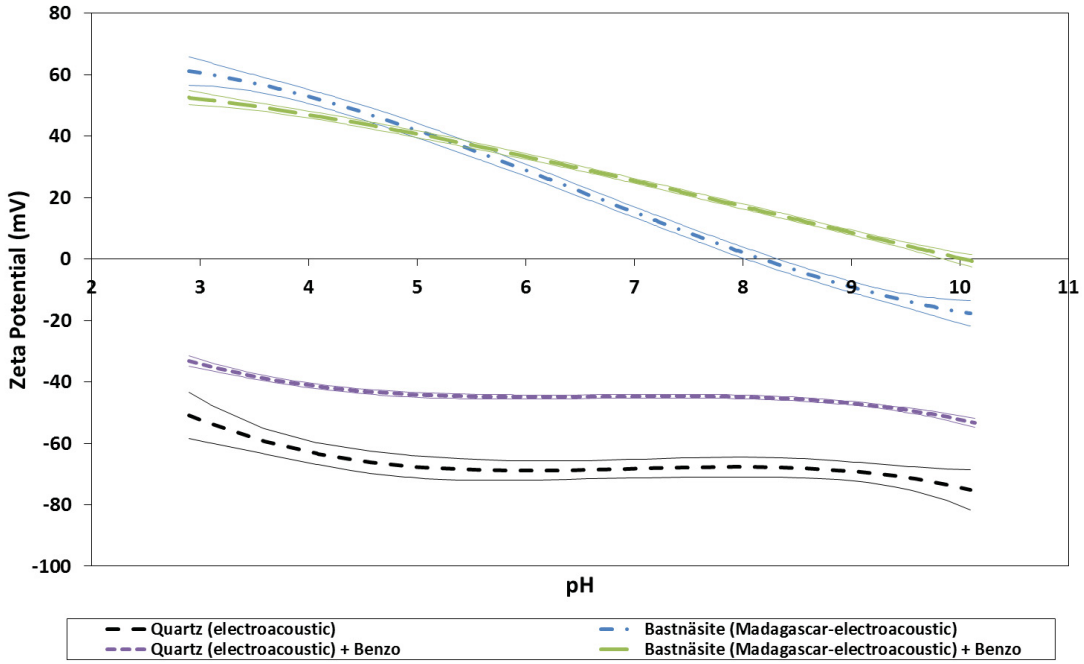

Figure 5.19 – Electroacoustic zeta potential trends of bastnäsite (Madagascar) and quartz without collectors (in 10^{-3} M KCl) and in the presence of 1.74 x 10^{-3} M benzohydroxamic acid. Confidence interval lines represent 95 % confidence about a third order polynomial trendline

5.4.3 Zeta potential with activating ions

Due to the similar zeta potential behaviour of quartz and allanite with various flotation collectors as well as difficulties in selectively floating allanite without floating quartz (further details in Section 5.5.2), the use of flotation activators was investigated for this mineral. In froth flotation if a given mineral is unrecoverable by direct addition of a collector, a potential solution is to add an activator to specifically adsorb to the mineral surface (Fuerstenau & Palmer, 1976). Activators may be simple metal cations or more complex molecules. In the case of flotation using anionic collectors, such as hydroxamates, common activators are polyvalent metal cations (Fuerstenau & Palmer,

1976). A classic example of activation can be seen in the adsorption of calcium ions onto the surface of quartz to enable flotation with a fatty acid collector (Fuerstenau & Palmer, 1976). The specific adsorption of metal cations onto a mineral surface has been shown to occur at a pH where the metal cation is in a monohydroxy state, suggesting that the monohydroxy species are the surface active species (Fuerstenau & Palmer, 1976). In the case of flotation with hydroxamates, it is important to choose a metal cation with a high metal-hydroxamate stability constant such that the additional collector adsorption sites on the mineral surface will be favourable for hydroxamate adsorption. Previous work by Herrera-Urbina & Fuerstenau (1987) has shown that a small amount of Fe ions introduced to a quartz suspension were able to cause unexpected hydroxamate adsorption onto the quartz mineral surfaces, thus resulting in mineral flotation. The effect of Fe ions on hydroxamate adsorption is intuitive as hydroxamates are known to form very stable chelates with Fe (Fuerstenau, 2005; Shuaib *et al.*, 1987). The effect of iron cations on the hydroxamate flotation of cassiterite has also been investigated with the observed maximum in recovery occurring at the pH at which the activating ion is present as a monohydroxy species (Sreenivas & Padmanabhan, 2002). It should also be noted that Sreenivas & Padmanabhan (2002) also observed a decrease in flotation at elevated dosages of Fe ions, which they speculated was due to the consumption of hydroxamate in the bulk by unadsorbed Fe ions. More recently, Anderson (2015) investigated the use of cobalt ions in high temperature hydroxamate flotation of the Mountain Pass bastnäsite ore at pH 9. The presence of these ions resulted in significantly improved REE recovery with an accompanying decrease in REE grade (Anderson, 2015). Based on these results the decision was made to investigate the use of ferric, ferrous and lead ions for the activation of allanite as both iron and lead cations have high stability constants with hydroxamic acids as well as monohydroxy speciation which overlaps with the pK_a of the benzohydroxamic acid collector.

The results of zeta potential measurements of allanite and quartz in the presence of ferric chloride may be seen in Figure 5.20. From literature the monohydroxy form of the trivalent Fe cation is present from pH 1 to pH 4 with a peak in concentration near pH 3 (Fuerstenau & Palmer, 1976). Figure 5.20 shows that the addition of $FeCl_3$ causes a positive shift in

zeta potential of allanite across the whole pH range investigated. This would appear to indicate that the adsorption of trivalent Fe cations onto the allanite surface is not limited to when the Fe is found in its monohydroxy state, $Fe(OH)^{2+}$. Above pH 4, trivalent Fe will start to precipitate as the insoluble hydroxide so the results in Figure 5.20 may also be indicative of the zeta potential of iron hydroxide (ferric hydroxide has a reported IEP of 8.6) (Parks, 1965). As the starting point for these measurements was near pH 3 the $Fe(OH)_3$ may be precipitating onto the allanite surface as well as in the bulk solution. The results with both $FeCl_3$ and benzohydroxamic acid show little change in the zeta potential which makes sense if the interaction of Fe and a hydroxamic acid is assumed to occur between the hydrolysed Fe cation and the undissociated hydroxamic acid with the resultant metal-hydroxamate complex having the same charge as the metal cation (Fuerstenau, 2005).

The results for quartz with $FeCl_3$ in Figure 5.20 show similar results in that there is a positive shift in zeta potential in the presence of trivalent Fe cations. The observed peak in zeta potential near pH 4-5 corresponds well with the expected adsorption mechanism of the monohydroxy species being the most favourable to adsorb onto the mineral surface. These results are also consistent with previous work employing ferric ions as activators for flotation with sodium oleate (Jie *et al.*, 2014). Contrary to the results for allanite, the zeta potential of quartz with $FeCl_3$ at alkaline pH (pH > 9) returns to a value comparable to that measured for quartz without reagents. This likely indicates that at alkaline pH most of the Fe ions have taken the form of solid iron hydroxide precipitates which do not interact with the mineral surface and since they are uncharged, have no additional impact on the zeta potential. The results with benzohydroxamic acid and iron chloride are similar to those for allanite in that there is little effect on zeta potential with the addition of benzohydroxamic acid.

The results of zeta potential measurements with allanite and quartz in the presence of divalent ferrous chloride may be seen in Figure 5.21. According to literature the speciation of divalent Fe cations is such that the monohydroxy species, $Fe(OH)^{+}$, is present from at least pH 6 to pH 11 with a peak near pH 9 (Fuerstenau & Palmer, 1976). As the ferrous

chloride is added to an agitated environment exposed to the atmosphere, it should be expected that a portion of the divalent ferrous ions will be oxidized to trivalent ferric cations. In Figure 5.21 the results are very similar to those in Figure 5.20, with adsorption across the entire pH range indicating that much of the iron seems to have been oxidized to its ferric form. While steps could be taken to minimize this oxidation, such as bubbling nitrogen through deionized water prior to preparing all solutions, it was felt that the initial experimental set up was more representative of the oxidative nature of industrial flotation separations.

For the results with quartz in Figure 5.21, once again a peak in zeta potential is observed near pH 4. As these peaks in zeta potential are much less evident with allanite in the presence of Fe cations it seems likely that the complex composition of allanite results in more complicated and varied interactions with Fe species in solution than are typically expected for a more well-researched silicate mineral such as quartz. The drop off in zeta potential at pH 3 may indicate that the oxidation of ferrous ions to ferric ions is not complete and consequently there are insufficient monohydroxy species for significant Fe adsorption onto the quartz surface. Similar to Figure 5.20, the zeta potential trend of benzohydroxamic acid with iron chloride shows little deviation from the trend with iron chloride alone. This appears to confirm that in all cases investigated it is the undissociated benzohydroxamic acid interacting with the Fe cations (the likelihood of no interaction at all between the benzohydroxamic acid and the mineral surface may be dismissed when these results are viewed along with the microflotation in Section 5.5.3).

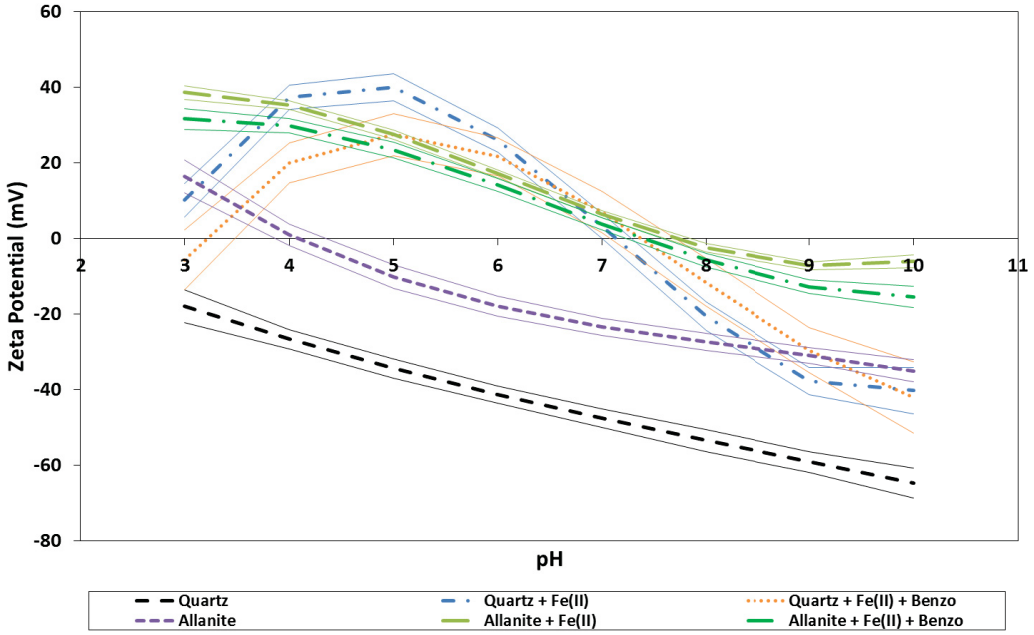

Figure 5.20 – Zeta potential as a function of pH for allanite and quartz without collector, in the presence of ferric ions, and in the presence of ferric ions followed by the addition of 5.83 x 10^{-4} M benzohydroxamic acid (Benzo). Confidence interval lines represent 95 % confidence about a third order polynomial trendline

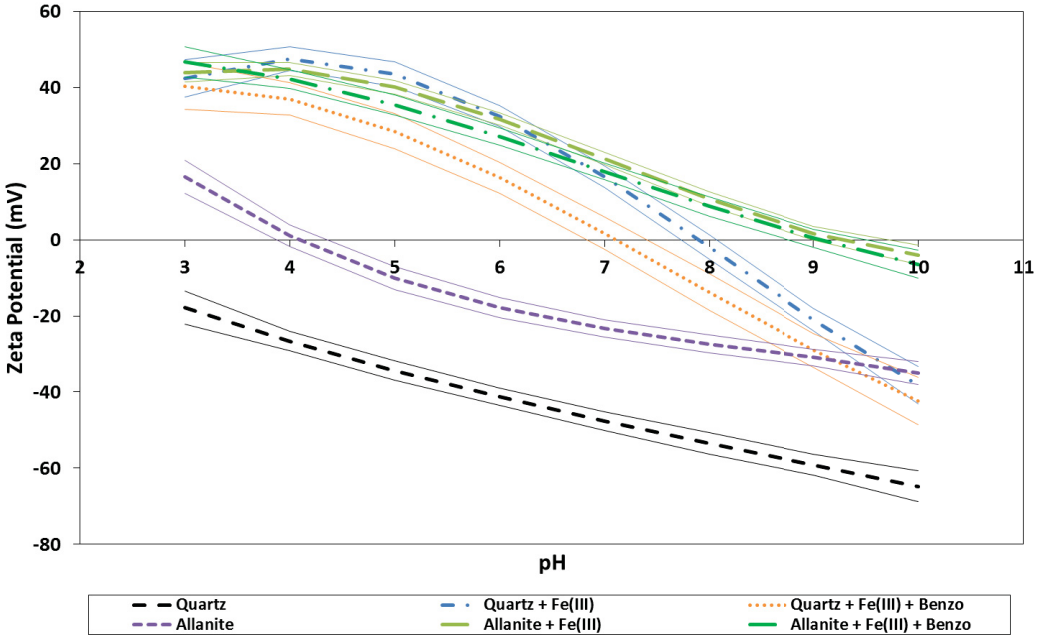

Figure 5.21 – Zeta potential as a function of pH for allanite and quartz without collector, in the presence of ferrous ions, and in the presence of ferrous ions followed by the addition of 5.83 x 10^{-4} M benzohydroxamic acid (Benzo). Confidence interval lines represent 95 % confidence about a third order polynomial trendline

The results of zeta potential measurements using $PbCl_2$ as an activator may be seen in Figure 5.22. The monohydroxy species, $Pb(OH)^+$, is found in the highest concentrations from pH 6 to pH 10 which corresponds well with the observed peak in allanite zeta potential near pH 8 in the presence of lead ions (Fuerstenau & Palmer, 1976). Surprisingly, the zeta potential of quartz with lead ions does not show much deviation from the trend of the pure mineral which is inconsistent with reported charge reversals occurring from pH 6 to 10 for the quartz-lead system (Fuerstenau & Palmer, 1976). The trends of both allanite and quartz with lead and benzohydroxamic acid show positive zeta potential values across the alkaline pH range, which agrees with the expected zeta potential of a silicate mineral in the presence of lead ions (*i.e.* the zeta potential should be positive for pH ~6-10) (Fuerstenau & Palmer, 1976). The positive zeta potential at alkaline pH with benzohydroxamic acid indicates that it is primarily the undissociated benzohydroxamic acid molecule interacting with the Pb ions on the mineral surfaces. This conclusion is further supported by the microflotation results discussed in Section 5.5.3.

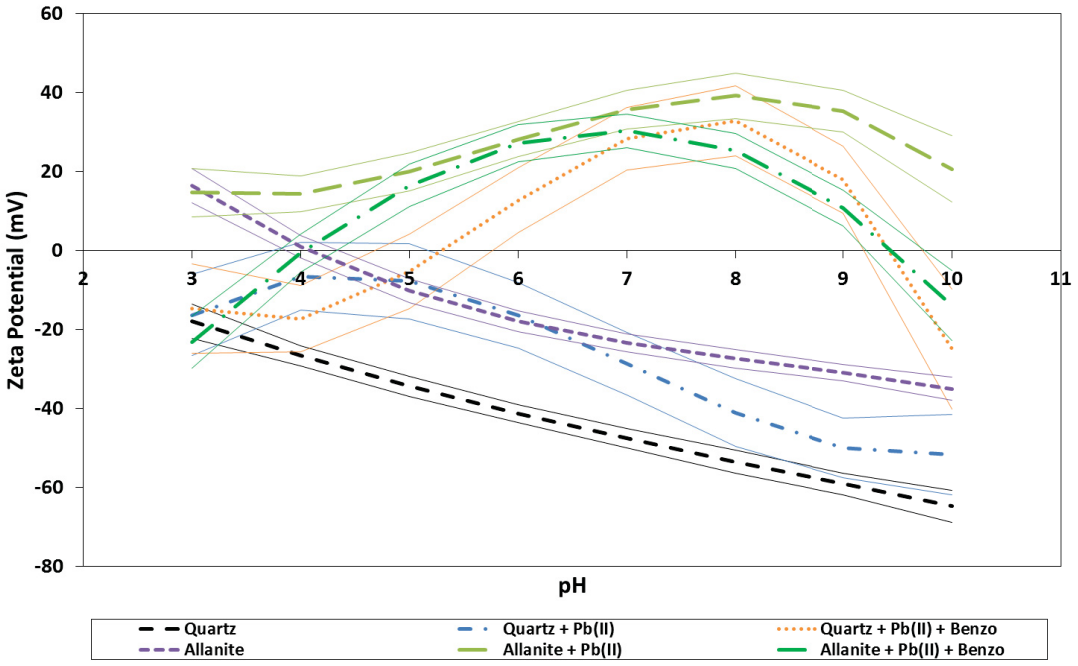

Figure 5.22 – Zeta potential as a function of pH for allanite and quartz without collector, in the presence of lead ions, and in the presence of lead ions followed by the addition of 5.83 x 10^{-4} M benzohydroxamic acid (Benzo). Confidence interval lines represent 95 % confidence about a third order polynomial trendline

5.5 Microflotation

5.5.1 Bastnäsite and quartz

The microflotation results of both quartz and bastnäsite in the presence of benzohydroxamic acid can be seen in Figure 5.23. The data illustrates an interesting finding from microflotation tests with benzohydramic acid, namely that the type of frother used has a significant impact on microflotation recoveries of bastnäsite. The benzohydroxamic acid microflotation tests on bastnäsite and quartz employed methyl isobutyl carbinol (MIBC), a weak frother, and F150, a relatively strong frother. The results clearly indicate that the reported strong collecting ability of hydroxamate at pH 9 for bastnäsite can only be achieved when the strong frother F150 is used. This may correspond well with the reported lack of frothing effects in the Chinese H_{205} collector (Chapter 3) which as a naphthyl hydroxamate is similar in structure to benzohydroxamic acid. The interaction between various frothers and hydroxamates should be investigated as hydroxamates become an increasingly prevalent collector. The data from Figure 5.23 also reinforce the high selectivity of hydroxamate for bastnäsite as well as the optimum pH for hydroxamate flotation occurring at pH 9. The flotation results for bastnäsite do not agree perfectly with previous Hallimond tube flotation tests on bastnäsite by Pradip (1981) who was able to achieve complete bastnäsite recovery from pH 5 to pH 9 using a similar hydroxamate concentration (3×10^{-4} M compared to 2.43×10^{-4} M in this work). Some important differences between these two sets of microflotation tests include the apparatus used, the bastnäsite origin as well as the hydroxamate used (K-octyl hydroxamate compared with benzohydroxamic acid).

Microflotation results for bastnäsite and quartz with sodium oleate and phosphoric acid ester collectors are shown in Figure 5.24. The sodium oleate results indicate that both quartz and bastnäsite are recovered to some extent at a dosage of 2000 g/ton (grams of collector per ton of mineral). The recovery of quartz is counterintuitive when compared to the zeta potential data for quartz in the presence of sodium oleate. The flotation of quartz may however be explained when viewed in light of recent work that has shown that sodium oleate may act to reduce mean bubble size (similar to frothers) at sufficiently high concentrations (Atrafi *et al.*, 2012). Atrafi *et al.* (2012) showed that above a concentration

of 10 mg/L (in this work 2000 g/ton = 33.33 mg/L) sodium oleate will significantly reduce the flotation bubble size. The microflotation recovery of quartz may therefore potentially be explained by non-selective entrainment associated with the increased bubble surface area flux (a measure of the instantaneous fraction of air passing the cross-section of the microflotation column) caused by a reduction in bubble size (Warren, 1984). This is only a hypothesis as the water overflow rate from the column was not measured during these experiments. An alternative explanation for the recovery of quartz may be due to the presence of small amounts of metal ion impurities in the quartz sample which can act as activators for the flotation of quartz in the presence of sodium oleate (Fuerstenau & Elgillani, 1967). The possibility of unintentional quartz activation and flotation using sodium oleate reinforces the need for depressants for silicate minerals in bastnäsite flotation as the use of sodium oleate in a mixed mineral system would likely result in increased quartz flotation (due to the increased presence of possible activating ions in the system). The results for Flotinor SM15 (phosphoric acid ester) indicate that it is a very strong collector of both quartz and bastnäsite at a high dosage of 2000 g/ton. At a lower dosage of 200 g/ton there appears to be some possibility of a selective separation of bastnäsite from quartz at pH 9. Similar to sodium oleate, this would likely require the use of a silicate-specific depressant. In the case of both sodium oleate and SM15 it appears that the optimum pH for bastnäsite flotation from quartz would be at pH 9, similar to the results for benzohydroxamic acid. This finding suggests that the optimum pH for bastnäsite flotation may be a function of the dissolution of this mineral as the species present in an aqueous suspension of bastnäsite will vary greatly as a function of pH (see Chapter 3).

In order to verify that the single mineral microflotation results shown in Figure 5.23 were applicable to the separation of bastnäsite from quartz, the benzohydroxamic acid reagent scheme was applied to binary mixtures of quartz and bastnäsite from Mountain Pass (as the supply of bastnäsite from Madagascar was at this point exhausted). The sample from Mountain Pass in single mineral flotation testing with benzohydroxamic acid at pH 9 exhibited a similar recovery (51 %) to that of the bastnäsite from Madagascar. The particle size of both the quartz and bastnäsite samples used in mixed mineral microflotation was

38-53 µm. The concentrate mass pull of these flotation tests was 35 +/- 12 % (1 standard deviation). X-ray diffraction (XRD) analysis of the feed and products of these mixed mineral tests can be seen in Figure 5.25. A table with semi-quantitative mineral contents (as determined by Xpert HighScore) can be seen in Table 5.2. While the semi-quantitative analyses from the XRD patterns are far from accurate due to the differences in mineral diffraction intensities (the 1:1 feed mixture was identified as being 96 % quartz), the XRD patterns in Figure 5.25 illustrate clearly the successful concentration of bastnäsite from quartz. This result is in agreement with the results of the single mineral flotation tests.

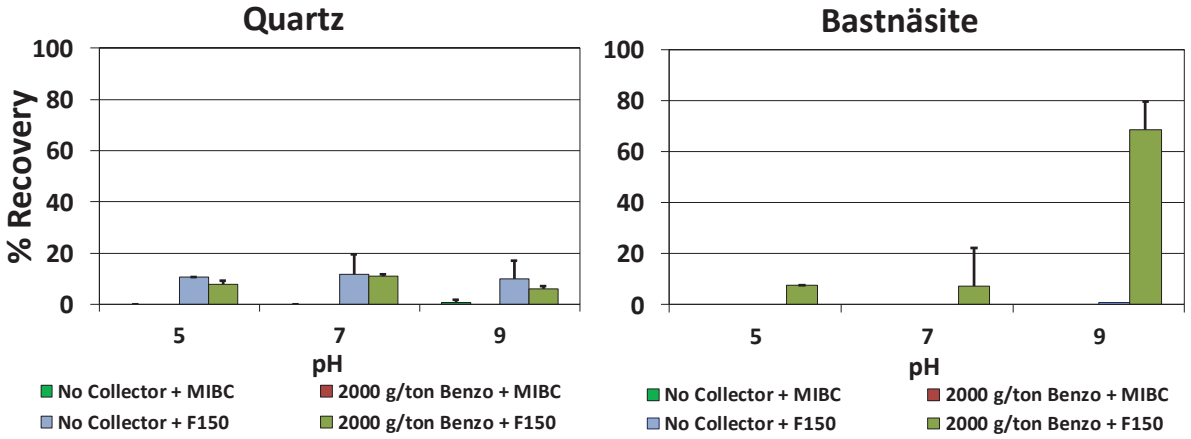

Figure 5.23 – Microflotation tests of quartz and bastnäsite with benzohydroxamic acid. Two different frothers are used (MIBC and F150). Error bars represent one standard deviation

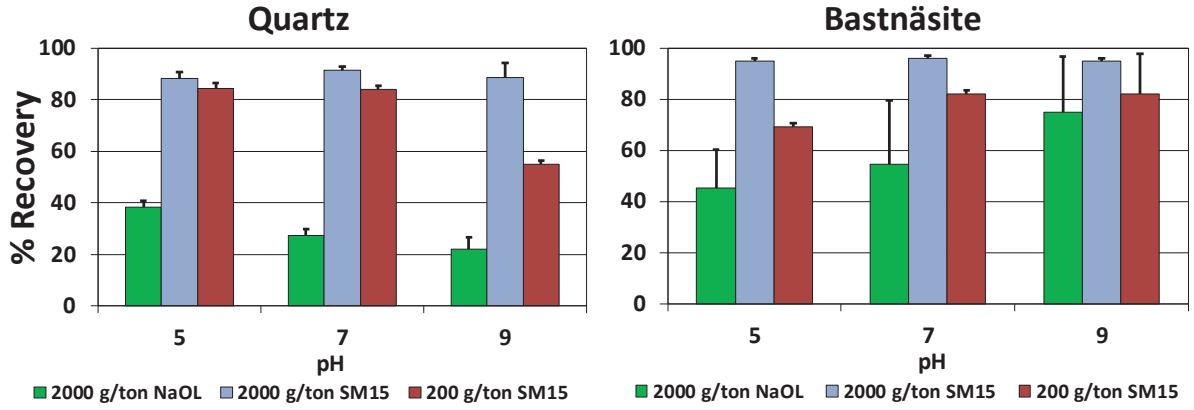

Figure 5.24 - Microflotation tests of quartz and bastnäsite with sodium oleate (NaOL) and phosphoric acid ester (SM15) collectors. Error bars represent one standard deviation

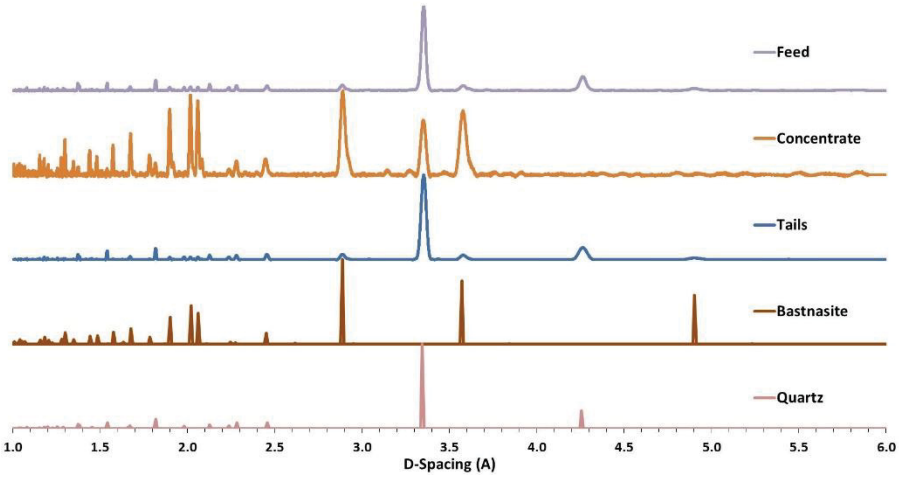

Figure 5.25 – Typical XRD patterns of concentrate and tails produced from binary bastnäsite-quartz mixed mineral microflotation along with feed (1:1 mixture) and reference patterns for both minerals

Table 5.2 – Semi-quantitative results from XRD analysis of mixed mineral microflotation

Mineral	Feed (%)	Conc. (%)	Tails (%)
Bastnäsite	4	49	2
Quartz	96	51	98

5.5.2 Allanite and quartz

Results from microflotation experiments with sodium oleate, dodecylamine and benzohydroxamic acid can be seen in Figure 5.26, Figure 5.27 and Figure 5.28 respectively. Initially, a dosage of 200 g/ton was tested for each collector. As can be seen from Figure 5.26 and Figure 5.28, these dosages of sodium oleate and benzohydroxamic acid do not result in any flotation of quartz or allanite. The results for the dodecylamine flotation (Figure 5.27) show recoveries of quartz in the range of 80-90 %. At 200 g/ton of dodecylamine, allanite is also floated (~60 % recovery) across the whole pH range. Given the successful flotation recoveries of allanite and quartz at 200 g/ton dodecylamine, the flotation recoveries of these two minerals as a function of time were examined by collecting concentrates at three different time intervals (maximum collection time of 2 minutes) as shown in Figure 5.29. The times required for flotation are important as if the rate of flotation of one mineral is significantly different than a second mineral it may be possible in a bank of flotation cells to selectively remove the mineral which floats faster in the first few flotation cells, leaving the slower floating mineral to be recovered further down

the bank. It should be noted that calculating the flotation rate constants for allanite and quartz was not considered for these microflotation experiments. The results from these experiments indicate that the bulk of both quartz and allanite flotation recovery occurs in the first 30 s of collection. It is therefore unlikely that these two minerals could be easily separated based on their flotation rates at 200 g/ton dodecylamine.

To determine conditions where a selective separation of quartz from allanite might be possible, the dosage of dodecylamine was reduced to 20 g/ton. The results from Figure 5.27 confirm the possibility of selective separation as at pH 7 the recovery of quartz is approximately 60 % with zero recovery of allanite. If one considers the zeta potential results from Figure 5.18 the apparent higher degree of adsorption of dodecylamine onto the quartz surface compared with allanite makes sense if the mechanism of collector adsorption is strictly via electrostatic interactions. As the magnitude of the negative zeta potential from pH 4 to pH 10 is larger for quartz than it is for allanite the attractive force between a cationic collector and the negatively charged mineral particle surface should be greater for the quartz surface relative to the surface of allanite. The drop-off of flotation recovery with dodecylamine at pH 10 may be explained by the fact that the concentrations used in these flotation tests (maximum of 1.8×10^{-5} M) are approaching the point of converting the $-NH_3^+$ group of the amine to $NH_{2(s)}$ and precipitating the amine out of solution (Smith & Scott, 1990).

The dosage of sodium oleate and benzohydroxamic acid were increased to the point where some flotation recovery was observed (Figure 5.26 and Figure 5.28). In the case of sodium oleate this required an addition of 1 kg/ton. At this elevated dosage the recovery of allanite and quartz are both increased however the only observable difference (using 95 % confidence intervals) between the two lies at pH 7. The bulk of the flotation with sodium oleate is likely driven by non-selective entrainment at this elevated dosage due to the frother-like properties of sodium oleate. At a concentration between 10 and 20 mg/L of sodium oleate (1 kg/ton = 16.67 mg/L in this system) a significant inhibition of bubble coalescence has been observed (Atrafi *et al.*, 2012). This coalescence inhibition results in a finer mean bubble size and, as a consequence, a much higher bubble surface area

flux as discussed in Section 5.5.1. As there is a statistically significant difference between allanite and quartz at pH 7 it seems that there must also be some degree of sodium oleate adsorption to the allanite surface (corresponding with the zeta potential results from Figure 5.16).

Flotation with benzohydroxamic acid required a much higher dosage of 32 kg/ton; however even at this elevated concentration the recovery of allanite is very poor. An experimental observation during the microflotation tests with benzohydroxamic acid was that the froth layer formed was much less stable than the froth layers formed with dodecylamine or sodium oleate. As a result it was decided to switch the frother from MIBC (a relatively weak frother) to F150 (a relatively strong frother) to investigate the possibility of improving flotation recoveries by stabilizing the froth. The results are shown in Figure 5.30. It appears that with an addition of F150 the increased frothing allows for an improvement in allanite recovery, especially at pH 4. This result agrees well with the zeta potential results from Figure 5.15 which indicates benzohydroxamic acid adsorption onto the allanite surface in acidic conditions (pH < 4). This result also corresponds well with results from bastnäsite microflotation experiments (Section 5.5.1). As the increased recovery is generally accompanied by an increase in quartz recovery it seems likely that this effect is non-selective, however the interactions of hydroxamate collectors with different frothers warrants further investigation.

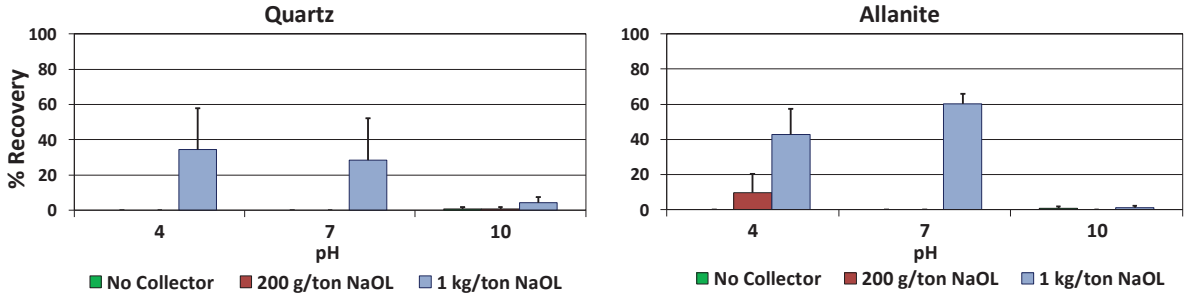

Figure 5.26 – Microflotation results of quartz and allanite using sodium oleate as a collector. Error bars represent one standard deviation

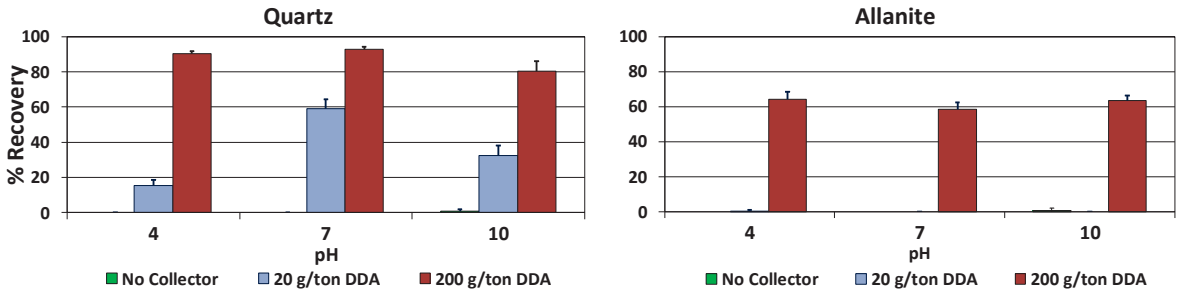

Figure 5.27 – Microflotation results of quartz and allanite using dodecylamine as a collector. Error bars represent one standard deviation

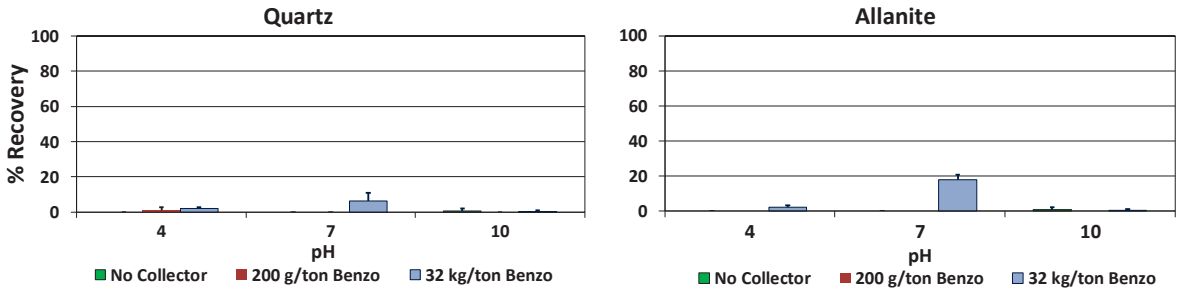

Figure 5.28 – Microflotation results of quartz and allanite using benzohydroxamic acid as a collector. Error bars represent one standard deviation

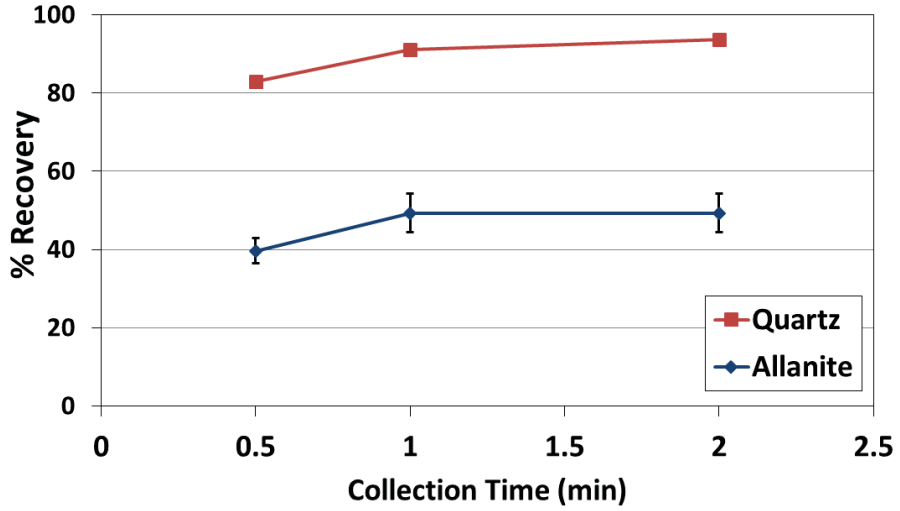

Figure 5.29 – Microflotation results of quartz and allanite as a function of time in the presence of 200 g/ton dodecylamine at pH 7. Error bars represent one standard deviation

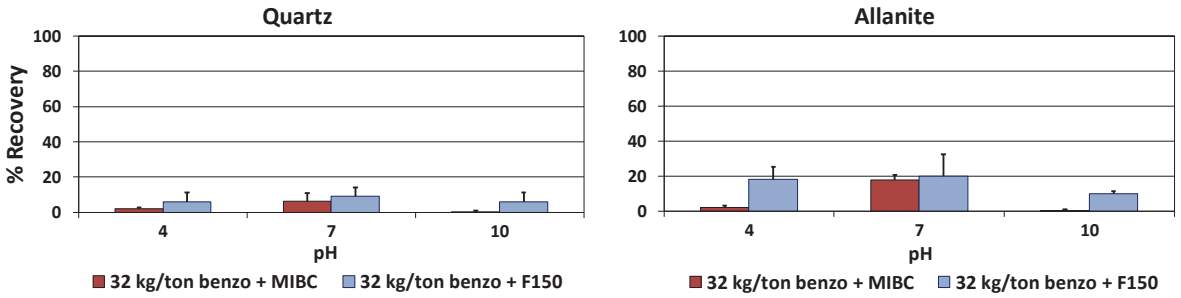

Figure 5.30 – Microflotation results of quartz and allanite using 32 kg/ton benzohydroxamic acid as a collector and either MIBC or F150 as a frother. Error bars represent one standard deviation

5.5.3 Allanite with activators

Due to the difficulties in floating allanite using benzohydroxamic acid it was decided to investigate the use of activating ions to improve hydroxamate adsorption and therefore improve allanite flotation. A more detailed discussion of the conditions investigated is presented in Chapter 4 and also in Section 5.4.3 along with zeta potential results for the three activating ions used (ferric ions, ferrous ions and lead ions).

Conditions for microflotation experiments were chosen based on zeta potential investigations as well as prior experience with hydroxamate flotation. Previous results in allanite microflotation (Figure 5.28) have shown that benzohydroxamic acid is an ineffective collector for allanite at all pH levels investigated. At very high benzohydroxamic dosages (32 kg/ton) a small increase in both allanite and quartz flotation was observed. Thus the selected benzohydroxamic dosage of 2000 g/ton would be expected to recover very little allanite or quartz.

Based on the observed peaks in Fe adsorption with quartz (Figure 5.20 and Figure 5.21) as well as knowledge of ferric ion speciation, microflotation was carried out at pH 4 (Figure 5.31). Microflotation experiments were also carried out at pH 9 since most hydroxamate-based REM flotation is carried out at this pH as high recoveries of bastnäsite are readily achievable under these conditions. This pH is also very close to the pK_a of benzohydroxamic acid, thereby providing the conditions necessary for multilayer adsorption of both the undissociated and dissociated forms of this reagent as suggested by Fuerstenau (2005).

The results of microflotation at pH 9 shown in Figure 5.31 indicate that no combination of either ferric chloride or ferrous chloride with benzohydroxamic acid was able to recover allanite. This makes sense as at this pH the trivalent Fe (in the case of ferrous chloride addition, much of it was oxidized) has precipitated out of solution, eliminating any charged Fe cations that might otherwise be available for interaction with the benzohydroxamic acid. If the ferric hydroxide has precipitated at the mineral surface it may even be the case that this hydroxide is blocking potential sites for collector adsorption.

The results of microflotation tests at pH 4 show flotation recoveries of approximately 10 % for both allanite and quartz when $FeCl_3$ is added, however when $FeCl_2$ is substituted the recoveries of allanite increase to approximately 50 % while the recovery of quartz increases only to 20 % (Figure 5.31). These flotation results are challenging to interpret without knowing the exact oxidation state of Fe after addition of the ferrous chloride. It seems reasonable however to assume that the ferrous chloride is incompletely oxidized to its ferric form, thereby allowing for the presence of monohydroxy species of both trivalent and divalent iron at pH 4. It may be that when only $FeCl_3$ is added the amount of monohydroxy species is quite low at pH 4 (as mentioned in Section 5.4.3 the reported peak concentration for this species occurs at pH 3) so there is insufficient Fe adsorption to the mineral surface. The justification for the larger increase in allanite flotation recovery relative to quartz can easily be explained if one considers the need for a critical amount of hydroxamate-favourable cations on the mineral surface to facilitate sufficient collector adsorption for recovery. As the allanite mineral already contains both REE ions and Fe ions it may be that the addition of $FeCl_2$ incrementally increases the potential sites of hydroxamate adsorption to the point where many more allanite particles may be collected.

The results of flotation with Pb ions (Figure 5.31) appear to present the most favourable conditions for selective separation of allanite from quartz using benzohydroxamic acid as the acidic pH required for flotation with Fe ions would be detrimental to bastnäsite flotation (Figure 5.23). For the conditions investigated > 35 % of the allanite is recovered compared with < 10 % for quartz. Similarly to the explanation for selectivity with Fe ions it is possible that the adsorbed lead ions produce a sufficient increase in potential binding sites on the

allanite surface that the mineral particles can then be collected successfully. Alternatively, Pb ions may selectively adsorb onto the allanite surface relative to quartz.

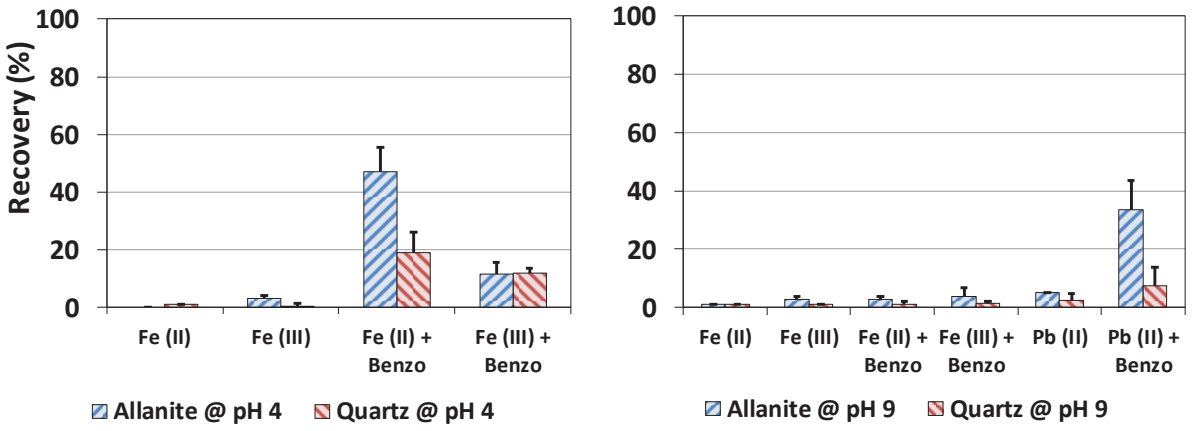

Figure 5.31 – Microflotation results of allanite and quartz with 2000 g/ton benzohydroxamic acid at a) pH 4 and b) pH 9. Error bars shown represent one standard deviation

5.5.4 Ore microflotation

After single mineral surface microflotation tests, a series of preliminary microflotation experiments were carried out on the Nechalacho ore using the reagents investigated for single minerals. Prior to microflotation the ore was subject to a pre-concentration stage using centrifugal gravity concentrators in order to concentrate high specific gravity REM. Two separate centrifugal gravity concentrators were used with their respective mass pulls shown in Table 5.3. To prevent accumulation on the magnetic stir bar used in microflotation, strongly magnetic material was removed prior to microflotation using a hand magnet. The percentage of each concentrate removed as the magnetic phase can be seen in Table 5.3. The flotation conditions investigated may be seen in Table 5.4.

Table 5.3 – Mass pull of centrifugal gravity concentrates with accompanying magnetic mass removed by hand magnet

Concentrator	Mass Pull (%)	Magnetics in Conc (%)
Knelson	4.5	4.9
Falcon	7.3	3.1

Table 5.4 – Summary of reagents, dosages and pH used in ore microflotation

Symbol	Collector	Dosage (g/ton)	Frother	pH
DDA	Dodecylamine	200	F150	7
NaOL	Sodium Oleate	2000	MIBC	9
Benzo	Benzohydroxamic Acid	20000	F150	9
SM15	Flotinor SM15	200	MIBC	7

The XRD patterns of the Knelson and Falcon concentrates after magnetic separation along with their respective separated magnetic phases are shown in Figure 5.32. As both Knelson and Falcon concentrators concentrated the high specific gravity minerals (S.G. ~ 5) found in the deposit the main product of the magnetic separation is expected to be magnetite due to its high density (S.G. = 5.2) and strong ferromagnetic properties. The patterns in Figure 5.32 indicate that the magnetic phase removed from the Knelson concentrate was almost entirely magnetite. Conversely, the magnetic phase separated from the Falcon concentrate showed peaks for both biotite and hematite (both of which are less strongly magnetic than magnetite) and a peak at 2.9 Å. As the major difference between the two centrifugal gravity concentrators is the addition of fluidizing water in the Knelson (the Falcon concentrator was operated using the smooth-walled ultra-fine bowl), the magnetic separation results may demonstrate the Knelson concentrator's improved ability to reject mixed particles of lower density such as magnetite/biotite (S.G. of biotite = 2.7-3.3).

The mass recoveries of the various microflotation tests may be seen in Figure 5.33. The results for the microflotation tests using traditional REM collectors (sodium oleate, benzohydroxamic acid and Flotinor SM15) show an increased mass recovery for the Knelson concentrate and conversely, tests using dodecylamine recovered more mass from the Falcon concentrate. As dodecylamine is a common collector for silicate minerals (Fuerstenau, 1956; Smith & Scott, 1990) the mass recoveries from microflotation suggest that the Falcon concentrate may contain an increased level of silicate gangue relative to the Knelson concentrate.

The XRD patterns for the various microflotation concentrates may be seen in Figure 5.34. It is interesting to first look at the major characteristic peaks for the feldspar minerals microcline and albite (3.25 and 3.2 Å respectively). As expected, the concentrates produced using dodecylamine exhibit the peaks for both these silicate gangue minerals whereas concentrates produced using the more selective benzohydroxamic acid collector do not. The Knelson concentrate does not have the albite or microcline peak after magnetic separation (Figure 5.32) however, after flotation with dodecylamine these peaks are again present, suggesting that the dodecylamine is in fact concentrating these gangue minerals. The concentrates produced using sodium oleate show little difference relative to the Falcon and Knelson concentrates respectively, further reinforcing that sodium oleate displays minimal selectivity for the REM in this deposit.

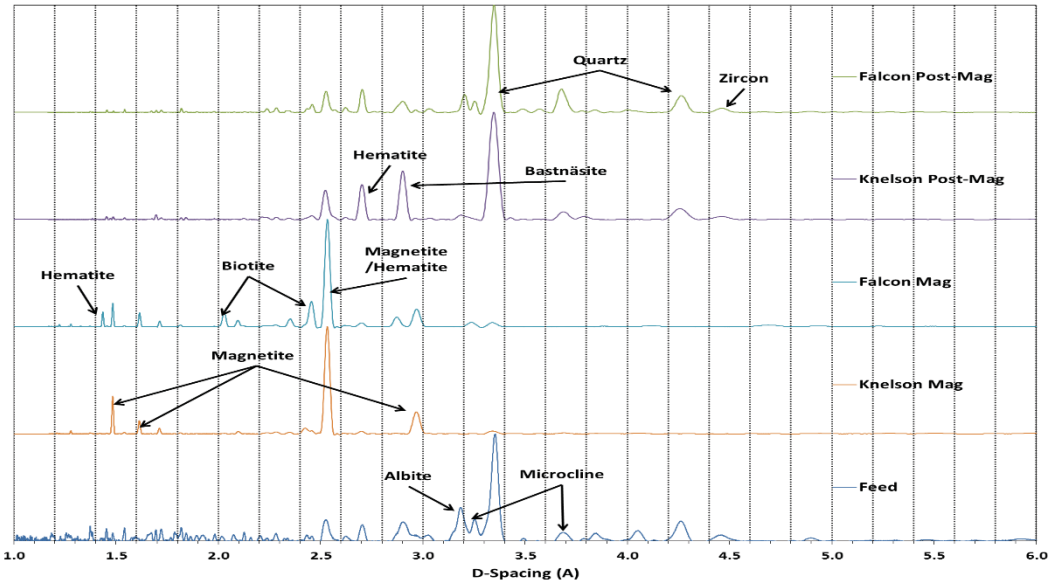

Figure 5.32 - XRD patterns of the Knelson and Falcon concentrates after magnetic separation, along with the magnetic fractions removed from the Knelson and Falcon concentrates, as well as the XRD pattern of the feed material to gravity concentration. All diffraction peaks have been normalized to the maximum peak intensity for each pattern.

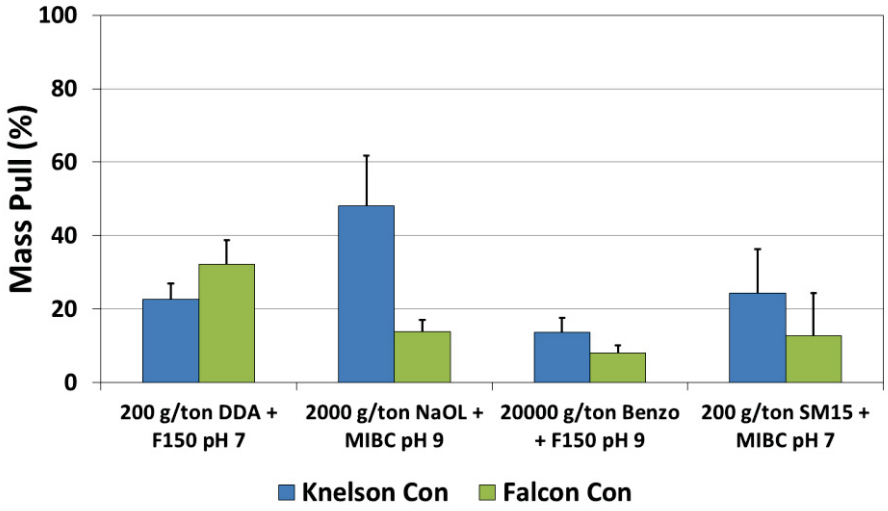

Figure 5.33 - Combined mass pulls of microflotation tests on the Knelson and Falcon concentrates after magnetic separation (DDA = dodecylamine, NaOL = sodium oleate, Benzo = benzohydroxamic acid, SM15 = Flotinor SM15). Error bars represent +/- one standard deviation.

The most successful combination of gravity separation and microflotation appears to be the combination of the Knelson concentrator and benzohydroxamic acid as the major peaks for both albite and microcline are not distinguishable however the characteristic peak of bastnäsite at 4.9 Å is present. It should be noted that the large peak at 3.35 Å in all concentrates is due to an overlap of mineral peaks including major mineral phases in the deposit such as quartz and zircon. The benzohydroxamic acid concentrate produced from the Knelson concentrate also has a peak at approximately 4.45 Å that is characteristic for zircon in this deposit. This is significant as the bulk of the REE in the deposit are found in zircon, as mentioned previously. One other interesting microflotation concentrate is the one produced from the Knelson concentrate using Flotinor SM15. This concentrate has no peak for albite and it has a strong zircon peak. Flotinor SM15 is marketed as a collector for zircon when $CuSO_4$ is added as an activator so this result is somewhat expected (Clariant, 2012). Unfortunately SM15 is also marketed as a collector of multiple other gangue minerals in the Nechalacho deposit including calcite, dolomite, hematite, magnetite and biotite so selective flotation of the REM in this deposit using SM15 would likely require multiple depressants (Clariant, 2012).

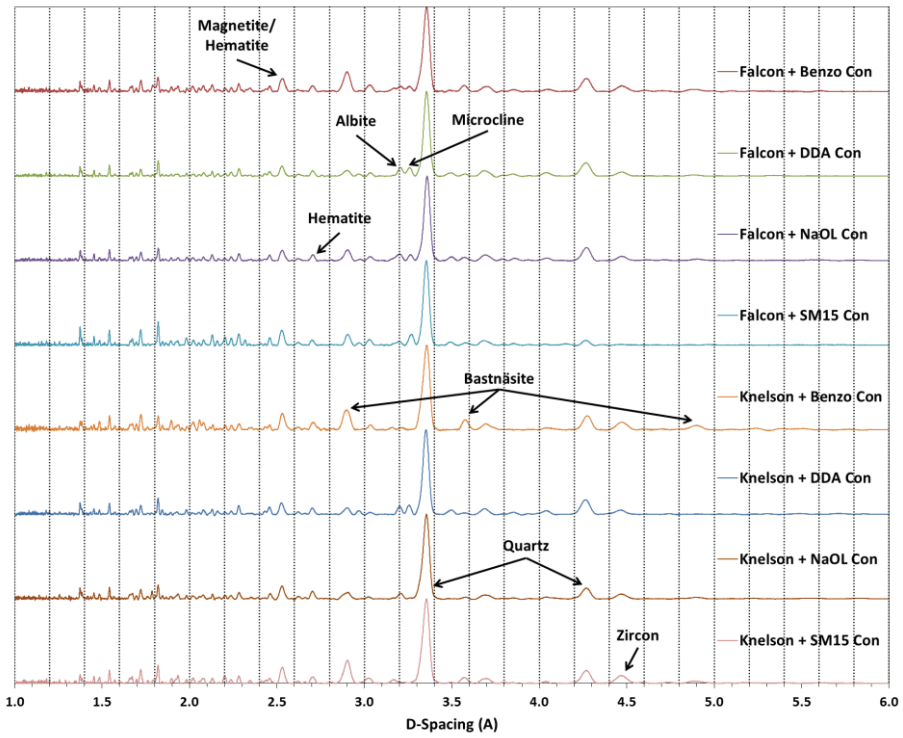

Figure 5.34 - XRD patterns of the microflotation concentrates produced from both Knelson and Falcon concentrates after magnetic separation (Benzo = benzohydroxamic acid, DDA = dodecylamine, NaOL = sodium oleate, SM15 = Flotinor SM15). All diffraction peaks have been normalized to the maximum peak intensity for each pattern.

5.6 Conclusions

This chapter presented the results of the measurement of physicochemical (bulk and surface) properties of many of the minerals found in the Nechalacho deposit. This information provides baseline information to predict mineral behaviour in larger scale separation operations. The results of these investigations have been fed forward to the design of a flowsheet to process the Nechalacho deposit using a variety of separation techniques.

6. Physical Separation

6.1 Introduction

This chapter details a series of gravity and magnetic separations applied to a bulk sample (Sample 2) of the Nechalacho ore in order to determine the optimum process for pre-concentration of the REM. The explicit goal of this process investigation is the production of a high-grade product to be fed to downstream flotation testwork. In order to fully understand the behaviour of the various value and gangue minerals through gravity and magnetic separations a series of characterisation tools have been used. The results of these investigations are presented below.

6.2 Feed composition

Analysis of the Nechalacho feed material using X-ray diffraction (XRD), Scanning Electron Microscopy (SEM), and Quantitative Evaluation of Minerals by Scanning Electron Microscopy (QEMSCAN) identified a number of silicates including biotite, plagioclase, quartz, K-feldspar, Fe-oxides (both magnetite and hematite), lesser proportions of muscovite/clays, chlorite, amphibole, carbonates, and trace proportions of other minerals (*e.g.*, fluorite). The REM include mainly allanite [$(Ca,Y)_2(Al,Fe,REE)_3Si_3O_{12}(OH)$], monazite [$(LREE,Y,Th)PO_4$], bastnäsite [$REE(CO_3)F$], synchysite [$Ca(REE)(CO_3)_2F$] and fergusonite [$(REE,Y)NbO_4$]. Zircon ($ZrSiO_4$) and ferrocolumbite-(Fe) ($FeNb_2O_6$) are not primary REM but are important REE-Y-Nb carriers. For the purpose of this analysis, synchysite refers to solid solution synchysite and parisite.

The processed data includes information such as mineral content (wt. %), liberation and association of the minerals, grain-size, and classification of the minerals by their specific gravity among other parameters. A summary of the mineralogy calculated for the feed sample and by size fraction (+20 µm and -20 µm) is given in Table 6.1. The mass distribution indicates that zircon is more abundant in the coarser fraction. This is also reflected in the elemental distribution between the two feed size fractions (Figure 6.1) as zircon in the Nechalacho deposit has been reported to host more of the HREE than other REM (Ciuculescu *et al.*, 2013; Grammatikopoulos *et al.*, 2013). In this figure, elemental content (as determined by ICP-MS) of the two feed size fractions is represented as a

positive or negative percentage of the expected value based on the mass split between +20 µm and -20 µm size fractions. In addition to the individual REE, Figure 6.1 also presents information on LREE, HREE, total REE (TREE) and the most valuable REE (Pr, Nd, Eu, Gd, Tb, Dy, Er and Y as discussed in Chapter 3). Both the HREE and Value REE show an increased concentration in the larger size fraction, indicating that targeting this size fraction may have a significant impact on project economics.

Table 6.1 – Nechalacho deposit mineralogy (in wt. %) as determined by QEMSCAN

Mineral Name	Total	+20 µm	-20 µm
REM			
Zircon	7.14	9.47	5.47
Bastnäsite	0.93	1.23	0.71
Synchysite	0.55	0.27	0.75
Allanite	0.58	0.68	0.52
Columbite (Fe)	0.42	0.59	0.31
Fergusonite	0.22	0.13	0.29
Other REM	0.49	0.18	0.71
Silicate Gangue			
K-Feldspar	21.84	23.39	20.73
Quartz	20.90	19.87	21.64
Plagioclase	18.59	25.62	13.53
Biotite	13.18	5.32	18.84
Other Gangue			
Fe-Oxides	9.50	9.37	9.59
Ankerite	2.87	1.58	3.80
Calcite	0.64	0.51	0.73
Fluorite	0.55	0.46	0.62
Other Gangue	1.59	1.33	1.78

The liberation characteristics of individual particles, as well as particle associations between various minerals in the feed, were also determined from QEMSCAN analysis. Due to the complex mineralogy of the deposit, the REM containing predominantly LREE (bastnäsite, synchysite, allanite, monazite) were grouped together for this analysis and collectively referred to as light REE minerals (LREM.) Figure 6.2 shows a summary of the liberation characteristics of the five mineral groups of interest [Fe-oxides, zircon, LREM, fergusonite and columbite (Fe)]. “Free” refers to particles with the mineral of interest having greater than 95% of the particle surface area, and “Liberated” refers to particles with less than 95% and greater than 80% of the surface area. It can be seen that for the

P_{80} of 40 µm chosen in this work, liberation ("Free+Liberated") for the iron oxides, zircon and LREM is higher than 70%, but it is lower for fergusonite and columbite. These particle mineral associations may be further broken down to include binary mixtures of a given mineral with a REM, binary mixtures of a given mineral with a gangue mineral and complex particles ("Binary-Value", "Binary-Gangue", and "Complex" respectively) (Figure 6.3). The data in Figure 6.3 demonstrates that many of the REM (zircon and LREM) liberate at relatively coarse (~30 µm) sizes whereas the iron oxides, and to an even greater extent fergusonite and columbite, have much smaller liberation sizes. Fergusonite is particularly fine-grained (liberation size of < 15 µm), which poses additional challenges in concentrating this mineral.

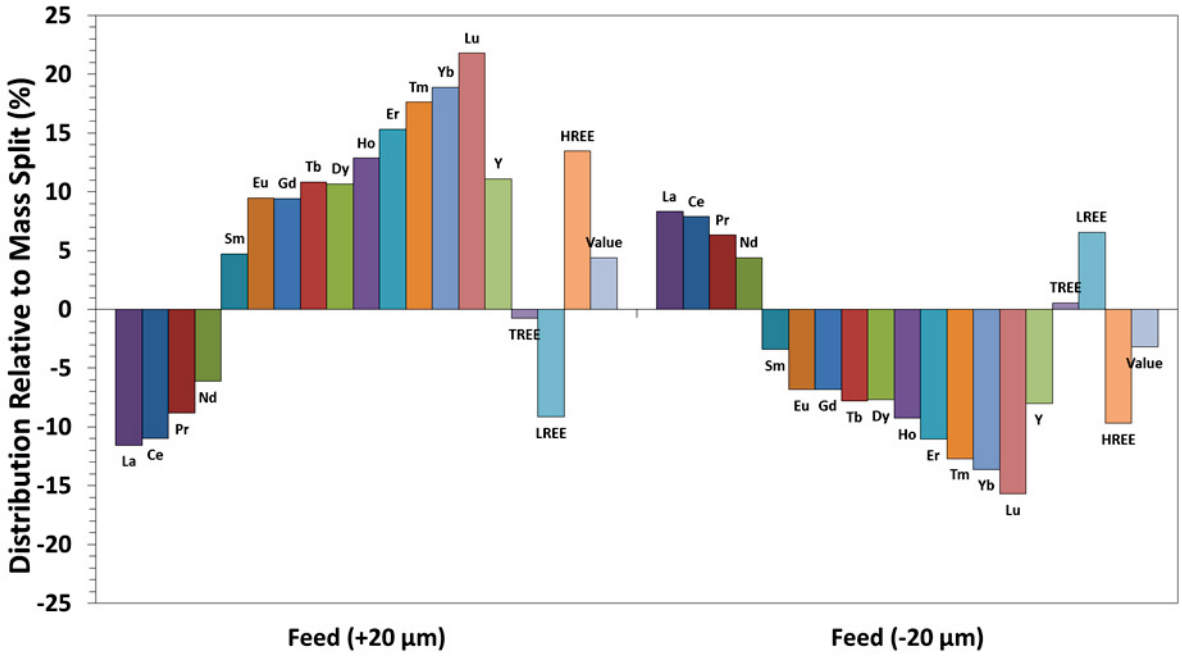

Figure 6.1 – Elemental content of different size fractions of the ground ore for all REE, Y, LREE (La-Sm), HREE (Eu-Lu+Y), TREE (REE+Y) and Value (Pr, Nd, Eu-Dy, Er+Y)

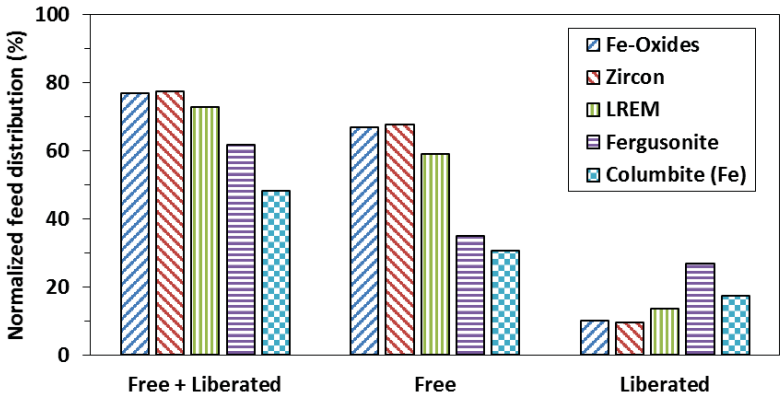

Figure 6.2 – Mineral liberation for the five mineral classes of interest in the Nechalacho deposit. LREM = bastnäsite, synchysite, allanite and monazite

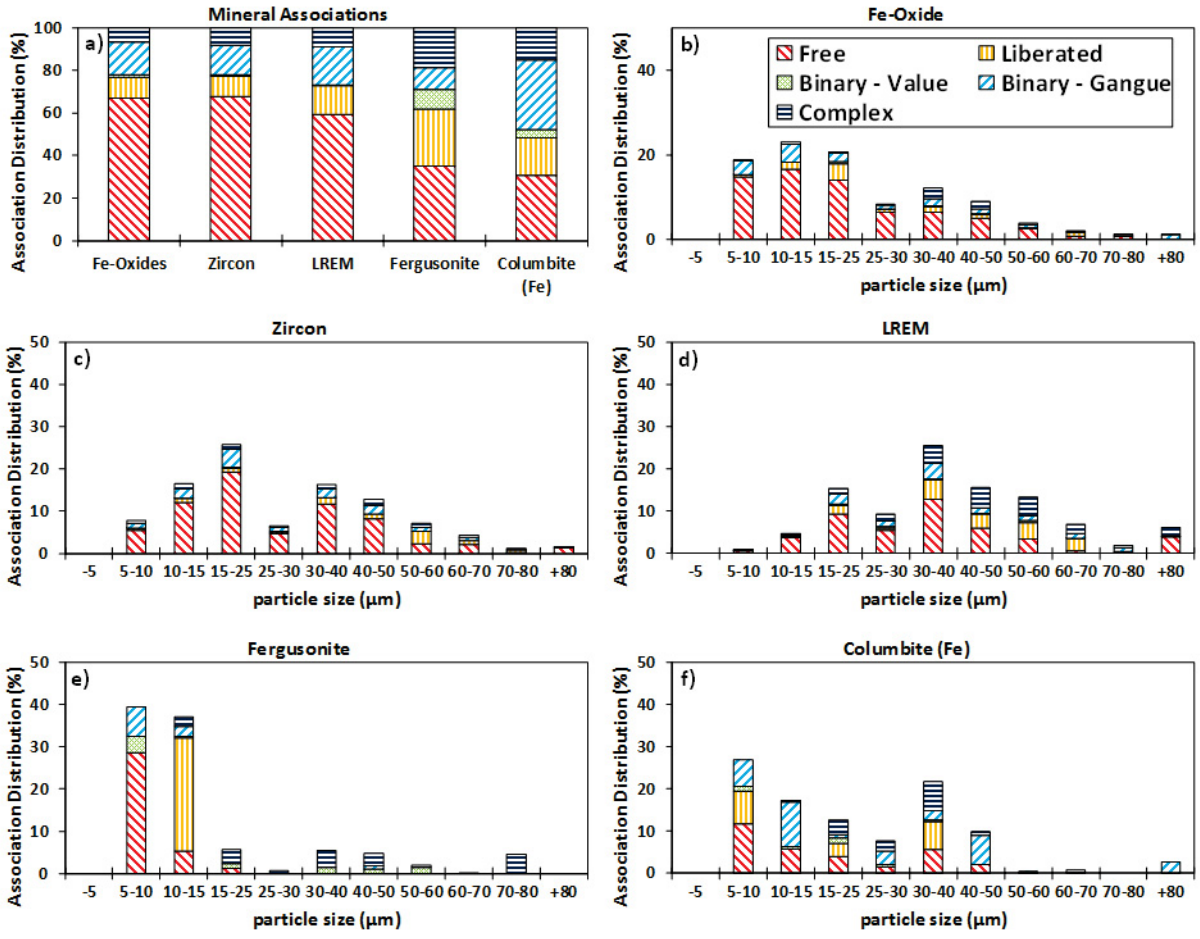

Figure 6.3 – Mineral associations in the Nechalacho deposit: a) total mineral association distribution for five mineral classes, b) to f) size-by-size mineral association distributions for iron oxides, zircon, LREM (bastnäsite, synchysite, allanite and monazite), fergusonite and columbite (Fe) respectively

6.3 Centrifugal gravity concentration with wet drum magnetic separation

6.3.1 Effect of particle size and specific gravity

The series of centrifugal gravity and drum magnetic concentration processes applied to the deposit is shown in Chapter 4. The mass pull and REO content of each different stream is provided in Table 6.2 (refer to Figure 4.4 for stream labels). The d_{50} and d_{80} particle sizes (as measured by QEMSCAN) and specific gravity of each stream can be found in Figure 6.4 and Figure 6.5, respectively. The particle size and specific gravities of each fraction demonstrate that the Knelson Concentrator acts as both a size separator and gravity concentrator. The gravity concentrate from the separator (KC) has a larger particle size and elevated specific gravity (SG) relative to the intermediate tailings (KT) and final gravity tailings (FT). The Falcon Concentrator by contrast seems to have no bias for particle size or specific gravity because the FC fraction shows little difference in particle size or SG relative to its feed (KT) and tailings (FT) streams. The flowrates for the tailings stream from both Knelson and Falcon are shown in Table 6.3. The data give an indication of the flow rates to the individual separators. The mass flow rate to the Falcon Concentrator was higher than that to the Knelson with greater variability (Table 6.3). This is to be expected as the control of mass flow rate is much easier in a lab scale when feeding dry material using a vibratory feeder (Knelson) as opposed to pumping a slurry (Falcon). This higher mass flow rate may be one factor accounting for the apparent lack of selectivity in terms of particle size or specific gravity with the Falcon Concentrator.

Table 6.2 – Mass pull and TREO content of the different streams from centrifugal gravity concentration and drum magnetic separation

Stream	Mass Pull (%)	TREO (%)
Feed		2.40
KC	6.83	5.17
KC Oversize	0.81	
KC Mag	2.29	2.45
KC RE Mag	1.43	6.81
KC Non-Mag	2.30	8.00
FC	3.01	3.38
FC Mag	1.63	3.98
FC RE Mag	0.40	4.36
FC Non-Mag	0.98	4.63
FC Tails	90.16	2.13

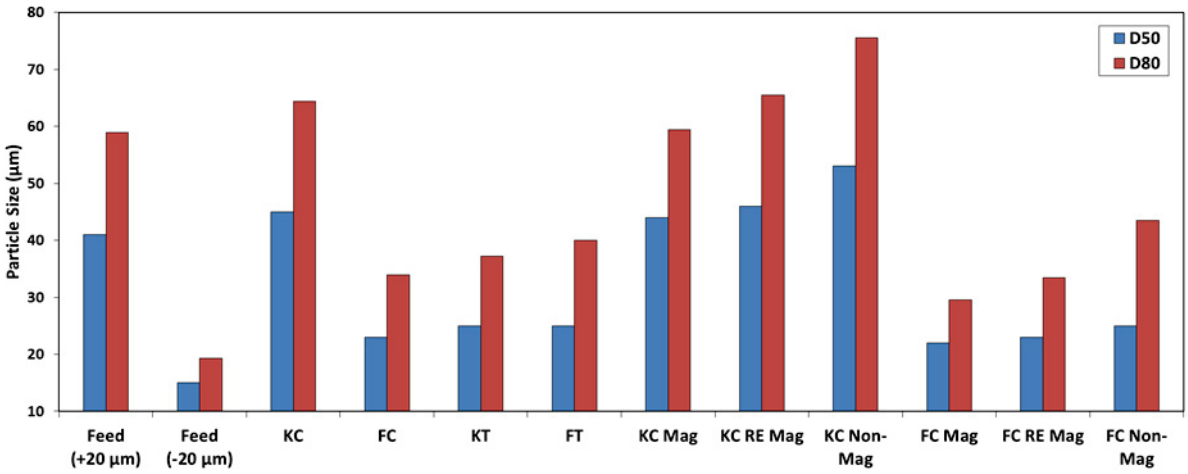

Figure 6.4 – Particle sizes (d_{50} and d_{80} values determined by QEMSCAN) of different products of centrifugal gravity concentration and drum magnetic separation

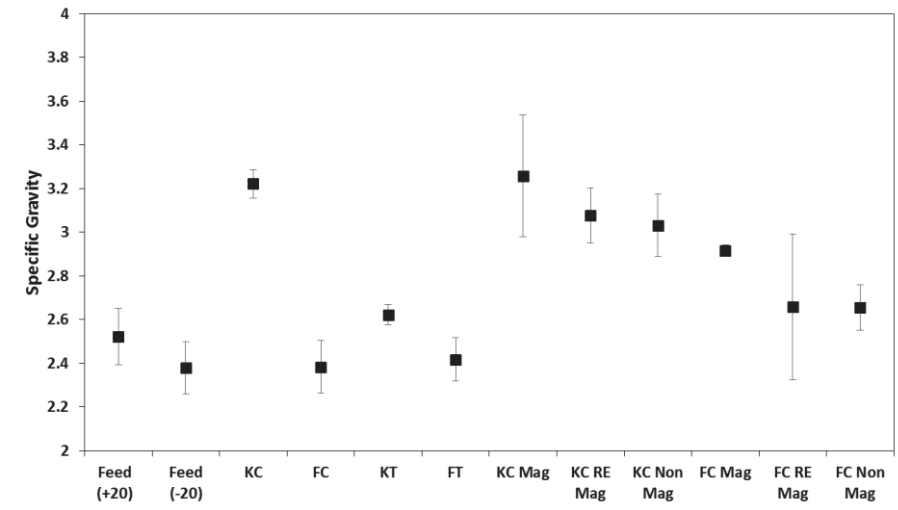

Figure 6.5 – Specific gravities (as determined by pycnometer measurement) of different products of centrifugal gravity concentration and drum magnetic separation. Error bars represent 95 % confidence intervals

Table 6.3 – Solid flow rates and percent solids for tailings streams from Knelson and Falcon

Stream	% Solids		Solids Flow (g/min)	
	Avg	*95% CI*	*Avg*	*95% CI*
KT	2.51	0.30	175	19
FT	9.06	2.07	300	68

The results of gravity separation can be better understood by using QEMSCAN data to assess recoveries of individual particles sorted by either size or specific gravity (SG). This

is possible by associating an SG value to each mineral in the deposit and then calculating the SG of each measured particle as a function of the different minerals within the particle. The volumetric composition of a particle is estimated from the two dimensional phase map of the particle as well as stereological corrections in the QEMSCAN software (Pascoe *et al.*, 2007). The particle SG is then calculated from the volumetric composition of the particle and the specific gravities of each mineral. Thus, it is possible to evaluate the recoveries achieved by both the Knelson and Falcon Concentrators by SG and size class. For this purpose the particles were split into 10 size classes from 5-10 µm up to +80 µm; and 18 different SG classes from < 2.5 to > 6.5. The resolution limitations of this technique must be acknowledged as particles of very fine sizes will have assigned specific gravities less than the lowest possible mineral SG (~2.5 for silicates). This is because the mounting material is assigned a specific gravity of 2 such that pixels at the interface of the mineral particle will have an assigned specific gravity that is lower than that of the actual mineral present on the surface of the particle. Thus, for very small particle sizes these “surface” pixels contribute significantly to the overall particle specific gravity and produce particles with lower SG values than would realistically be possible for this mineral system.

A composite view of the distribution of SG across the various size fractions in the feed material is shown in Figure 6.6. It can be seen that at very fine size ranges there are more particles of low SG (< 2 .5) and high SG (> 5.0), while at the coarsest particle sizes (+80 µm) the SG of all particles is 2.5-5. This is a reflection of the fine grained nature of the REM as the coarsest particles contain both high and low SG minerals.

A comparison of the total (Knelson + Falcon) gravity recovery at the fine and coarse particle sizes is shown in Figure 6.7. It is noted that there are certain categories of grouping particles by SG and size in which there are no corresponding feed particles. That is, if a distribution of particle sizes and SGs is divided arbitrarily in sufficiently small intervals, some of the intervals will contain no particles. Therefore, the zero recoveries shown are actually due to the lack of particles and not due to a lack of recovery. For example, Figure 6.7b shows that there are no coarse particles (> 60 µm) in the feed,

which have a particle SG within the range of 4.75-5.00 or 5.25-5.50. It is clear from Figure 6.7 that coarse particle recovery, even at low particle SG, is quite high, whereas fine particles (< 15 µm in diameter) have very low recoveries (as would be expected). The gravity recoveries for each separator are compared in Figure 6.8 for small (< 30 µm) particle sizes to compare the efficiency of fine particle collection between the two centrifugal gravity concentrators. The Knelson concentrator shows a clear size effect across all particle SGs, where recovery drops off dramatically with decreasing particle size. Additionally, the values for the recovery of 15-30 µm particles increase significantly with increasing SG, indicating that the Knelson concentrator is selectively concentrating high SG material. This effect is much less evident for the Falcon concentrator (Figure 6.8b), where recoveries show a very minimal increase with increasing SG and a much less pronounced decrease in recovery with decreasing particle size. This reinforces the conclusions from Figure 6.4 and Figure 6.5 that the Falcon concentrator in this process shows very low selectivity.

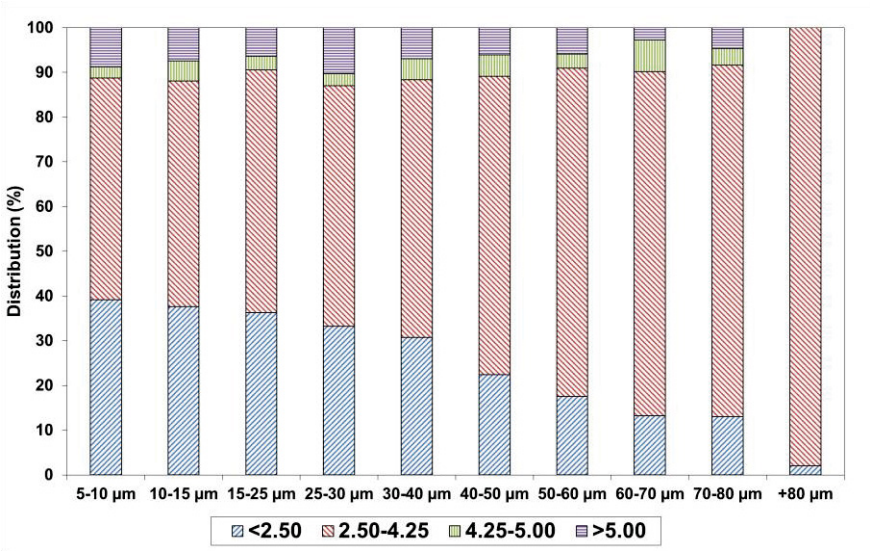

Figure 6.6 – Normalized distribution of particle densities across different feed size fractions. Legend entries refer to particle specific gravity

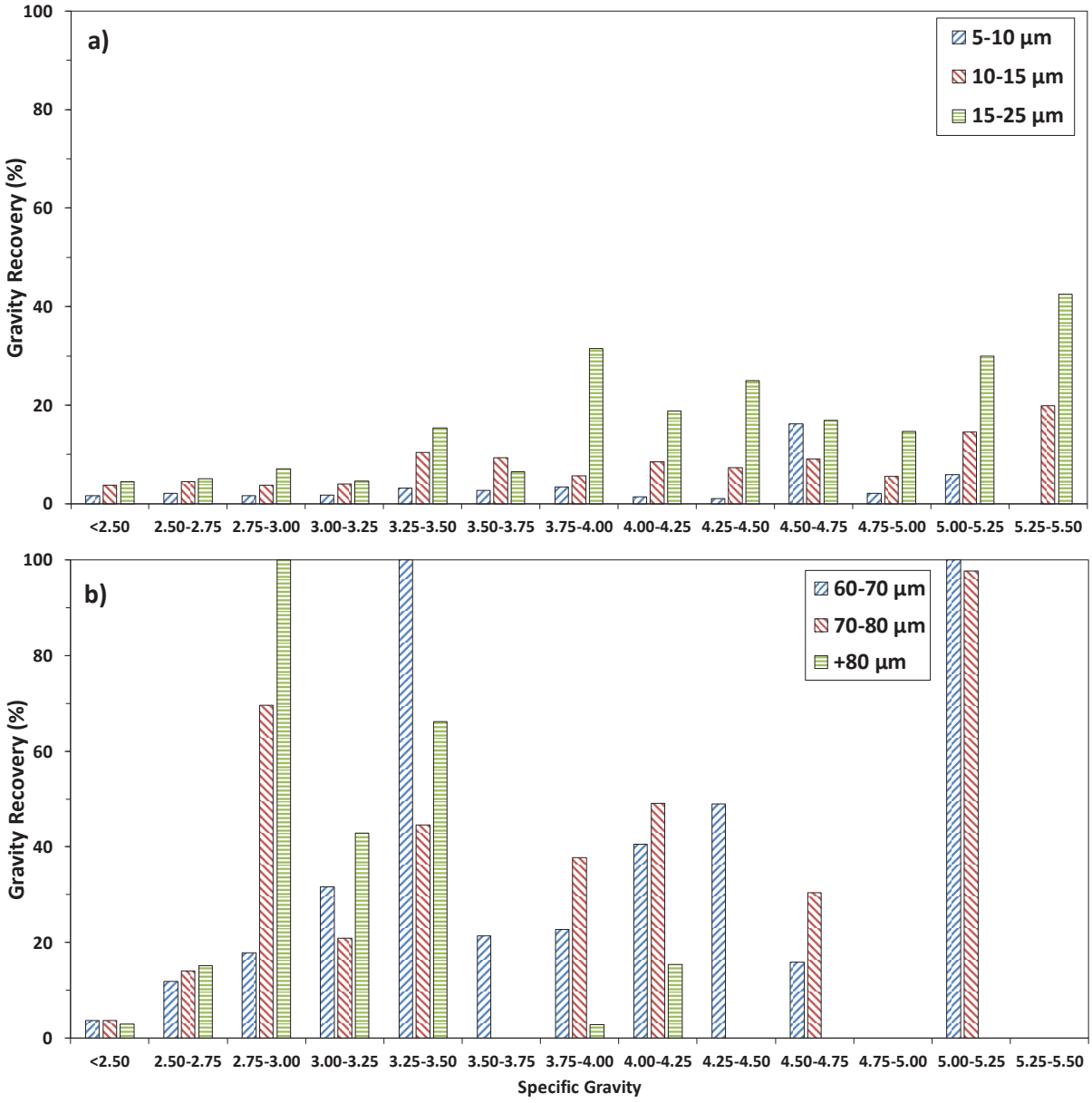

Figure 6.7 – Comparison of total gravity recovery (Knelson + Falcon) across particle specific gravity size classes for a) fine particle sizes and b) coarse particle sizes

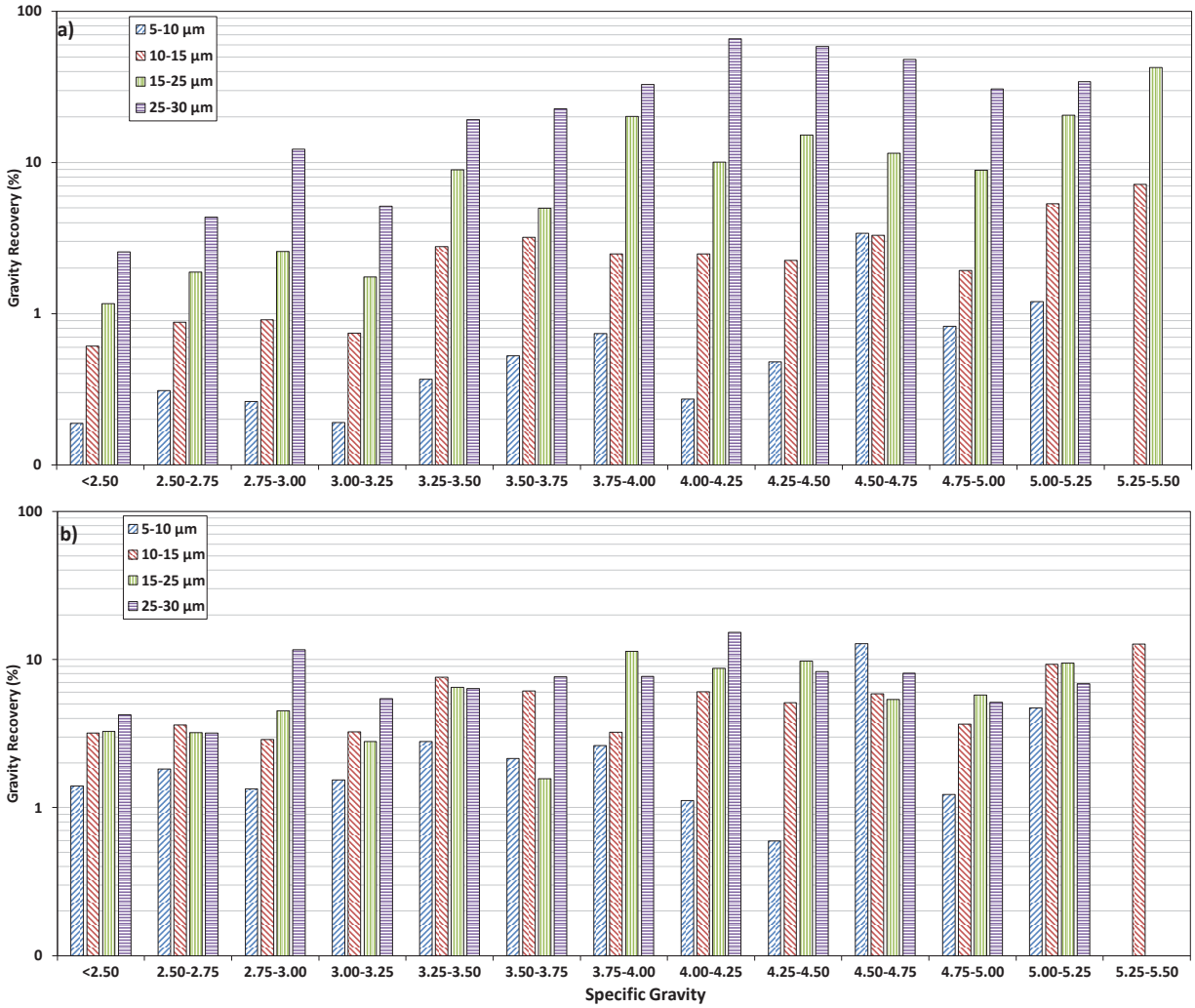

Figure 6.8 – Gravity recovery for small (< 30 µm) particles across particle specific gravity size classes for a) Knelson gravity concentrate and b) Falcon gravity concentrate

The particle size and SG information can also be filtered to select particles by the minerals contained in each particle. This allows for the evaluation of the distribution of particles containing a specific mineral across size classes (Figure 6.9). The Knelson and Falcon gravity concentrates were compared using the distribution of iron oxides, zircon and all particles across all size classes at 3 different SG levels. A more visual representation of this information is provided by QEMSCAN particle maps for the three same SGs (Figure 6.10). These two figures confirm the finding that the Knelson Concentrator in this process configuration has preferentially concentrated the coarser particles (independent of particle SG). Furthermore, zircon recovered in the Knelson gravity concentrate is highly

liberated at a particle SG of 4.25-4.50 (higher zircon recoveries for particles of this SG) (Figure 6.9 (e, f)), whereas in the Falcon gravity concentrate, zircon recovery is primarily due to the recovery of high SG (5.0-5.25), mixed mineral particles. This inference is confirmed by the particle maps shown in Figure 6.10 (c, d).

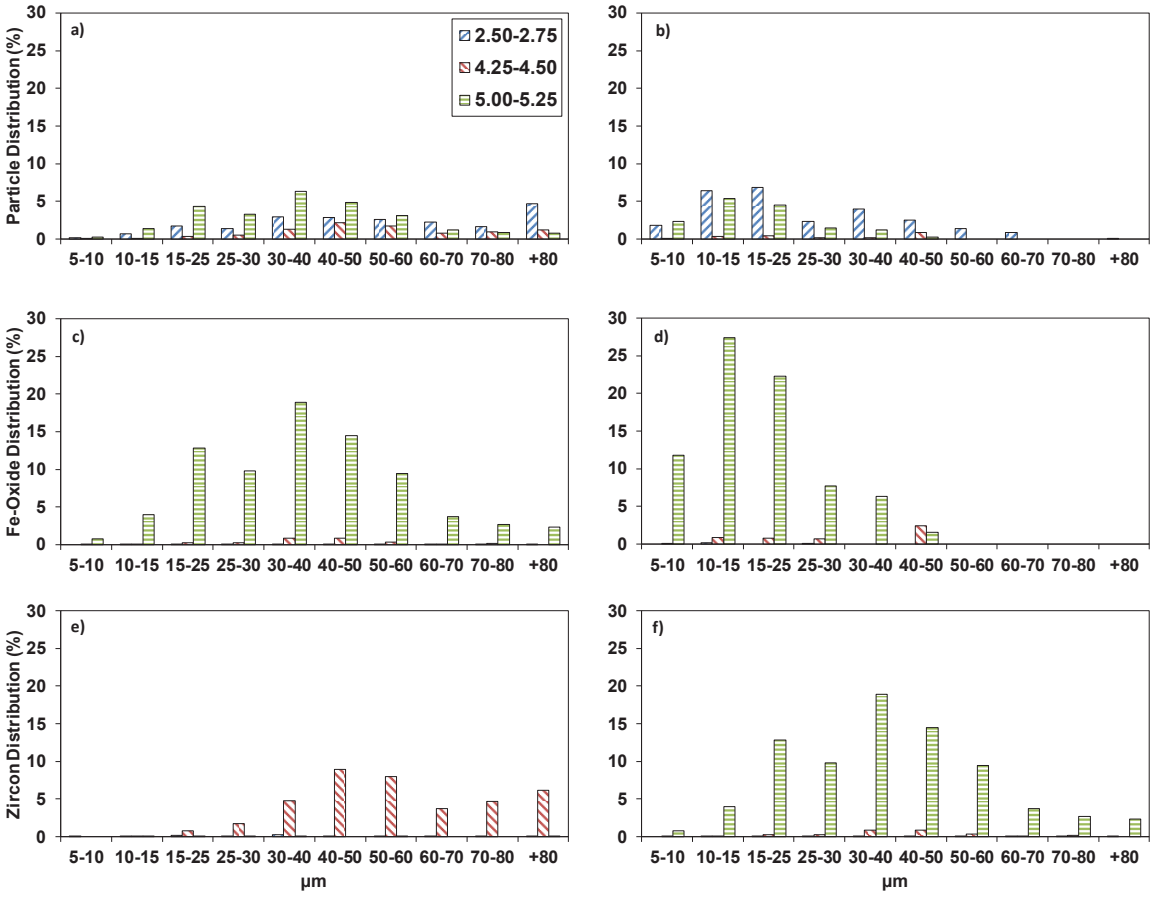

Figure 6.9 – Distribution of particles (a, b), particles containing iron oxide minerals (c, d) and particles containing zircon (e, f), for three different particle specific gravities across all size classes. Figures on the left (a, c, e) represent the Knelson gravity concentrate, and those one the right (b, d, f) represent the Falcon gravity concentrate

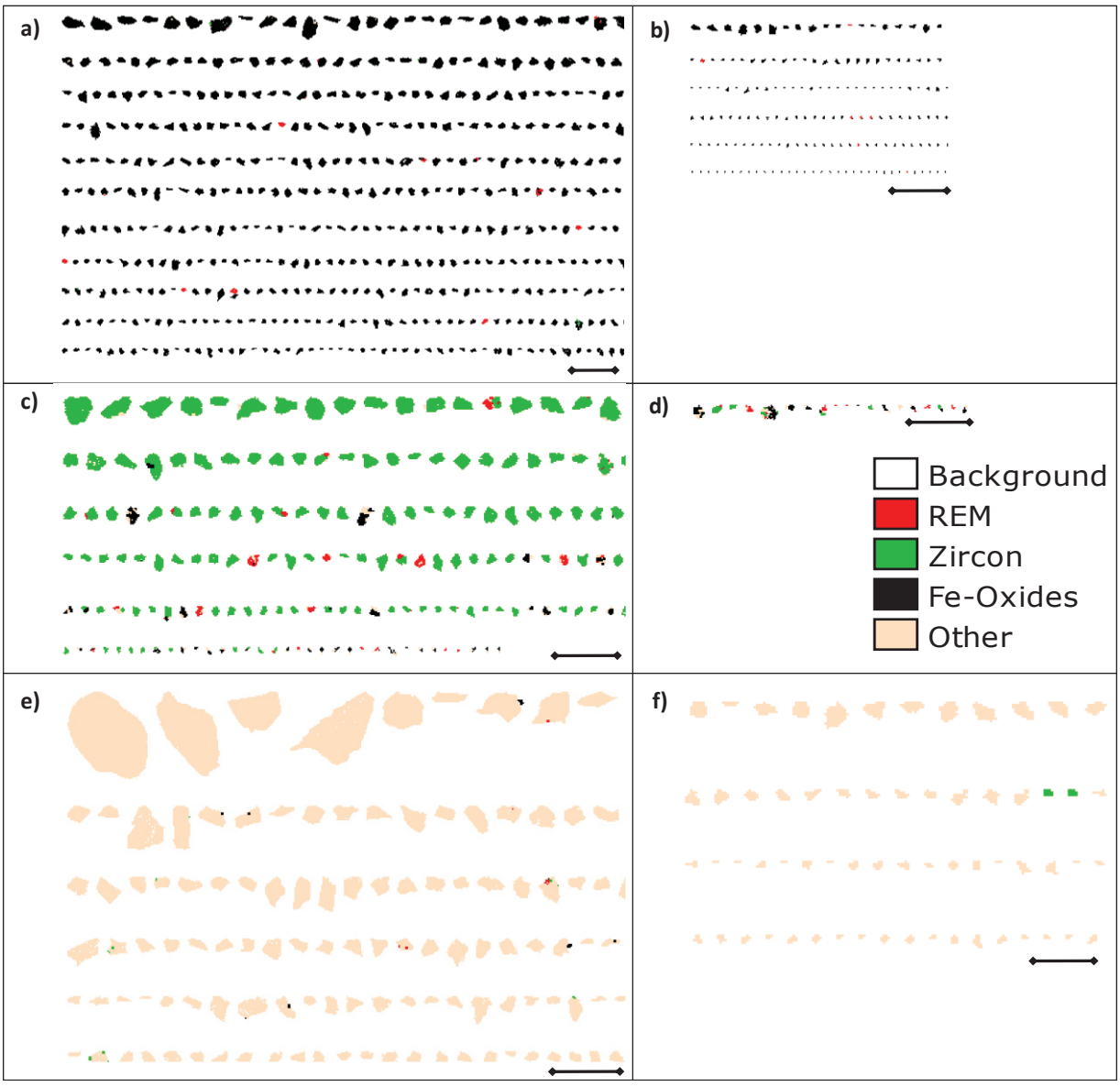

Figure 6.10 - Particle maps of high specific gravity (5.0-5.25) [a, b], intermediate specific gravity (4.25-4.5) [c,d] and low specific gravity (2.5-2.75) [e,f]. Particle maps on the left (a, c, e) represent the Knelson gravity concentrate and particle maps on the right (b, d, f) represent the Falcon gravity concentrate. Phase identification is limited to four mineral classes: iron oxides, zircon, REM (all other REM) and other (all other minerals in the deposit). Scale bars represent 250 µm (a, c, e) and 100 µm (b, d, f)

6.3.2 Deportment of magnetic phases

The choice of magnetic separation steps in this flowsheet (as detailed in Chapter 4) is motivated by the downstream flotation requirement of prior removal of iron-bearing gangue minerals. Additionally, many of the REM in the deposit have been previously

determined to be paramagnetic, and thus have the potential to be concentrated by a medium intensity magnetic drum separator (Chapter 5). In order to understand the deportment of magnetic minerals in this process, samples from each stream were analysed in a VSM to determine the magnetic properties of the sample. This technique, when applied to pure mineral samples, can be used to characterise magnetic properties. VSM results from mixed mineral samples provide general information as to the relative amount of magnetism in a sample. If there is only one main ferromagnetic mineral, then the data can be used to indirectly measure the concentration of this magnetic phase. Figure 6.11 shows VSM results for the feed to the centrifugal gravity and drum magnetic process as well as samples from all process streams. Paramagnetic minerals will have a positive linear slope, while ferromagnetic minerals will show a rapid increase in magnetisation followed by a plateau at the minerals saturation magnetisation (a characteristic property of ferromagnetic materials). A more detailed explanation of mineral magnetism along with VSM measurement of some pure REM is available in Chapters 2 and 5 respectively.

The coarse fraction of the feed exhibits a lower degree of ferromagnetism (Figure 6.11a) and indicates that there is either a higher concentration of ferromagnetic minerals or more strongly ferromagnetic minerals present in the finer size fraction. Based on the feed mineralogy (Table 6.1), the only minerals expected to exhibit ferromagnetic behaviour are the iron oxides (likely to be a mixture of magnetite and hematite). Likewise, the similar mineral concentrations (as measured by QEMSCAN) between the size fractions lead to the conclusion that the fine (< 20 μm) size fraction contains an elevated concentration of a strongly ferromagnetic iron oxide such as magnetite. The results (Figure 6.11b) show a higher ferromagnetic character for the Knelson gravity concentrate than that in the Falcon gravity concentrate, but both have a higher saturation magnetisation than the feed. The analysis of the two gravity tailings streams (Figure 6.11c) shows that after gravity separation the remaining mass in the tailings (~90 % of the feed) is most similar in magnetic behaviour to the fine size fraction of the feed. This is intuitive in the context of the results presented in Section 6.3.1 which demonstrated the preferential recovery of coarse particles in the gravity separation step. The results for the magnetic fractions

recovered from low intensity magnetic separation (Figure 6.11d) and medium intensity separation (Figure 6.11e) show that the Knelson gravity concentrate contains ferromagnetic material, which is primarily recovered at low intensity, while the Falcon gravity concentrate's magnetic products from both low and medium intensity magnetic separation have similar magnetic properties. This is, once again, likely due to particle size effects where the Knelson gravity concentrate contains larger liberated ferromagnetic particles that report to the magnetic fraction of a wet drum magnetic separator at lower applied magnetic field strengths. This is confirmed by the iron oxide d_{50} grain sizes calculated from QEMSCAN, which show the low intensity and medium intensity magnetic fractions from the Knelson gravity concentrate are larger (32 and 26 μm, respectively) than those produced from the Falcon (15 and 14 μm, respectively). Figure 6.11f shows a lack of ferromagnetism indicating that both non-magnetic products from medium intensity wet drum magnetic separation have very low concentrations of strongly ferromagnetic iron oxide minerals.

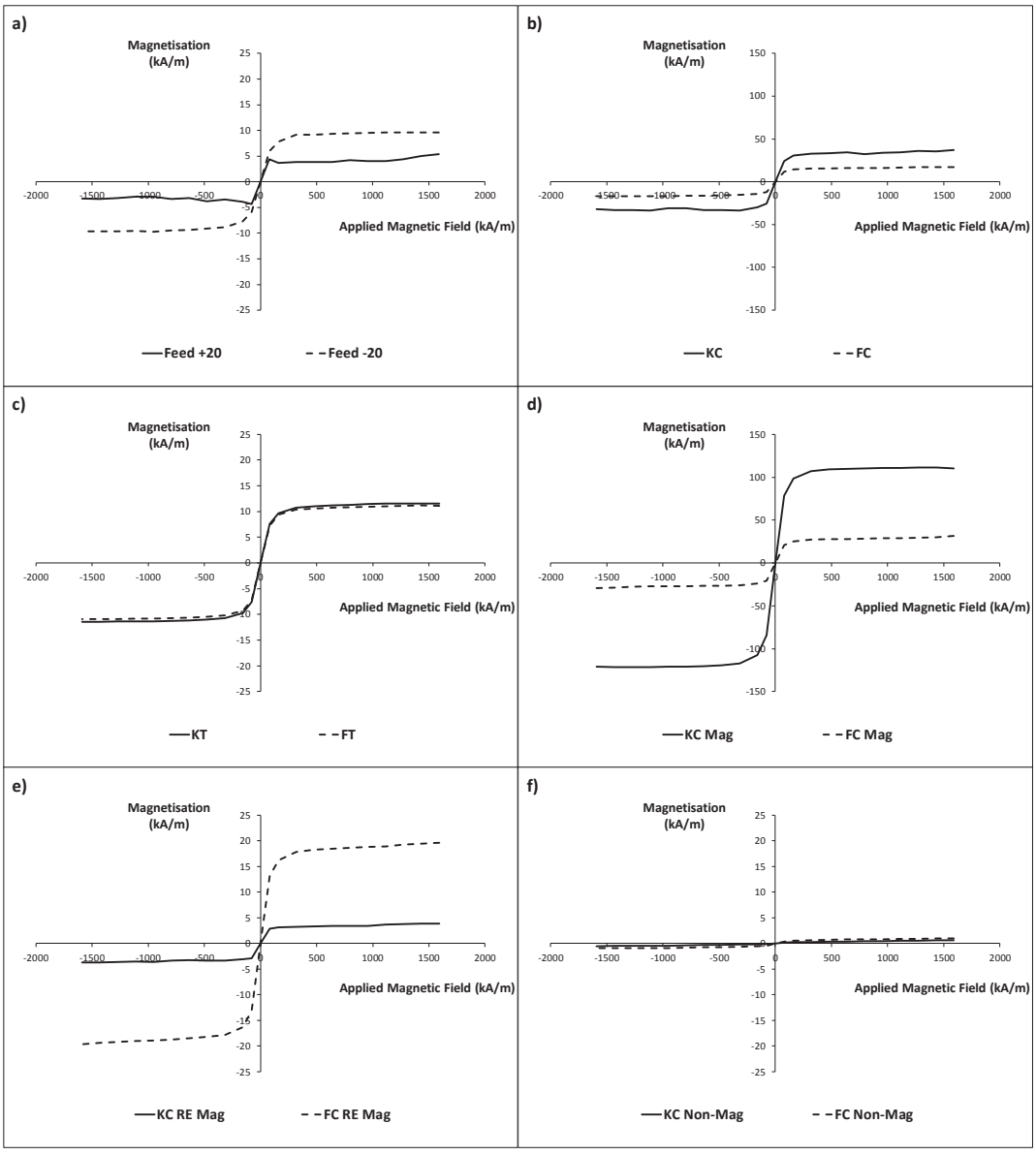

Figure 6.11 – Magnetic behaviour (magnetisation as a function of applied magnetic field) of samples from centrifugal gravity + wet drum magnetic flowsheet as determined by VSM for: a) feed, b) gravity concentrates, c) gravity tailings, d) low intensity magnetic fraction, e) medium intensity magnetic fraction, f) non-magnetic fraction

If the oversimplification of treating all samples in this flowsheet as binary mixtures of a paramagnetic mineral and a ferromagnetic mineral is made, then it is possible to semi-quantitatively evaluate and compare the ferromagnetic mineral content of each sample using Honda-Owen analysis. This analysis is more typically used in the elimination of the effects of a ferromagnetic impurity from VSM data for a paramagnetic sample (Chapter

5). Table 6.4 shows the results of this analysis assuming magnetite is the lone ferromagnetic mineral in the deposit. Although this might be incorrect it does provide a means of quantitatively comparing the VSM results.

Table 6.4 – Calculated magnetite content of different separation products from Honda-Owen analysis of VSM data

Stream Designation	Calculated Magnetite Content (%)
Feed +20	0.75
Feed -20	1.95
KC	6.70
FC	3.17
KT	2.33
FT	2.22
KC Mag	23.24
KC RE Mag	0.62
KC Non-Mag	0.00
FC Mag	5.59
FC RE Mag	3.74
FC Non-Mag	0.12

6.3.3 Grade and recovery of REM

In order to evaluate the effect of the centrifugal gravity concentration and wet drum magnetic separation circuit on the recovery of REM, the size-by-size recoveries of zircon, LREM and iron oxides are shown in Figure 6.12 (due to low concentration and fine grain sizes, data for fergusonite and columbite were excluded from this analysis). It can be seen from Figure 6.12 (a, b) that coarse zircon recovery occurs exclusively in the Knelson Concentrator while the Falcon Concentrator recovers fine-grained LREM (Figure 6.12 (c, d)). Recovery of coarse iron oxides occurs in the Knelson, while fine grained iron oxide in the Falcon shows higher recovery (Figure 6.12 (e, f)). For the Knelson gravity concentrate, the low intensity magnetic fraction has the highest recovery of iron oxides while the non-magnetic product from medium intensity magnetic separation contains the highest recoveries of zircon (Figure 6.12a and Figure 6.12e). This suggests that the wet drum magnetic separation is efficiently rejecting iron oxide minerals which are collected in the gravity separation stage.

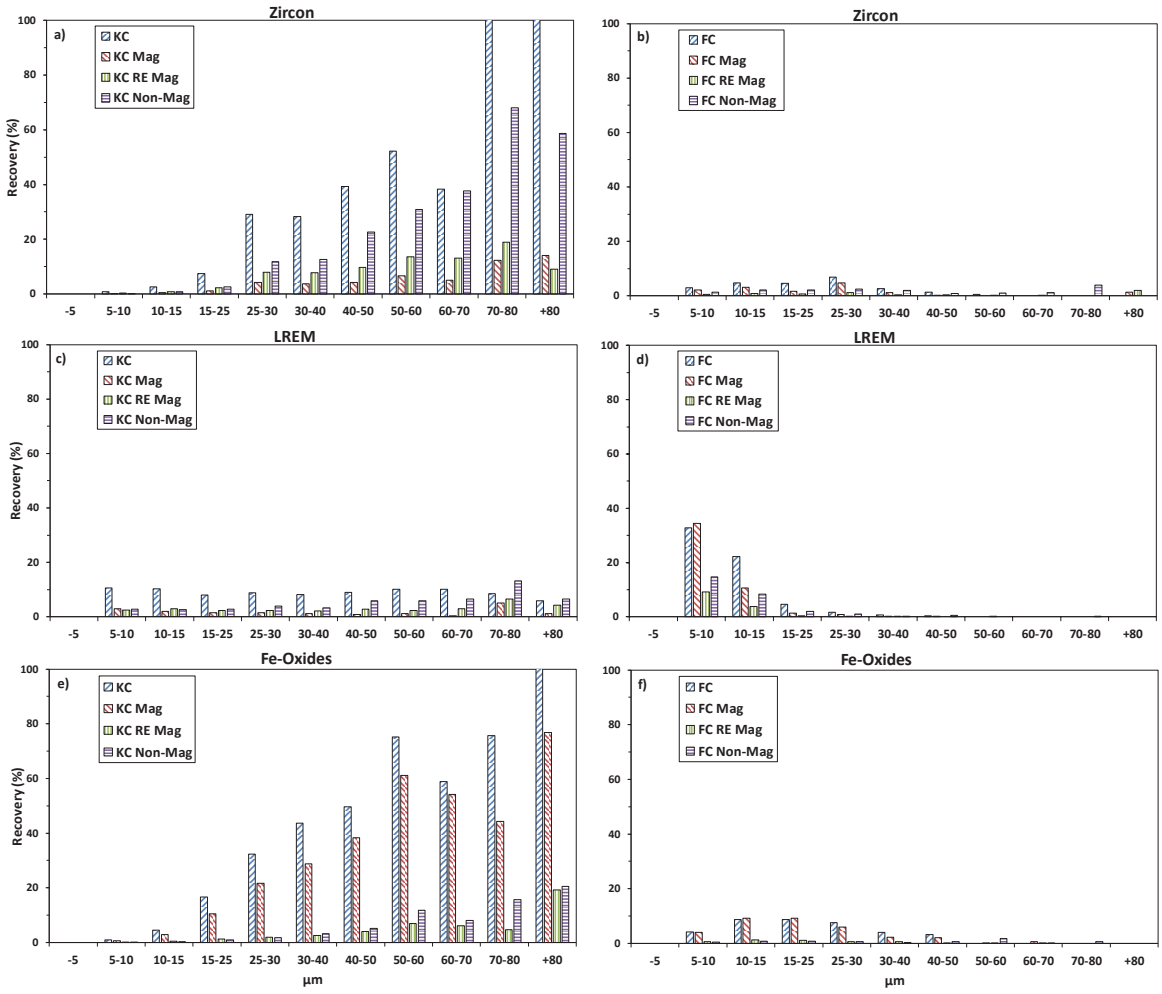

Figure 6.12 – Size-by-size recoveries of: zircon (a, b), LREM (c, d) and iron oxide minerals (e, f). The left column represents the Knelson gravity concentrate and associated downstream magnetic separation products while the right represents the Falcon gravity concentrate and associated downstream magnetic separation products

To further examine the different streams in terms of the grade and recovery of value REM as well as gangue, grade-recovery plots of zircon as well as three of the main gangue minerals (iron oxides, quartz and K-feldspar) are shown in Figure 6.13. The highest grade zircon stream can be seen to be the non-magnetic fraction produced from the Knelson gravity concentrate (KC Non-Mag) (Figure 6.13a). The highest-grade iron oxide stream (Figure 6.13b) is the low intensity magnetic fraction produced from the Knelson gravity concentrate (KC Mag), while the KC Non-Mag stream has low recovery of iron oxides at a grade approximately equivalent to the feed. The two silicate gangue minerals (Figure

6.13c, d) are rejected in every stream shown (grades below feed grade) with the KC Non-Mag fraction showing low grades and recoveries of both these minerals. Therefore, the KC Non-Mag fraction appears to have successfully concentrated the targeted REM, zircon.

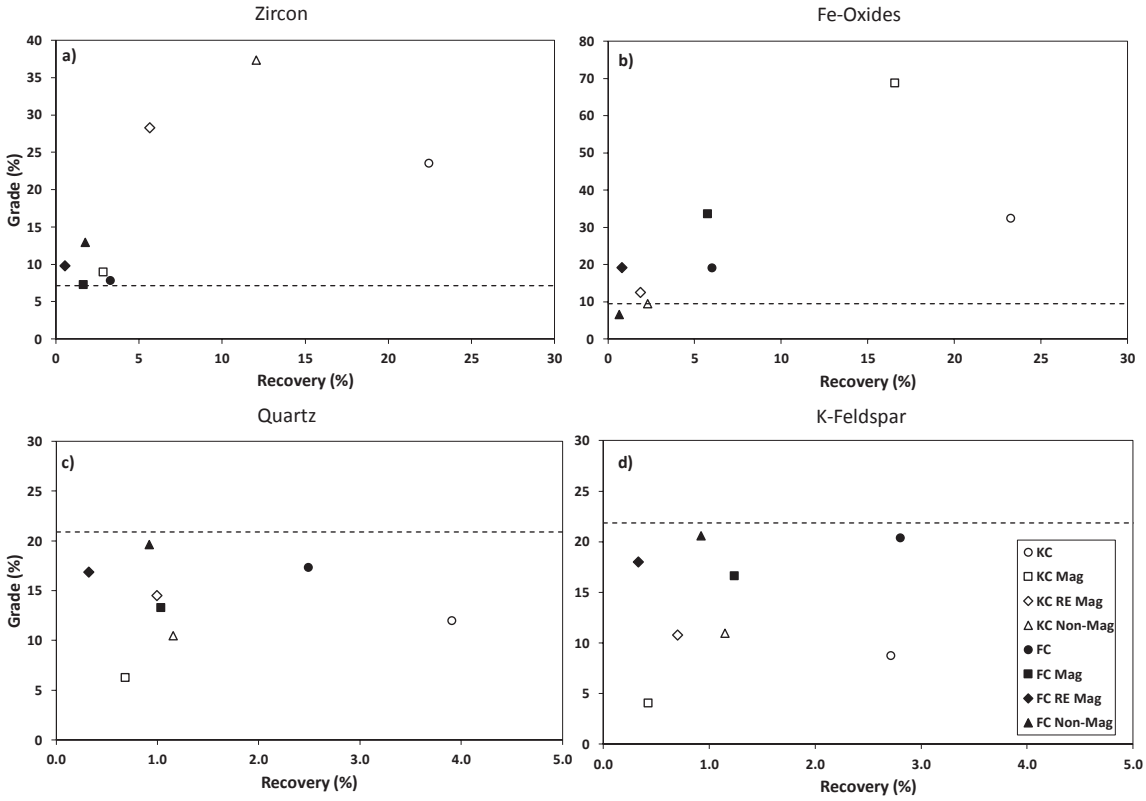

Figure 6.13 – Grade and recovery of: a) zircon, b) iron oxides, c) quartz and d) K-feldspar as calculated from QEMSCAN. Dashed lines in all figures represent feed grade

Figure 6.14 is the elemental [expressed as rare earth oxide (REO)] grade-recovery for the same streams and it illustrates that the KC Non-Mag fraction has the highest REO grade. However, it is significant that the recovery in the KC Non-Mag fraction is much lower than that achieved in the Knelson gravity concentrate prior to magnetic separation. This implies that there are significant losses of REM in the wet drum magnetic products. It is also interesting to note that recoveries of the HREO and Value REO in the KC Non-Mag fraction are higher than those for LREO. This may be attributed to the concentration of heavy REE-bearing zircon without similar recoveries of light REE-bearing minerals. A

further discussion of the optimum fraction for downstream flotation is presented in Section 6.6.

Scanning electron microscopy and energy dispersive X-ray spectroscopy were used to qualitatively identify important elements (Zr, Fe, La, Ce, Nd, and Y) as well as REM in the feed (Figure 6.15) and products of gravity (Figure 6.16) and magnetic separation (Figure 6.17 and Figure 6.18). The SEM images in Figure 6.15 and Figure 6.16 illustrate the differences between the Knelson and Falcon gravity concentrates in terms of particle size as well as demonstrating the successful concentration of Zr, Fe and REM into the gravity concentrates. The images of the products of magnetic separation of the Knelson gravity concentrate (Figure 6.17) show that fine Fe particles are concentrated into the low-intensity magnetic product with coarse REM remaining in the medium-intensity magnetic and non-magnetic products. Figure 6.18 shows a similar trend for the recovery of REM in the non-magnetic fractions of the Falcon gravity concentrate but the removal of Fe-bearing minerals occurs over both low-intensity and medium-intensity magnetic products.

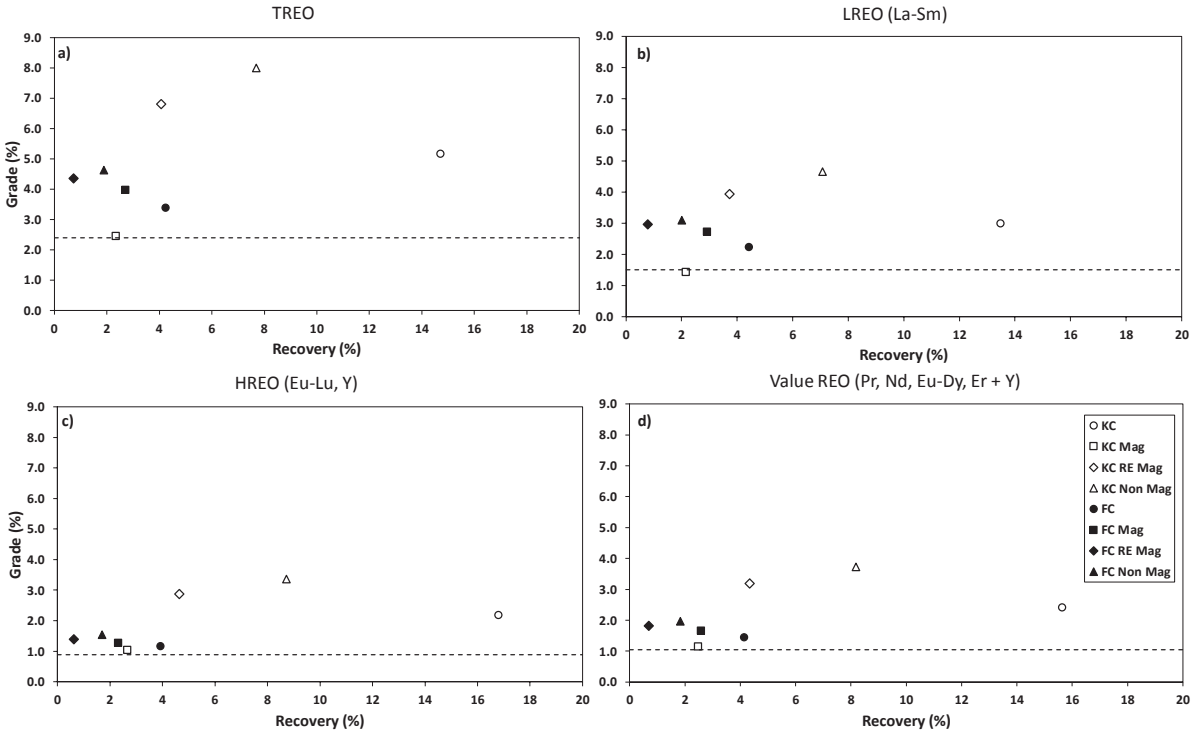

Figure 6.14 – Grade and recovery of: a) total REO, b) light REO, c) heavy REO and d) most valuable REO as determined by ICP-MS. Dashed lines in all figures represent feed grade

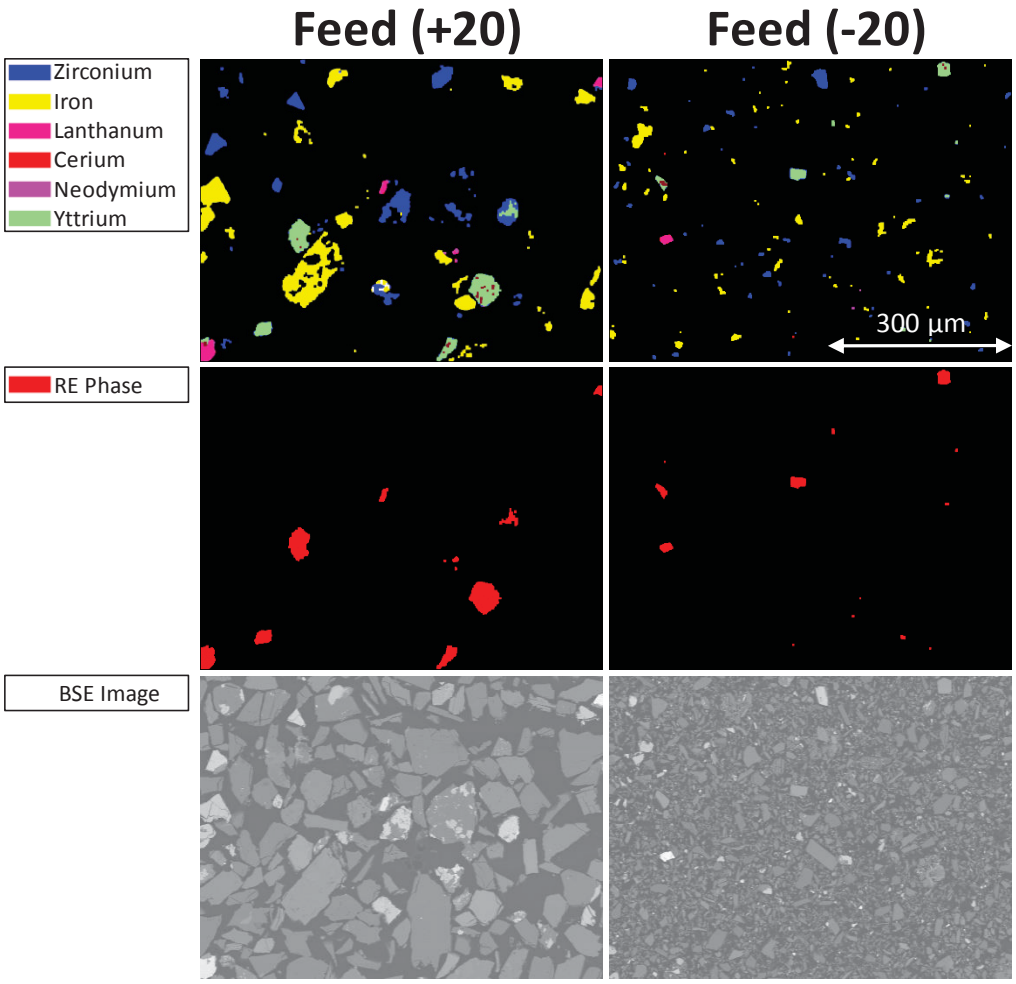

Figure 6.15 – SEM images of the feed (+20 µm and -20 µm) to gravity and magnetic separation including elemental (Zr, Fe, La, Ce, Nd, Y) phase identification, REM identification and backscattered electron (BSE) images

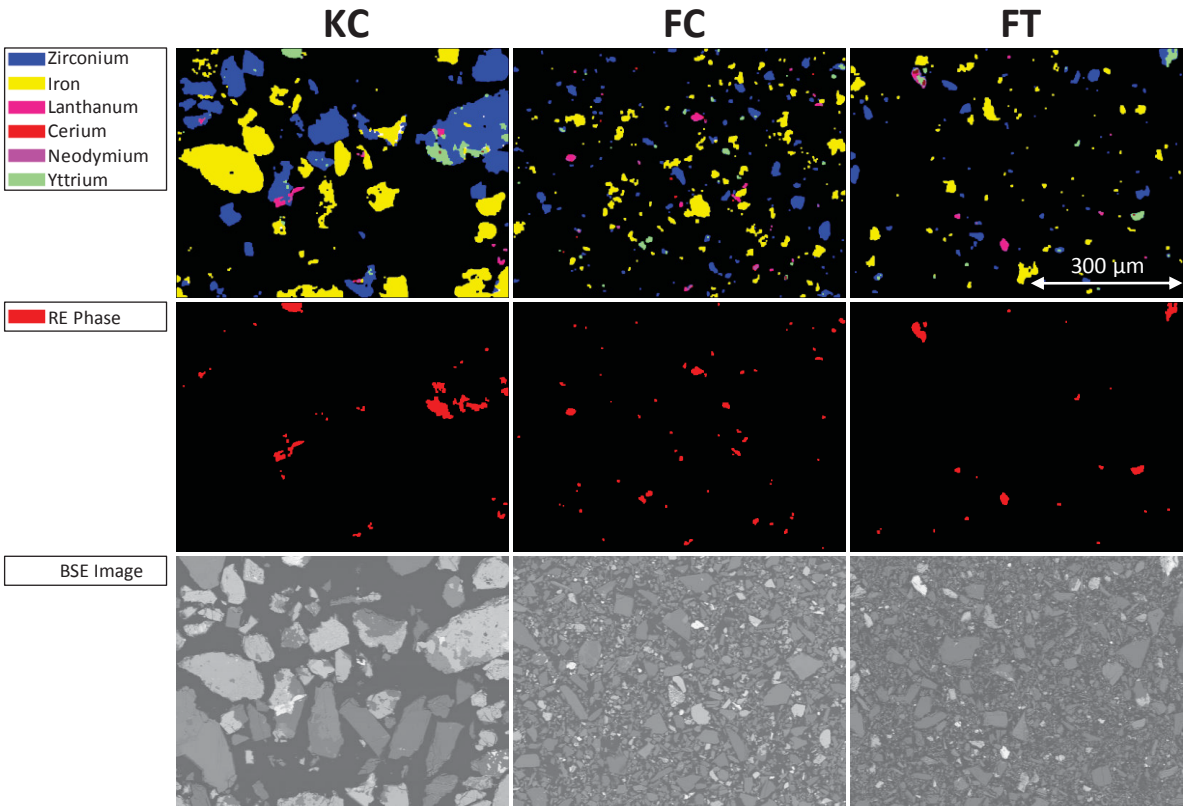

Figure 6.16 – SEM images of the Knelson Con (KC), Falcon Con (FC) and Falcon Tailings (FT) including elemental (Zr, Fe, La, Ce, Nd, Y) phase identification, REM identification and backscattered electron (BSE) images

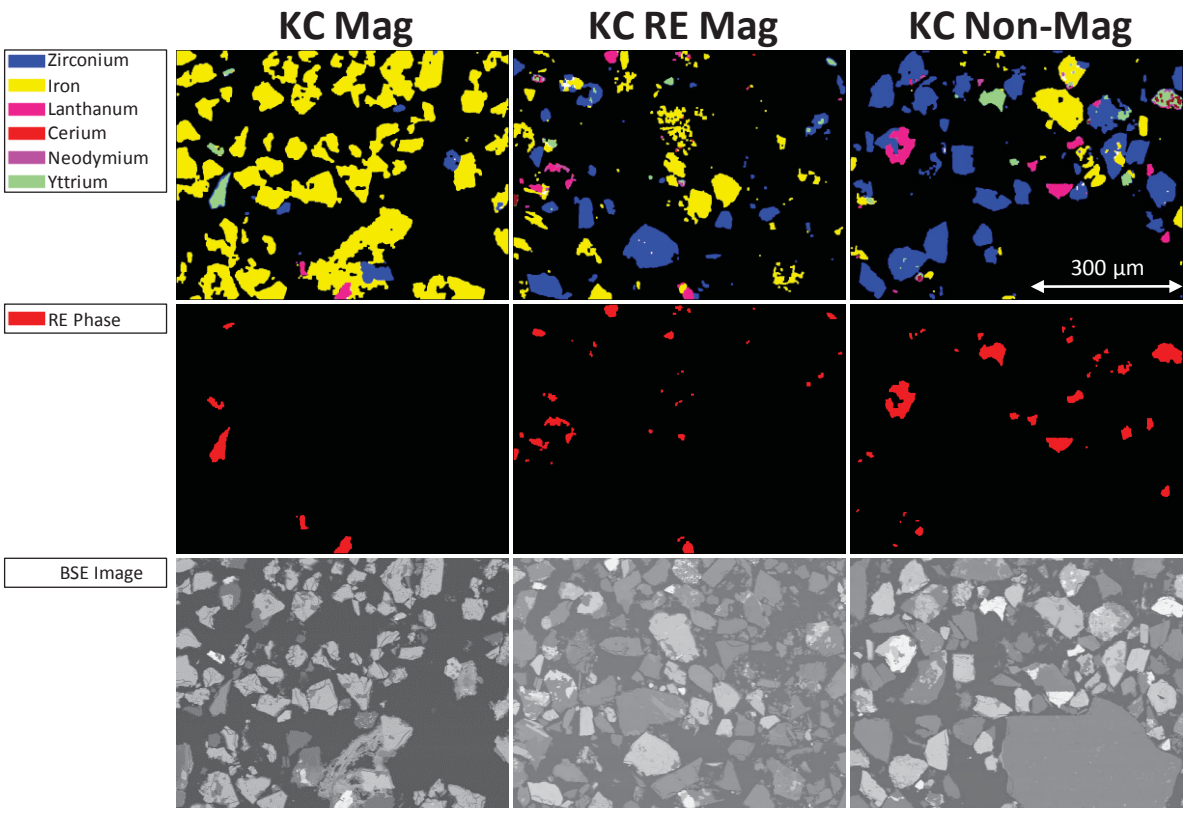

Figure 6.17 – SEM images of the Knelson Con low intensity magnetic product (KC Mag), Knelson Con medium intensity magnetic product (KC RE Mag) and Knelson Con non-magnetic product (KC Non-Mag) including elemental (Zr, Fe, La, Ce, Nd, Y) phase identification, REM identification and backscattered electron (BSE) images

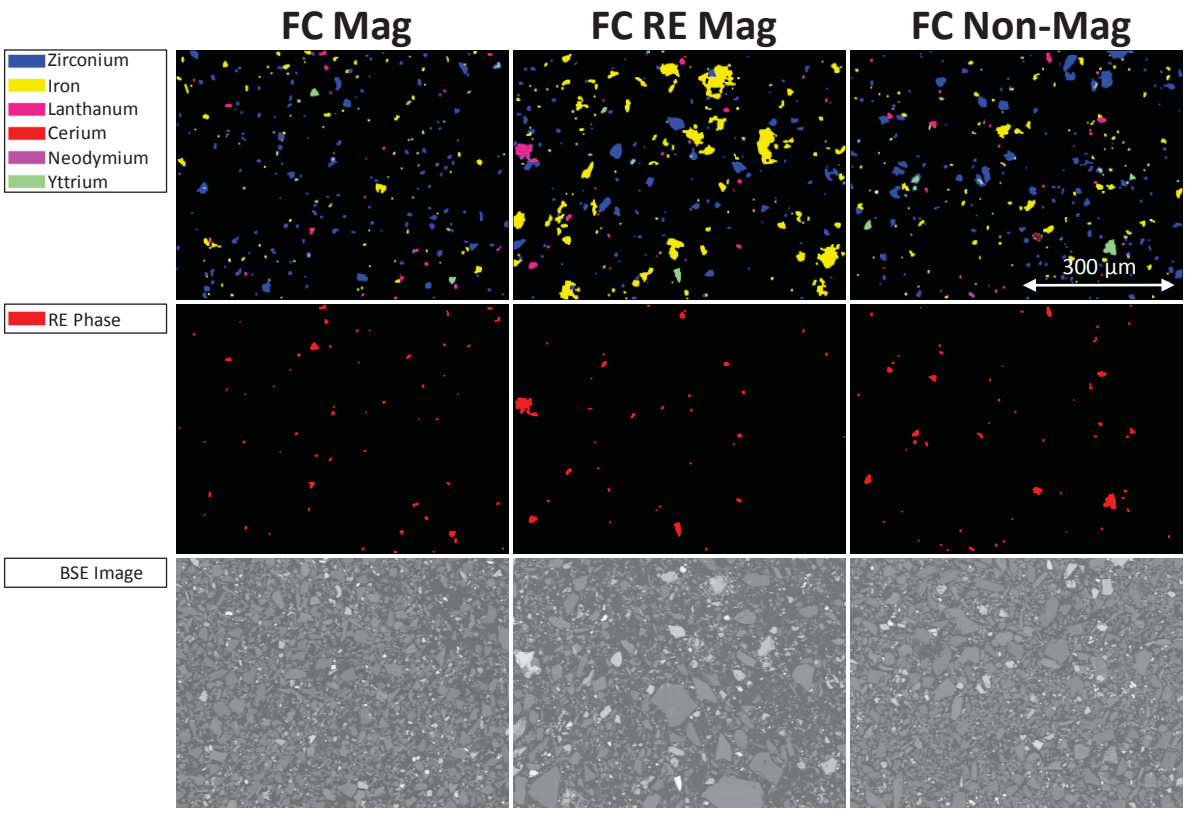

Figure 6.18 – SEM images of the Falcon Con low intensity magnetic product (FC Mag), Falcon Con medium intensity magnetic product (FC RE Mag) and Falcon Con non-magnetic product (FC Non-Mag) including elemental (Zr, Fe, La, Ce, Nd, Y) phase identification, REM identification and backscattered electron (BSE) images

6.4 Dry magnetic separation

Prior to the wet drum magnetic separation steps (Figure 4.5) the Knelson gravity concentrate was screened at 300 µm, as particles coarser than this would not be expected to respond well to wet drum magnetic separation. This coarse material was then screened into five different size fractions and submitted for QEMSCAN analysis (Table 6.5). The mass pull to the oversize (+300 µm) fraction (KC Oversize in Table 6.2) was 0.81 wt. % with the largest size fraction by mass being the 600-1180 µm fraction. The mineralogy (Table 6.5) shows that both zircon and iron oxides are enriched in the oversize material, indicating that the Knelson gravity concentration step has had some concentrating effect for higher SG minerals, even at very coarse particle sizes. The mineral associations of the zircon, iron oxides and LREM are shown in Figure 6.19. As expected, there is very little liberation at these size ranges, with the exception being the

iron oxide minerals which show slightly higher degrees of liberation at smaller particle sizes (up to 17 % free+liberated for the 300-425 µm size fraction).

As a result of the presence of significant concentrations of iron oxide minerals in the oversize material, a series of dry induced roll magnetic separation steps were carried out to investigate the possibility of further concentrating REM by eliminating magnetic iron oxides. The flowsheet for this magnetic separation process (Figure 4.4) has four of the size fractions fed separately to this process (the +1700 µm fraction did not have enough mass to warrant further separation). The mass pull as a function of magnetic field strength is shown in Figure 6.20. The mass pull of ~40-50 % indicates that the bulk of the iron oxide minerals are likely to report to the magnetic fraction at a magnetic field strength of 0.5 T. This mass pull is much higher than the iron oxide content of the KC Oversize fraction (Table 6.5), indicating that the bulk of the iron oxide minerals are being recovered as mixed particles. The slightly lower mass pull of the smaller size fractions (Figure 6.20) is indicative of the increase in iron oxide liberation at these sizes.

Efforts to analyse the products of dry magnetic separation using XRD were unsuccessful due to the difficulty in sampling representatively from such a small amount of coarse material. Therefore, it is not possible to comment on the efficiency of the dry magnetic separation process. Nevertheless, the grain sizes of the KC Oversize stream measured from QEMSCAN (Figure 6.21) suggest that a secondary comminution step after screening of the centrifugal gravity concentrate could achieve high degrees of liberation at much larger particle sizes (~100 µm) than the initial grinding stage. The resultant liberated material could then be easily concentrated using additional gravity, magnetic and/or flotation separation.

Table 6.5 – Mineralogy (in wt. %) of Knelson gravity concentrate oversize by size fraction as determined by QEMSCAN

Mineral Name	+1700 µm	-1700 +1180 µm	-1180 +600 µm	-600 +425 µm	-425 +300 µm	Combined
REM						
Zircon	19.68	14.01	12.05	9.08	9.56	12.55
Bastnäsite	1.38	1.21	1.80	1.77	1.96	1.64
Synchysite	0.31	0.23	0.50	0.55	0.47	0.42
Allanite	0.57	1.02	0.57	0.52	0.66	0.67
Columbite (Fe)	0.52	0.53	0.60	0.61	0.48	0.56
Fergusonite	0.25	0.14	0.14	0.22	0.17	0.17
Other REM	0.18	0.29	0.37	0.28	0.22	0.30
Silicate Gangue						
K-Feldspar	11.82	16.79	20.45	21.01	21.91	18.95
Quartz	19.20	18.39	15.30	15.72	16.40	16.62
Plagioclase	11.02	13.74	18.67	21.14	20.82	17.39
Biotite	11.25	10.02	9.87	9.85	9.48	10.01
Other Gangue						
Fe-Oxides	17.06	15.82	12.05	11.92	11.52	13.36
Ankerite	2.63	3.53	3.69	3.20	3.00	3.37
Calcite	0.99	0.73	0.89	0.71	0.75	0.82
Fluorite	1.36	1.97	1.04	1.27	1.01	1.32
Other Gangue	1.78	1.57	2.02	2.15	1.58	1.86

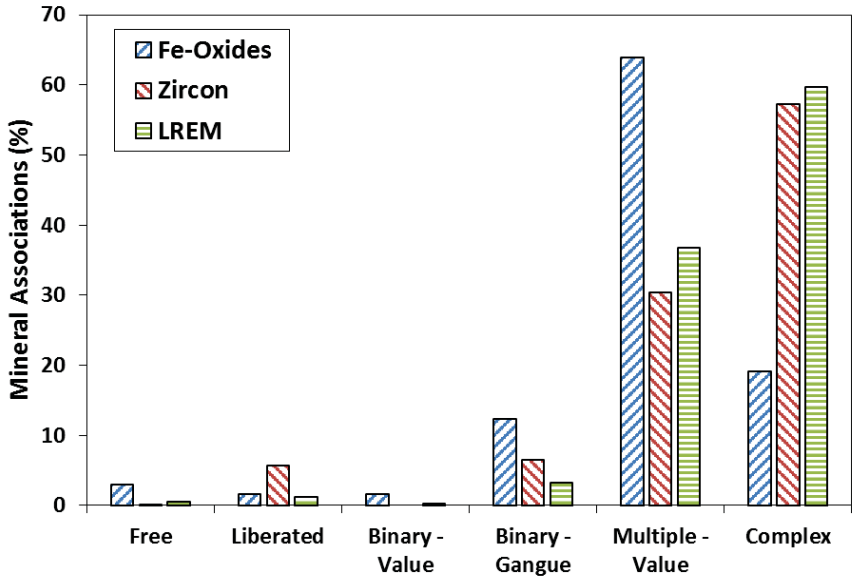

Figure 6.19 – Mineral liberation characteristics of iron oxide minerals, zircon and LREM in the Knelson gravity concentrate oversize fraction calculated from QEMSCAN. LREM = bastnäsite, synchysite, allanite and monazite

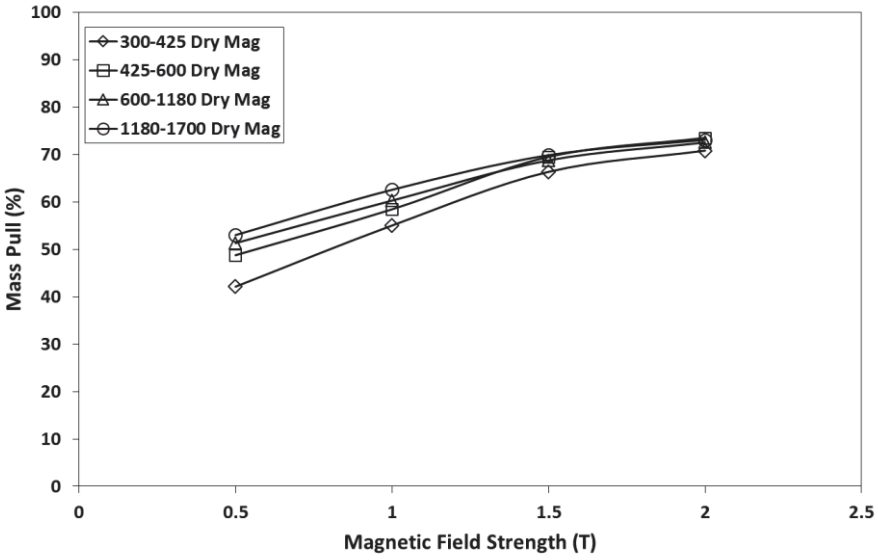

Figure 6.20 – Mass pull to the magnetic fraction of the dry variable magnetic separation process as a function of applied magnetic field strength for four different size fractions from the Knelson gravity concentrate oversize fraction

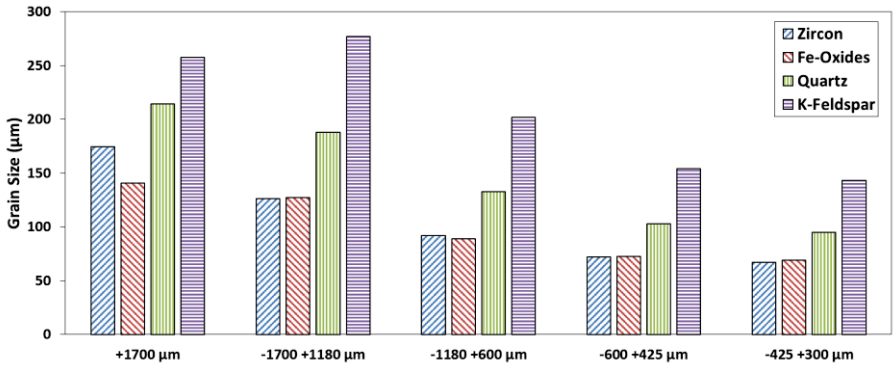

Figure 6.21 – Grain size of zircon, iron oxide minerals, quartz and K-feldspar as measured by QEMSCAN for five different size fractions of the Knelson gravity concentrate oversize fraction

6.5 Wet variable intensity magnetic separation

The two non-magnetic fractions produced from medium intensity drum magnetic separation of the centrifugal gravity concentrates were shown in Section 6.3.3 to still contain iron oxide minerals at levels as high as the initial feed grade (Figure 6.13b). To determine whether the remaining iron oxides in the KC Non-Mag and FC Non-Mag fractions (Table 6.6) could be removed by further magnetic separation, each of these streams was then fed to a series of WHIMS stages (Figure 4.6). This is the next logical

step after medium intensity drum magnetic separation to target finer particles of ferromagnetic minerals as well as strongly paramagnetic mineral particles. Figure 6.22 shows the mass pull of this series of separations (as a function of applied magnetic field strength). These mass split results are much lower compared to previous work which fed the Knelson and Falcon gravity concentrates directly to the WHIMS step, with mass pulls as high as 65 % at 0.94 T reported (preliminary gravity and magnetic separation work not included in this thesis can be found in Appendix A).

The products from the WHIMS process were then analysed using XRD to identify the major phases (Figure 6.23 and Figure 6.24). It can be concluded that iron oxide minerals (magnetite and hematite) were concentrated in each magnetic fraction produced from both feeds. The non-magnetic products from WHIMS show a significantly larger peak for feldspar minerals (albite and microcline) indicating that they were efficiently rejected through the WHIMS process. The presence of REM (zircon, allanite and bastnäsite) in some of the magnetic concentrates indicate that these minerals either experienced sufficient magnetic force to report to the magnetic fraction directly, or that they were recovered as part of a mixed mineral particle containing an iron oxide mineral. The clear difference between the WHIMS process applied to the KC Non-Mag and FC Non-Mag streams is the difference in the distribution of REM in that there are larger peaks corresponding to zircon in the KC WHIMS magnetic fractions and larger peaks for allanite and bastnäsite in the FC WHIMS magnetic fractions. The higher concentration of allanite and bastnäsite in the FC WHIMS magnetic fractions does not correspond well with the concentrations of each mineral in the feed to the WHIMS process (Table 6.6) as the KC Non-Mag stream is enriched in all REM relative to the FC Non-Mag stream. However, this may be explained in the differences in particle size of these two streams (d_{50} values of 53 and 25 µm, respectively) such that the FC Non-Mag stream contains more well-liberated allanite and bastnäsite particles. Additionally, the mineral associations of LREM (bastnäsite, synchysite, allanite and monazite) into the KC Non-Mag and FC Non-Mag streams is shown in Figure 6.25. There is a clear size difference in the mineral association data between the two fractions with the KC Non-Mag stream containing liberated LREM across many size fractions, while the FC Non-Mag stream contains liberated LREM only

at very fine sizes. This suggests that liberated allanite and bastnäsite in the deposit are found over a narrowly distributed, fine size range, and thus, it would be expected to report to the WHIMS magnetic fraction only at very high magnetic field strengths (Figure 6.24).

Table 6.6 – Mineralogy (in wt. %) of the non-magnetic products of medium intensity wet drum magnetic separation as determined by QEMSCAN

Mineral Name	KC Non-Mag	FC Non-Mag
REM		
Zircon	37.36	12.91
Bastnäsite	3.70	1.65
Synchysite	1.38	1.05
Allanite	1.56	0.76
Columbite (Fe)	1.22	1.13
Fergusonite	0.91	0.51
Other REM	0.89	0.63
Silicate Gangue		
K-Feldspar	10.91	20.56
Quartz	10.49	19.61
Plagioclase	12.95	18.57
Biotite	4.20	9.65
Other Gangue		
Fe-Oxides	9.52	6.54
Ankerite	1.57	3.33
Calcite	0.35	0.43
Fluorite	0.63	0.84
Other Gangue	2.36	1.83

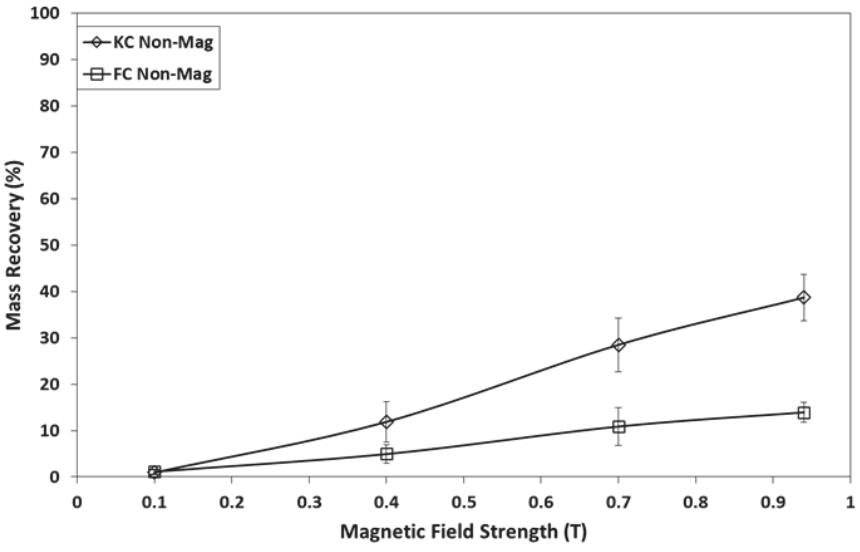

Figure 6.22 - Mass pull as a function of applied magnetic field strength for the wet high intensity magnetic separation of the non-magnetic product of medium intensity wet drum magnetic separation from the Knelson and Falcon gravity concentrates. Error bars represent 95 % confidence intervals

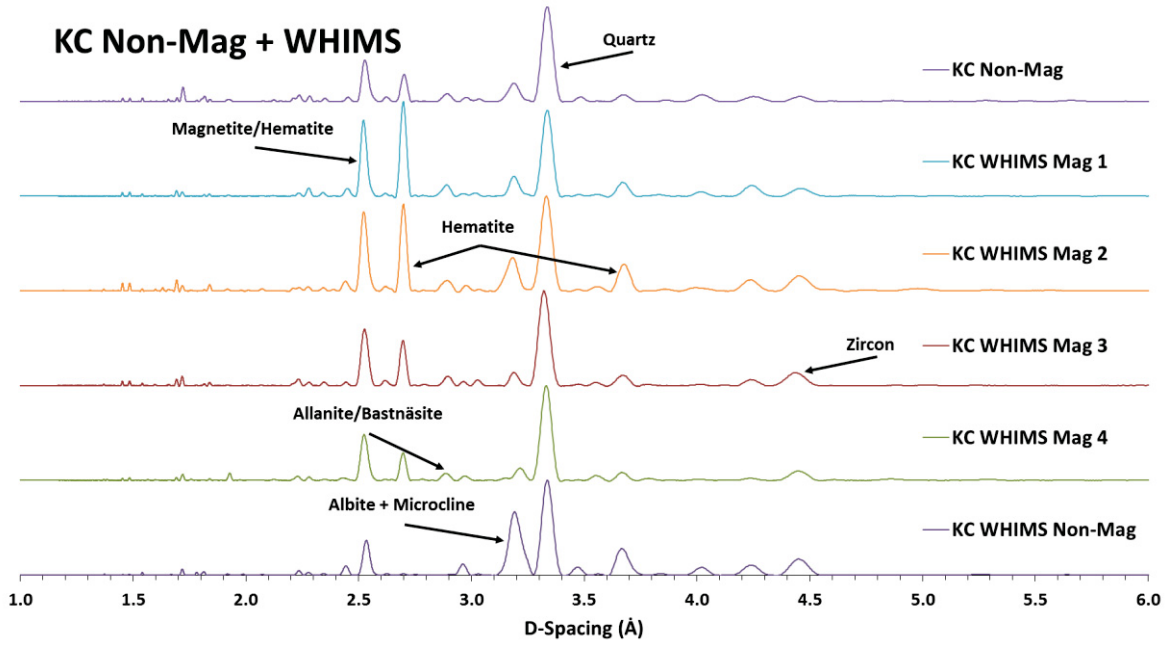

Figure 6.23 – X-ray diffraction patterns of the wet high intensity magnetic separation of the non-magnetic product of medium intensity wet drum magnetic separation from the Knelson gravity concentrate. All peak heights are normalized against the maximum peak intensity in each pattern

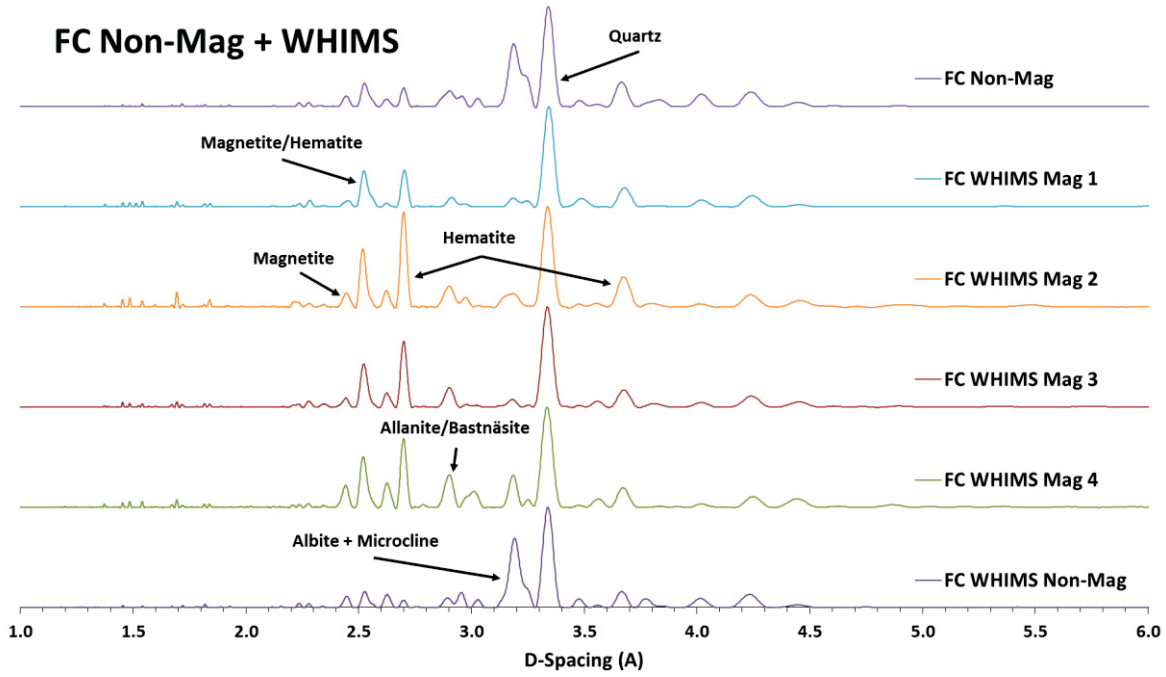

Figure 6.24 – X-ray diffraction patterns of the wet high intensity magnetic separation of the non-magnetic product of medium intensity wet drum magnetic separation from the Knelson gravity concentrate. All peak heights are normalized against the maximum peak intensity in each pattern

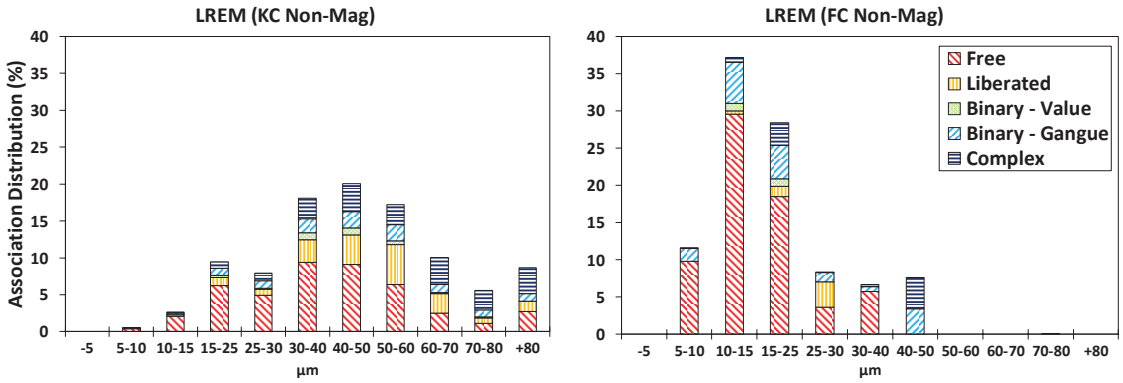

Figure 6.25 – Mineral associations of LREM across all sizes in the non-magnetic fractions from medium intensity wet magnetic separation applied to the Knelson and Falcon gravity concentrates

6.6 Selection of optimal fraction for downstream processing

The ultimate goal of the processes presented in Sections 6.3 to 6.5 was to produce an optimal product for downstream froth flotation. The requirements for this product include: rejection of iron-bearing gangue (detrimental to flotation with hydroxamates); rejection of silicate gangue and maximizing the grade and recovery of REE, in particular the heavy REE which have the greatest economic impact to a potential REE mine. In order to combine mineralogical and elemental grade and recovery data for many different minerals and elements and many different product streams, graphs of upgrade ratio versus recovery were created. On such a graph, different minerals from the same sample will form a linear line with the length of the line between points indicating the selectivity of that sample for one mineral (or group of minerals) over another. The point at the upper right of such a graph is the mineral which is being concentrated to the greatest extent and the point at the lower left is the mineral being rejected to the greatest extent. Upgrade ratio is a better indicator than grade, in systems with multiple value minerals, as the change in grade may not be indicative of the degree to which a given mineral is concentrated if the initial concentration of the mineral is relatively low.

Graphs of upgrade ratio versus recovery were created for the streams produced from centrifugal gravity concentration and wet drum magnetic separation (Figure 6.26 (a, b)); for different combinations of these product streams such as the combined magnetic fractions from low intensity drum magnetic separation (Mags); the combined magnetic

fractions from medium intensity drum magnetic separation (RE Mags); the combined non-magnetic fractions from medium intensity drum magnetic separation (Non-Mags); and several others (Figure 6.26 (c, d)).

Figure 6.26a illustrates that the centrifugal gravity concentration steps preferentially upgrade iron oxides, and that those iron oxides are even further upgraded by low intensity magnetic separation. The non-magnetic fractions from the medium intensity magnetic separation are enriched in zircon and other REM, while the magnetic fraction from medium intensity magnetic separation of the Falcon gravity concentrate is actually enriched with iron oxides (Figure 6.26b). This suggests that the medium intensity magnetic separation may only be necessary to remove iron oxide minerals from the Falcon gravity concentrate stream. Figure 6.26c shows combinations of these streams, with the Mag product showing the best upgrade ratio and recovery of iron oxide minerals while the RE Mag + Non-Mag shows the best results for zircon and REM. Several other combinations of the RE Mag and Non-Mag streams are shown in Figure 6.26d, where it can be seen that a combination of the RE Mag and Non-Mag streams from the Falcon gravity concentrate offers very low recoveries and upgrade ratios. The other three stream combinations are very difficult to differentiate.

As one of the criteria for the final fraction from this process is to maximize the recovery of HREE, graphs of elemental upgrade ratio versus recovery are shown in Figure 6.27 for the four stream options selected from Figure 6.26 with the best REM upgrade ratios and recovery. The results show that all four options considered preferentially concentrate the HREE with the Non-Mag (KC) stream providing the highest upgrade ratio and the combination of all RE Mag and Non-Mag streams providing the highest recovery values.

The final decision on which fraction to carry forward for downstream flotation was based on two factors: maximizing both REO grade and recovery; and avoiding an unnecessarily complex physical separation process. For this reason the RE Mag and Non-Mag fractions from the Knelson gravity concentrate were selected as the feed to downstream flotation processes as this achieves a high upgrade ratio (Figure 6.27b), while also eliminating

everything but the Knelson Concentrator and low intensity wet drum magnetic separation process steps from the initially investigated process flowsheet (Figure 4.4).

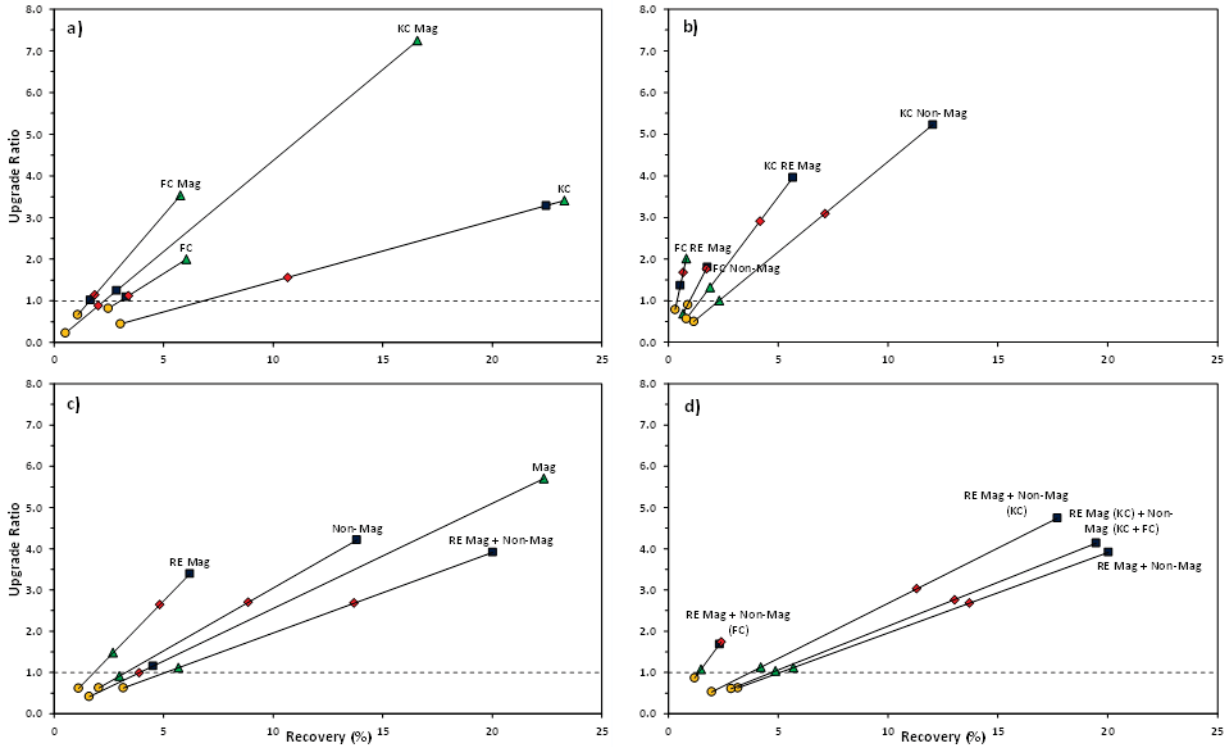

Figure 6.26 – Upgrade ratio versus recovery as determined by QEMSCAN for different product streams and combination of product streams: a) gravity concentrates and low intensity magnetic fractions, b) medium intensity magnetic and non-magnetic fractions, c) combinations of low intensity magnetic, medium intensity magnetic and non-magnetic product streams, d) alternate combinations of the non-magnetic products from low intensity magnetic separation. In each figure the symbol represents the upgrade ratio and recovery of: zircon [squares], all other REM [diamonds], iron oxide minerals [triangles] and silicate gangue (quartz, K-feldspar, plagioclase and biotite) [circles]

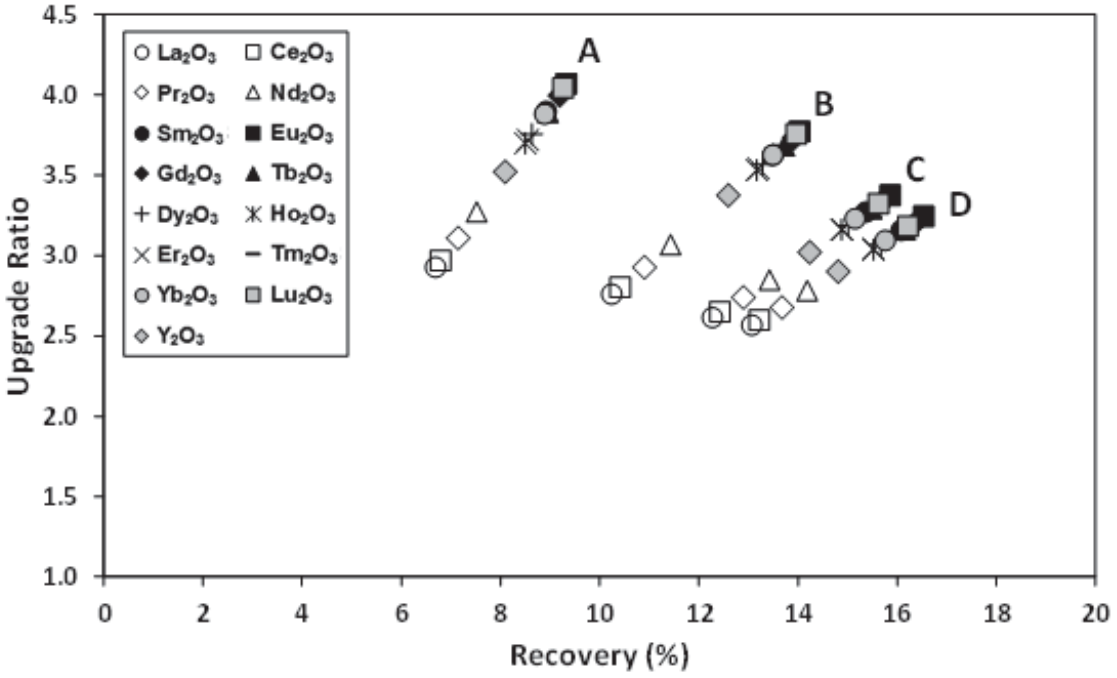

Figure 6.27 – Upgrade ratio versus recovery for individual REO as determined by ICP-MS: a) Non-Mag (KC), b) RE Mag + Non-Mag (KC), c) RE Mag (KC) + Non-Mag (KC + FC), d) RE Mag + Non-Mag.

Similar graphs of upgrade ratio versus recovery were also created for the oversize material screened from the Knelson gravity concentrate (Figure 6.28). It is interesting to note that a simple gravity concentration step applied to very coarse particles in the feed material was able to produce upgrade ratios between 2 and 3 for zircon (although at very low recoveries). A particle map of this oversize material sorted by particle size and calculated particle specific gravity similar to Figure 6.10 was created and is shown in Figure 6.29. It can be seen visually in this figure that the particles in the Knelson gravity concentrate oversize fraction with specific gravities between 3.25 and 4.5 are enriched in zircon across a wide size range. This suggests that grain size differences in the deposit may present opportunities for selective comminution.

An expansion of this work to develop a stage grinding, gravity and magnetic separation circuit could include a grind to a much coarser particle size (~300 microns) followed by a centrifugal gravity concentration step (or an alternative gravity separation), followed by

further grinding of the gravity concentrate, with a final low intensity magnetic separation step to separate coarsely liberated iron oxide minerals from the enriched RE mineral fraction. Such a flowsheet, while not suitable for processing the entire Nechalacho deposit, could present opportunities to minimise grinding costs while producing an initial high grade REE concentrate for hydrometallurgical processing or as part of a pre-concentration process prior to REM flotation. Such a process could certainly be expected to be easier to commission in an industrial setting than novel REM flotation schemes which typically include reagents with minimal in-plant testing and validation. The proposed process would be analogous to the use of centrifugal gravity concentration in gold processing flowsheets to target gravity recoverable gold recovery initially during plant start-up and commissioning to provide an early revenue stream, and thereby improve project economics.

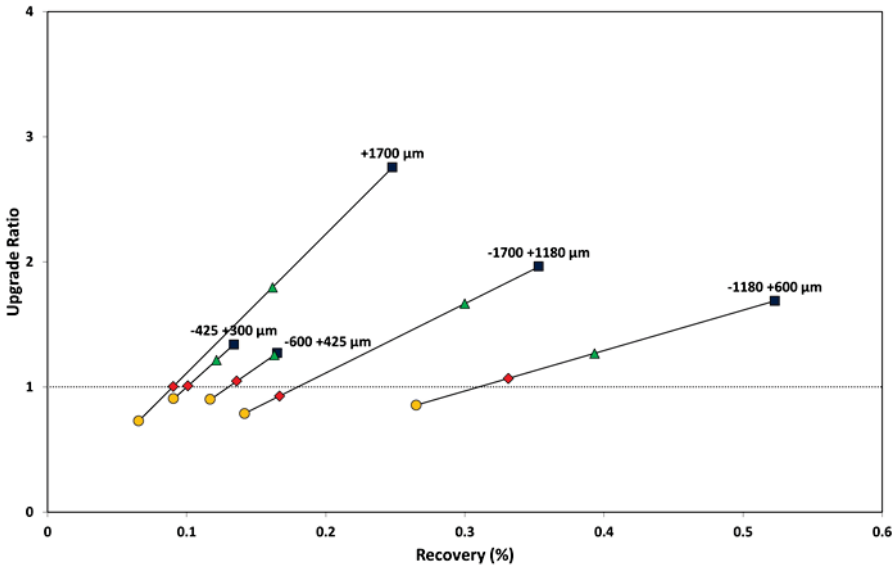

Figure 6.28 – Upgrade ratio versus recovery as determined by QEMSCAN for different size fractions of the Knelson gravity concentrate oversize material. In each figure the symbol represents the upgrade ratio and recovery of: zircon [squares], all other REM [diamonds], iron oxide minerals [triangles] and silicate gangue (quartz, K-feldspar, plagioclase and biotite) [circles]

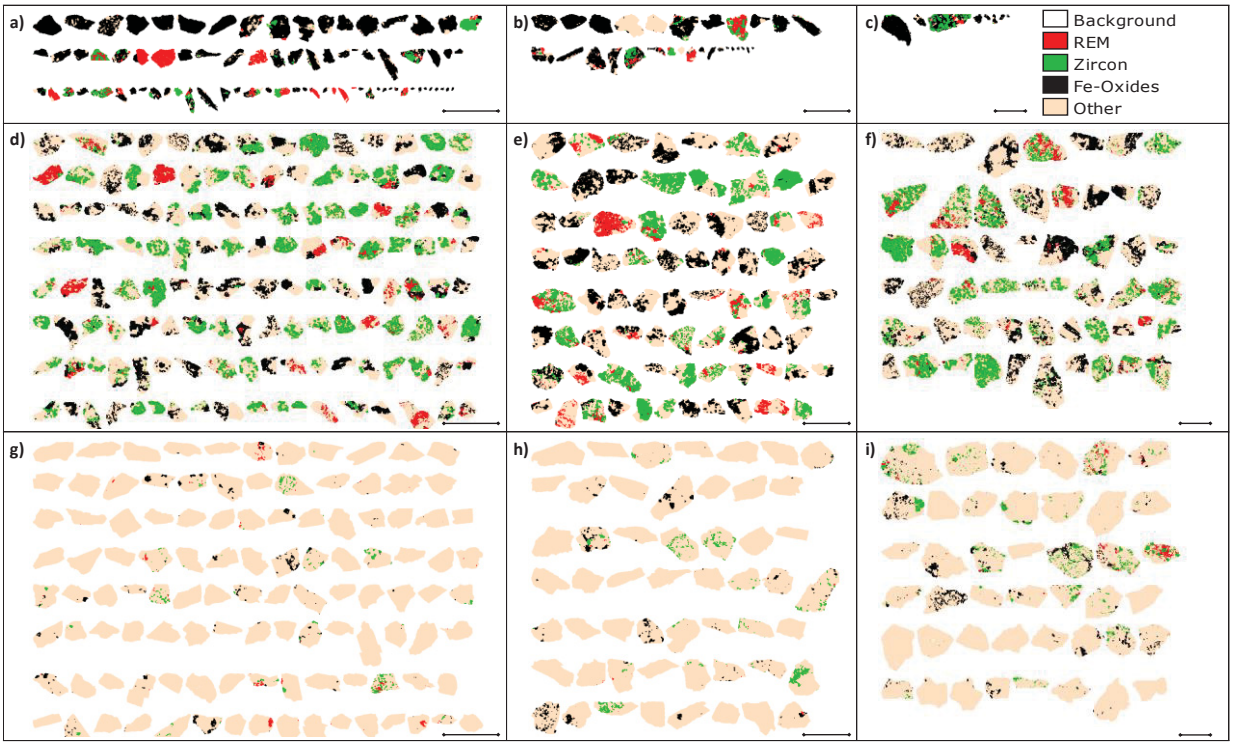

Figure 6.29 - Particle maps of high specific gravity (> 4.5) [a, b, c], intermediate specific gravity (3.25-4.5) [d, e, f] and low specific gravity (2.5-3.25) [g, h, i]. Particle maps on the left (a, d, g) represent the 300-425 µm fraction of the Knelson gravity concentrate, particle maps in the middle of the figure (b, e, h) represent the 425-600 µm fraction of the Knelson gravity concentrate, and particle maps on the right (c, f, i) represent the 600-1180 µm fraction of the Knelson gravity concentrate. Phase identification is limited to four mineral classes: iron oxides, zircon, REM (all other REM) and other (all other minerals in the deposit). Scale bars represent 1 mm

6.7 Conclusions

This chapter has presented the development of a pre-concentration process for the Nechalacho deposit using gravity and magnetic separation. With information provided from characterisation techniques such as QEMSCAN, XRD, SEM and VSM it was determined that the optimum pre-concentration flowsheet was a combination of a Knelson Concentrator to concentrate high specific gravity minerals followed by a low intensity magnetic separation step to remove ferromagnetic iron oxide gangue minerals. The specific conclusions of this chapter are:

- The coarse size fraction of the feed material to the process has increased concentrations of heavy REM (*i.e.* zircon) and consequently higher HREE grades

- Centrifugal gravity concentration is effective at concentrating REM from this deposit, with recovery decreasing with decreasing particle size
- The Knelson Concentrator in this process exhibited greater selectivity for particle size and particle specific gravity compared to the Falcon Concentrator. This may be due to the lack of fluidizing water in the Falcon (different bowl geometry), higher centrifugal accelerations experienced by the particles or the different distribution of mineral particles fed to the Falcon as opposed to the Knelson
- The Knelson Concentrator in conjunction with low intensity wet drum magnetic separation is able to achieve high rejection of strongly ferromagnetic iron-bearing gangue minerals
- The oversize material in the Knelson gravity concentrate is enriched with zircon, suggesting that a coarser initial grind size should be investigated with centrifugal gravity separation and low intensity magnetic separation to produce a heavy REE-enriched concentrate
- The use of WHIMS after wet drum magnetic separation of the centrifugal gravity concentrates may be able to reject additional iron oxide gangue and concentrate strongly paramagnetic REM while rejecting silicate gangue into the non-magnetic tailings
- The optimal fraction from this process to send to a downstream flotation stage is the non-magnetic fraction left after low intensity wet drum magnetic separation of the Knelson gravity concentrate with a total RE oxide (TREO) recovery of 11.75 % and a grade of 7.50 % TREO

7. Flotation

7.1 Introduction

The objective of this chapter is to determine the flotation characteristics of the various REM present in the Nechalacho REE deposit through lab-scale flotation testing with a hydroxamate-based collector. Through the use of QEMSCAN, ICP-MS and the first-order flotation rate model, baseline flotation behaviours of the different REM are assessed. After the initial flotation recovery, three different reconditioning steps are investigated to determine the best approach for improving REM recoveries.

7.2 Flotation Feed

Prior to flotation, the ore was subject to a series of gravity and magnetic pre-concentrations steps as detailed in Chapter 6. The highest grade product (k_{50} = 50 µm) from the gravity and magnetic separation process was selected for downstream flotation experiments to determine the flotation behaviour of the different REM in the deposit. A high grade feed is important to this work as direct flotation of the ore would be much less likely to produce flotation concentrates with high enough grades of the minor REM to reliably assess their floatability (which may have a significant effect on the overall grade and recovery of REE). The mineralogy of the flotation feed may be seen in Table 7.1.

Table 7.1 – Mineralogy of flotation feed (determined by QEMSCAN)

Mineral	Grade (wt. %)
Columbite(Fe)	1.06
Fergusonite	0.64
Bastnäsite	2.82
Synchysite	1.68
Allanite	1.66
Monazite	0.84
Zircon	35.25
Quartz	11.82
Plagioclase	14.15
K-Feldspar	10.22
Fe-Oxides	10.16
Other	9.70

7.3 Mass Recovery

The cumulative mass pull from the Nechalacho flotation tests as a function of concentrate collection time can be seen in Figure 7.1. The results indicate that the changes in reagent addition after reconditioning produced pronounced differences in mass recovery. Without additional reagent addition, the bulk of the mass recovery occurs over the first 2 min of flotation, indicating the kinetics of flotation are quite rapid with this collector (benzohydroxamic acid). After reconditioning, the baseline condition (no further reagent addition) shows little additional mass recovery. In contrast, the secondary addition of collector shows a significant increase in mass recovery, with the bulk of the mass recovered in the first minute of collection after reconditioning. The third condition with both Pb and benzohydroxamic acid additions at the reconditioning stage produces an even more significant increase in mass recovery, with the bulk of this recovery again occurring within the first minute of concentrate collection.

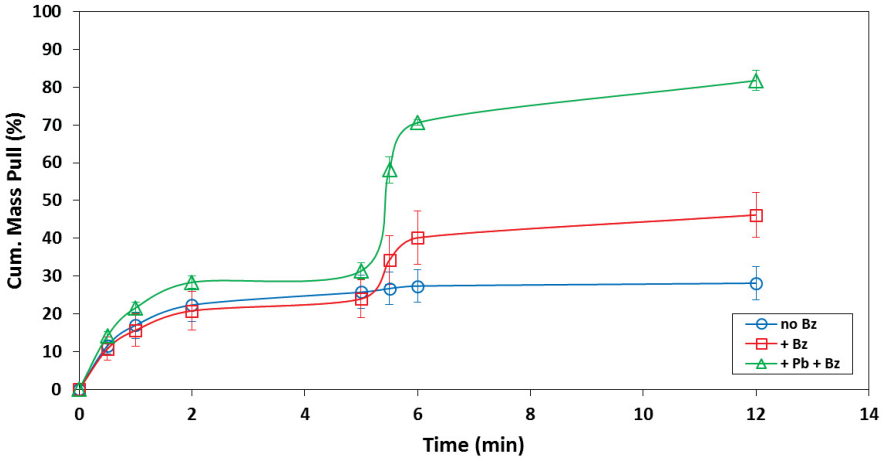

Figure 7.1 – Cumulative mass pull versus time for the three different flotation conditions investigated including reconditioning without collector addition (no Bz), reconditioning with a secondary addition of collector (+ Bz), and reconditioning with lead ions followed by a secondary addition of collector (+Pb +Bz). Error bars represent 95% confidence intervals

7.4 Water Recovery

The cumulative water recoveries associated with the three flotation conditions are shown in Figure 7.2. It can be concluded from this figure that there is little difference in water recovery between flotation conditions. The relatively high levels of water recovery are a

result of the repeated adjustment of pulp level after each concentrate collection by adding additional water. It can also be inferred from Figure 7.2, thanks to the well-established correlation of fine particle entrainment with water recovery shown by Trahar (1981) and others, that the observed differences in mass recovery in Figure 7.1 are not due simply to an increase in non-selective entrainment.

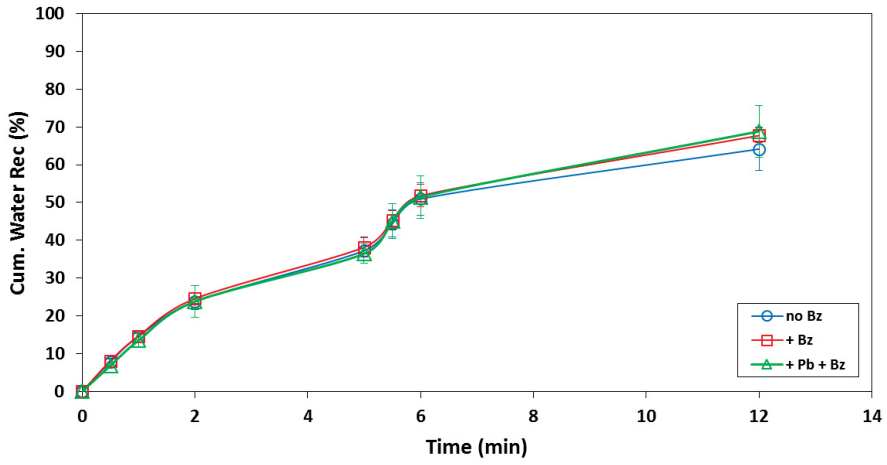

Figure 7.2 – Cumulative water recovery as a function of time for the three different flotation conditions investigated including reconditioning without collector addition (no Bz), reconditioning with a secondary addition of collector (+ Bz), and reconditioning with lead ions followed by a secondary addition of collector (+Pb +Bz). Error bars represent 95% confidence intervals

7.5 Mineral Recovery

In order to compare the differences between reconditioning steps, the concentrates produced after reconditioning are considered as distinct products from the initial flotation stage. The recoveries for post-reconditioning concentrates are calculated as a percentage of the initial flotation feed but are not considered cumulative with the initial 5 minute collection time. The recoveries versus time for different minerals in the flotation feed may be seen in Figure 7.3 to Figure 7.5 for all REM as well as the major gangue minerals (Table 7.1). The conditions include the initial flotation over a five minute period as well as the seven minute collection after reconditioning with additional benzohydroxamic acid, and lead ions. The recoveries of four REM (bastnäsite, synchysite, fergusonite and columbite) are shown in Figure 7.3 grouped together due to their observed similar flotation response. Similarly the major silicate gangue minerals

(quartz, plagioclase and K-feldspar) are shown in Figure 7.4. These two groups of minerals respond similarly regardless of flotation conditions. Whether this observed similarity is due to true flotation behaviour or mineral association, the two groups are treated as single phases (light REM and silicates, respectively) in order to simplify further analysis. The remaining major constituents of the flotation feed (allanite, monazite, zircon and iron oxides) are shown in Figure 7.5. These four minerals do not show any obvious correlations, and thus are treated individually in subsequent sections.

A comparison of the different flotation conditions in Figure 7.3 shows that the initial flotation recovery prior to reconditioning functions very well at collecting this group of light REM. The addition of further collector in Figure 7.4 has little effect on the collection of silicate gangue minerals. However the presence of lead prior to further collector addition significantly increases the recovery of these gangue minerals (especially quartz). The results in Figure 7.4 also indicate that quartz recovery is more sensitive to the addition of lead than feldspar recovery. A similar effect is illustrated in Figure 7.5 where the addition of lead increases the recovery of allanite, monazite, zircon and iron oxides. Allanite in particular exhibits an increase of approximately 40% due to the addition of lead.

These results agree with a previous investigation by Xia *et al.* (2015) into the use of lead and hydroxamic acid for the flotation of this deposit. In the previous work, flotation with lead was found to preferentially increase the recovery of REE along with silicate minerals (Xia *et al.*, 2015). The selectivity of lead for quartz over feldspar is also confirmed in this work by the observation of an increased concentration of Si surface ions in the flotation concentrate without a corresponding increase in Na, K or Al ions present in feldspar minerals (Xia *et al.*, 2015). However, the results in this study do not completely agree with the work of Xia *et al.* (2015). Key differences between the two studies include the use of: a lab-scale Denver flotation cell rather than microflotation, a pre-concentrated REM feed rather than direct ore flotation, $PbCl_2$ instead of $Pb(NO_3)_2$, different hydroxamic acid collectors, different collector dosages, and the lack of depressant or heated flotation pulps (approximately 45-55 °C) in this work.

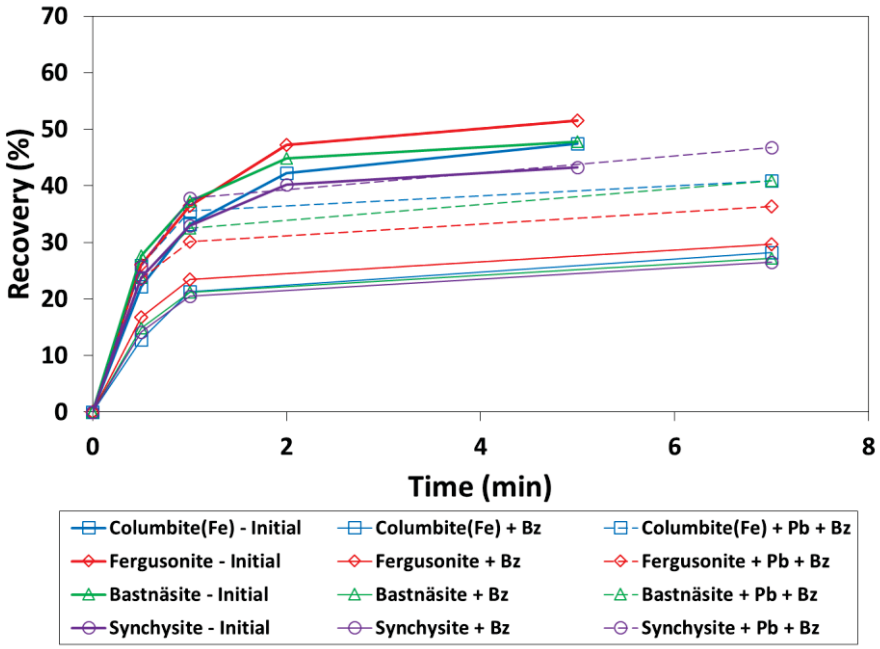

Figure 7.3 – Mineral recovery as a function of time for three different conditions (initial flotation recovery, recovery after reconditioning with additional benzohydroxamic acid, recovery after reconditioning with lead ions followed by additional benzohydroxamic acid) corresponding to thick solid lines, thin solid lines and dashed lines respectively. The four minerals presented here are columbite(Fe), fergusonite, bastnäsite and synchysite

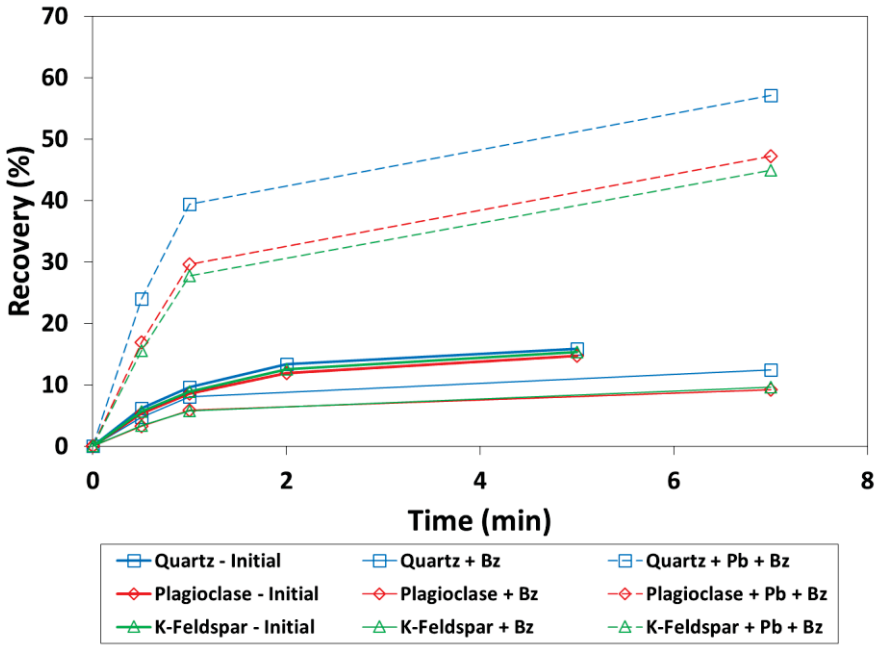

Figure 7.4 – Mineral recovery as a function of time for three different conditions (initial flotation recovery, recovery after reconditioning with additional benzohydroxamic acid, recovery after reconditioning with lead ions followed by additional benzohydroxamic acid) corresponding to thick solid lines, thin solid lines and dashed lines respectively. The three minerals presented here are quartz, plagioclase and K-feldspar

7.6 Grade-recovery comparison

While the increased recovery of REM due to the addition of collector (and lead) during the reconditioning stages of flotation is illustrated by Figure 7.3 to Figure 7.5 it is important to also consider the grade of these flotation concentrates. The ultimate goal of any REM beneficiation process for this deposit is to recover as much of the value REE as possible, while simultaneously minimizing the presence of gangue minerals with significant processing costs (i.e. silicates and iron oxides) in downstream metallurgical processes. The grade-recovery relationships for various minerals in this deposit are shown in Figure 7.6 for both the initial flotation concentrates collected prior to reconditioning and all three sets of flotation concentrates collected after reconditioning.

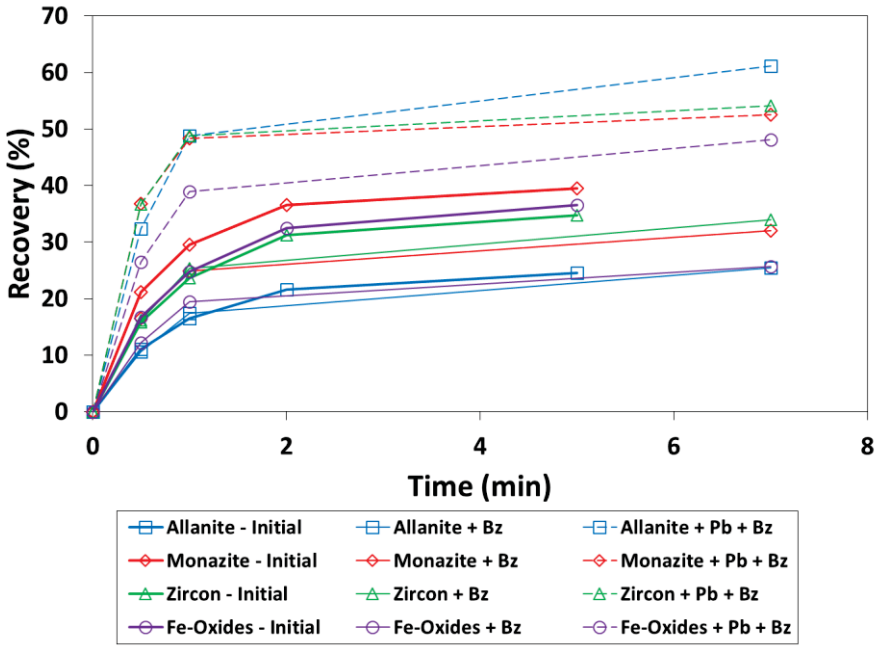

Figure 7.5 – Mineral recovery as a function of time for three different conditions (initial flotation recovery, recovery after reconditioning with additional benzohydroxamic acid, recovery after reconditioning with lead ions followed by additional benzohydroxamic acid) corresponding to thick solid lines, thin solid lines and dashed lines respectively. The four minerals presented here are allanite, monazite, zircon and Fe-oxides

Figures 7.6a and 7.6e illustrate that the initial flotation conditions (addition of 5 kg/ton benzohydroxamic acid and flotation for 5 minutes) produce the best grade and recovery for both LREM and iron oxide minerals. This may indicate the preference of benzohydroxamic acid for these minerals, which is problematic as iron oxides are a deleterious gangue mineral in this deposit. Conversely, the addition of benzohydroxamic acid (in combination with lead) at the reconditioning stage produces significantly better results for allanite, zircon and to some extent monazite (Figure 6b-d). The poor flotation of allanite without the addition of lead to act as an activator has been confirmed with this reagent in single mineral microflotation and surface chemistry studies (Chapter 5). Potential explanations for this include a lack of sufficient REE cations on the allanite surface or differences in mineral structure and solubility relative to more traditional REM, for which hydroxamic acids are very successful collectors, such as bastnäsite. The grade and recovery for silicates indicates that prolonged flotation times result in an increase in

silicate grade and recovery for all flotation conditions (Figure 7.6f). The addition of lead ions in particular, causes a significant increase in silicate recovery.

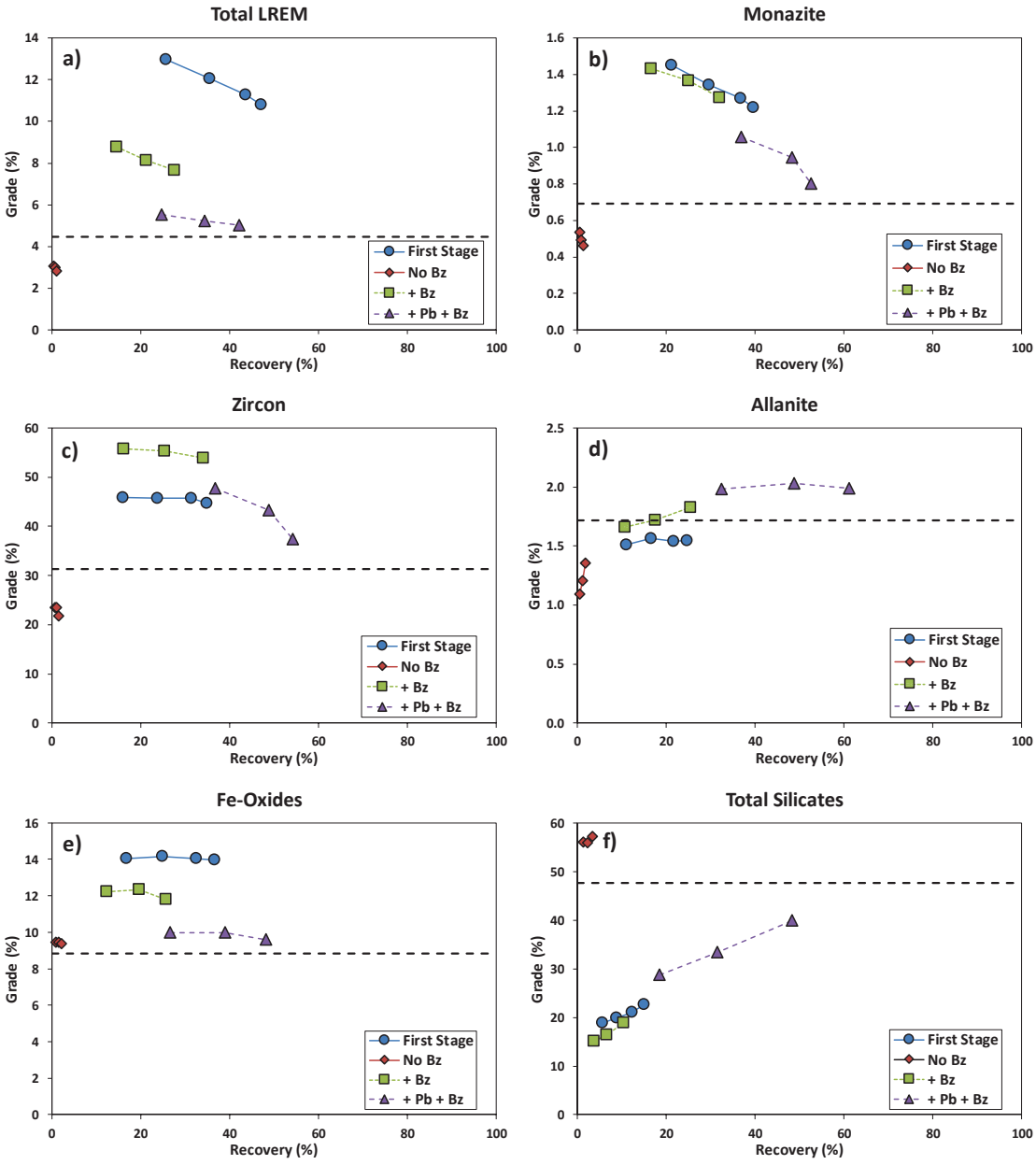

Figure 7.6 – Cumulative grade and recovery of flotation concentrates produced before reconditioning and after reconditioning. In the cases of flotation concentrates produced after reconditioning they have been treated as distinct from the initial flotation stage and are therefore not cumulative with the initial flotation stages. Minerals represented here include: a) LREM (columbite, fergusonite, bastnäsite and synchysite), b) monazite, c) zircon, d) allanite, e) iron oxides and f) silicates (quartz and feldspars). Dashed horizontal lines represent feed grades

7.7 REM kinetics

In order to understand the flotation behaviour of the various minerals on a relative basis the initial (i.e. first 5 minutes) recovery data as a function of time was fitted to the first order flotation rate equation, as discussed in Chapter 2, Section 2.5.1.2, using the statistical software Stata13 (StataCorp, USA) to perform non-linear regressions. The outputs of these regressions (maximum recovery, flotation rate constant, and modified flotation rate constant) and the major metal cation composition information for the given minerals are shown in Table 7.2. The minerals are sorted by decreasing modified flotation rate constant. Bastnäsite shows the highest flotation rate and feldspar the lowest. The data indicate a clear differentiation of flotation kinetic behaviour according to mineral type. Carbonates and niobates show the highest flotation rates and silicates the lowest. This trend may be due to the effect of differences in mineral solubility on hydroxamate flotation as proposed by Assis *et al.* (1996) with carbonates expected to have a much higher degree of solubility than silicates. Another identifiable trend is the decrease in flotation associated with a decrease in metal cations on which benzohydroxamic acid is likely to preferentially adsorb. Hydroxamic acids in general will prefer the formation of stable chelates with REE, Fe and to some extent Nb and Zr over Na, K or Si (Fuerstenau, 2005; Gibson *et al.*, 2015; Pavez & Peres, 1993).

Table 7.2 – Output of non-linear regression fitting to first-order flotation rate equation for major minerals from the Nechalacho deposit along with mineral type and selected chemical composition information (from QEMSCAN mineral definition database) for each mineral

Mineral	Type	R_{max} (%)	k (min^{-1})	k_M	REE (%)	Fe (%)	Nb (%)	Zr (%)	Total (%)
Bastnäsite	Carbonate	47.2	1.7	**79.0**	63.6	0.1	-	-	**63.7**
Fergusonite	Niobate	51.3	1.3	**67.9**	40.0	0.7	32.2	-	**72.9**
Synchysite	Carbonate	42.9	1.5	**66.4**	46.5 - 63.6	0.10	-	-	**55.1**
Columbite(Fe)	Niobate	47.2	1.2	**58.0**	0.4	14.8	49.4	-	**64.6**
Monazite	Phosphate	39.2	1.5	**57.8**	59.1	0.1	-	-	**59.2**
Fe-Oxides	Oxide	36.4	1.2	**42.7**	-	70.0 - 77.7	-	-	**73.9**
Zircon	Silicate	34.8	1.2	**40.7**	2.3	0.9	0.4	44.8	**48.4**
Allanite	Silicate	24.5	1.2	**28.2**	22.6	11.1	-	-	**33.7**
Quartz	Silicate	15.9	0.9	**14.9**	-	-	-	-	**0.00**
Feldspar	Silicate	15.0	0.9	**12.9**	-	-	-	-	**0.00**

Similar regressions were also completed for the flotation recoveries after different reconditioning stages. Using the fitted parameters from these non-linear regressions the selectivity index, a ratio of modified rate constants as discussed in Chapter 2, Section 2.5.1.2, of each mineral relative to the major gangue minerals (silicates and iron oxides) was calculated. A comparison of the selectivity indices between different conditions is shown in Figure 7.7. Figure 7.7a and 7.7c indicate that the most selective flotation condition for the LREM (fergusonite, columbite, bastnäsite and synchysite) is the initial flotation stage with only benzohydroxamic acid. Conversely, the flotation of allanite, zircon and monazite has increased selectivity relative to silicates (Figure 7.7b) after reconditioning with benzohydroxamic acid. The flotation of iron oxides is a special case where these minerals are floated preferentially (relative to silicates) with benzohydroxamic acid collector (Figure 7.7b). However, the addition of lead ions appears to slightly improve the selectivity of allanite, zircon and monazite relative to iron oxide minerals (Figure 7.7d).

A more traditional representation of the selectivity of different flotation conditions for zircon (the major heavy REM) versus bastnäsite (a major light REM) is shown in Figure 7.8. Based on this figure and the preceding kinetic information it seems likely that staged additions of benzohydroxamic acid could be beneficial to the flotation of this deposit due to the different flotatabilities of the various REMs and the rapid kinetics of flotation with benzohydroxamic acid in general.

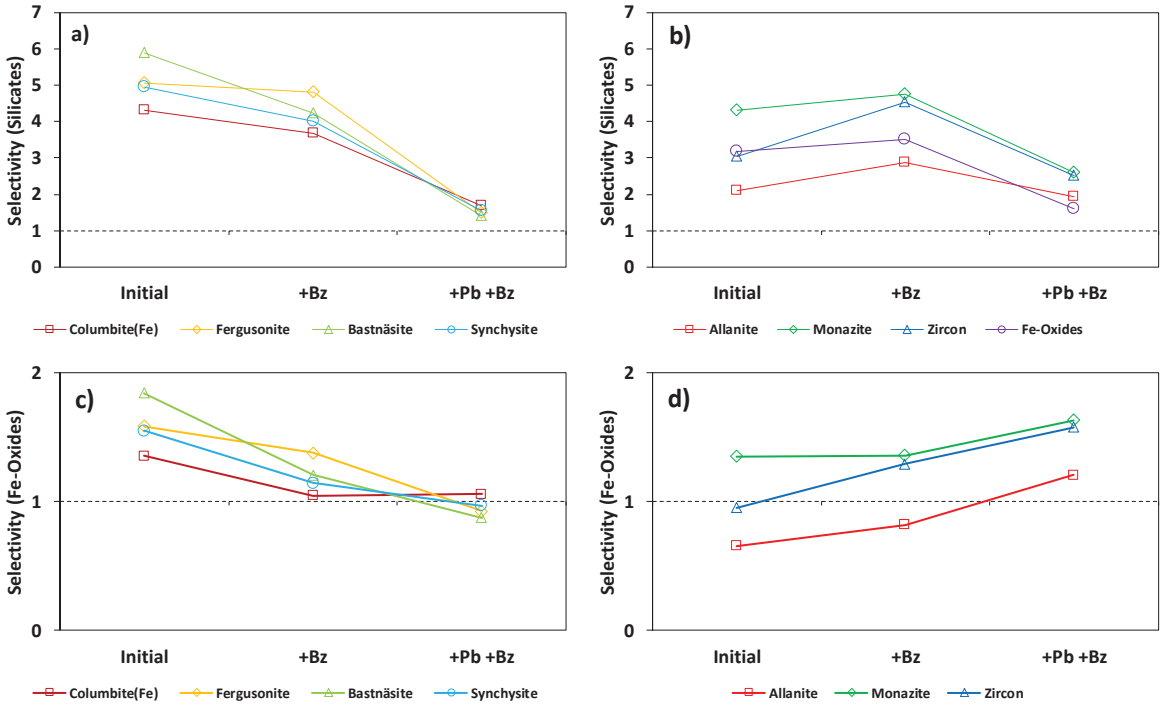

Figure 7.7 – Comparison of selectivity index for columbite, fergusonite, bastnäsite and synchysite (a, c) and allanite, monazite and zircon (b, d) relative to silicates (a, b) and iron oxides (c, d). The selectivity of iron oxides over silicates is shown in b). The selectivities of these minerals are compared between the initial flotation condition, the flotation after reconditioning with additional collector (+Bz) and flotation after reconditioning with lead and collector (+Pb +Bz)

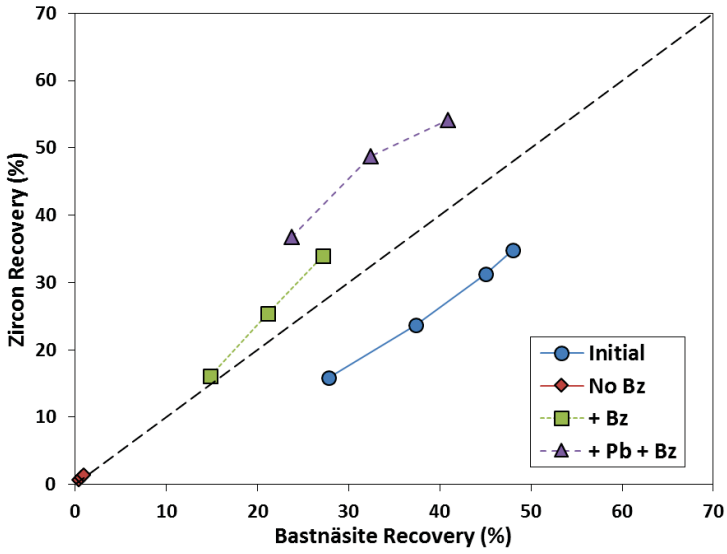

Figure 7.8 – Selectivity of zircon versus bastnäsite for different flotation conditions including initial flotation with benzohydroxamic acid, flotation after reconditioning with additional collector (+Bz) and flotation after reconditioning with lead and collector (+Pb +Bz)

The use of total mineral recoveries for flotation kinetic modelling is a very common method however these total recovery numbers may mask the impact of mineral associations, especially in systems comprised of multiple value minerals. In the case of the Nechalacho deposit it is important to differentiate the flotation of mixed particles containing fast-floating and slow-floating minerals (*e.g.* bastnäsite:allanite) from fully liberated particles when assessing flotation kinetics. The data obtained from QEMSCAN allows the isolation of only "free" (> 95% of particle surface comprised of a single mineral) particles for this purpose. After calculating recoveries of these "free" particles the data was fed to the same non-linear regression as discussed previously. The results of this analysis can be seen in Table 7.3. This data confirms the rapid flotation kinetics of both carbonates and niobates in this system and the general trend of decreasing flotation with decreasing solubility initially observed in Table 7.2.

Table 7.3 – Output of non-linear regression fitting to first-order flotation rate equation for "free" REM particles along with mineral type and selected chemical composition information (from QEMSCAN mineral definition database) for each mineral

Mineral	Type	R_{max} (%)	k (min^{-1})	k_M	REE + Fe + Nb (%)
Fergusonite	Niobate	85.6	1.7	**144.3**	**72.9**
Bastnäsite/Synchysite	Carbonate	66.7	1.8	**118.6**	**55.1**
Columbite(Fe)	Niobate	73.1	1.2	**88.1**	**64.6**
Monazite	Phosphate	44.7	1.5	**65.4**	**59.2**
Fe-Oxides	Oxide	47.8	1.2	**56.8**	**73.9**
Zircon	Silicate	39.2	1.2	**45.1**	**48.4**
Allanite	Silicate	32.8	1.2	**40.2**	**33.7**

7.8 Elemental grade and recovery

The grade and recovery of the different flotation conditions is shown in Figure 7.9 on an elemental basis for Fe, Zr, light REE (La to Sm), heavy REE (Eu-Lu + Y) and U and Th. Figure 7.9c indicates that the optimum condition for light REE concentration is the initial flotation stage, which agrees with the mineral results presented in previous sections. This initial flotation stage also results in the highest Fe grades (Figure 7.9a). Figures 7.9b and 7.9d show the highest recoveries for Zr and heavy REE occur after reconditioning with lead, corresponding to increased zircon recoveries. This is significant as the demand (and therefore price) is much higher for many heavy REE (Binnemans *et al.*, 2013). Additionally, the response of the various REM in downstream processes is very different (leaching and digestion of zircon is orders of magnitude more difficult than similar processing of bastnäsite). These factors suggest that production of two flotation concentrates, one enriched in LREE-bearing minerals such as bastnäsite and the other enriched in HREE-bearing minerals such as zircon, may be advisable.

A final consideration for this flotation process is the concentration of deleterious elements along with the desired REM such as radioactive U and Th. Grades and recoveries of these two elements are shown in Figures 7.9e and 7.9f. As the feed grades of U and Th in this work are 80 ppm and 320 ppm respectively, it can be seen from these two figures that the flotation concentrates in all scenarios are enriched in both U and Th. This is unavoidable as U is found in fergusonite, columbite and zircon with Th occurring in fergusonite, columbite, monazite, zircon and allanite.

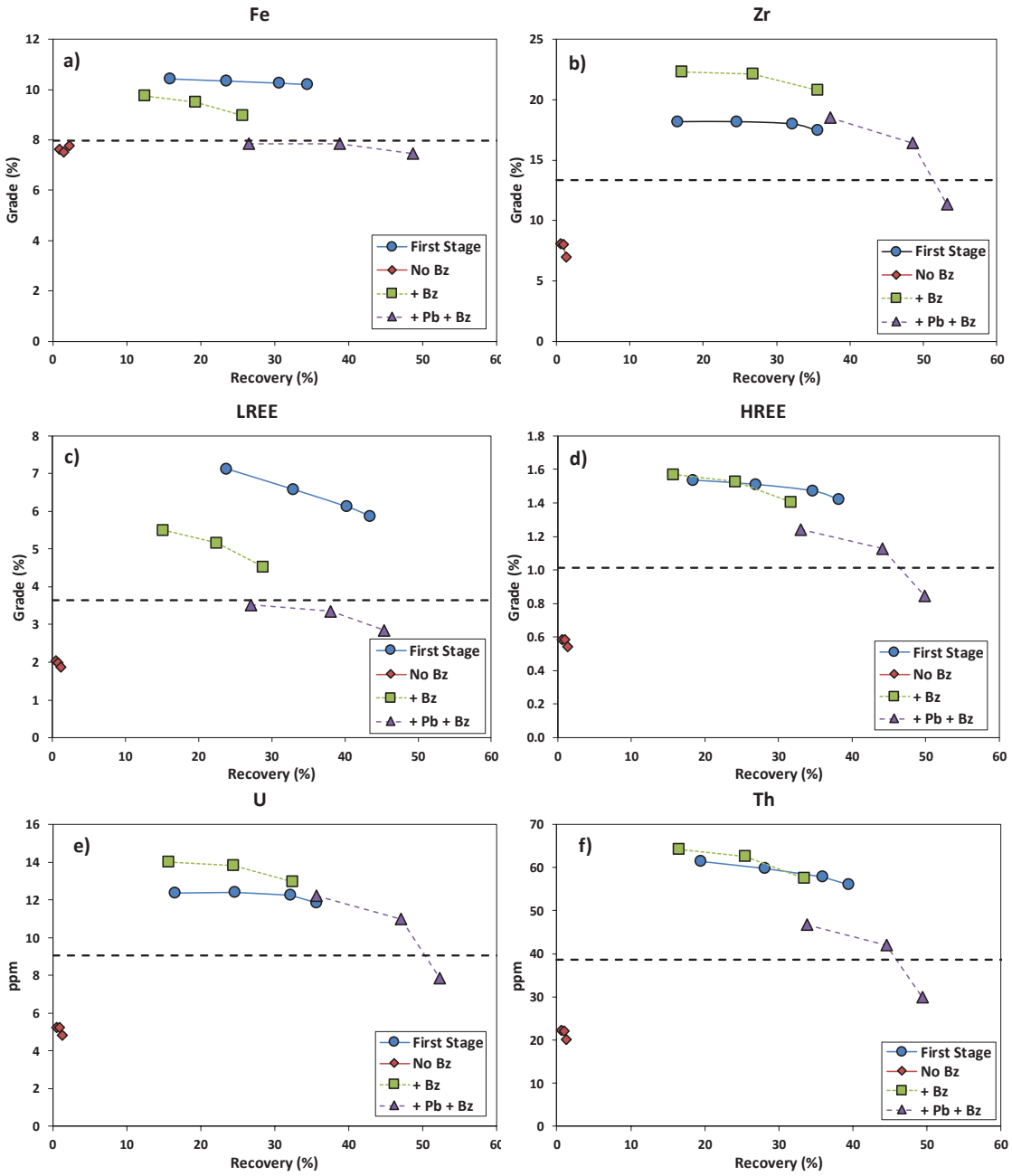

Figure 7.9 - Cumulative elemental grade and recovery of flotation concentrates produced before reconditioning and after reconditioning. In the cases of flotation concentrates produced after reconditioning they have been treated as distinct from the initial flotation stage and are therefore not cumulative with the initial flotation stages. Elements represented here include: a) iron, b) zirconium, c) light REE, d) heavy REE, e) uranium, f) thorium. Dashed horizontal lines represent feed grades

7.9 Implications for industrial flotation

The grade, recovery and kinetic flotation results described in previous sections have implications for the design of a multiple stage industrial flotation process for this deposit. In envisioning such a process, an initial rougher flotation step with benzohydroxamic acid as the collector might be focused on light REM recovery with a secondary rougher using a secondary addition of collector to produce a concentrate more enriched in heavy REE. Scavenger flotation stages could potentially employ lead ions as an activator to maximize REM recovery (by targeting the recovery of less floatable REM). Depending on economic and environmental concerns (lead can be very environmentally concerning if present in the plant tailings stream), it might also be possible to use less collector, combined with lead ions, for the initial rougher flotation stages. Finally, as the work of Anderson (2015) suggests, lead is not the only metal cation which may be used as an activator for REM.

Based on the rapid kinetics of REM flotation with benzohydroxamic acid, the final grade and recovery of a combined concentrate (initial & post-reconditioning) was calculated including only the first 2 min of initial flotation and first minute of collection after reconditioning. The grade and recovery of these products are shown graphically in Figure 7.10 and listed in Table 7.4. It can be seen that the reconditioning stage with only benzohydroxamic acid is the most selective (highest rejection of silicates), while reconditioning with the addition of lead ions achieves the highest recovery of REM. In both cases the grade of iron oxides is increased, indicating that the examined flotation reagent combinations are ineffective at rejecting this gangue mineral.

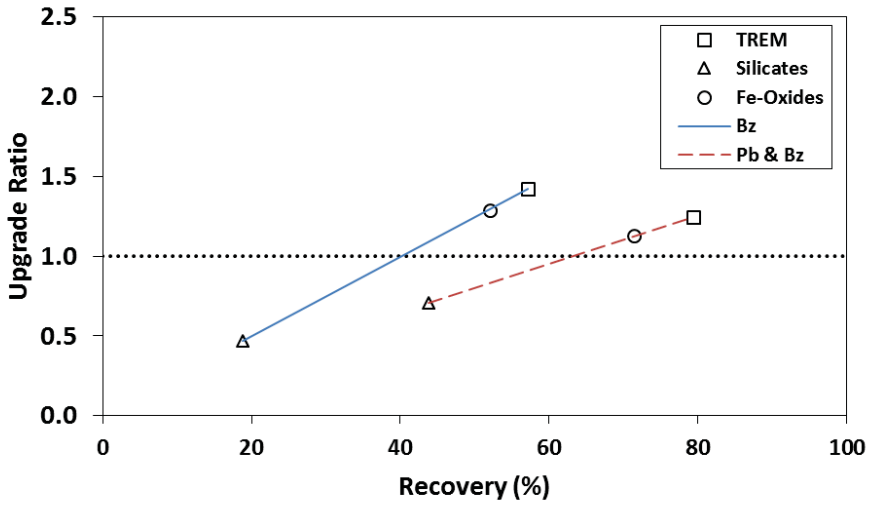

Figure 7.10 – Upgrade ratio versus recovery for combined products from initial flotation (first 2 min) combined with: post-reconditioning collection for 1 min with benzohydroxamic acid (Bz), and post-reconditioning collection for 1 min with lead ions and benzohydroxamic acid (Pb & Bz). The three minerals shown are total REM (square), quartz and feldspar (triangle), and iron oxides (circle)

Table 7.4 – Grade and recovery of combined flotation concentrates

Number	Product	Reagent	Total REM		Silicates		Fe-Oxides	
			Recovery	*Grade*	*Recovery*	*Grade*	*Recovery*	*Grade*
1	First Stage (2 min)	Bz	32.7	59.8	12.3	21.1	32.5	14.0
2	Post-Recondition (1 min)	Bz	24.5	66.5	6.5	16.4	19.5	12.3
3	Post-Recondition (1 min)	Pb & Bz	46.7	51.4	31.4	33.4	39.0	10.0
	Combined 1 (1 & 2)	Bz	57.2	62.5	18.8	19.2	52.0	13.3
	Combined 2 (2 & 3)	Pb & Bz	79.5	54.6	43.7	28.7	71.5	11.5
	Feed			**43.8**		**40.8**		**10.2**

The two optimal conditions (reconditioning with benzohydroxamic acid and reconditioning with both lead and benzohydroxamic acid) from Table 7.4 are shown in Figure 7.11 for each individual REM. For each REM the idealized grade-recovery curve, as determined from QEMSCAN, is also shown. The idealized grade-recovery curve is produced by assuming the ideal situation where the mineral of interest is recovered sequentially as a function of particle surface exposure (degree to which the particle surface is composed of the mineral of interest) and then calculating the corresponding cumulative grade and recovery for each population of particles with decreasing surface exposure. Empirical flotation results rarely match up with this ideal grade-recovery curve but it is a useful comparative tool for the purposes of determining how to further improve the flotation process.

The implicit assumption in these calculations is that only the mineral of interest is recovered so the comparison of empirical results to the ideal curve in a system containing multiple value minerals will always have poorer grades than expected. Nevertheless, the results in Figure 7.11b illustrate the effectiveness of the lead addition in pushing REM recoveries for every REM above 70 %. Regrettably, this increased recovery is accompanied with significant decreases in grade relative to the conditions shown in Figure 7.11a. The low grades for many of the REM indicate indicated in Figure 7.11 clearly illustrate the differences between these two reagent conditions and provides useful insight into the possibility of developing distinct separation processes for the different REM in this deposit based on varying flotation responses.

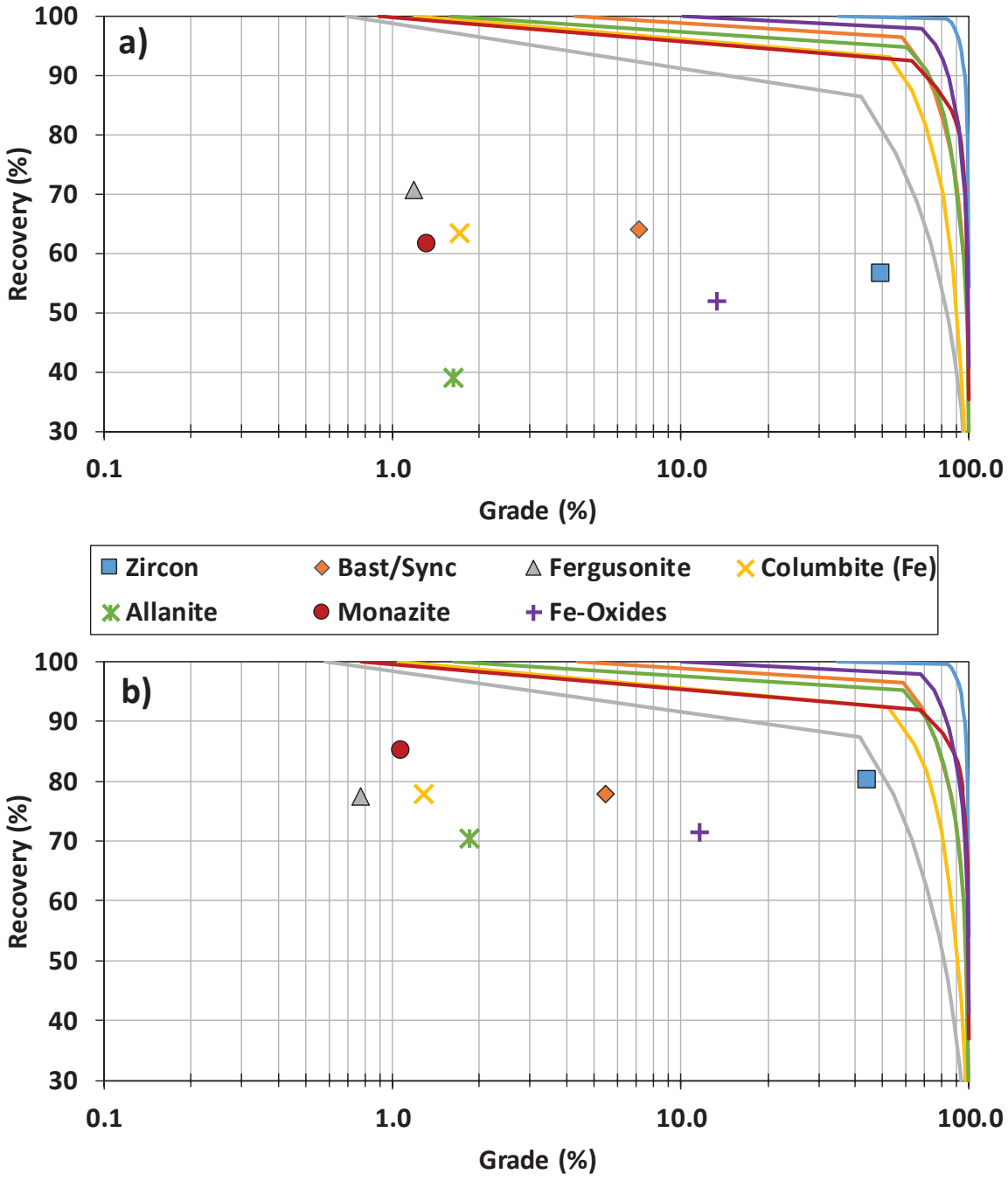

Figure 7.11 – Optimum grade-recovery results of REM compared to ideal grade-recovery as determined by QEMSCAN. Results shown are for: a) First stage flotation with benzohydroxamic acid for 2 min followed by reconditioning with additional benzohydroxamic acid and floating for 1 min (+ Bz), and b) First stage flotation with benzohydroxamic acid for 2 min followed by reconditioning with lead ions and additional benzohydroxamic acid and floating for 1 min (+ Pb + Bz)

7.10 Conclusions

This chapter presents the results of flotation experiments conducted on a pre-concentrated REM feed to evaluate different reagent combinations including initial flotation using a benzohydroxamic acid collector, reconditioning with additional collector and reconditioning with an addition of lead as an activator followed by benzohydroxamic acid. The conclusions of this chapter are as follows:

- The relative flotation kinetics of the REM in this deposit with benzohydroxamic acid (in decreasing order) are:
    - bastnäsite > fergusonite > synchysite > columbite(Fe) > monazite > zircon > allanite

- Benzohydroxamic acid is a much more effective collector for REM with relatively high degrees of solubility and higher REE contents (*i.e.* bastnäsite vs. allanite)

- A secondary addition of benzohydroxamic acid results in improved flotation of important REM such as zircon

- The addition of lead ions as an activator increases the recovery of less floatable REM such as zircon and allanite while also increasing the recovery of silicate gangue minerals (with some selectivity for quartz over feldspar)

- The results of this work support the design of a flotation process for this deposit which does not treat all REM as having identical flotation behaviours. A staged addition of benzohydroxamic acid coupled with the addition of activating ions may present an improved, efficient flotation process for this deposit

8. Conclusions, Contributions and Future Work

8.1 Conclusions

This chapter summarizes the main conclusions from this thesis, details the claims to original work as well as highlighting the areas identified throughout the research program as being in need of further work.

This research program has focused on the dual goals of: developing a fundamental body of knowledge surrounding the beneficiation of REM which have been the subject of minimal prior research; and constructing a process for the beneficiation of the Nechalacho REM deposit that is based on sound mineral processing fundamentals. Within the field of REM-related research this thesis presents an attempt at identifying many of the major gaps in literature (unknown physicochemical properties of many minerals, reported processes which are overly ore specific, lack of sufficiently detailed explanations of established processing methodologies *etc.*) and then begins the work of developing this knowledge base through experimental investigations. The conclusions of this work are as follows:

- Multiple individual REM such as bastnäsite and allanite were obtained and purified, using gravity and magnetic separation, for a range of particle sizes in order to proceed with fundamental investigations of mineral properties tied to beneficiation

- Key physicochemical characteristics including bulk (*e.g.* magnetic properties) and surface properties (*e.g.* zeta potentials) of individual REM have been measured and modified using different experimental conditions in order to provide an indication of separability from a common silicate gangue mineral. These investigations contributed to the selection of downstream processing conditions such as magnetic field strengths and flotation reagents
    - All of the REM tested were found to possess paramagnetic properties with fergusonite having the highest paramagnetic susceptibility and zircon the lowest

- The separation of bastnäsite from quartz was investigated using fatty acid, hydroxamate and phosphoric acid ester collectors. The optimum flotation reagent for this separation was determined to be benzohydroxamic acid
- The separation of allanite from quartz was investigated using fatty acid, hydroxamate and amine collectors. The optimum reagent for this separation was determined to be dodecylamine in a reverse flotation process
- The effect of iron and lead ions as activators for the flotation of allanite using benzohydroxamic acid was investigated with the best activator for the allanite-quartz system determined to be lead ions

- The response of the Nechalacho deposit to a variety of gravity and magnetic separations has been investigated in terms of grade, recovery and mineralogy
  - The mineralogical analysis identified a significant opportunity for upgrading the ore using selective comminution
  - The result of the gravity and magnetic separation experiments was the selection of a simple physical separation flowsheet employing a Knelson centrifugal gravity concentrator and a low intensity drum magnetic separator for effective upgrading of the ore prior to downstream flotation

- The flotation response of a pre-concentrated REM feed to flotation with benzohydroxamic acid was investigated in terms of grade, recovery, kinetics and mineralogy
  - Three different reagent schemes were investigated including flotation with benzohydroxamic acid only, the addition of a benzohydroxamic acid reconditioning step and the addition of a lead ion activator and benzohydroxamic acid at the reconditioning step
  - The flotation kinetics with benzohydroxamic acid of the various minerals in the Nechalacho deposit were investigated with the kinetic behaviour of the mineral found to depend on mineral solubility as well as metal cation content

- The addition of additional collector at the reconditioning stage was found to improve the flotation of zircon however other silicate REM (*e.g.* allanite) still exhibited poor floatability
- The lead ion activator was found to vastly improve recoveries of all REM (in particular allanite) with a corresponding, relatively small decrease in REM grade (due to increased silicate gangue recovery)

8.2 Contributions to original knowledge

The work in this thesis involved the application of established mineral characterisation and separation techniques to a novel class of minerals. As such, a listing of specific contributions to original knowledge would involve reiterating much of the information included in the preceding chapters. The contributions of this work may be better stated as the development of a consolidated framework of REM beneficiation knowledge which future researchers will be able to build on. The major contributions are summarised as follows:

- Direct measurement and quantification of the magnetic properties of multiple REM

- Development of a physical separation (gravity and magnetic) process capable of upgrading the Nechalacho deposit by concentrating the coarse fraction (which is enriched in heavy REE-bearing zircon)

- Investigation of the flotation separation of REM from silicate gangue using surface chemistry, single mineral flotation, batch flotation and automated mineralogy

- Investigation of the flotation of allanite, a common silicate REM found in many deposits worldwide, from the perspective of surface chemistry as well as in the flotation of a real ore

- Investigation into the differences in flotation behaviour between REM dependent on their solubility on multiple scales (single mineral tests as well as flotation of a real ore)

- The application of metal ion activators in REM flotation using hydroxamic acids on a fundamental (surface chemistry, single mineral flotation) and applied (batch flotation tests) basis

8.3 Future work

The field of REM beneficiation will require a great deal of future research work. As discussed in the previous section, this thesis provides a framework on which to build up the processing knowledge surrounding these minerals. Certain specific areas in need of investigation for the field of REM beneficiation include:

- Fundamental physicochemical characterisation of other valuable REM to determine bulk properties (specific gravities, magnetic properties) and surface properties (zeta potential, isoelectric point, mineral-reagent interactions) which control separation behaviour
    - In particular, the role of iron and silicate depressants requires extensive investigation for these minerals
    - Additionally the role of activating ions with REM should be investigated

- Fundamental investigations of synthetic mineral mixtures with hydroxamate-based collectors to clearly define the role of mineral solubility in the collection mechanism of these reagents. Such investigations should involve a series of minerals with different solubilities as well as operating at different solids concentrations

- The frothing action of hydroxamates and hydroxamate-frother blends should be investigated in terms of gas dispersion properties as experiments in the present

research program have suggested that bubble size may be affected by the addition of these reagents

- The investigation of highly specific oxide flotation collectors with multiple points of functionality to act as “selective flocculants”
    - Such selective flocculants could also be applied prior to gravity and magnetic separation of fine particle streams in order to improve REM collection

- An economic analysis of future REE demand should be applied to the valuation of REM such that rather than targeting all REM in a poly-mineral REE deposit, only the REM with the highest value (*i.e.* highest heavy REE content) should be targeted

In the context of the Nechalacho deposit the following areas should be investigated:

- The application of selective comminution to remove coarse zircon particles and treat them as a different stream

- Multiple stages of centrifugal gravity concentration (similar to a Gravity Recoverable Gold test) to determine the maximum REM recovery obtainable with this separation technique

- The use of dense media separation should be investigated and compared against gravity separation results

- The use of pilot-scale HGMS (*i.e.* SLon) on fine particle streams to attempt to magnetically concentrate weakly paramagnetic REM

- The application of gravity and magnetic separation after flotation to remove gangue minerals which are difficult to remove through flotation (*e.g.* iron oxides)

- Locked cycle flotation tests to determine hydroxamate dosages and determine the viability of a two-stream flotation process for this deposit treating the LREE-bearing minerals separately from the HREE-bearing minerals
    - Such a process would likely have a significant impact on downstream processing such as leaching and solvent extraction

- The use of alternate metal ion activators in hydroxamate flotation which are more environmentally friendly (*e.g.* cobalt) but have the correct speciation to be effective

- The investigation of specific depressants for silicate gangue and iron oxides

- Alternate flotation reagents such as cationic amines should be investigated for certain flotation applications (*e.g.* the separation from allanite from quartz in a scavenger stage)

References

Abeidu, A.M. (1972). The Separation of Monazite from Zircon by Flotation. Journal of the Less-Common Metals, 29: 113-119.

Abreu, R.D. and Morais, C.A. (2014). Study on separation of heavy rare earth elements by solvent extraction with organophosphorus acids and amine reagents. Minerals Engineering, 61: 82-87.

Agrawal, Y.K. and Kapoor, H.L. (1977). Stability constants of rare earths with hydroxamic acids. Journal of Inorganic Nuclear Chemistry, 39: 479-482.

Agrawal, Y.K. and Tandon, S.G. (1972). Thermodynamic dissociation constants of N-phenylbenzohydroxamic acids and benzohydroxamic acid. Talanta, 19: 700-706.

Alex, P., Suri, A. and Gupta, C. (1998). Processing of xenotime concentrate. Hydrometallurgy, 50 (3): 331-338.

Amer, T.E., Abdella, W.M., Abdel Wahab, G.M. and El-Sheikh, E.M. (2013). A suggested alternative procedure for processing of monazite mineral concentrate. International Journal of Mineral Processing, 125: 106-111.

Anand, T., Mishra, B., Apelian, D. and Blanpain, B. (2011). The case for recycling of rare earth metals - A CR3 communication. JOM, 63 (6): 8-9.

Anderson, C. (2015). Improved understanding of rare earth surface chemistry and its application to froth flotation. Metallurgical and Materials Engineering. PhD Thesis, Colorado School of Mines. 268.

Anthony, J.W., Bideaux, R.A., Bladh, K.W. and Nichols, M.C. (2001). Handbook of Mineralogy. Mineralogical Society of America, Chantilly, VA, USA.

Arbiter, N., Cooper, H., Fuerstenau, M.C., Harris, C.C., Kuhn, M.C., Miller, J.D. and Yap, R.F. (1985). Flotation Kinetics. SME Mineral Processing Handbook. ed. Weiss, N.L. Society of Mining Engineers, New York, USA. 94-98.

Arbiter, N., Harris, C.C. and Yap, R.F. (1976). The air flow number in flotation machine scale-up. International Journal of Mineral Processing, 3: 257-280.

Argus (2015). Argus Rare Earths Monthly Outlook. 1-13.

Assis, S.M., Montenegro, L.C.M. and Peres, A.E.C. (1996). Utilisation of hydroxamates in minerals froth flotation. Minerals Engineering, 9 (1): 103-114.

Atrafi, A., Gomez, C.O., Finch, J.A. and Pawlik, M. (2012). Frothing behavior of aqueous solutions of oleic acid. Minerals Engineering, 36-38: 138-144.

Bau, M. (1991). Rare-earth element mobility during hydrothermal and metamorphic fluid-rock interaction and the significance of the oxidation state of europium. Chemical Geology, 93: 219-230.

Binnemans, K., Jones, P.T., Blanpain, B., Van Gerven, T., Yang, Y., Walton, A. and Buchert, M. (2013a). Recycling of rare earths: a critical review. Journal of Cleaner Production, 51: 1-22.

Binnemans, K., Jones, P.T., Van Acker, K., Blanpain, B., Mishra, B. and Apelian, D. (2013b). Rare-earth economics: the balance problem. JOM, 65 (7): 846-848.

Browning, P.E. (1908). Introduction to the Rarer Elements. 2nd edn. John Wiley & Sons, New York, USA.

Bulatovic, S. (1988). Froth Flotation of Bastnaesite. ed. Office, U.S.P.Falconbridge Ltd, Toronto, CAN and Highwood Resources Ltd., Vancouver, CAN, Canada. 1-5.

Bulatovic, S. (2007). Collectors. Handbook of Flotation Reagents: Chemistry, Theory and Practice - Flotation of Sulfide Ores. Elsevier, Amsterdam, NL. 5-42.

Bulatovic, S. and Willett, G. (1991). A Monazite Beneficiation Process. ed. Organization, W.I.P. Carr Boyd Minerals Ltd., West Perth, AU, Australia. 1-40.

Bulatovic, S. and Wyslouzil, D.M. (1999). Process Development for Treatment of Complex Perovskite, Ilmenite and Rutile Ores. Minerals Engineering, 12: 1407-1417.

Bulatovic, S.M. (2010). Flotation of REO Minerals. Handbook of Flotation Reagents: Chemistry, Theory and Practice: Flotation of Gold, PGM and Oxide Minerals. 1st ed. Elsevier Science, Amsterdam, NL. 151-173.

Cappuccitti, F. and Finch, J.A. (2008). Development of new frothers through hydrodynamic characterization. Minerals Engineering, 21 (12–14): 944-948.

Carlston, J. (2014). New and innovative rare earth technology for low-level phosphorous removal. Conference of Metallurgists 2014, Canadian Institute of Mining, Metallurgy and Petroleum, Vancouver, CA. 1-12.

Cesbron, F.P. (1986). Mineralogy of the Rare-Earth Elements. Lanthanides, Tantalum and Niobium: Mineralogy, Geochemistry, Characteristics of Primary Ore Deposits, Prospecting, Processing and Applications, eds. Moller, P., Cerny, P., Saupe, F. Society for Geology Applied to Mineral Deposits, Berlin. 3-26.

Chan, T.N. (1992). A new beneficiation process for the treatment of supergene monazite ore. Rare Earths: Extraction, Preparation and Applications, eds. Bautista, R.G., Jackson, N. TMS and AusIMM, San Diego, USA. 77-94.

Chander, S. and Hogg, R. (1984). Physical and surface characterization for mineral processing. Minerals and Metallurgical Processing, 65: 152-163.

Chehreh Chelgani, S., Hart, B. and Xia, L. (2013). A TOF-SIMS surface chemical analytical study of rare earth element minerals from micro-flotation tests products. Minerals Engineering, 45: 32-40.

Chen, Z. (2011). Global rare earth resources and scenarios of future rare earth industry. Journal of Rare Earths, 29 (1): 1-6.

Chen, L., Qian, Z., Wen, S. and Huang, S. (2012). High-Gradient Magnetic Separation of Ultrafine Particles with Rod Matrix. Mineral Processing and Extractive Metallurgy Review, 34 (5): 340-347.

Cheng, T.W. (2000). The point of zero charge of monazite and xenotime. Minerals Engineering, 13 (1): 105-109.

Cheng, T.W., Holtham, P.N. and Tran, T. (1993). Froth flotation of monazite and xenotime. Minerals Engineering, 6 (4): 341-351.

Cheng, T.W., Partridge, A.C., Tran, T.A.M. and Wong, P.L.M. (1994). The surface properties and flotation behaviour of xenotime. Minerals Engineering, 7 (9): 1085-1098.

Chi, R., Xu, S., Zhu, G., Xu, J. and Qiu, X. (2001). Beneficiation of rare earth ore in china. Light Metals 2001: Technical Sessions at the 130th TMS Annual Meeting, ed. Anjier, J.L. TMS Aluminum Committee, New Orleans, USA. 1159-1165.

China, P.R. (2012). Situation and Policies of China's Rare Earth Industry. Information Office of the State Council, Beijing, CHN. 1-18.

Cho, Y.S. and Laskowski, J.S. (2001). Bubble coalescence and its effect on dynamic foam stability. Canadian Journal of Chemical Engineering, 80 (2): 299-305.

Chowdhury, R. and Antolasic, F. (2012). Structural analysis of hydroxamate reagents by X-ray diffraction. Journal of Earth Science and Engineering 2: 584-589.

Ciuculescu, T., Foo, B., Gowans, R., Hawton, K., Jacobs, C. and Spooner, J. (2013). Technical report disclosing the results of the feasibility study on the Nechalacho rare earth elements project. 1-307.

Clariant (2012). Beneficiation of Frequently Occurring Minerals. Clariant, The Woodlands, TX, USA. 1-3.

Cordier, D. (2011). Rare Earths. Mineral Commodity Summaries 2011, United States Geological Survey, Reston, VA, USA. 128-129.

Cordier, D. (2012). Rare Earths. Mineral Commodity Summaries 2012, United States Geological Survey, Reston, VA, USA. 128-129.

Cox, J.J., Ciuculescu, T., Goode, J.R. and Hains, D.H. (2011). Avalon Rare Metals - Technical Report on the Thor Lake Project: NI 43-101 Report - August 25, 2011. Toronto, ON, CA. 1-293.

Cross, W.M. and Miller, J.D. (1989). Bubble attachment time measurements for selected rare-earth phosphate minerals in oleate solutions. Rare Earths: Extraction, Preparation and Applications, eds. Bautista, R.G., Wong, M.M. TMS Reactive Metals Commitee, Las Vegas, USA. 45-55.

Crow, J.M. (2011). 13 exotic elements we can't live without. The New Scientist (2817): 36-41.

Cui, J., Hope, G.A. and Buckley, A.N. (2012). Spectroscopic investigation of the interaction of hydroxamate with bastnaesite (cerium) and rare earth oxides. Minerals Engineering, 36-38: 91-99.

Cuthbertson, R.E. (1952). Froth Flotation of Monazite from Heavy Gravity Minerals. ed. Office, U.S.P.Climax Molybdenum Company, United States. 1-3.

Darcy, J.W., Dhammika Bandara, H.M., Mishra, B., Blanplain, B., Apelian, D. and Emmert, M.H. (2013). Challenges in Recycling End-of-Life Rare Earth Magnets. JOM, 65 (11): 1381-1382.

Dehaine, Q. and Filippov, L.O. (2014). Rare earth (La, Ce, Nd) and rare metals (Sn, Nb, W) as by-product of kaolin production, Cornwall: Part 1: Selection and characterisation of the valuable stream. Minerals Engineering, 76: 141-153.

Deju, R.A. and Bhappu, R.B. (1967). Mineral Beneficiation - A chemical interpretation of surface phenomena in silicate minerals. Transactions of the Metallurgical Society of AIME: 329-332.

Delaney, K.A. (2010). Challenges Facing New Global Rare Earth Separation Plants - Presentation at the Critical & Rare Metals Summit III. Rare Earth Industry and Technology Association, Washington, DC, USA. 1-18.

Do, S.-S. (2003). Hydrodynamic characterization of a Denver laboratory flotation cell. Department of Mining and Materials Engineering. MEng Thesis, McGill University, Montreal, Canada.

Ebner, A.D., Ritter, J.A. and Ploehn, H.J. (1997). Feasibility and limitations of nanolevel high gradient magnetic separation. Separation and Purification Technology, 11 (3): 199-210.

Elshkaki, A. and Graedel, T.E. (2014). Dysprosium, the balance problem, and wind power technology. Applied Energy, 136: 548-559.

Eyring, L. (1964). Progress in the Science and Technology of the Rare Earths. Pergamon Press Ltd., Oxford, New York.

Falconer, A. (2003). Gravity Separation: Old Technique/New Methods. Physical Separation in Science and Engineering, 12 (1): 31-48.

Fangji, L., Juying, W. and Xinglan, Z. (1989). A process on the recovery of RE minerals with chelating collector. Rare Earths: Extraction, Preparation and Applications, eds. Bautista, R.G., Wong, M.M. TMS Reactive Metals Committee, Las Vegas, USA. 71-79.

Fangji, L. and Xinglan, Z. (2003). Maoniuping Bastnasite Separation Process (in Chinese). Journal of Shanghai Polytechnic University, 1: 10-16.

Fangji, L., Xinglan, Z. and Yingjiang, Z. (2002). Application of Collector L102 in Changlan Rare Earth Processing Plant (in Chinese). Chinese Rare Earths, 23: 1-5.

Feasby, G. (1966). Investigation of Hallimond-Tube Flotation of Low Grade Phosphate Material. Mineral Research Laboratory, NC State University, USA.

Ferron, C.J., Bulatovic, S.M. and Salter, R.S. (1991). Beneficiation of Rare Earth Oxide Minerals. International Conference on Rare Earth Minerals and Minerals for Electronic Uses, eds. Siribumrungsukha, B., Arrykul, S., Sanguansai, P., Pungrassami, T., Sikong, L., Kooptarnond, K. Prince Songkla University, Hat Yai, THL. 251-269.

Fitzgibbon, K. (1990). Thermally Assisted Liberation - A Review. Minerals Engineering, 3 (1): 181-185.

Foner, S. (1959). Versatile and Sensitive Vibrating-Sample Magnetometer. The Review of Scientific Instruments, 30 (7): 548-557.

Foner, S. (1956). Vibrating Sample Magnetometer. The Review of Scientific Instruments, 27 (7): 548.

Fuerstenau, D.W. (1956). Streaming Potential Studies on Quartz in Solutions of Aminium Acetates in Relation to the Formation of Hemi- micelles at the Quartz-Solution Interface. The Journal of Physical Chemistry, 60 (7): 981-985.

Fuerstenau, D.W., Metzger, P. and Seele, G. (1957). How to use this modified Hallimond tube for better flotation testing. Engineering and Mining Journal, 158 (March): 93-95.

Fuerstenau, D.W. and Pradip (1991). The role of inorganic and organic reagents in the flotation separation of rare-earth ores. International Journal of Mineral Processing, 32: 1-22.

Fuerstenau, D.W. and Pradip (2005). Zeta potentials in the flotation of oxide and silicate minerals. Advances in Colloid and Interface Science, 114-115: 9-26.

Fuerstenau, D.W., Pradip and Herrera-Urbina, R. (1992). The surface chemistry of bastnaesite, barite and calcite in aqueous carbonate solutions. Colloids and Surfaces, 68: 95-102.

Fuerstenau, D.W., Pradip, Khan, L.A. and Raghavan, S. (1982). An alternate reagent scheme for the flotation of mountain pass rare-earth ore. Proceedings of the 14th International Mineral Processing Congress, ed. Maltby, P.D.R.CIM, Toronto, Canada. 6.1-6.12.

Fuerstenau, M.C. (2005). Chelating Agents as Flotation Collectors. Innovations in natural resource processing: proceedings of the Jan D. Miller symposium, eds. Young, C.A., Kellar, J.J., Free, M.L. Society for Mining, Metallurgy & Exploration, Salt Lake City, USA. 33-56.

Fuerstenau, M.C. and Elgillani, D.A. (1967). Minerals Beneficiation - Calcium Activation in Sulfonate and Oleate Flotation of Quartz. Transactions of the Metallurgical Society of AIME. American Institute of Mining, Metallurgical and Petroleum Engineers, New York, USA. 405-413.

Fuerstenau, M.C., Jameson, G.J. and Yoon, R.H. (2007). Froth Flotation: A Century of Innovation. SME, USA.

Fuerstenau, M.C. and Palmer, B. (1976). Anionic Flotation of Oxides and Silicates Flotation: A.M. Gaudin Memorial Volume. ed. Fuerstenau, M.C. Port City Press, Baltimore, MD, USA.

Fullam, M. and Grewal, I. (2001). The Knelson Continuous Variable Discharge (CVD) Concentrator. The Knelson Group. 1-6.

http://www.flsmidth.com/~/media/PDF%20Files/FLSmidth%20Knelson/Papers/20010618ContinuousConcentratorGainsIndustryAcceptance.ashx (Dec. 7, 2015)

Gambogi, J. (2015). Rare Earths. Mineral Commodity Summaries 2015, United States Geological Survey, Reston, VA, USA. 128-129.

Gao, L. and Chen, Y. (2010). A study on the rare earth ore containing scandium by high gradient magnetic separation. Journal of Rare Earths, 28 (4): 622-626.

Gee, B., Holtham, P., Dunne, R. and Gregory, S. (2005). Recovery of fine gold particles using a Falcon ‘ B ’ separator. International Symposium on the Treatment of Gold Ores, eds. Deschenes, G., Hodouin, D., Lorenzen, L.CIM, Calgary, CAN. 3-15.

Gibson, C.E., Kelebek, S., Aghamirian, M. and Yu, B. (2015). Flotation of pyrochlore from low grade carbonatite gravity tailings with benzohydroxamic acid. Minerals Engineering, 71: 97-104.

Girgin, E., Do, S.-S., Gomez, C.O. and Finch, J.A. (2006). Bubble size as a function of impeller speed in a self-aeration laboratory flotation cell. Minerals Engineering, 19: 201-203.

Ginzburg, A.I. (1963). New data on Rare Element Mineralogy. Consultants Bureau, New York, USA.

Golev, A., Scott, M., Erskine, P.D., Ali, S.H. and Ballantyne, G.R. (2014). Rare earths supply chain: Current status, constraints and opportunities. Resources Policy, 41: 52-59.

Gorken, A., Perez, W. and Ravishankar, S.A. (2005). Flotation purification of kaolin clay with hydroxamate collectors. Centenary of Flotation Symposium, Australasian Institute of Mining and Metallurgy and the Society for Mining, Metallurgy and Exploration Brisbane, Australia.

Graedel, T.E., Harper, E.M., Nassar, N.T. and Reck, B.K. (2013). On the materials basis of modern society. Proceedings of the National Academy of Sciences USA, 112 (20): 6295-6300.

Gramaccioli, C.M. and Segalstad, T.V. (1978). A uranium- and thorium-rich monazite from a south-alpine pegmatite at Piona, Italy. American Mineralogist, 63: 757-761.

Grammatikopoulos, T., Mercer, W. and Gunning, C. (2013). Mineralogical characterization using QEMSCAN of the Nechalacho heavy rare earth metal deposit, Northwest Territories, Canada. Canadian Metallurgical Quarterly, 52 (3): 265-277.

Greenwood, R. (2003). Review of the measurement of zeta potentials in concentrated aqueous suspensions using electroacoustics. Advances in Colloid and Interface Science, 106: 55-81.

Gromet, L.P. (1983). Rare earth element distributions among minerals in a granodiorite and their petrogenetic implications. Geochimica et Cosmochimica Acta, 47: 925-939.

Guney, A., Onal, G. and Celik, M. (1999). A new flowsheet for processing chromite fines by column flotation and the collector adsorption mechanism. Minerals Engineering, 12 (9): 1041-1049.

Gupta, C.K. and Krishnamurthy, N. (2005). Extractive Metallurgy of Rare Earths. CRC Press, Boca Raton, Florida.

Gupta, C.K. and Krishnamurthy, N. (1992). Extractive Metallurgy of Rare Earths. International Materials Reviews, 37 (5): 197-248.

Guy, P.J., Bruckard, W.J. and Vaisey, M.J. (2000). Beneficiation of Mt Weld Rare Earth Oxides by Gravity Concentration, Flotation, and Magnetic Separation. Seventh Mill Operators' Conference, AusIMM, Kalgoorlie, AUS. 197-205.

Harris, C.C. (1974). Impeller speed, air, and power requirements in flotation machine scale-up. International Journal of Mineral Processing, 1: 51-64.

Harris, C.C. and Mensah-Biney, R.K. (1977). Aeration characteristics of laboratory flotation machine impellers. International Journal of Mineral Processing, 4: 51-67.

Hedrick, J. (2009). Rare Earths. Mineral Commodity Summaries 2009, United States Geological Survey, Reston, VA, USA. 130-131.

Hedrick, J. (2010). Rare Earths. Mineral Commodity Summaries 2010, United States Geological Survey, Reston, VA, USA. 128-129.

Hedrick, J.B., Sinha, S.P. and Kosynkin, V.D. (1997). Loparite, a rare-earth ore (Ce, Na, Sr, Ca)(Ti, Nb, Ta, Fe+3)O3. Journal of Alloys and Compounds, 250: 467-470.

Herrera-Urbina, R. and Fuerstenau, D.W. (1987). The effect of trace metal ion impurities on the hydroxamate flotation of quartz. International Journal of Mineral Processing, 21: 307-310.

Herrera-Urbina, R., Pradip and Fuerstenau, D.W. (2013). Electrophoretic mobility and computations of solid-aqueous solution equilibria for the bastnaesite-H2O system. Minerals and Metallurgical Processing, 30 (1): 18-23.

Higashiyama, Y. and Asano, K. (2007). Recent Progress in Electrostatic Separation Technology. Particulate Science and Technology, 16 (1): 77-90.

Holland-Batt, A.B. and Holtham, P.N. (1991). Particle and fluid motion on spiral separators. Minerals Engineering, 4 (3–4): 457-482.

Hope, G., Woods, R., Parker, G.K., Buckley, A.N. and McLean, J. (2010). A vibrational spectroscopy and XPS investigation of the interaction of hydroxamate reagents on copper oxide minerals. Minerals Engineering, 23: 952-959.

Horny, P., Lifshin, E., Campbell, H. and Gauvin, R. (2010). Development of a new quantitative X-ray microanalysis method for electron microscopy. Microscopy and Microanalysis, 16 (6): 821-830.

Houot, R. (1982). Beneficiation of Phosphatic Ores Through Flotation: Review of Industrial Applications and Potential Developments. International Journal of Mineral Processing, 9: 353-384.

Houot, R., Cuif, J.-P., Mottot, Y. and Samama, J.-C. (1991). Recovery of Rare Earth Minerals with Emphasis on Flotation Process. International Conference on Rare Earth Minerals and Minerals for Electronic Uses, eds. Siribumrungsukha, B., Arrykul, S., Sanguansai, P., Pungrassami, T., Sikong, L., Kooptarnond, K. Prince Songkla University, Hat Yai, THA. 301-324.

Hunter, R.J. (1998). Recent developments in the electroacoustic characterisation of colloidal suspensions and emulsions. Colloids and Surfaces A: Physicochemical and Engineering Aspects, 141: 37-65.

Ito, S., Yotsumoto, H. and Sakamoto, H. (1991). Magnetic Separation of Monazite and Xenotime. Proceedings of the International Conference on Rare Earth Minerals and Minerals for Electronic Uses, eds. Siribumrungsukha, B., Arrykul, S., Sanguansai, P., Pungrassami, T., Sikong, L., Kooptarnond, K. Prince Songkla University, Hat Yai, THA. 279-299.

Jakubovics, J.P. (1994). Magnetism and Magnetic Materials (2nd Edition). Maney Publishing for IOM3, the Institute of Materials, Minerals and Mining.

Jianzhong, C., Yunbing, H. and Liping, C. (2007). Flotation Separation on Rare Earth Minerals and Gangues. Journal of Rare Earths, 25 (1): 62-66.

Jie, Z., Weiqing, W., Jing, L., Yang, H., Qiming, F. and Hong, Z. (2014). Fe(III) as an activator for the flotation of spodumene, albite and quartz minerals. Minerals Engineering, 61: 16-22.

Jiles, D. (1990). Introduction to Magnetism and Magnetic Materials. Chapman & Hall, London.

Jorjani, E. and Bagherieh, A.H. (2007). Determination of Rare Earth Elements in Products of Chadormalu Iron Ore Concentrator Plant (Iran) from Beneficiation Point of View. Iran Journal of Chemistry and Chemical Engineering, 26 (4): 11-18.

Jun, R. (1989). Practice and Process Improvement of Baotou Rare Earth Flotation (in Chinese). Nonferrous Metals (Mineral Processing), 6: 15-19.

Jun, R. (1992). Studies of Synergistic Effects of Reagents for Rare Earth Flotation (in Chinese). Nonferrous Metals (Mineral Processing), 3: 6-9.

Jun, R., Wenmei, W., Jiake, L., Gaoyun, Z. and Fangqiong, T. (2003). Progress of Flotation Reagents of Rare Earth Minerals in China. Journal of Rare Earths, 21 (1): 1-8.

Kanazawa, Y. and Kamitani, M. (2006). Rare earth minerals and resources in the world. Journal of Alloys and Compounds, 408-412: 1339-1343.

Kasey, J.B. (1956). Method of Treating Rare Earth Ores. ed. Office, U.S.P.John Bryant Kasey. 1-5.

Kelly, E.G. and Spottiswood, D.J. (1989a). The theory of electrostatic separations: a review - part II. particle charging. Minerals Engineering, 2 (2): 193-205.

Kelly, E.G. and Spottiswood, D.J. (1989b). The theory of electrostatic separations: a review - part III. the separation of particles. Minerals Engineering, 2 (3): 337-349.

Kelly, E.G. and Spottiswood, D.J. (1989c). The theory of electrostatic separations: a review - part I. fundamentals. Minerals Engineering, 2 (1): 33-46.

Knelson, B. (1992). The Knelson concentrator. metamorphosis from crude beginning to sophisticated world wide acceptance. Minerals Engineering, 5 (10–12): 1091-1097.

Kosmulski, M. (2001a). Surface Charging in Absence of Strongly Adsorbing Species. Chemical Properties of Material Surfaces. Marcel Dekker, Inc., New York, USA. 90-155.

Kosmulski, M. (2001b). Chemical Properties of Material Surfaces. Marcel Dekker, New York, USA.

Kosmulski, M. (2002). The pH-dependent surface charging and the points of zero charge. Journal of Colloid and Interface Science, 253: 77--87.

Kosmulski, M. (2004). pH-dependent surface charging and points of zero charge II. Update. Journal of Colloid and Interface Science, 275: 214-224.

Kosmulski, M. (2006). pH-dependent surface charging and points of zero charge III. Update. Journal of Colloid and Interface Science, 298: 730-741.

Kosmulski, M. (2009). pH-dependent surface charging and points of zero charge. IV. Update and new approach. Journal of Colloid and Interface Science, 337: 439-448.

Kroll-Rabotin, J.-S., Climent, E. and Bourgeois, F. (2011). Beneficiation of concentrated ultrafine suspensions with a Falcon UF concentrator. Canadian Institute of Mining Journal, 2 (4): 189-198.

Laplante, A. (1993). A comparative study of two centrifugal concentrators. 25th annual meeting of the Canadian Mineral Processors, Canadian Mineral Processors Division of the CIM, Ottawa. 18.

Laplante, A.R., Buonvino, M., Veltmeyer, A., Robitaille, J. and Naud, G. (1994). A Study of the Falcon Concentrator. Canadian Metallurgical Quarterly, 33 (4): 279-288.

Levy, S.I. (1924). The Rare Earths. 2nd Ed. edn. Edward Arnold & Co., London.

Li, H.C. and De Bruyn, P.L. (1966). Electrokinetic and adsorption studies on quartz. Surface Science, 5 (2): 203-220.

Li, L., Xu, S., Ju, Z. and Wu, F. (2009). Recovery of Ni, Co and rare earths from spent Ni-metal hydride batteries and preparation of spherical Ni(OH)2. Hydrometallurgy, 100: 41-46.

Liley, P.E., Thomson, G.H., Friend, D.G., Daubert, T.E. and Buck, E. (1997). Physical and Chemical Data. Perry's Chemical Engineering Handbook. eds. Perry, R.H., Green, D.W., Maloney, J.O., 7th ed. McGraw-Hill, New York, USA.

Lin, S.T. (1959). Magnetic Properties of Hematite Single Crystals. I. Magnetization Isotherms, Antiferromagnetic Susceptibility, and Weak Ferromagnetism of a Natural Crystal. Physical Review, 116 (6): 1447-1452.

Lins, F.F., Veiga, M.M., Stewart, J.A., Papalia, A. and Papalia, R. (1992). Performance of a new centrifuge (Falcon) in concentrating a gold ore from texada island, B.C., Canada. Minerals Engineering, 5 (10–12): 1113-1121.

Lister, T.E., Wang, P. and Anderko, A. (2014). Recovery of critical and value metals from mobile electronics enabled by electrochemical processing. Hydrometallurgy, 149: 228-237.

Long, K.R., Van Gosen, B.S., Foley, N.K. and Cordier, D. (2010). The Principal Rare Earth Elements Deposits of the United States — A Summary of Domestic Deposits and a Global Perspective - U.S. Geological Survey Scientific Investigations Report 2010-5220. Reston, VA, USA. 1-104.

Lu, Y., Drelich, J. and Miller, J.D. (1998). Oleate Adsorption at an Apatite Surface Studied by Ex-Situ FTIR Internal Reflection Spectroscopy. Journal of Colloid and Interface Science, 202: 462-476.

Luo, J. and Chen, X. (1984). Research into the recovery of high-grade rare-earth concentrate from Baotou complex iron ore, China. Mineral Processing and Extractive Metallurgy, eds. Jones, M.J., Gill, P., Hui, Z.J.S.X. IMM and Chinese Society of Metals, Kunming, Yunnan Province, CHN. 663-675.

Luttrell, G.H., Phillips, D.I. and Honaker, R.Q. (1995). Enhanced gravity separators: New alternatives for fine coal cleaning. Coal Prep '95, Lexington, USA. 282-292.

Male, S.E. (1980). Magnetic measurements on coal. Journal of Physics D: Applied Physics, 13: L67-70.

Marion, C., Jordens, A., McCarthy, S., Grammatikopoulos, T. and Waters, K.E. (2015). An investigation into the flotation of muscovite with an amine collector and calcium lignin sulfonate depressant. Separation and Purification Technology, 149: 216-227.

Massari, S. and Ruberti, M. (2013). Rare earth elements as critical raw materials: Focus on international markets and future strategies. Resources Policy, 38: 36-43.

Matis, K.A., Mavros, P. and Kydros, C.A. (1991). A dissolved-air flotation microcell for floatability tests with particulate systems. Separations Technology, 1: 255-258.

McAndrew, J. (1957). Calibration of a frantz isodynamic separator and its application to mineral separation. Proceedings of the Australian Institute of Mining and Metallurgy, 181: 59-73.

Menzel, K., Lindner, J. and Nirschl, H. (2012). Removal of magnetite particles and lubricant contamination from viscous oil by High-Gradient Magnetic Separation technique. Separation and Purification Technology, 92: 122-128.

Meyer, L. and Bras, B. (2011). Rare earth metal recycling. 2011 IEEE International Symposium on Sustainable Systems and Technology (ISSST), Institute of Electrical and Electronics Engineers, Chicago, IL, USA. 1-6.

Michaud, D. (2013). Froth Flotation Process Explained. 911 Metallurgist Blog. http://www.911metallurgist.com/blog/froth-flotation-process (Dec. 7, 2015)

Ming, Z. (1993). The Process of Rare Earth Element Synthetical Recovery from Baogang Tailings (in Chinese). China Mine Engineering, 1: 52-56.

Mishra, S.K. (1982). Electrokinetic properties and flotation behaviour of apatite and calcite in the presence of sodium oleate and sodium metasilicate. International Journal of Mineral Processing, 9: 59-73.

Miyawaki, R. and Nakai, I. (1993). Crystal structures of rare earth minerals. Handbook on the Physics and Chemistry of Rare Earths. eds. Gschneider Jr., K.A., Eyring, L. Elsevier, Amsterdam, NL. 249-518.

Morrice, E. and Wong, M.M. (1983). Flotation of Rare Earths from Bastnasite Ore - Report for the Federal Bureau of Mines. Reno, NV, USA. 1-13.

Moustafa, M.I. and Abdelfattah, N.A. (2010). Physical and Chemical Beneficiation of the Egyptian Beach Monazite. Resource Geology, 60 (3): 288-299.

Murariu, V. and Svoboda, J. (2003). The applicability of Davis tube tests to ore separation by drum magnetic separators. Physical Separation in Science and Engineering, 12 (1): 1-11.

Nagaraj, D.R. (1988). The chemistry and application of chelating or complexing agents in minerals separations. Reagents in Mineral Technology. eds. Somasundaran, P., Moudgil, B.M. Marcel Dekker, New York, USA.

Neiheisel, J. (1962). Heavy-Mineral Investigation of Recent and Pleistocene Sands of Lower Coastal Plain of Georgia. Geological Society of America Bulletin, 73 (March): 365-374.

Ni, X., Parrent, M., Cao, M., Huang, L., Bouajila, A. and Liu, Q. (2012). Developing flotation reagents for niobium oxide recovery from carbonatite Nb ores. Minerals Engineering.

Nosrati, A., Addai-Mensah, J. and Skinner, W. (2011). Influence of mineral chemistry on electrokinetic and rheological behavior of aqueous muscovite dispersions. Industrial and Engineering Chemistry Research, 50: 11087-11096.

O'Driscoll (1991). An Overview of Rare Earth Minerals Supply and Applications. International Conference on Rare Earth Minerals and Minerals for Electronic Uses, eds.

Siribumrungsukha, B., Arrykul, S., Sanguansai, P., Pungrassami, T., Sikong, L., Kooptarnond, K. Prince Songkla University, Hat Yai, THA. 409-420.

Oberteuffer, J. (1974). Magnetic Separation: A review of principles, devices, and applications. IEEE Transactions on Magnetics, 10 (2): 223-238.

Ozbayoglu, G. and Atalay, U. (2000). Beneficiation of bastnaesite by a multi-gravity separator. Journal of Alloys and Compounds, 303-304: 520-523.

Ozkan, A. and Yekeler, M. (2003). A new microcolumn flotation cell for determining the wettability and floatability of minerals. Journal of Colloid and Interface Science, 261: 476-480.

Parak, T. (1973). Rare Earths in the Apatite Iron Ores of Lappland Together With Some Data About the Sr, Th and U Content of These Ores. Economic Geology, 68: 210-221.

Parks, G.A. (1965). The isoelectric points of solid oxides, solid hydroxides, and aqueous hydroxo complex systems. Chemical Reviews, 65: 177-198.

Partridge, A.C. and Smith, G.W. (1971). Small-sample flotation testing: A new cell. Transactions of the Institute of Mining and Metallurgy, 80: C199-C200.

Pascoe, R.D., Power, M.R. and Simpson, B. (2007). QEMSCAN analysis as a tool for improved understanding of gravity separator performance. Minerals Engineering, 20: 487-495.

Pavez, O., Brandao, P.R.G. and Peres, A.E.S. (1996). Technical Note - Adsorption of Oleate and Octyl-Hydroxamate on to Rare-Earths Minerals. Minerals Engineering, 9 (3): 357-366.

Pavez, O. and Peres, A.E.C. (1994). Technical note - Bench scale flotation of a brazilian monazite ore. Minerals Engineering, 7 (12): 1561-1564.

Pavez, O. and Peres, A.E.C. (1993). Effect of Sodium Metasilicate and Sodium Sulphide on the Floatability of Monazite-Zircon-Rutile with Oleate and Hydroxamates. Minerals Engineering, 6 (3): 69-78.

Pitts, M. (2011). Endangered Elements. The Chemical Engineer (844): 48-51.

Pol'kin, S.I., Ilie, P., Solnyshkin, V.I. and Zakharov, A.E. (1967). Selective Desorption of Sodium Oleate from Pyrochlore, Zircon and Monazite by Sodium Sulfide. Flotation Properties of Rare Metal Minerals. ed. Plaksin, I.N. Primary Sources, New York, USA. 46-56.

Pope, M.I. and Sutton, D.I. (1973). The Correlation between Froth Flotation Response and Collector Adsorption from Aqueous Solution. Part I. Titanium Dioxide and Ferric Oxide Conditioned in Oleate Solutions. Powder Technology, 7: 271-279.

Pradip (1981). The Surface Properties and Flotation of Rare-Earth Minerals. Department of Materials Science and Mineral Engineering. PhD Thesis, University of California, Berkeley, Berkeley. 1-225.

Pradip and Fuerstenau, D.W. (1983). The Adsorption of Hydroxamate on Semi-Soluble Minerals. Part I: Adsorption on Barite, Calcite and Bastnaesite. Colloids and Surfaces, 8: 103-119.

Pradip and Fuerstenau, D.W. (1985). Adsorption of hydroxamate collectors on semi-soluble minerals. Part II: Effect of temperature on adsorption. Colloids and Surfaces, 15: 137-146.

Pradip and Fuerstenau, D.W. (2013). Design and development of novel flotation reagents for the beneficiation of Mountain Pass rare-earth ore. Minerals and Metallurgical Processing, 30 (1): 1-9.

Preinfalk, C. and Morteani, G. (1986). The Industrial Applications of Rare Earth Elements. Lanthanides, Tantalum and Niobium: Mineralogy, Geochemistry, Characteristics of Primary Ore Deposits, Prospecting, Processing and Applications. eds. Moller, P., Cerny, P., Saupe, F. Society for Geology Applied to Mineral Deposits, Berlin, DE. 359-370.

Rao, S.R. (2004). Surface Chemistry of Froth Flotation. Kluwer Academic, New York, USA.

Raslan, M.F. (2009). Mineralogical and Minerallurgical Characteristics of Samarskite-Y, Columbite and Zircon from Stream Sediments of the Ras Baroud Area, Central Eastern Desert, Egypt. Studia i Materialy, 128 (36): 179-194.

Ren, J. (1993). Flotation Behaviour and Mechanism of Bastnaesite with N-Hydroxyl Phthalicimide. Acta Metallurgica Sinica Series B, 6 (6): 432-438.

Ren, J., Lu, S., Song, S. and Niu, J. (1997). A new collector for rare earth mineral flotation. Minerals Engineering, 10 (12): 1395-1404.

Ren, J., Song, S. and Lopez-Valdivieso, A. (2000). Selective flotation of bastnaesite from monazite in rare earth concentrates using potassium alum as depressant. International Journal of Mineral Processing, 59: 237-245.

Research, T.M. (2015). Technology metals research advanced rare-earth projects index. www.techmetalsresearch.com

Resende, L.V. and Morais, C.A. (2015). Process development for the recovery of europium and yttrium from computer monitor screens. Minerals Engineering, 70: 217-221.

Riley, J. (2005). Charge in Colloidal Systems. Colloid Science: Principles, methods and applications. ed. Cosgrove, T. Blackwell Publishing. 14-35.

Ring, R., Soldenhoff, K., Bellingham, A., Brown, S., Collier, D., Day, A., Levins, D., Quan, C., Secomb, R., Tapsell, G., Kingsnorth, D. and Chan, M. (1993). Development of a Process for Recovery of Rare Earths from the Mt Weld Orebody. XVIII International Mineral Processing Congress, AusIMM, Sydney. 1239-1244.

Rosenblum, S. and Brownfield, I.K. (1999). Magnetic Susceptibilities of Minerals - Report for U.S. Geological Survey. 1-33.

Roy, S. (2011). Recovery Improvement of Fine Magnetic Particles by Floc Magnetic Separation. Mineral Processing and Extractive Metallurgy Review, 33 (3): 170-179.

Samson, B., Sandi, G., Lionel, F., Rosemary, F. and Mpho, M. (2013). Electrostatic concentration of phosphate flotation concentrate. International Journal of Mining Science and Technology, 23 (3): 403-406.

Schnetzler, C.C. and Philpotts, J.A. (1970). Partition coefllcients of rare-earth elements between igneous matrix material and rock-forming mineral phenocrysts-II. Geochimic et Cosmochimica Acta, 34: 331-340.

Schoeller, W.R. and Powell, A.R. (1955). The Analysis of Minerals and Ores of the Rarer Elements. 3rd edn. Charles Griffin and Company, London.

Shrivastava, A. and Ghosh, K.K. (2007). Determination of pKa's of hydroxamic acids by nucleophilic substitution reaction. Indian Journal of Chemistry, 46A: 1630-1634.

Shuaib, N., Marafie, H., Hassan, M. and El-Ezaby, M.S. (1987). Complexes of hydroxamates III. Equilibrium and kinetic studies on the reactions of iron (III) with monohydroxamic acids. Journal of Inorganic Biochemistry, 31: 171-185.

Seredin, V.V. (2010). A new method for primary evaluation of the outlook for rare earth element ores. Geology of Ore Deposits, 52 (5): 428-433.

Simandl, G.J. (2012). Geology and Economic Significance of Current and Future Rare Earth Element Sources. Conference of Metallurgists 2012 - Rare Earths, eds. Goode, J.R., Moldoveanu, G., Rayat, M.S.Met Soc, Niagara Falls, ON, CA. 15-30.

Smith, R. and Scott, J.L. (1990). Mechanisms of Dodecylamine Flotation of Quartz. Mineral Processing and Extractive Metallurgy Review, 7 (2): 81-94.

Smith, R.W. and Shonnard, D. (1986). Electrokinetic Study of the Role of Modifying Agents in Flotation of Salt-type Minerals. AIChE Journal, 32 (5): 865-868.

Sorensen, E. and Lundgaard, T. (1966). Selective Flotation of Steenstrupine and Monazite from Kvanefjeld Lujavrite - Report for the Danish Atomic Energy Commission. Roskilde, DK.

Spedding, F.H. (1975). Contributions of the Rare Earths to Science and Technology. Symposium on the effects of rare earths on the properties of metals and alloys, ASM, Cincinnati. 1-11.

Spedding, F.H. and Daane, A.H. (1961). The Rare Earths. John Wiley & Sons, New York, USA.

Sreenivas, T. and Padmanabhan, N.P.H. (2002). Surface chemistry and flotation of cassiterite with alkyl hydroxamates. Colloids and Surfaces A: Physicochemical and Engineering Aspects, 205: 47-59.

Srinivas, K., Sreenivas, T. and Venugopal, R. (2004). Studies on the Application of Alkyl Phosphoric Acid Ester in the Flotation of Wolframite. Mineral Processing and Extractive Metallurgy Review, 25: 253-267.

Steinberg, G.M. and Swidler, R. (1965). The Benzohydroxamate Anion. Journal of Organic Chemistry, 30 (7): 2362-2365.

Svoboda, J. and Fujita, T. (2003). Recent developments in magnetic methods of material separation. Minerals Engineering, 16 (9): 785-792.

Taikang, D. and Yingnan, H. (1980). Studies on High Grade Rare Earth Flotation Technology (in Chinese). Multipurpose Utilization of Mineral Resources, 1: 27-33.

Tien, J.C. (2013). China's rare earth minerals: Reserves, supply and demand. Mining Engineering(December 2013): 44-49.

Topp, N.E. (1965). The chemistry of the rare-earth elements. Elsevier, Amsterdam, NL.

Trahar, W.J. (1981). A rational interpretation of the role of particle size in flotation. International Journal of Mineral Processing, 8 (4): 289-327.

Tran, T. (1991). New Developments in the Processing of Rare Earths. International Conference on Rare Earth Minerals and Minerals for Electronic Uses, eds.

Siribumrungsukha, B., Arrykul, S., Sanguansai, P., Pungrassami, T., Sikong, L., Kooptarnond, K. Prince Songkla University, Hat Yai, THA. 337-353.

Trifonov, D.N. (1963). The Rare-Earth Elements. Macmillan, New York.

Tu, Y.-J., Lo, S.-C. and You, C.-F. (2015). Selective and fast recovery of neodymium from seawater by magnetic iron oxide Fe3O4. Chemical Engineering Journal, 262: 966-972.

Uda, T., Jacob, K.T. and Hirasawa, M. (2000). Technique for Enhanced Rare Earth Separation. Science, 289: 2326-2329.

Vijayan, S., Melnyk, A.J., Singh, R.D. and Nuttall, K. (1989). Rare earths: Their mining, processing, and growing industrial usage. Mining Engineering, 41: 13-18.

Warren, L.J. (1984). Determination of the contributions of true flotation and entrainment in batch flotation tests. International Journal of Mineral Processing, 14: 33-44.

Waters, K.E., Rowson, N.A., Greenwood, R.W. and Williams, A.J. (2007). Characterising the effect of microwave radiation on the magnetic properties of pyrite. Separation and Purification Technology, 56: 9-17.

Wills, B.A. and Finch, J.A. (2016). Wills' Mineral Processing Technology. Butterworth-Heinemann, Oxford, UK.

Wu, C. (2008). Bayan Obo Controversy: Carbonatites versus Iron Oxide-Cu-Au-(REE-U). Resource Geology, 58 (4): 348-354.

Xia, L., Hart, B. and Loshusan, B. (2015). A Tof-SIMS analysis of the effect of lead nitrate on rare earth flotation. Minerals Engineering, 70: 119-129.

Xie, F., Zhang, T.A., Dreisinger, D. and Doyle, F. (2014). A critical review on solvent extraction of rare earths from aqueous solutions. Minerals Engineering, 56: 10-28.

Xu, M. (1998). Modified flotation rate constant and selectivity index. Minerals Engineering, 11 (3): 271-278.

Yan, J. (1991). Application of the New Collector H205 in Rare Earth Flotation (in Chinese). Science and Technology of Baotou Steel (Group) Corporation, 4: 33-35.

Yang, J., Matsui, M., Kawa, M., Ohta, H., Michioka, C., Dong, C., Wang, H., Yuan, H., Fang, M. and Yoshimura, K. (2009). Magnetic and Superconducting Properties of Single Crystals of Fe1+δ Te1−x Sex System. arXiv preprint arXiv:0911.4758.

Yang, X., Satur, J.V., Sanematsu, K., Laukkanen, J. and Saastamoinen, T. (2015). Beneficiation studies of complex REE ore. Minerals Engineering, 71: 55-64.

Yu, B., Che, X. and Zheng, Q. (2014). Flotation of ultra-fine rare-earth minerals with selective flocculant PDHA. Minerals Engineering, 60: 23-25.

Zakharov, A.E., Ilie, P., Pol'kin, S.I. and Solnyshkin, V.I. (1967). Reaction of Sodium Sulfide with Pyrochlore, Zircon and Monazite in Flotation with Sodium Oleate. Flotation Properties of Rare Metal Minerals. ed. Plaksin, I.N. Primary Sources, New York, USA. 71-82.

Zhang, X., Du, H., Wang, X. and Miller, J.D. (2013). Surface chemistry considerations in the flotation of rare-earth and other semisoluble salt minerals. Minerals and Metallurgical Processing, 30 (1): 24-37.

Zhang, J. and Edwards, C. (2012). A Review of Rare Earth Mineral Processing Technology. 44th Annual Meeting of The Canadian Mineral Processors, eds. Leroux, D., Zinck, J. CIM, Ottawa, CAN. 79-102.

Zhang, W., Nesset, J.E., Rao, R. and Finch, J.A. (2012). Characterizing frothers through critical coalescence concentration (CCC)95-Hydrophile-Lipophile Balance (HLB) Relationship. Minerals, 2: 208-227.

Appendix

MAGNETIC PROCESSING OF A RARE EARTH ELEMENT BEARING ORE

*Adam Jordens[1], Richard S. Sheridan[2], Neil A. Rowson[3], Kristian E. Waters[1]
[1]*Department of Mining and Materials Engineering*
McGill University
3610 University Street
Montreal, Quebec, Canada H3A 0C5
*(*Corresponding author: adam.jordens@mail.mcgill.ca)*

[2] *School of Metallurgy and Materials*
University of Birmingham
Edgbaston, Birmingham, United Kingdom B15 2TT

[3] *School of Chemical Engineering*
University of Birmingham
Edgbaston, Birmingham, United Kingdom B15 2TT

MAGNETIC PROCESSING OF A RARE EARTH ELEMENT BEARING ORE

ABSTRACT

Along with gravity separation and froth flotation, magnetic separation is one of the most common techniques for separating minerals. Minerals are separated by a magnetic force that is dependent on a combination of the applied magnetic field, the magnetic field gradient and the magnetic properties of the minerals themselves. Minerals may be classified as diamagnetic, paramagnetic or ferromagnetic based on the way they interact in a magnetic field. The magnetic susceptibility of a material may be determined by using a vibrating sample magnetometer to determine the magnetic moment of the material in an applied magnetic field and then converting this measured moment into the material's magnetic susceptibility. In the case of rare earth minerals, magnetic separation is commonly used to remove ferromagnetic iron-bearing gangue minerals and to concentrate paramagnetic valuable minerals such as monazite and xenotime. These magnetic separation steps are frequently preceded by a gravity separation step as many iron oxides and rare earth minerals have specific gravities that are much larger than those of typical gangue minerals. By varying the magnetic field intensity it may be possible to use magnetic separation to selectively separate the paramagnetic and ferromagnetic minerals that report to the concentrate after gravity separation. Test work on a Canadian rare earth ore has shown that a gravity concentration step using a Knelson concentrator was able to selectively concentrate heavy magnetic minerals as evidenced by increased recoveries, relative to the Knelson tailings and fresh feed, after processing through a wet variable intensity magnetic separator. Mass pull to the Knelson concentrate was 4.5 % and the magnetic recovery of this concentrate, at 0.94 T, was approximately 40 % higher than the magnetic recovery from the Knelson tailings (70 % versus 30 %). The products of the wet high intensity magnetic separation were also analysed using a vibrating sample magnetometer to determine the magnetic susceptibilities of the various concentrate and tailings products.

KEYWORDS

Rare Earth Elements, Rare Earth Minerals, Magnetic Separation, Gravity Separation, Vibrating Sample Magnetometer

INTRODUCTION

Rare Earth Mineral Beneficiation

Rare earth (RE) minerals are minerals which contain at least one of the lanthanide elements (La to Lu) or yttrium. These elements are used in numerous applications including high-strength permanent magnets, phosphors for electronic displays, and as metal alloying elements (Crow, 2011; Meyer & Bras, 2011; Preinfalk & Morteani, 1986). Recent export restrictions by China, which is currently responsible for 97 % of the world's RE production, have resulted in a significant increase in exploration and development of new RE deposits in the world outside of China (Chen, 2011; Chi, Xu, Zhu, Xu, & Qiu, 2001). These exploration activities combined with the limitations of existing rare earth literature have resulted in a need to research the physicochemical properties of these minerals, as well as how the different RE minerals behave in mineral processing unit operations.

The beneficiation of rare earth minerals typically involves many different unit operations including gravity, magnetic and flotation separations. Many rare earth minerals have high specific gravities and exhibit some degree of paramagnetism, making them good candidates for both gravity and magnetic separation

(Jordens, Cheng, & Waters, 2013). For further information on rare earth mineral beneficiation recent reviews by Zhang and Edwards (2012) and Jordens et al. (2013) should be consulted.

Gravity Separation

Gravity separations exploit differences in the specific gravity of minerals to achieve separation. Various separators are utilized to allow fine, high specific gravity material to separate from coarse, lower specific gravity particles (Falconer, 2003). Two commonly used separators are spiral separators and centrifugal gravity concentrators.

In a spiral separator, a mineral slurry flows along an inclined helical path where centrifugal and gravitational forces act to bring the densest particles towards the central column of the separator where they form the concentrate (Falconer, 2003). Spiral separators afford improvements over cone separators and jigs as the increased force felt by the particle, in conjunction with a lower slurry density, can achieve higher upgrade ratios and an improved treatment of fines (Falconer, 2003). Within the spiral trough there are two distinct zones; an inner zone near the column which acts to control concentrate grade and an outer zone that handles the bulk of the slurry flow and must allow heavy particles to settle to the spiral surface so that they can migrate towards the concentrate (Holland-Batt & Holtham, 1991).

Centrifugal gravity separators are employed for very fine particle sizes as they are able to increase the force on a particle to many times that of gravity. One of the most common centrifugal separators is the Knelson concentrator which passes material through a rapidly spinning bowl so that high specific gravity material is held against the wall of the bowl while low specific gravity particles are carried with the slurry up the wall and out of the bowl (Fullam & Grewal, 2001). The bowl's sides are lined with ridges to trap dense particles and each of the ridges has inlets where fluidizing water is continuously fed so that unintentional entrapment of low specific gravity particles into the concentrate phase is minimized (Fullam & Grewal, 2001). The Knelson concentrator is able to produce forces on a particle that are up to 60 times the force of gravity (Fullam & Grewal, 2001).

Magnetic Separation

The magnetic response of a material to an applied magnetic field is due to the presence of unpaired electrons which induce magnetic dipoles in the material. These magnetic dipoles possess individual magnetic moments and the alignment of these magnetic moments with an applied magnetic field will produce a resultant magnetic force on the material. The magnetisation of a material is a measure of the density of magnetic dipoles induced in the material. A good introduction into the concepts of magnetism can be found in Jiles (1990).

The magnetic recovery in a magnetic separation operation depends on the magnetic force felt by the particles and this force is proportional to the magnetic field gradient, the applied magnetic field intensity and the mineral's magnetic susceptibility (Waters, Rowson, Greenwood, & Williams, 2007). The equation for magnetic force felt by a mineral particle may be stated as (Oberteuffer, 1974; Svoboda & Fujita, 2003):

$$\boldsymbol{F_x = V(\chi_p - \chi_m) H \frac{dB}{d_x}} \quad (1)$$

where Fx is the magnetic force on a particle (N), V is the volume of the particle (m^3), χ is the magnetic susceptibility of the particle/medium, H is the applied magnetic field (A/m) and dB/dx is the gradient of the magnetic induction (T/m or N/Am^2). The particle size limit at which magnetic separation is effective depends on the interplay of three different forces, drag forces from the fluid medium, the force of gravity and the magnetic force as described above (Oberteuffer, 1974). For small particles fluid drag forces will vary proportionally with particle radius, r, while the gravitational force on a particle will vary proportionally with r^3 (Oberteuffer, 1974). For an optimized magnetic separator, the magnetic force can be shown to vary proportionally with r^2 (Oberteuffer, 1974). This means that at very small particle size, fluid drag forces will predominate and at very large particle sizes gravitational forces will be much stronger than any other force

(Oberteuffer, 1974). There is therefore a small range of particle sizes (typically 5 μm to 1 mm) where effective magnetic separation is possible (Oberteuffer, 1974).

A mineral particle may behave in three different manners when exposed to an external magnetic field gradient. Diamagnetic minerals will be repelled along magnetic field lines, paramagnetic minerals will be attracted along magnetic field lines and ferromagnetic minerals will be strongly attracted along magnetic field lines (Jiles, 1990). The key difference between paramagnetic and ferromagnetic materials is that the magnetic dipoles of a ferromagnetic material will align themselves much more rapidly than a paramagnetic material at a given applied magnetic field strength (Jiles, 1990).

Vibrating Sample Magnetometer

The vibrating sample magnetometer (VSM) was invented by Foner and first reported in scientific literature in 1956 (Foner, 1956). This equipment may be used to measure the magnetic moment of samples by suspending a sample in a uniform magnetic field (i.e. no magnetic field gradient), vibrating the sample and measuring the resultant oscillations in magnetic field via detection coils which surround the sample (Foner, 1959). These magnetic moment measurements are then completed at a series of different magnetic field strengths (Foner, 1959). The main advantage offered by the VSM compared with other means of measuring magnetic moments is that the sample moves perpendicular to the applied magnetic field, thereby simplifying the design of the magnet and detection coil assembly (Foner, 1959).

The data obtained from VSM measurements give the measured magnetic moment of the sample as a function of applied magnetic field. By dividing the magnetic moment by the volume of the sample being measured it is possible to generate a graph of magnetisation, M, as a function of applied magnetic field, H. An example of this type of figure is shown in Figure 1.

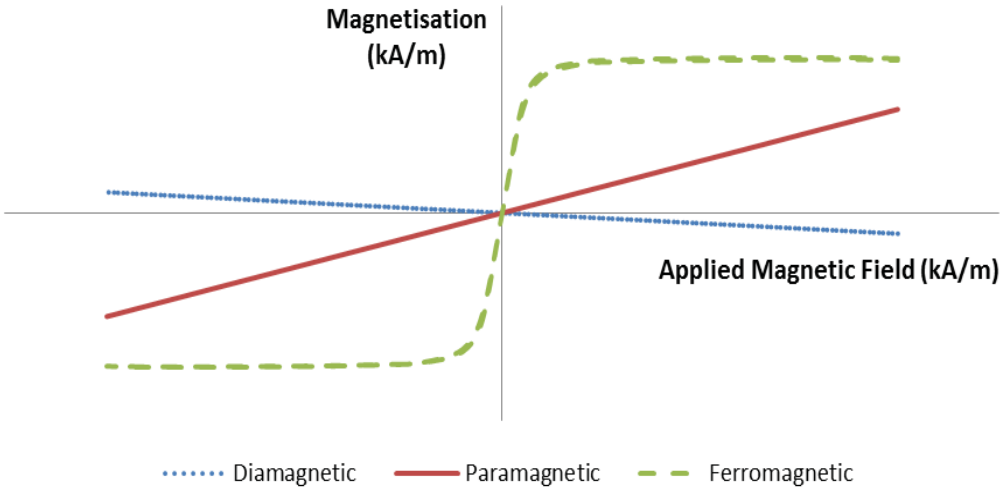

Figure 1 – Magnetisation curves for the three major forms of magnetic behaviour

The three trends shown in Figure 1 are typical of diamagnetic, paramagnetic, and ferromagnetic material (Waters et al., 2007). In a diamagnetic material the magnetic moments of the atoms result in a weak force that repels the material along the lines of the applied magnetic field (Jiles, 1990; Waters et al., 2007). This is represented in Figure 1 by a slight negative linear slope as the magnetisation decreases with increasing applied magnetic field (Jiles, 1990; Waters et al., 2007). Paramagnetic materials exhibit a positive linear slope (Figure 1) as the applied magnetic field causes the magnetic dipoles in the material to align, resulting in an attractive force on the material along the direction of the applied magnetic field lines (Jiles, 1990;

Waters et al., 2007). Ferromagnetic materials exhibit a non-linear variation of magnetisation with applied magnetic field as the atoms in a ferromagnetic material can undergo exchange coupling such that their magnetic dipoles will permanently align with one another to form magnetic domains (Jiles, 1990; Waters et al., 2007). These domains can then rapidly align themselves with an applied magnetic field. This allows the material to reach its saturation magnetisation (the plateau of the ferromagnetic trend in Figure 1) at relatively low applied magnetic field strengths, where almost all of the available magnetic domains have aligned themselves with the applied magnetic field and little further increase in magnetisation is possible (Jiles, 1990). The saturation magnetisation is a unique characteristic of ferromagnetic materials and can be used to identify the ferromagnetic component in a paramagnetic-ferromagnetic binary mixture of materials using a Honda-Owen plot of magnetic susceptibility of the material as a function of inverse applied magnetic field strength (Waters et al., 2007).

Previous work using magnetisation curves of minerals (obtained using VSM measurements as well as other undisclosed methods) has focused on understanding and altering the magnetic properties of pyrite as well as the removal of pyrite from coal (Male, 1984; Waters et al., 2007; Waters, Rowson, Greenwood, & Williams, 2008).

EXPERIMENTAL

Raw Materials

We obtained the raw material used in this work from a RE deposit located in the Northwest Territories, Canada. This deposit contains a series of RE minerals with very fine-grained mineralization (approximately 10–20 μm). There is also a significant amount of iron present in the deposit in the form of iron oxides. The major minerals present in the deposit are listed in Table 1 along with their specific gravities and magnetic properties. Most of the RE minerals present in this deposit have high specific gravities (relative to gangue minerals such as silica and feldspar) and some degree of paramagnetic behaviour.

Table 1 – Mineralogy of RE Deposit along with Specific Gravities and Magnetic Properties (Anthony, Bideaux, Bladh, & Nichols, 2001; Long, Van Gosen, Foley, & Cordier, 2010; Rosenblum & Brownfield, 1999)

Mineral	Weight %	Nominal S.G.	Magnetic Properties
Columbite(Fe)	0.5	6.30	Paramagnetic
Fergusonite	0.3	5.05	Paramagnetic
Bastnasite	1.3	4.98	Paramagnetic
Synchysite	0.2	4.03	N/A
Allanite	0.1	3.75	Paramagnetic
Monazite	0.2	5.15	Paramagnetic
Zircon	4.1	4.65	Diamagnetic
Apatite	0.2	3.18	Diamagnetic
Quartz	35.1	2.63	Diamagnetic
Plagioclase	10.5	2.68	Diamagnetic
K-Feldspar	20.5	2.57	Diamagnetic
Biotite	9.6	3.10	Paramagnetic
Calcite	1.9	2.71	Diamagnetic
Dolomite	1.8	2.85	Diamagnetic
Ankerite	3.7	3.05	Paramagnetic
Fluorite	0.3	3.18	Diamagnetic
Fe-Oxides	8.3	5.30	Ferromagnetic

We initially crushed all of the material using a jaw and cone crusher to achieve a 100 % -850 μm particle size. The size distribution of the ore after crushing can be seen in Figure 2. We produced feed material for the Knelson Concentrator and subsequent wet variable intensity magnetic separation by pulverizing this

100 % -850 µm material for approximately 4.5 minutes in 1 kg batches to produce material with 80 % passing 53 µm.

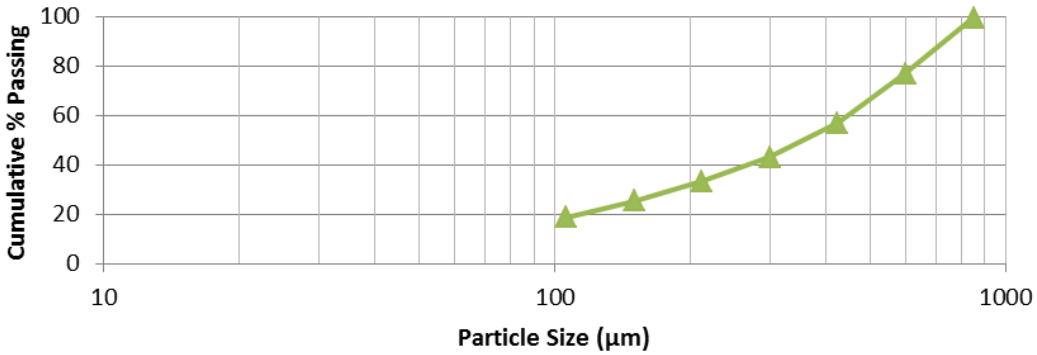

Figure 2 – Particle size distribution of ore after crushing to 100 % - 850 µm

Gravity Pre-Concentration

Spiral Concentrator

The spiral concentrator we used in this work was a four-turn helical spiral with a pitch of 15° manufactured by Walkabout Mineral Technologies (Australia) and includes a single splitter to produce a single concentrate and a single tailings stream. We produced the feed to the spiral by slurrying batches of approximately 4 kg with water in a 40 litre tank at 10 wt. % solids. We then fed the resultant slurry to the spiral with a constant splitter setting. Feed material for the spiral separation step had a particle top size of 850 µm however we further separated both the spiral concentrate and tailings streams by screening material to produce a single size fraction (212–425 µm) from each stream.

Knelson Concentrator

The Knelson concentrator we used in this work was a KC MD3 model manufactured by FLSmidth Knelson. We operated the concentrator at a mass flowrate of 300 – 400 g/min, a water pressure of 2.5–3 psi, slurrying water feed rate of approximately 2.5 L/min and a fluidizing water feed rate that varied between 6 and 9 L/min. Every 4 minutes we stopped the concentrator to remove the accumulated concentrate.

Magnetic Separation

Dry Variable Intensity Magnetic Separator (DVIMS)

We conducted dry magnetic separation in this work using a dry induced roll magnetic separator manufactured by BoxMag (UK). This separator allows for the manipulation of the magnetic field strength by varying the current supplied to the electromagnet coils. We used a gauss meter to establish a calibration curve between the current supplied to the separator and the strength of the induced magnetic field.

We passed approximately 150 g of material through the magnetic separator for each experiment with the tailings of each successive magnetic separation step reprocessed at increasing field strengths (increments of ~0.2 T with a maximum of 1.2 T). The feed material consisted of the untreated ore as well as the concentrate and tailings of the spiral separation step.

Wet High Intensity Magnetic Separator (WHIMS)

We conducted wet magnetic separation in this work using a wet high intensity magnetic separator manufactured by BoxMag (UK). This separator allows for the manipulation of the magnetic field strength by varying the current supplied to the electromagnet. In order to establish a calibration curve between the current supplied to the separator and the strength of the induced magnetic field we used a gauss meter. In this separator material is passed through a funnel containing a ferromagnetic matrix. This ferromagnetic matrix serves to produce a number of points with very high field gradient, thereby providing more points of attraction for small paramagnetic and ferromagnetic particles. In order to remove the magnetic particles after the applied magnetic field has been turned off, wash water is used to rinse the matrix material and remove any trapped magnetic particles.

For each experiment, we passed approximately 50 g of material through the wet magnetic separator at approximately 17 wt. % solids with the tailings of each successive magnetic separation step reprocessed at increasing field strengths (0.11 T, 0.41 T, 0.70 T and 0.94 T). The feed material consisted of the untreated ore as well as the concentrate and tailings of the Knelson gravity separation step. The general flow diagram for the magnetic and gravity separation steps can be seen in Figure 3.

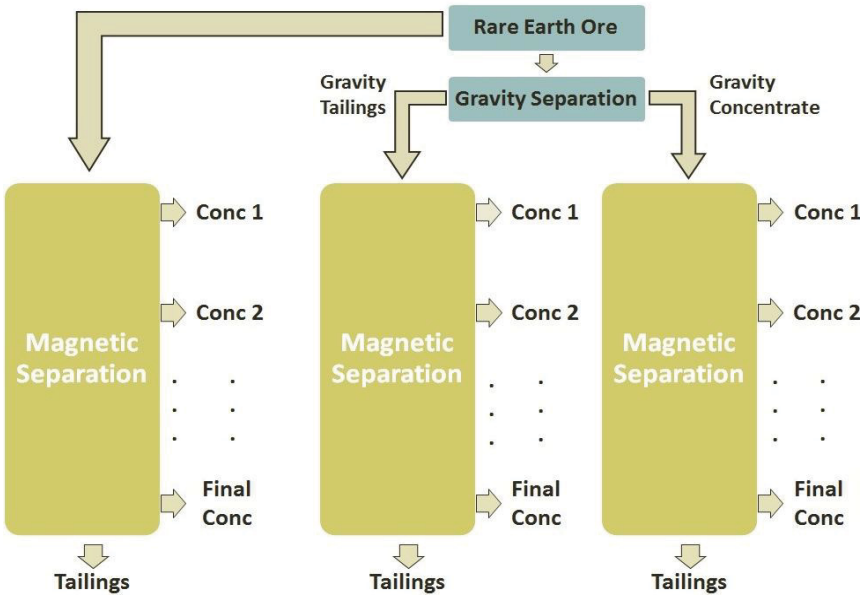

Figure 3 – Schematic of gravity pre-concentration followed by magnetic separation

Vibrating Sample Magnetometer

We obtained the vibrating sample magnetometer (VSM) measurements in this work from a 7300 series VSM manufactured by LakeShore (USA). For each sample measured 50–100 mg of sample (in the form of fine particles) is placed into a cylindrical VSM sample holder and attached to the end of an oscillating rod. The sample is saddled so that it sits in the middle of 4 pick-up coils and a hall probe. The rod is then oscillated about this central point as a magnetic field is applied to the sample to create a full hysteresis loop between +2 Tesla and -2 Tesla with measurements taken every 0.1 Tesla. The empty sample holder is also measured, and the magnetic moment associated with it subtracted from the sample data. The data output of the VSM consists of measured magnetic moment as a function of magnetic induction. We converted magnetic moment data output from the VSM to magnetisation by dividing by the volume of the samples. The magnetic induction is converted to magnetic field strength by dividing by the permeability of free space, $4\pi \times 10^{-7}$ Vs/Am.

RESULTS

The mass recovery from the spiral and Knelson gravity separation steps respectively can be seen in Table 2.

Table 2 – Mass Pull to Gravity Concentrate

	Mass Recovery
Knelson Concentrate	4.5 %
Spirals Concentrate	34.7 %

Dry Magnetic Separation

After gravity separation, we sized the concentrate and tailings of the spiral separation step to produce a suitable size fraction for dry magnetic separation. Next we put these two streams, along with a similar size fraction of the untreated ore through a series of dry magnetic separation steps as described above. The cumulative concentrate mass pull from this separation step can be seen in Figure 4. The results appear to indicate that the spiral separation step was ineffective at concentrating any high specific gravity, magnetic minerals as there was no significant difference in magnetic recovery seen between the spirals concentrate and spirals tailings. This is as expected since the particle size used for the spiral separation step was sufficiently large that there would likely be no fully liberated particles present.

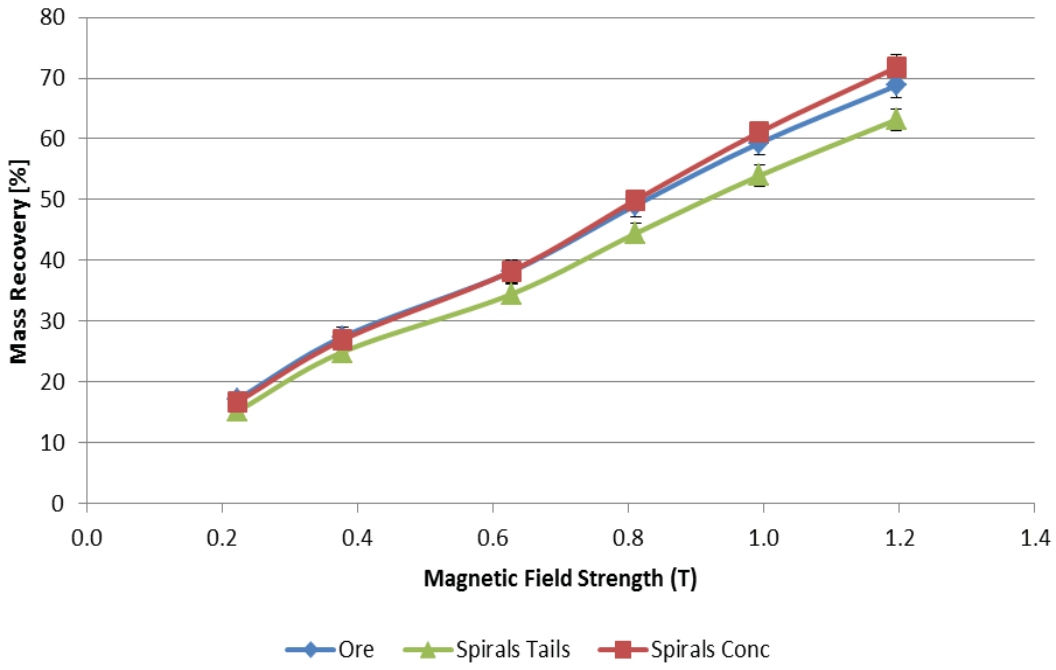

Figure 4 – Cumulative Mass Pull to the Concentrate from DVIMS (212–425 µm size fraction). Error bars indicate 95 % confidence intervals

Wet Magnetic Separation

We passed the products of the Knelson separation step and a sample of untreated ore (P_{80} of 53 µm) through a series of wet magnetic separations as described above and shown schematically in Figure 3.

Cumulative mass pull to the magnetic fraction can be seen in Figure 5. A much higher total magnetic recovery is seen for the Knelson concentrate stream (70 % as compared to 30 % for both the Knelson tails and the untreated ore), likely indicating that the Knelson separation step is able to concentrate heavy, magnetic minerals present in the ore such as iron oxides or paramagnetic RE minerals. The mass recovery from the Knelson tails stream is statistically identical to the untreated ore for all points except for the magnetic concentrate produced at 0.41 T. At this magnetic field strength the Knelson tails has a cumulative magnetic recovery of 13.1 % with a 95 % confidence interval of 2.1 % while the untreated ore has a cumulative magnetic recovery of 9.7 % with a 95 % confidence interval of 1.3 %. This minor difference can likely be explained by minor changes in the washing step used to release magnetic particles from the ferromagnetic matrix of the WHIMS.

We confirmed the effectiveness of the Knelson + WHIMS separation steps at concentrating particles of higher specific gravity by experimentally determining the densities of the products of the WHIMS via density bottle measurements. These data can be seen in Figure 6. The densities of all four magnetic concentrates produced from the Knelson concentrate are significantly larger than those of the magnetic concentrates produced from the Knelson tails or the untreated ore. The densities of all three magnetic tails have comparably low densities, reinforcing the hypothesis that the WHIMS has concentrated magnetic, high specific gravity minerals in all three feed streams.

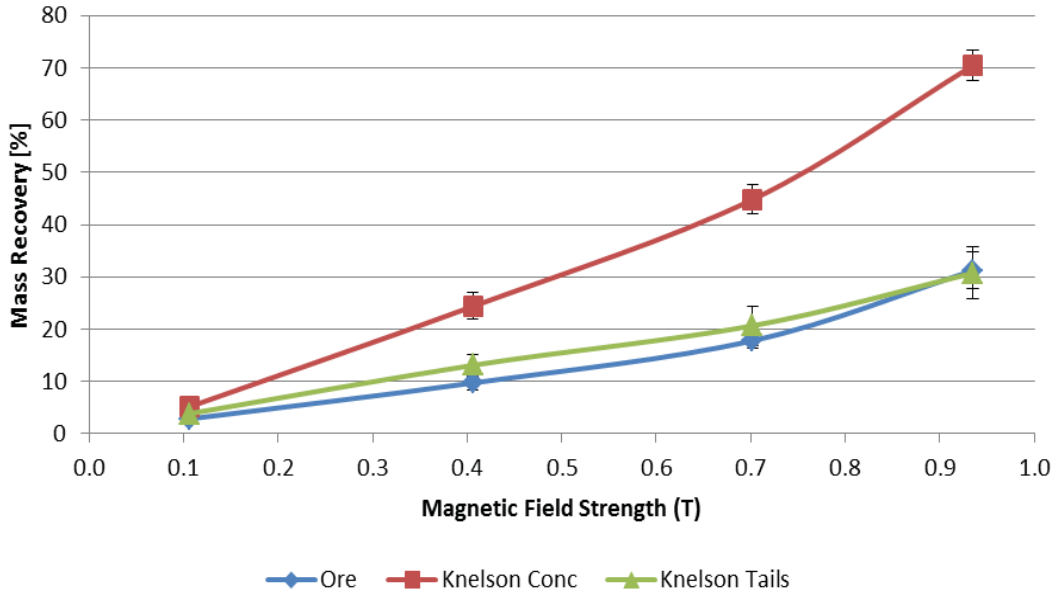

Figure 5 – Cumulative mass pull to the concentrate from WHIMS. Error bars indicate 95 % confidence intervals

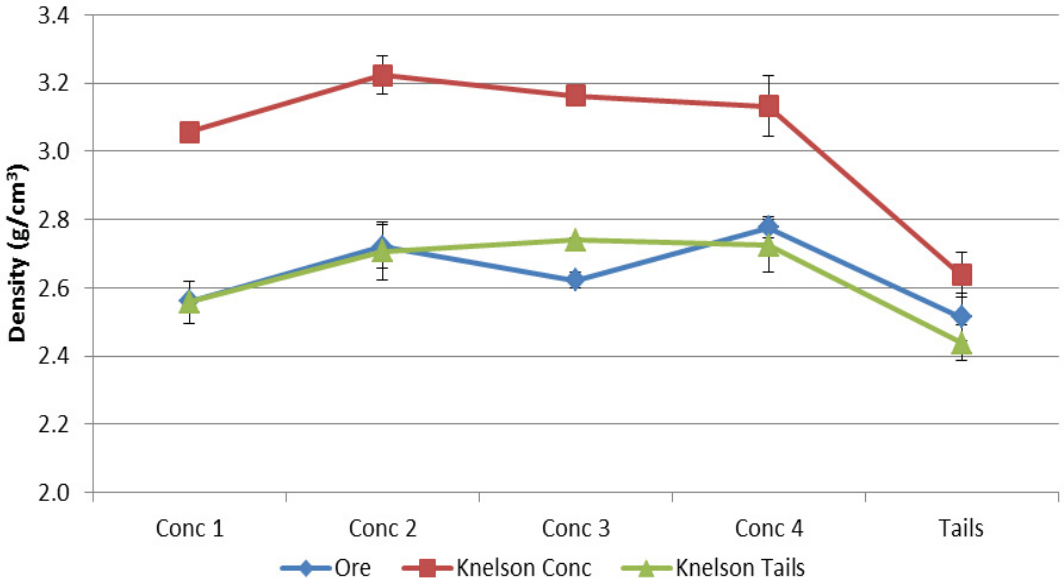

Figure 6 – Experimentally determined densities of the products of WHIMS. Error bars indicate 95 % confidence intervals

We also analysed the products from the WHIMS using a VSM to determine their magnetic characteristics. The results are shown in Figures 7–10 as plots of magnetisation as a function of applied magnetic field strength. The VSM data for the first three magnetic concentrates (Figures 7–9) display the expected trend of decreasing ferromagnetic tendency with increasing magnetic concentration field strength. The initial magnetic concentration step at 0.11 T would be expected to attract the most ferromagnetic material first with subsequent reprocessing of the tailings resulting in increased recovery of weakly paramagnetic material that is not concentrated at lower magnetic field strengths. This trend is not observed however in the fourth magnetic concentrate which is by far the most ferromagnetic for all three feed streams with saturation magnetisations that are almost an order of magnitude greater than those observed for the first three magnetic concentration steps (Figure 10). VSM measurements were also conducted on the magnetic tails from each stream however these results are not included as all three magnetic tails exhibited very small magnetisations (<0.2 kA/m) at all applied magnetic field strengths.

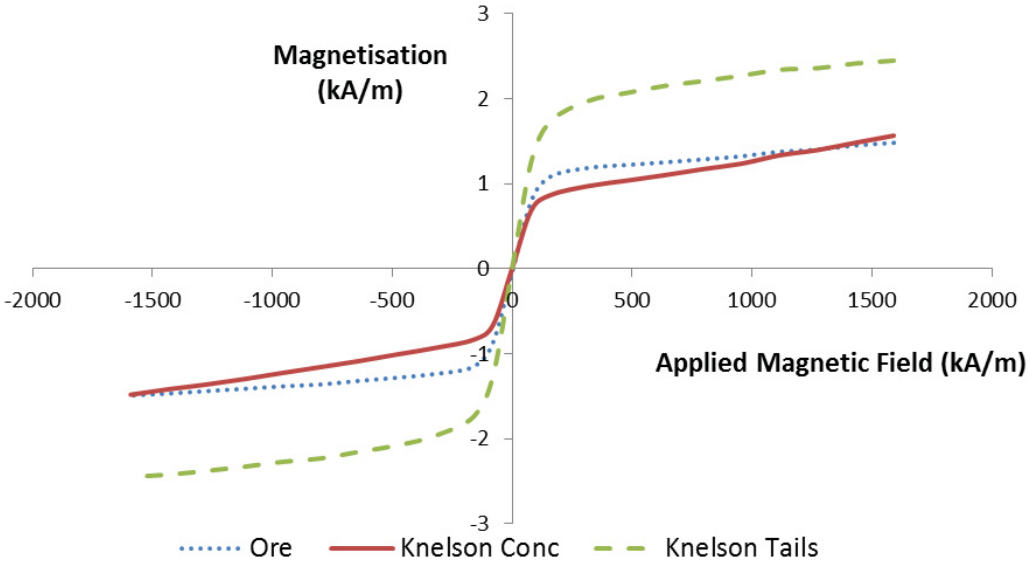

Figure 7 – Magnetisation behaviour (determined by VSM) of the first WHIMS concentrate (produced at 0.11 T) obtained from three different feeds

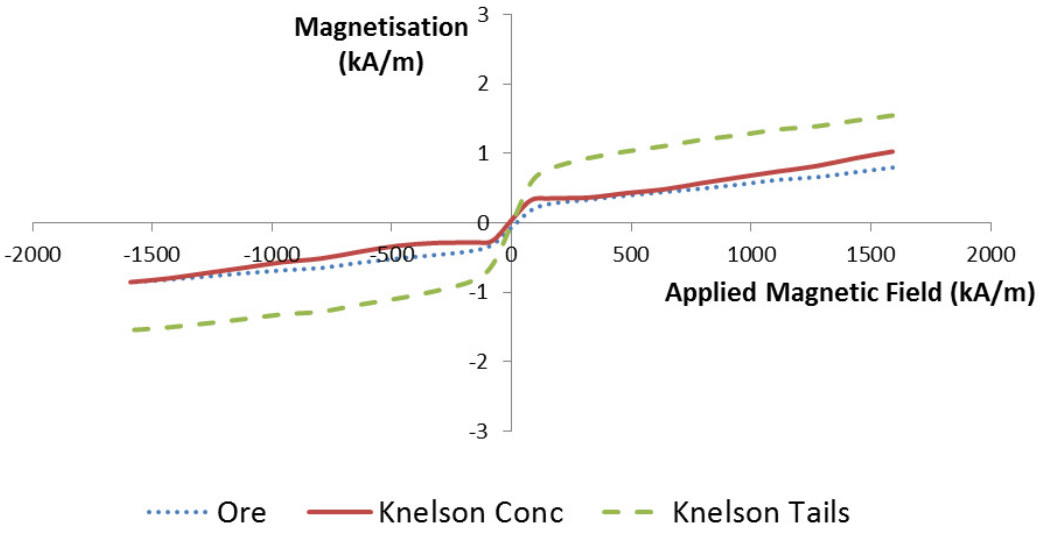

Figure 8 – Magnetisation behaviour (determined by VSM) of the second WHIMS concentrate (produced at 0.41 T) obtained from three different feeds

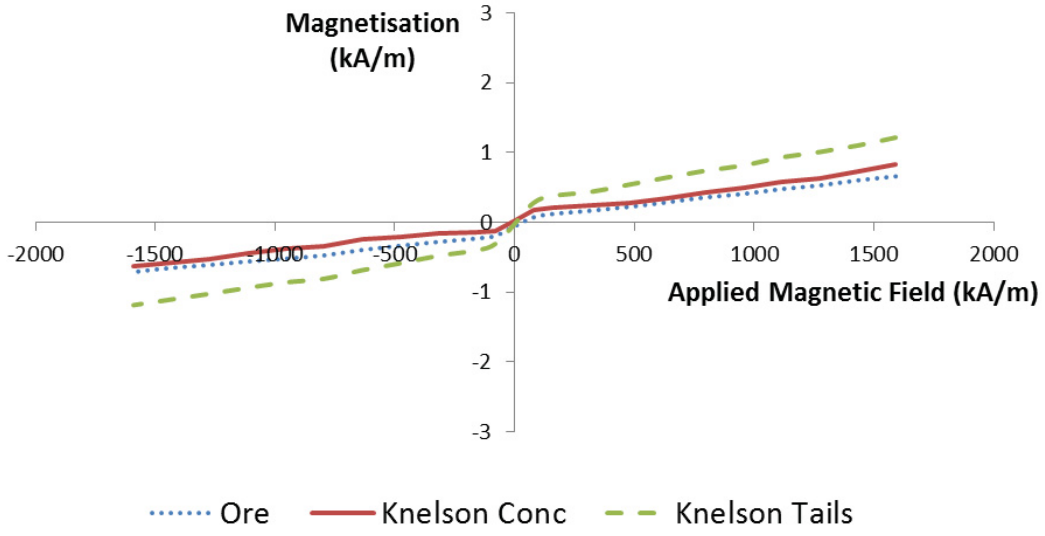

Figure 9 – Magnetisation behaviour (determined by VSM) of the third WHIMS concentrate (produced at 0.70 T) obtained from three different feeds

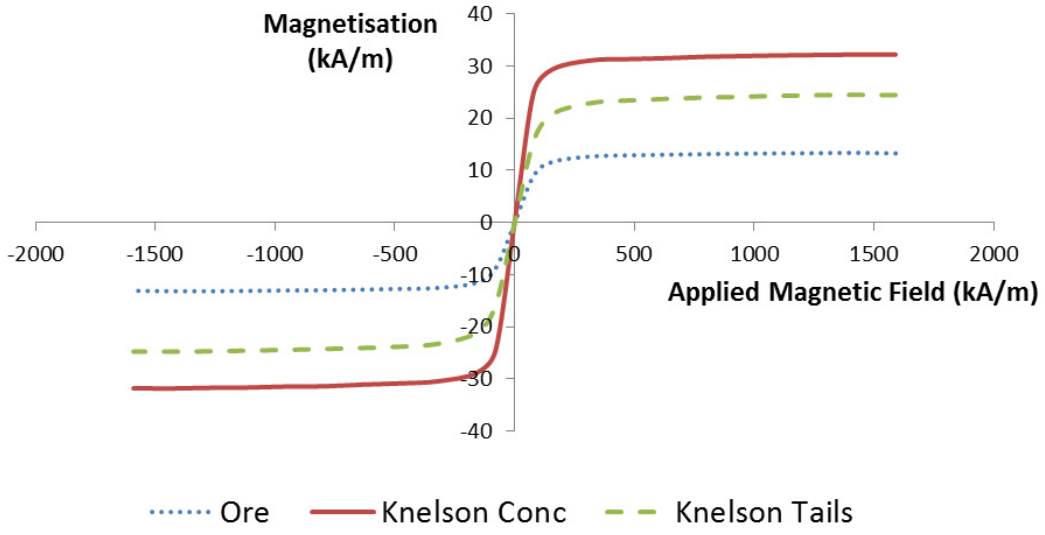

Figure 10 – Magnetisation behaviour (determined by VSM) of the fourth WHIMS concentrate (produced at 0.94 T) obtained from three different feeds

A proposed explanation for the unexpected behaviour of the fourth concentrate is that there is a particle size effect at work in the WHIMS steps so that relatively coarser particles are concentrated first, with the finest particles only concentrated once the magnetic field (and corresponding magnetic force) has increased to the point where it is able to overcome the hydrodynamic drag forces at work in the WHIMS. To confirm this, we analysed the particle size of all of the magnetic concentrates by wet screening at 25 µm. The results of this sizing step can be seen in Figure 11. The magnetic concentrates from the Knelson concentrate and Knelson tails do not exhibit a steady decrease in particle size therefore it is unlikely that this

unexpected VSM behaviour can be fully explained by a particle size effect. Another possible explanation for the VSM results may be that the most strongly ferromagnetic particles are not easily removed from the matrix material in the WHIMS by washing and are only released after the magnetic separator is disassembled and thoroughly washed to produce the final magnetic concentrate.

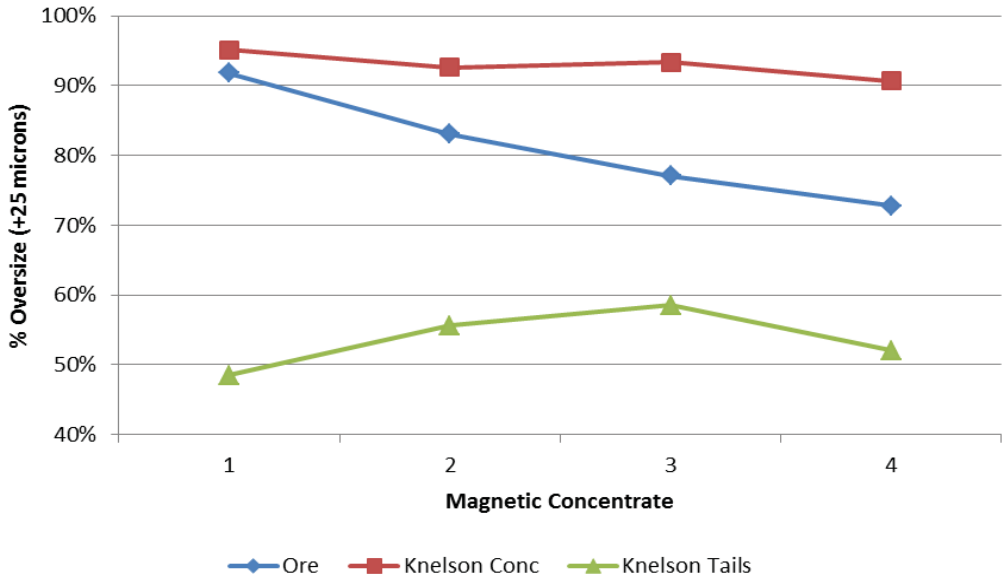

Figure 11 – Fraction of material retained on a 25 μm screen for the concentrates produced from WHIMS

Another unexpected result from the VSM analysis is that the magnetic concentrates produced from the Knelson tails exhibits a higher level of magnetisation than the Knelson concentrate for the first three magnetic concentrates (Figures 7–9). Looking only at the mass recovery results from the WHIMS the magnetic concentrates produced from the Knelson concentrate would be expected to display a higher degree of magnetisation to go along with the increased mass recovery observed in Figure 5. For the final magnetic concentrate the trend is as expected with the Knelson concentrate stream displaying the highest degree of magnetisation. Based on the VSM results it seems likely that multiple magnetic mineral phases (of varying magnetic characteristics) are present in this ore. Accurate interpretation of the trends of magnetisation as a function of applied magnetic field will only be possible once chemical assays have been completed to determine the mineralogical composition of each concentrate. Unfortunately, such information has not yet been obtained as the analysis of RE minerals in this ore is quite challenging.

CONCLUSIONS

Based on the results of this work it can be seen that a combination of centrifugal gravity pre-concentration combined with WHIMS was able to successfully concentrate heavy, magnetic minerals into the magnetic concentrate streams produced from the wet magnetic separator. Combining the mass recovery results with the experimentally measured densities of the various magnetic products suggests that the tailings of the magnetic separation step likely have elevated concentrations of low specific gravity gangue minerals such as feldspar, plagioclase or quartz (nominal specific gravities of 2.57–2.68). Similarly, it is appropriate to infer that the magnetic concentrates produced from the concentrate of a Knelson pre-concentration step contain increased amounts of ferromagnetic and paramagnetic minerals with high specific gravities such as bastnäsite, fergusonite, columbite, monazite and iron oxides (nominal specific gravities of 4.98–6.30). Without specific elemental and mineralogical composition information it is impossible to determine the efficacy of these separation steps at concentrating the desired RE minerals as opposed to unwanted iron oxides and other paramagnetic gangue minerals such as biotite and ankerite. The unexpected VSM results

(general trends indicating magnetic behavior as well as magnitudes of magnetisation) obtained in this work for the magnetic concentrates suggests that there is likely considerable variation in composition between the magnetic concentrates produced at various magnetic field strengths. It may be possible, with additional experiments, to suggest a specific magnetic field strength to target the optimal recovery of RE minerals while minimizing the recovery of paramagnetic gangue minerals.

Future work on this deposit will involve inductively coupled plasma mass spectrometry measurements to determine elemental composition of the different streams as well as QEMSCAN analysis on selected streams to determine mineralogical composition. Based on the small grain size of the deposit, additional gravity and magnetic separations may be carried out at finer particle sizes to attempt to take advantage of enhanced liberation.

ACKNOWLEDGMENTS

The authors would like to acknowledge the Natural Sciences and Engineering Research Council (NSERC) for funding a CGS M scholarship for A. Jordens as well as Avalon Rare Metals for supporting this work.

REFERENCES

Anthony, J. W., Bideaux, R. A., Bladh, K. W., & Nichols, M. C. (2001). Handbook of Mineralogy. Retrieved July 16, 2012, from Mineralogical Society of America http://www.handbookofmineralogy.org/

Chen, Z. (2011). Global rare earth resources and scenarios of future rare earth industry. *Journal of Rare Earths, 29*(1), 1–6.

Chi, R., Xu, S., Zhu, G., Xu, J., & Qiu, X. (2001, Feb. 11–15, 2001). *Beneficiation of rare earth ore in china.* Paper presented at the Light Metals 2001: Technical Sessions at the 130th TMS Annual Meeting, New Orleans.

Crow, J. M. (2011). 13 exotic elements we can't live without. *The New Scientist,* 36–41.

Falconer, A. (2003). Gravity Separation: Old Technique/New Methods. *Physical Separation in Science and Engineering, 12*(1), 31–48.

Foner, S. (1956). Vibrating Sample Magnetometer. *The Review of Scientific Instruments, 27*(7), 548.

Foner, S. (1959). Versatile and Sensitive Vibrating-Sample Magnetometer. *The Review of Scientific Instruments, 30*(7), 548–557.

Fullam, M., & Grewal, I. (2001). The Knelson Continuous Variable Discharge (CVD) Concentrator (pp. 1–6): The Knelson Group.

Holland-Batt, A. B., & Holtham, P. N. (1991). Particle and fluid motion on spiral separators. *Minerals Engineering, 4*(3–4), 457–482.

Jiles, D. (1990). *Introduction to Magnetism and Magnetic Materials*. London: Chapman & Hall.

Jordens, A., Cheng, Y. P., & Waters, K. E. (2013). A review of the beneficiation of rare earth element bearing minerals. *Minerals Engineering, 41*, 97–114.

Long, K. R., Van Gosen, B. S., Foley, N. K., & Cordier, D. (2010). The Principal Rare Earth Elements Deposits of the United States — A Summary of Domestic Deposits and a Global Perspective - U.S. Geological Survey Scientific Investigations Report 2010-5220 (pp. 1–104). Reston, VA, USA.

Male, S. E. (1984). Magnetic susceptibility and separation of inorganic material from UK coals. *Journal of Physics D: Applied Physics, 17*(1), 155.

Meyer, L., & Bras, B. (2011). *Rare earth metal recycling.* Paper presented at the 2011 IEEE International Symposium on Sustainable Systems and Technology (ISSST), Chicago, IL, USA.

Oberteuffer, J. (1974). Magnetic Separation: A review of principles, devices, and applications. *IEEE Transactions on Magnetic, 10*(2), 223–238.

Preinfalk, C., & Morteani, G. (1986). The Industrial Applications of Rare Earth Elements. In P. Moller, P. Cerny & F. Saupe (Eds.), *Lanthanides, Tantalum and Niobium: Mineralogy, Geochemistry, Characteristics of Primary Ore Deposits, Prospecting, Processing and Applications.* (pp. 359–370). Berlin, DE: Society for Geology Applied to Mineral Deposits.

Rosenblum, S., & Brownfield, I. K. (1999). Magnetic Susceptibilities of Minerals - Report for U.S. Geological Survey (pp. 1–33).

Svoboda, J., & Fujita, T. (2003). Recent developments in magnetic methods of material separation. *Minerals Engineering, 16*(9), 785–792.

Waters, K. E., Rowson, N. A., Greenwood, R. W., & Williams, A. J. (2007). Characterising the effect of microwave radiation on the magnetic properties of pyrite. *Separation and Purification Technology, 56*, 9–17.

Waters, K. E., Rowson, N. A., Greenwood, R. W., & Williams, A. J. (2008). The effect of heat treatment on the magnetic properties of pyrite. *Minerals Engineering, 21*, 679–682.

Zhang, J., & Edwards, C. (2013). Review of rare earth mineral processing technology. *CIM Journal 4*(1), 38–52.

Minerals Engineering 62 (2014) 9–18

Contents lists available at ScienceDirect

Minerals Engineering

journal homepage: www.elsevier.com/locate/mineng

Processing a rare earth mineral deposit using gravity and magnetic separation

Adam Jordens [a,*], Richard S. Sheridan [b], Neil A. Rowson [c], Kristian E. Waters [a]

[a] Department of Mining and Materials Engineering, McGill University, 3610 University Street, Montreal, Quebec H3A 0C5, Canada
[b] School of Metallurgy and Materials, University of Birmingham, Edgbaston, Birmingham B15 2TT, United Kingdom
[c] School of Chemical Engineering, University of Birmingham, Edgbaston, Birmingham B15 2TT, United Kingdom

ARTICLE INFO

Article history:
Available online 15 October 2013

Keywords:
Rare earth minerals
WHIMS
Knelson Concentrator
Falcon Concentrator
Vibrating sample magnetometer

ABSTRACT

Rare earth (RE) mineral deposits are typically processed using several different unit operations including flotation, gravity, magnetic and electrostatic separation techniques. Two of the most important beneficiation techniques for RE minerals are gravity and magnetic separation. Many RE minerals are found alongside low specific gravity gangue minerals thereby permitting the use of gravity separations to concentrate the heavy value RE minerals. Magnetic separation is used primarily to remove ferromagnetic gangue minerals as well as to separate individual paramagnetic rare earth minerals.

This work investigated the use of a wet high intensity magnetic separation (WHIMS) in conjunction with gravity pre-concentration steps (Knelson and Falcon centrifugal concentrators) to beneficiate a rare earth ore. The results of these separation steps are related to the magnetic properties of RE minerals, based on literature and measurements conducted using a vibrating sample magnetometer (VSM).

1. Introduction

1.1. Rare Earth minerals

Rare earth (RE) element bearing minerals are composed of at least one of the fifteen lanthanide elements or yttrium. Rare earth elements are used in a diverse range of applications including high strength magnets, phosphors, alloying elements, catalysts and polishing compounds (Crow, 2011; Meyer and Bras, 2011; Preinfalk and Morteani, 1986). There are many different RE minerals and these minerals can be found in many locations throughout the world; the bulk of currently operating RE mines are located in China.

Recently, the Chinese government has begun imposing strict export quotas on the RE industry thereby driving RE exploration and mine development in many other regions of the world (Chen, 2011). The three most common RE minerals mined are bastnäsite, monazite and xenotime, however the new deposits under development contain many new minerals with unknown characteristics. Most RE mineral deposits are beneficiated through a combination of unit operations such as gravity concentration, magnetic separation and froth flotation (Zhang and Edwards, 2012). Due to their relatively high specific gravities (between 4 and 7) gravity separation can be used to concentrate RE minerals by eliminating low specific gravity gangue minerals such as quartz (Ferron et al., 1991). In the context of RE mineral beneficiation, magnetic separation is typically used for two purposes: low intensity magnetic separation is used to remove ferromagnetic gangue minerals such as iron oxides and high intensity magnetic separation is used to separate monazite and xenotime from other heavy minerals (Gupta and Krishnamurthy, 1992).

For further information on rare earth physical beneficiation recent reviews by Zhang and Edwards (2012) and Jordens et al. (2013a) should be consulted.

1.2. Gravity separation

Gravity separation is used in mineral processing to separate minerals based on differences in specific gravity. The most common and successful type of gravity separator used for fine particle sizes is a centrifugal gravity concentrator (Falconer, 2003). These separators introduce a mineral slurry into a rapidly rotating bowl to generate centrifugal forces on the particles that are much higher than the force of gravity and therefore decrease the lower size limit for effective gravity separation (Falconer, 2003). The centrifugal forces on the particles trap high specific gravity material against the sides of the bowl to become the gravity concentrate while lower specific gravity material is carried along with the flowing fluid to report to the gravity tailings (Falconer, 2003). These concentrators are operated in a semi-continuous mode where the accumulated

* Corresponding author. Tel.: +01 5143984755X09503.
E-mail address: adam.jordens@mail.mcgill.ca (A. Jordens).

0892-6875/$ - see front matter © 2013 Elsevier Ltd. All rights reserved.
http://dx.doi.org/10.1016/j.mineng.2013.09.011

concentrate is periodically removed by washing (Fullam and Grewal, 2001).

One of the most common centrifugal separators is the Knelson Concentrator, which employs an inclined bowl lined with collecting ridges where the heavy (specific gravity >4) value mineral is collected (Ferron et al., 1991; Fullam and Grewal, 2001). These ridges contain perforations through which water is pumped in order to fluidize the material collecting in the ridges and allow for the exchange of low specific gravity material (which may have initially reported to the concentrate) with high specific gravity material (Fullam and Grewal, 2001; Knelson, 1992). The Knelson Concentrator works very well for applications where the desired high specific gravity mineral is present in very low concentrations (ppm) but runs into operational difficulties processing ores with higher contents (typically >1%) of high specific gravity material as the concentrate accumulates very rapidly (Fullam and Grewal, 2001). If the accumulated gravity concentrate is not flushed promptly the selectivity of the separation will suffer significantly (Fullam and Grewal, 2001; Knelson, 1992). An additional limitation to the Knelson Concentrator is that the efficiency of the concentration step decreases with feed fineness (Laplante, 1993). Laplante (1993) suggested that for the specific case of gold particles, the poor performance of the Knelson Concentrator in treating fine feeds (<75 μm) is more likely attributable to the shape of the fine gold particles rather than their size.

The Falcon Ultra-Fine (UF) Concentrator is designed specifically to process very fine particle sizes. It lacks the fluidizing water used in other centrifugal concentrators; instead relying on the geometry of the bowl walls to retain the high specific gravity material (Lins et al., 1992). This design changes the mechanism of high specific gravity particle collection as there is no opportunity for particle exchange once a particle has been deposited on the wall of the spinning bowl (Kroll-Rabotin et al., 2011). Laplante et al. (1994) showed that there are three steps in a Falcon Concentrator separation: initial unselective deposition of material on the concentrate bed along the bowl wall, selective concentration until the concentrate bed is saturated, and finally minimal recovery as the concentrate bed is unable to accept additional particles. It can be seen from these three phases of material recovery that it is crucial to ensure that the concentrator is stopped at suitable time intervals to maximize the separator's efficiency by not operating with a fully-loaded bowl.

1.3. Magnetic separation

Magnetic separation of minerals is based on different behaviours of mineral particles when in an applied magnetic field. Unpaired electrons present in certain types of atoms cause magnetic dipoles which lead to the creation of magnetic moments in a material that can in turn result in a magnetic force on the material when these moments are aligned by an externally applied magnetic field. In mineral processing terminology there are three distinct behaviours that a mineral particle may exhibit: Ferromagnetic and paramagnetic mineral particles will both be attracted along the lines of an applied magnetic field whereas a diamagnetic mineral particle will be repelled along the magnetic field lines. The main difference in ferromagnetic and paramagnetic minerals is that a ferromagnetic material is able to much more rapidly align its magnetic moments so that the magnetisation (and consequently the magnetic force felt by the particles) is much higher at lower applied magnetic field strengths. An excellent introduction to magnetism in materials and other associated concepts can be found in the work of Jiles (1990).

The magnetic recovery in a magnetic separator is dependent on the applied magnetic field strength, the magnetic field gradient and the magnetic susceptibility of the mineral particles and accompanying fluid medium as can be seen in the following equation (Oberteuffer, 1974):

$$F_x = V(\chi_p - \chi_m)H\frac{dB}{dx} \quad (1)$$

In this equation F_x is the magnetic force felt by a particle (N), V is the particle volume (m^3), χ_p is the dimensionless volume magnetic susceptibility of the particle, χ_m is the volume magnetic susceptibility of the fluid medium, H is the applied magnetic field strength (A/m) and dB/dx is the magnetic field gradient ($T/m = N/Am^2$) (Oberteuffer, 1974; Svoboda and Fujita, 2003). The magnetic force on a particle in a magnetic separator may be controlled by varying the magnetic susceptibility of the particle/medium, the applied magnetic field or the magnetic field gradient.

The size range at which magnetic separation is effective depends on which of the three main forces on a particle (gravitational, magnetic and fluid drag) is dominant at a particular size (Oberteuffer, 1974). The fluid drag forces on a particle are proportional to the radius, r, while the magnetic force on a particle is proportional to r^2 (Oberteuffer, 1974). Similarly the force due to gravity can be shown to scale with r^3 so that for particles of very small radius the fluid drag forces are dominant while for a much larger particle radius gravitational forces are the most significant forces on a particle (Oberteuffer, 1974). The particle radius at which magnetic separation may be effective has been determined to be approximately 5 μm up to 1 mm (Oberteuffer, 1974) however the recovery of increasingly fine magnetic material (down to even nano-scale particles) is an area of active research (Chen et al., 2012; Ebner et al., 1997; Menzel et al., 2012; Roy, 2011).

1.4. Measuring the magnetic properties of materials

As stated in Section 1.3 all minerals may be classified (for simplicity) into three categories of magnetic behaviour. The specific behaviour of a single mineral may be analysed by looking at the magnetisation of the material as a function of applied magnetic field. One method of obtaining this information is by using a vibrating sample magnetometer (VSM) which suspends a small quantity of mineral from an oscillating rod (Foner, 1959). The material is then subjected to a series of uniform magnetic fields of varying strength and the changes in magnetisation within the material are measured by a series of detection coils (Foner, 1956). The direct measurement output of the VSM is the magnetic moment of the sample, which is converted to magnetisation by dividing by the volume of the sample.

An example of typical diamagnetic, paramagnetic and ferromagnetic behaviour may be seen in Fig. 1. A diamagnetic material, due to its unaligned magnetic dipoles, will be repelled along the lines of an applied magnetic field and as such it will exhibit a slightly negative linear variation of magnetisation with increasing applied magnetic field as shown in Fig. 1 (Jiles, 1990; Waters et al., 2007). On the same graph a paramagnetic material will show a positive linear increase in magnetisation as higher applied magnetic field strengths will cause more of the magnetic dipoles

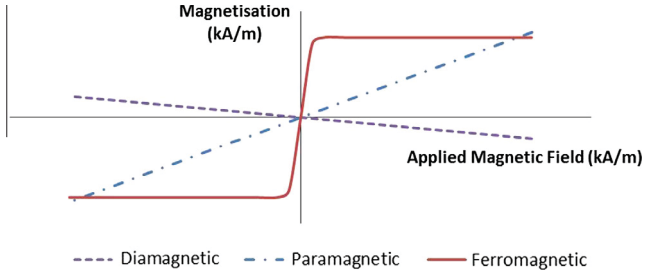

Fig. 1. Typical VSM results for diamagnetic, paramagnetic and ferromagnetic material.

present in the material to align (Waters et al., 2007). A ferromagnetic material will rapidly increase in magnetisation at relatively low applied magnetic field strengths until it reaches its saturation magnetisation at which point increased applied magnetic field strength will have a minimal effect on magnetisation (see Fig. 1) (Waters et al., 2007). The explanation for this rapid increase is that magnetic dipoles in a ferromagnetic material are able to interact with one another to form magnetic domains which then allow for rapid alignment of the magnetic dipoles at relatively low magnetic field strengths (Jiles, 1990). The plateau in magnetisation that occurs at a ferromagnetic material's saturation magnetisation is due to the fact that once all the magnetic domains in a material are aligned there is a very limited ability for any further dipole alignment to occur (Jiles, 1990). The saturation magnetisation is characteristic of a given ferromagnetic material and may be used to determine the ferromagnetic fraction of a binary mixture of para- and ferromagnetic materials (Waters et al., 2007).

In the case of a binary mixture of a paramagnetic and a ferromagnetic material the trend of magnetisation as a function of applied magnetic field strength will be a combination of both materials (as shown in Fig. 2) (Waters et al., 2007). If the slope (or susceptibility) of the linearly sloped portion of the binary mixture trend is extracted and plotted as a function of the inverse applied magnetic field (Fig. 3) it is possible to identify the paramagnetic material's volume susceptibility from the intercept of this graph (Waters et al., 2007; Yang et al., 2009). The slope of the graph in Fig. 3 is then equivalent to the fraction of the mixture taken up by the ferromagnetic material multiplied by the saturation magnetisation of the given ferromagnetic material (Waters et al., 2007; Yang et al., 2009). This technique may allow the estimation of the concentration of the ferromagnetic component in a binary mixture (Male, 1980) or it may allow the determination of the susceptibility of the paramagnetic component, by removing the effects of any ferromagnetic impurities (Yang et al., 2009).

This paper investigates the magnetic properties of several different RE minerals and their associated gangue minerals through the use of a VSM. These magnetic properties are then exploited using a series of wet high intensity magnetic separation (WHIMS) steps in conjunction with gravity pre-concentration steps to concentrate the valuable RE minerals from a Canadian RE deposit.

2. Methods

2.1. Raw material

The raw material used in this work originated from the Nechalacho deposit (Avalon Rare Metals, Inc.) located in the Northwest Territories, Canada. The ore was initially crushed to a top size of 850 μm using a jaw and cone crusher. The composition of the Nechalacho deposit can be seen in Table 1 with the important RE minerals highlighted. This deposit has 88.5 million tonnes of inferred resources at a grade of 1.53% total rare earth oxide (TREO) (Cox et al., 2011). The most important RE mineral in this deposit is zircon as it has been reported to host over 65% of all rare earth elements (REE) in the deposit (Cox et al., 2011). The major gangue minerals are quartz, K-feldspar, plagioclase, biotite and iron oxides.

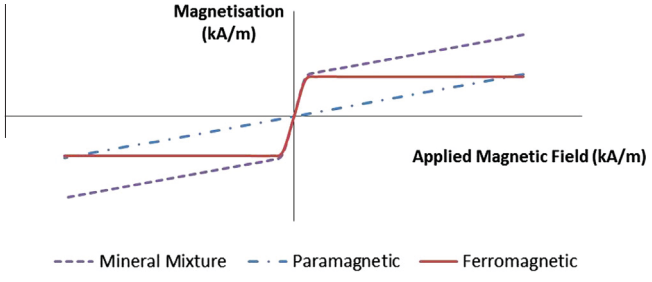

Fig. 2. VSM results for a binary mixture of paramagnetic and ferromagnetic mineral along with the extracted individual paramagnetic and ferromagnetic trends (from Honda–Owen plot).

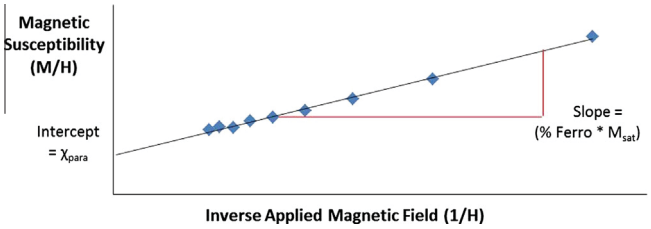

Fig. 3. Honda–Owen plot to determine paramagnetic and ferromagnetic of a binary mixture.

After crushing, a portion of the ore was stage pulverized in a ring mill to 80% passing 53 μm to be fed to the Knelson Concentrator and a second portion of the ore was ground dry for 15 min in a rod mill before being stage pulverized to 80% passing 44 μm and fed to the Falcon Concentrator. The different comminution steps were chosen to maximize mineral liberation without compromising gravity concentrator effectiveness, while also avoiding the overproduction of excessively fine (<5 μm) material.

Pure mineral samples examined in this work were obtained from Gregory, Bottley and Lloyd (UK) and identified using X-ray diffraction.

2.2. Vibrating sample magnetometer

The vibrating sample magnetometer measurements (VSM) were conducted using a LakeShore 7300 series VSM. All mineral samples, with the exception of two zircon crystals which were analysed intact, were pulverized in a T100 ring and disc pulveriser (Siebtechnik) prior to VSM measurements. To conduct the measurements 50–100 mg of powdered sample was placed into the cylindrical VSM sample holder (for the case of zircon, a single crystal was suspended from the sample holder) and attached to the end of an oscillating rod. The sample is positioned such that it sits in the middle of 4 pick-up coils and a hall probe. The rod is then oscillated about this central point as a magnetic field is applied to the sample to create a full hysteresis loop between +2 T and −2 T with measurements taken every 0.1 T. Measurements were also con-

Table 1
Mineralogical composition of the Nechalacho deposit along with specific gravity and magnetic property data (Anthony et al., 2001; Long et al., 2010; Rosenblum and Brownfield, 1999).

Mineral	Weight%	Nominal S.G.	Magnetic properties
Quartz	35.1	2.63	Diamagnetic
K-feldspar	20.5	2.57	Diamagnetic
Plagioclase	10.5	2.68	Diamagnetic
Biotite	9.6	3.10	Paramagnetic
Fe-Oxides	8.3	5.30	Ferromagnetic
Zircon	4.1	4.65	Diamagnetic
Ankerite	3.7	3.05	Paramagnetic
Calcite	1.9	2.71	Diamagnetic
Dolomite	1.8	2.85	Diamagnetic
Bastnasite	1.3	4.98	Paramagnetic
Columbite (Fe)	0.5	6.30	Paramagnetic
Fluorite	0.3	3.18	Diamagnetic
Fergusonite	0.3	5.05	Paramagnetic
Monazite	0.2	5.15	Paramagnetic
Apatite	0.2	3.18	Diamagnetic
Synchysite	0.2	4.03	N/A
Allanite	0.1	3.75	Paramagnetic

ducted on the empty sample holder so that any magnetic contribution of the sample holder may be subtracted from the sample data. The measured magnetic moment data (as a function of magnetic field) was converted into magnetisation by dividing by the sample volume. The magnetic induction values were converted into magnetic field strength by dividing by the constant of permeability of free space, $4\pi \times 10^{-7}$ Vs/Am.

Samples of fergusonite, bastnäsite, allanite and two different types of zircon were analysed in the VSM to experimentally determine the magnetic behaviour of these minerals prior to any attempts to concentrate the RE minerals present in the Nechalacho deposit. In addition, samples of several of the gangue minerals (including quartz, hematite and magnetite) found in the Nechalacho deposit were also examined.

2.3. Knelson Concentrator

The Knelson separator used in this work was a KC MD3 model (FLSmidth Knelson, Canada) operated at a material flow rate of 300–400 g/min. The slurrying water flow rate varied from 2.3 to 2.9 L/min, the fluidizing water flow rate varied from 6 to 9 L/min and the operating water pressure was 2.5–3 psi. During the operation the Knelson Concentrator was stopped every 4 min to remove the accumulated concentrate.

2.4. Falcon Concentrator

The Falcon Concentrator used in this work was a SB-6A model (Sepro Mineral Systems, Canada). The bowl used in the Falcon Concentrator was the ultra-fine bowl, designed especially for concentrating high specific gravity fines, which is smooth-walled and has no fluidizing water. The slurrying water flow rate was 4.7 L/min and the mass flow rate was approximately 400 g/min. During operation, the Falcon Concentrator was stopped every 4 min to remove the accumulated concentrate.

2.5. Wet high intensity magnetic separation (WHIMS)

Wet magnetic separation was carried out in this work using a wet high intensity magnetic separator (BoxMag, UK). Slurried material was passed through a ferromagnetic matrix to provide as many points of high magnetic field gradient as possible. The separator also allows for the variation of applied magnetic field strength by varying the current supplied to the separator. In order to control the magnetic separator by varying the applied current, a gauss meter was used to generate a calibration curve.

For each test approximately 50 g of material was slurried with water to achieve 17 wt.% solids. This slurry was then washed through the magnetic separator with a minimum of 250 mL of additional water to minimize the build-up of any magnetic material at the entrance to the magnetic separator that could lead to the entrainment of non-magnetic particles in the magnetic concentrate. After each separation step the ferromagnetic matrix was completely removed from the magnetic separator and thoroughly washed to fully remove all magnetic particles. The tailings of each separation step were reprocessed at increasing magnetic field strengths (0.10 T, 0.41 T, 0.70 T and 0.94 T).

Five different feed materials were used as feeds for wet magnetic separation: the untreated ore, the Knelson concentrate and tailings and the Falcon concentrate and tailings. A basic flowsheet of the different processing routes for the ore prior to WHIMS can be seen in Fig. 4.

2.6. X-ray Diffraction (XRD)

X-ray Diffraction analysis was conducted using a Bruker D8 Discovery X-ray Diffractometer equipped with a copper X-ray generating source. The resultant diffraction patterns were processed using Xpert High Score software (PANalytical) to identify peaks and relate them to selected mineral phases present in the Nechalacho ore.

3. Results and discussion

3.1. VSM measurements

The magnetisation as a function of magnetic field strength for the gangue minerals (magnetite, hematite and quartz) can be seen in Fig. 5. As expected, magnetite (Fe_3O_4) exhibits a clear ferromagnetic tendency with a large saturation magnetisation value while hematite exhibits a slight ferromagnetic tendency with a much smaller saturation magnetisation. While magnetite is in fact ferrimagnetic (with magnetic moments of unequal magnitude aligned in an antiparallel orientation such that the material experiences a net magnetic moment) its magnetic response in the VSM can, for our purposes, be considered to be identical to that of a ferromagnetic material (Jakubovics, 1994). Two different samples of quartz were analysed with both exhibiting an unexpected ferromagnetic behaviour. This is likely due to the presence of ferromagnetic impurities originating from the quartz crystals or introduced during pulverising. In order to remove the effect of the ferromagnetic impurity on the silica 2 trend the silica data was analysed using a Honda–Owen plot. In order for this analysis to be valid the silica must be assumed to be present in a binary mixture with the ferromagnetic impurity. The resultant diamagnetic and ferromagnetic trends can be seen in Fig. 6. The resolved diamagnetic susceptibility of the silica sample is -7.25×10^{-6}, which is within the expected range for a diamagnetic material (Jiles, 1990).

The VSM results for bastnäsite and fergusonite can be seen in Fig. 7. Both of these minerals are reported in literature to be paramagnetic and it can be seen that the general trend for both minerals also is a linear, paramagnetic, trend. The fergusonite sample is not completely pure and as such the trend seems to indicate that there may be a competing diamagnetic mineral present as well in the sample that was analysed. No prior work has reported the susceptibilities of these two minerals however there is reported empirical evidence to suggest that fergusonite is more strongly paramagnetic than bastnäsite (Rosenblum and Brownfield, 1999).

The VSM results for two different zircon samples, from two different localities, can also be seen in Fig. 7. The zircons, similar to the silica samples, exhibit a slight ferromagnetic trend. If one were to assume a binary mixture of ferromagnetic impurity and zircon mineral we can then determine the zircon's magnetic susceptibility from a Honda–Owen plot. The results of this analysis can be seen in Figs. 8 and 9. The zircon crystals from Brazil and Sri Lanka, after removing the ferromagnetic aspect from each VSM trend, exhibit magnetic susceptibilities of 2.50×10^{-6} and 2.77×10^{-6} respectively. This indicates that both zircons are slightly paramagnetic. This is in disagreement with the generally reported data on the magnetic behaviour of zircon (Moustafa and Abdelfattah, 2010; Rosenblum and Brownfield, 1999) although zircon may also have different magnetic properties dependent on its composition (Raslan, 2009).

As the zircons analysed were single crystals there was no possibility of a ferromagnetic impurity being introduced during pulverising or any other sample preparation. Therefore the ferromagnetic and paramagnetic tendencies measured must be due to the presence of magnetic elements within the crystal lattices of the two

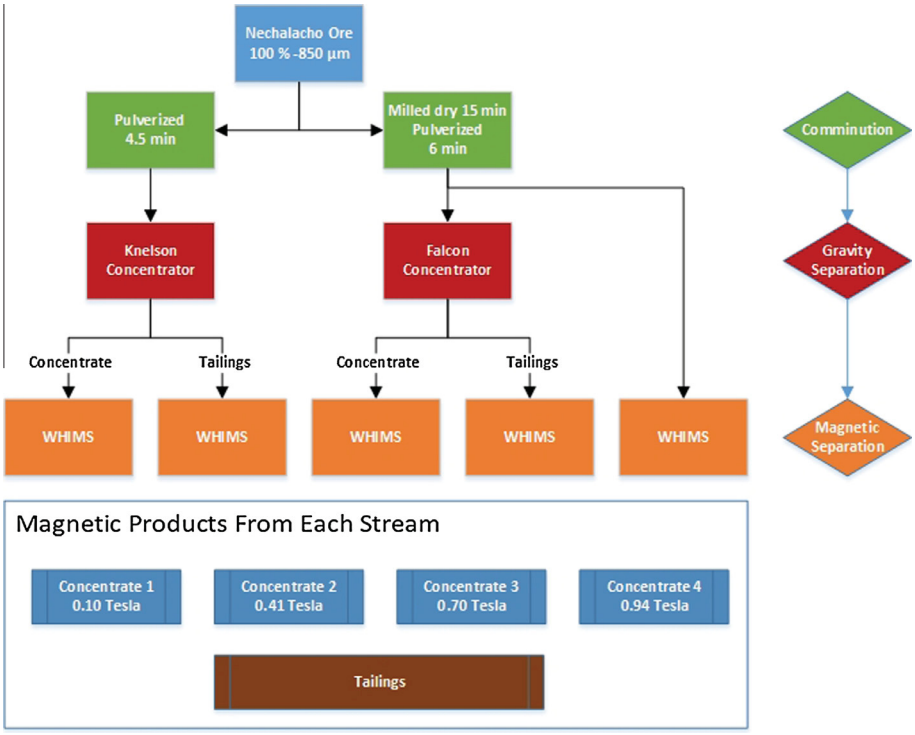

Fig. 4. Flow sheet of WHIMS experiments with and without gravity pre-concentration.

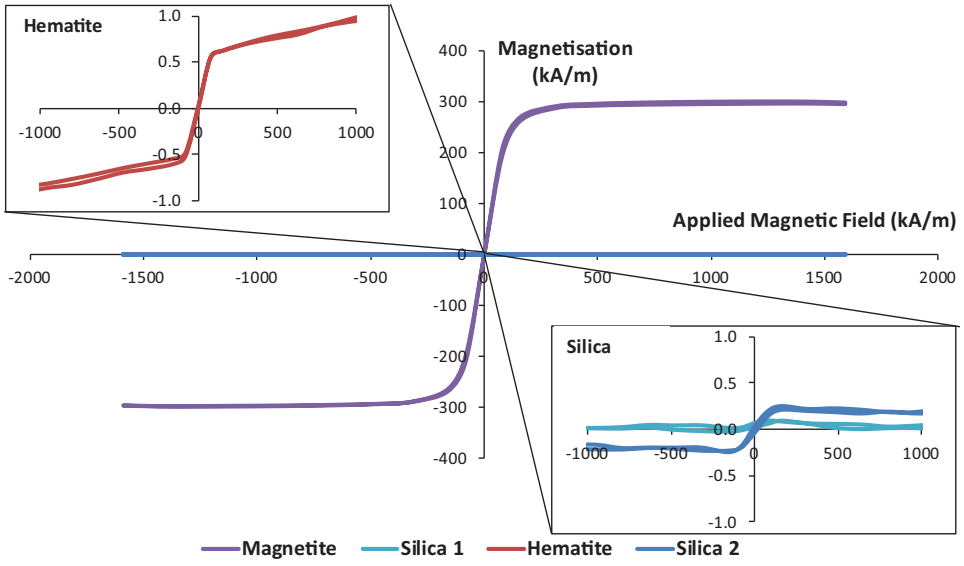

Fig. 5. VSM results for magnetite, hematite and quartz.

zircon minerals. Given the significant concentration of rare earth elements within the crystal structure of zircon from the Nechalacho deposit it seems likely that the magnetic behaviour of the RE-bearing zircon would also be non-diamagnetic as many of the RE elements have significant paramagnetic properties due to their unpaired electrons (Ito et al., 1991).

The VSM results for allanite appear to indicate both ferromagnetic behaviour and paramagnetic behaviour (as can be seen in Fig. 10) therefore a Honda–Owen analysis was conducted on the allanite data. The resolved ferromagnetic and paramagnetic components of the allanite trend are also shown in Fig. 10. As allanite has been reported to be paramagnetic, the underlying assumption in the Honda–Owen analysis is that there is a ferromagnetic impurity present along with allanite (Rosenblum and Brownfield, 1999). The calculated magnetic susceptibility of the paramagnetic component (5.15×10^{-4}) corresponds to published data, which indicate that allanite is more strongly paramagnetic than bastnäsite and has a similar magnetic susceptibility to fergusonite (Rosenblum and Brownfield, 1999). A summary of all VSM findings may be seen in Table 2.

3.2. WHIMS results

The Nechalacho ore was processed using a combination of WHIMS and gravity pre-concentration using either a Knelson (80% – 53 µm feed) or a Falcon (80% – 44 µm feed) Concentrator

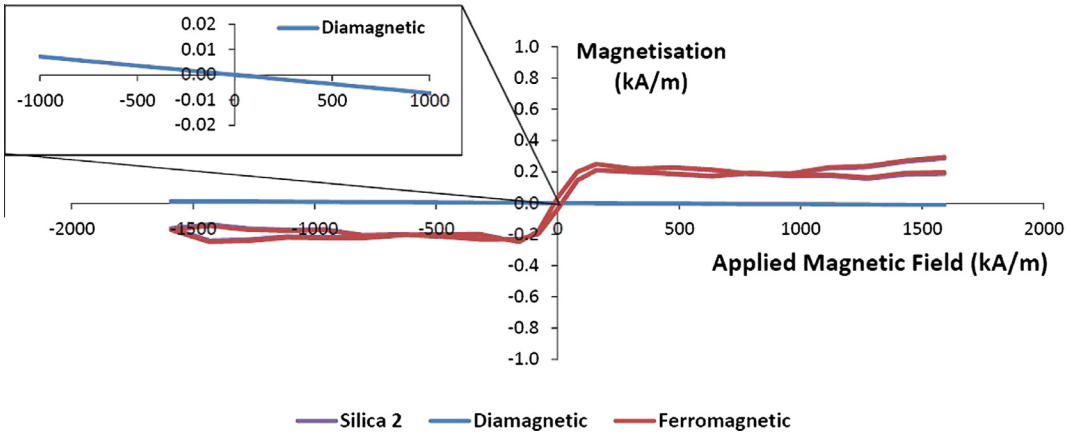

Fig. 6. VSM results for silica including diamagnetic and ferromagnetic trends calculated via Honda–Owen analysis.

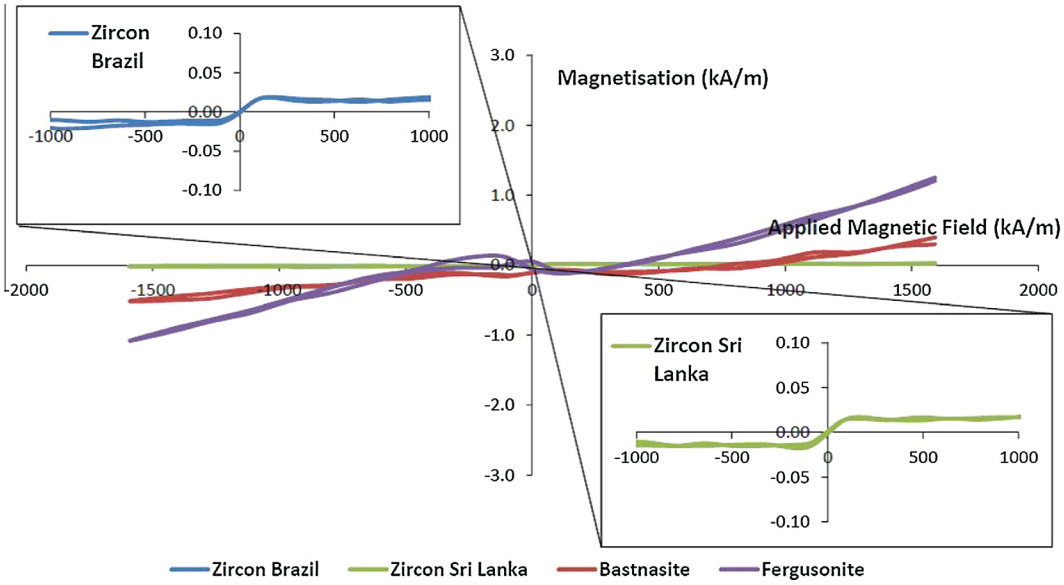

Fig. 7. VSM results for zircon, bastnäsite and fergusonite.

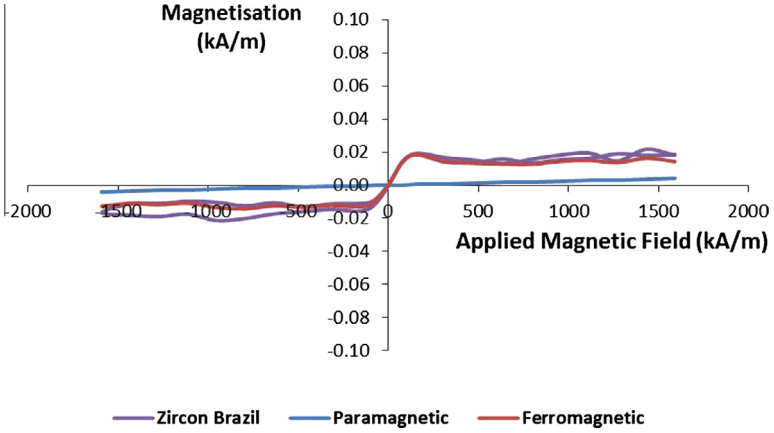

Fig. 8. VSM results for zircon (Brazil) including paramagnetic and ferromagnetic trends calculated via Honda–Owen analysis.

to exploit the differences in specific gravity and magnetic properties of the different minerals in order to achieve separation. Gravity pre-concentration steps were designed to eliminate low specific gravity gangue minerals and magnetic separation steps were conducted at varying magnetic field strengths to either remove unwanted ferromagnetic gangue minerals or concentrate valuable paramagnetic RE minerals.

The mass recovery to the Knelson concentrate was 4.5% whereas the Falcon recovered 7.3% of the mass. The Knelson concentrate and tailings were each processed through a series of

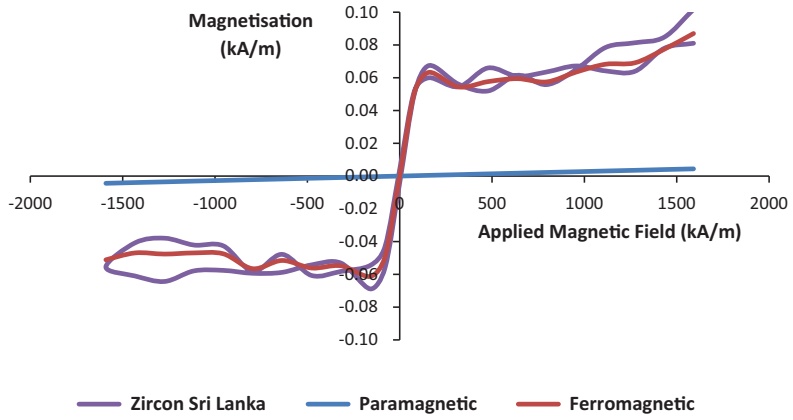

Fig. 9. VSM results for zircon (Sri Lanka) including paramagnetic and ferromagnetic trends calculated via Honda–Owen analysis.

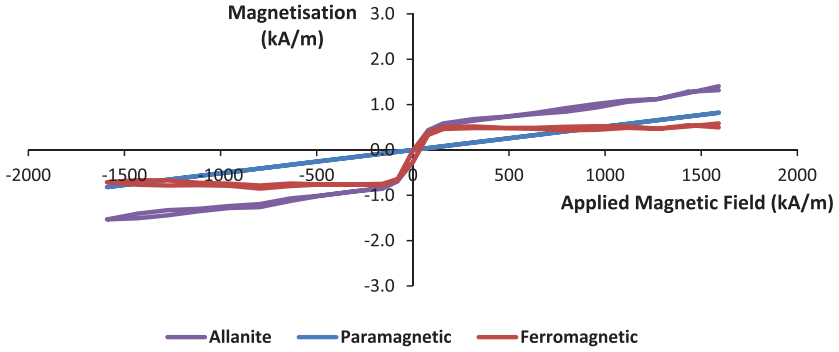

Fig. 10. VSM results for allanite including paramagnetic and ferromagnetic trends calculated via Honda–Owen analysis.

Table 2
Summary of VSM results.

Mineral	Magnetic properties	Magnetic susceptibility	Saturation magnetisation (kA/m)
Magnetite	Ferrimagnetic		291
Hematite[a]	Para/ Ferromagnetic	4.06×10^{-4}	5.60×10^{-1}
Silica	Diamagnetic	-7.25×10^{-6}	
Bastnäsite	Paramagnetic	2.12×10^{-4}	
Allanite	Paramagnetic	4.63×10^{-4}	
Fergusonite	Paramagnetic	6.01×10^{-4}	
Zircon (Brazil)	Paramagnetic	2.50×10^{-6}	
Zircon (Sri Lanka)	Paramagnetic	2.77×10^{-6}	

[a] Note that hematite may have both paramagnetic and ferromagnetic behaviour (Lin, 1959). Values shown for hematite were calculated from a Honda–Owen plot for this mineral.

WHIMS steps with the resultant cumulative mass recoveries to the magnetic fraction shown in Fig. 11. Other work has shown that the WHIMS mass recoveries of the Knelson tailings and Knelson feed are essentially identical (Jordens et al., 2013b). The increased mass recovery to the Knelson concentrate appears to indicate that the combination of gravity pre-concentration and magnetic separation has been able to successfully recover magnetic, high specific gravity minerals into the WHIMS concentrates produced from the Knelson concentrate.

The Falcon feed, concentrate and tailings were all fed through the same series of WHIMS steps with the resultant cumulative magnetic recovery shown in Fig. 12. Unlike with the Knelson Concentrator the Falcon concentrate displays a diminished magnetic recovery relative to the Falcon tailings and Falcon feed. This diminished magnetic recovery for the Falcon concentrate suggests that either the Falcon Concentrator was ineffective at concentrating the higher specific gravity minerals in the ore or the finer sized feed to the Falcon translated into increased liberation of zircon (which lacked sufficient magnetic susceptibility to report to the concentrates of WHIMS).

A selection of the XRD patterns from the gravity and magnetic separations can be seen in Figs. 13 and 14 along with highlighted peaks corresponding to different minerals present in the Nechalacho ore. A key difficulty in XRD analysis of this ore is that the major gangue mineral, quartz, has its most intense diffraction peak immediately adjacent to the most intense peak for the major RE value mineral, zircon. This results in serious difficulties when attempting to discern any differences in zircon concentrations. Nevertheless Fig. 13 does appear to indicate an enhanced zircon concentration (identified using a secondary peak of the standard zircon pattern) in the 0.10 T magnetic concentrate produced from the Falcon concentrate. This would seem to suggest that the zircon in the Nechalacho ore possesses a high degree of para/ferromagnetism or is often found locked with some other highly magnetic phase such as magnetite. Fig. 13 also shows that K-feldspar (microcline) and plagioclase (albite) gangue minerals were rejected into the tailings of the Falcon gravity concentration step and then subsequently rejected into the WHIMS tailings produced from the Falcon gravity tailings. Magnetite and hematite are both heavily indicated in the 0.10 T magnetic concentrate produced from the Falcon concentrate, which is as expected as the ferromagnetic iron oxides should be preferentially recovered initially at the lowest applied magnetic field strengths. The large peak shown in Fig. 13 for the 0.94 T magnetic concentrate produced from the Falcon concen-

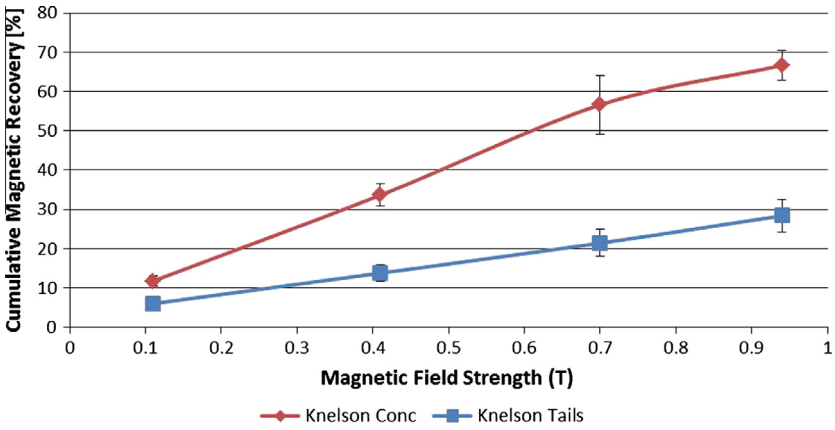

Fig. 11. Mass recovery from WHIMS with Knelson concentrate and tailings as feed materials to magnetic separation. Error bars represent 95% confidence intervals.

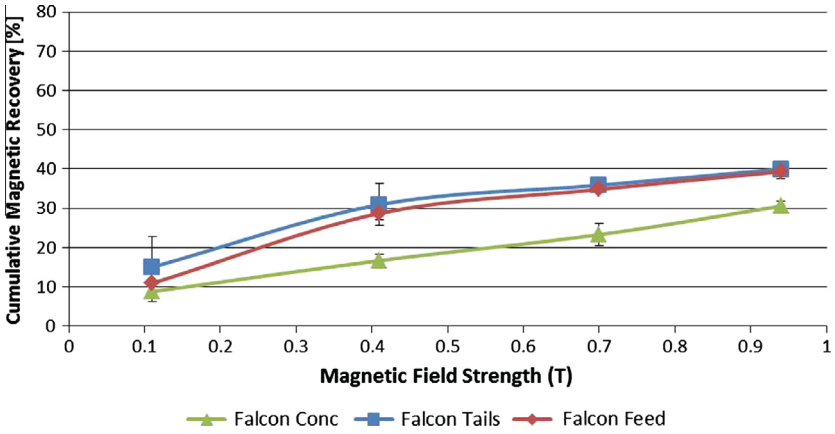

Fig. 12. Mass recovery from WHIMS with Falcon feed, concentrate and tailings as feed materials to magnetic separation. Error bars represent 95% confidence intervals.

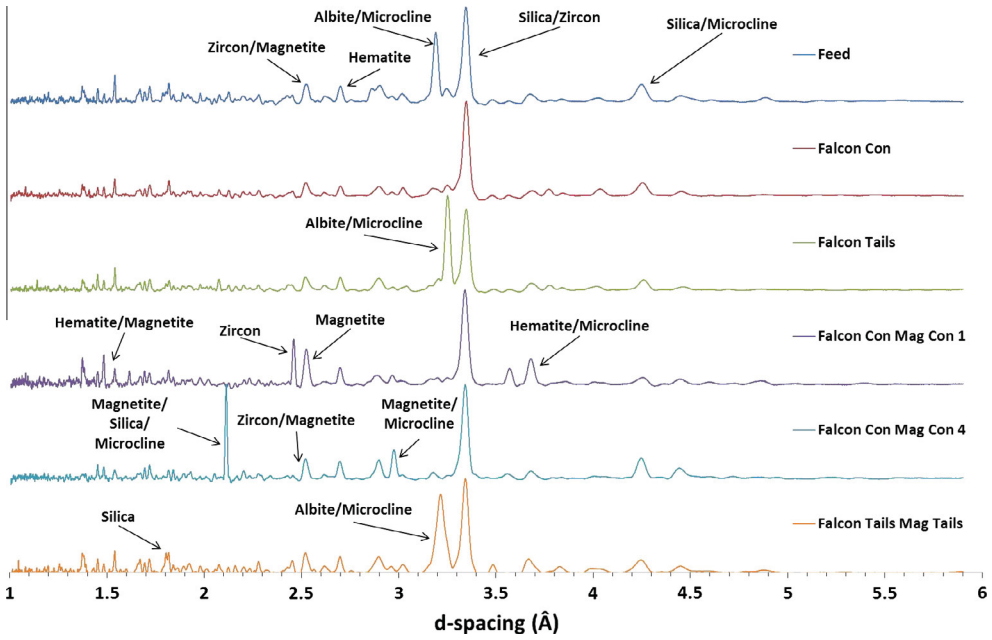

Fig. 13. X-ray diffraction patterns for selected gravity/magnetic separation products from the Falcon concentration step. All diffraction peaks have been normalized to the maximum peak intensity for each pattern.

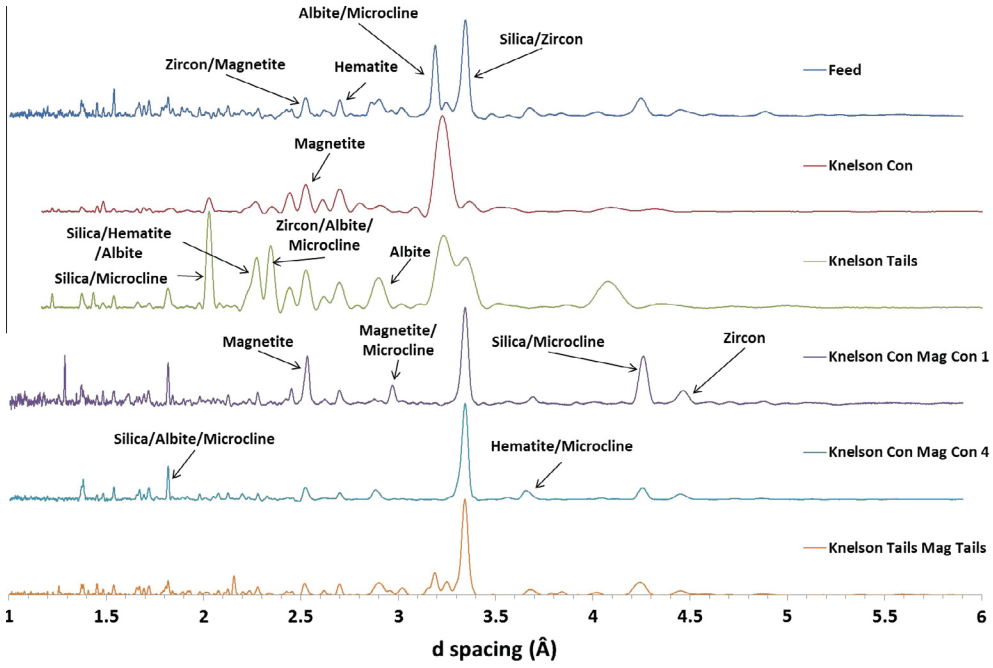

Fig. 14. X-ray diffraction patterns for selected gravity/magnetic separation products from the Knelson concentration step. All diffraction peaks have been normalized to the maximum peak intensity for each pattern.

trate is difficult to resolve as it corresponds to peaks for several different phases present in the Nechalacho ore. It may also correspond to a concentration of a completely different mineral phase as only the patterns for the major components of the Nechalacho ore (quartz, K-feldspar, plagioclase, hematite, magnetite and zircon) were checked in order to simplify the analysis.

Similarly Fig. 14 provides some useful information in identifying a magnetite peak present in the 0.10 T magnetic concentrate produced from the Knelson concentrate as well as a zircon peak. Beyond this information the data is inconclusive as many of the XRD peaks correspond to multiple phases. In particular there is a much smaller difference between the XRD patterns for the Knelson concentrate and tailings then was observed for the Falcon concentrate and tailings. The explanation for this is likely that the finer particle size of the feed to the Falcon Concentrator and WHIMS separation steps increases the liberation of the minerals in the ore, thereby allowing for more effective separation.

When viewed relative to one another Figs. 13 and 14 suggest that the combination of Falcon Concentrator and WHIMS was more effective in concentrating the valuable heavy, magnetic minerals in this deposit. It should be noted that these XRD results are not even semi-quantitative in nature but they do appear to indicate significant differences between the various products of the gravity and magnetic separation steps discussed in this paper.

4. Conclusions

This work investigated the magnetic behaviour of several different RE minerals and then compared these results with the behaviour of a RE ore through various gravity and magnetic separation operations. The conclusions are as follows:

(1) XRD results of the products of Falcon gravity concentration followed by WHIMS indicate that diamagnetic, low specific gangue minerals in the RE ore such as K-feldspar and plagioclase are rejected into the tails of the Falcon concentration step and when these tails are fed to a series of WHIMS steps the same minerals report to the non-magnetic fraction.

(2) Comparison of the VSM results for bastnäsite, fergusonite and allanite appears to indicate that the magnetic susceptibility of fergusonite and allanite are of similar magnitude with both larger than the susceptibility of bastnäsite. This would imply that fergusonite and allanite would require a lower applied magnetic field strength for magnetic recovery than bastnäsite.

(3) The VSM results for zircon originating from two different locations shows that these two minerals are very slightly para- or ferromagnetic, and the XRD analysis of the WHIMS of gravity concentrates produced from the RE ore suggest that the zircon in the ore behaves in a para- or ferromagnetic manner as well. One possible explanation for this is that the zircon grains contain many rare earth elements whose unpaired electrons cause the material to be paramagnetic. An alternate explanation is that insufficient liberation has resulted in many zircon grains associated with ferromagnetic iron oxides in locked particles. The ferromagnetic component of these locked particles would then be expected to cause the locked particle to report to the magnetic concentrate after WHIMS.

(4) XRD analysis of the WHIMS first concentrate (lowest applied magnetic field strength) produced from the Falcon concentrate show clear signs of magnetite and hematite, indicating that the ferromagnetic iron oxide gangue minerals in the RE ore may potentially be removed from a future gravity concentrate using low intensity magnetic separation. This may be a very important finding as removal of unwanted iron-bearing minerals from a potential flotation feed could be a critical process step depending on the selection of flotation collector.

Acknowledgments

The authors would like to acknowledge the Natural Sciences and Engineering Research Council of Canada (NSERC) and Avalon Rare Metals and for providing funding for this work through the Collaborative Research and Development (CRD) Program

(444537-12). The authors would also like to acknowledge funding for A. Jordens from NSERC, Avalon Rare Metals and the McGill Engineering Doctoral Award. The authors gratefully acknowledge the assistance of Ray Langlois with the Knelson and Falcon concentration steps.

References

Anthony, J.W., Bideaux, R.A., Bladh, K.W., Nichols, M.C., 2001. Handbook of mineralogy. Mineralogical Society of America, Chantilly, VA, USA.

Chen, L., Qian, Z., Wen, S., Huang, S., 2012. High-gradient magnetic separation of ultrafine particles with rod matrix. Mineral Processing and Extractive Metallurgy Review 34 (5), 340–347.

Chen, Z., 2011. Global rare earth resources and scenarios of future rare earth industry. Journal of Rare Earths 29 (1), 1–6.

Cox, J.J., Ciuculescu, T., Goode, J.R., Hains, D.H., 2011. Avalon Rare Metals – Technical Report on the Thor Lake Project: NI 43-101 Report – August 25, 2011, Toronto, ON, CA, pp. 1–293.

Crow, J.M., 2011. 13 Exotic Elements We Cannot Live Without. The New Scientist, London, UK, pp. 36–41 (Issue 2817).

Ebner, A.D., Ritter, J.A., Ploehn, H.J., 1997. Feasibility and limitations of nanolevel high gradient magnetic separation. Separation and Purification Technology 11 (3), 199–210.

Falconer, A., 2003. Gravity separation: old technique/new methods. Physical Separation in Science and Engineering 12 (1), 31–48.

Ferron, C.J., Bulatovic, S.M., Salter, R.S., 1991. Beneficiation of Rare Earth Oxide Minerals. In: International Conference on Rare Earth Minerals and Minerals for Electronic Uses. Prince Songkla University, Hat Yai, TH, 1991, pp. 251–269.

Foner, S., 1956. Vibrating sample magnetometer. The Review of Scientific Instruments 27 (7), 548.

Foner, S., 1959. Versatile and sensitive vibrating-sample magnetometer. The Review of Scientific Instruments 30 (7), 548–557.

Fullam, M., Grewal, I., 2001. The Knelson Continuous Variable Discharge (CVD) Concentrator. In: The Knelson Group, pp. 1–6.

Gupta, C.K., Krishnamurthy, N., 1992. Extractive metallurgy of rare earths. International Materials Reviews 37 (5), 197–248.

Ito, S., Yotsumoto, H., Sakamoto, H., 1991. Magnetic Separation of Monazite and Xenotime. In: Proceedings of the International Conference on Rare Earth Minerals and Minerals for Electronic Uses. Prince Songkla University, Hat Yai, TH, 1991, pp. 279–299.

Jakubovics, J.P., 1994. Magnetism and Magnetic Materials, second ed. Maney Publishing for IOM3, the Institute of Materials, Minerals and Mining.

Jiles, D., 1990. Introduction to Magnetism and Magnetic Materials. Chapman & Hall, London.

Jordens, A., Cheng, Y.P., Waters, K.E., 2013a. A review of the beneficiation of rare earth element bearing minerals. Minerals Engineering 41, 97–114.

Jordens, A., Sheridan, R.S., Rowson, N.A., Waters, K.E., 2013. Magnetic Processing of A Rare Earth Element Bearing Ore. In: 23rd World Mining Congress. CIM, Montreal, QC, Canada.

Knelson, B., 1992. The Knelson concentrator. Metamorphosis from crude beginning to sophisticated world wide acceptance. Minerals Engineering 5 (10–12), 1091–1097.

Kroll-Rabotin, J.-S., Climent, E., Bourgeois, F., 2011. Beneficiation of concentrated ultrafine suspensions with a Falcon UF concentrator. Canadian Institute of Mining Journal 2 (4), 189–198.

Laplante, A.R., Buonvino, M., Veltmeyer, A., Robitaille, J., Naud, G., 1994. A study of the Falcon concentrator. Canadian Metallurgical Quarterly 33 (4), 279–288.

Laplante, A., 1993. A Comparative Study of Two Centrifugal Concentrators. In: 25th Annual Meeting of the Canadian Mineral Processors. Canadian Mineral Processors Division of the CIM, Ottawa, pp. 18.

Lin, S.T., 1959. Magnetic properties of hematite single crystals. I. magnetization isotherms, antiferromagnetic susceptibility, and weak ferromagnetism of a natural crystal. Physical Review 116 (6), 1447–1452.

Lins, F.F., Veiga, M.M., Stewart, J.A., Papalia, A., Papalia, R., 1992. Performance of a new centrifuge (Falcon) in concentrating a gold ore from texada island, B.C., Canada. Minerals Engineering 5 (10–12), 1113–1121.

Long, K.R., Van Gosen, B.S., Foley, N.K., Cordier, D., 2010. The principal rare earth elements deposits of the United States — A summary of domestic deposits and a global perspective - U.S. Geological Survey Scientific Investigations Report 2010-5220, Reston, VA, USA, pp. 1-104.

Male, S.E., 1980. Magnetic measurements on coal. Journal of Physics D: Applied Physics 13, L67–L70.

Menzel, K., Lindner, J., Nirschl, H., 2012. Removal of magnetite particles and lubricant contamination from viscous oil by High-Gradient Magnetic Separation technique. Separation and Purification Technology 92, 122–128.

Meyer, L., Bras, B., 2011. Rare Earth Metal Recycling. In: 2011 IEEE International Symposium on Sustainable Systems and Technology (ISSST). Institute of Electrical and Electronics Engineers, Chicago, IL, USA, pp. 1–6.

Moustafa, M.I., Abdelfattah, N.A., 2010. Physical and chemical beneficiation of the Egyptian beach monazite. Resource Geology 60 (3), 288–299.

Oberteuffer, J., 1974. Magnetic separation: a review of principles, devices, and applications. IEEE Transactions on Magnetics 10 (2), 223–238.

Preinfalk, C., Morteani, G., 1986. The Industrial Applications of Rare Earth Elements. In: Moller, P., Cerny, P., Saupe, F. (Eds.), Lanthanides, Tantalum and Niobium: Mineralogy, Geochemistry, Characteristics of Primary Ore Deposits, Prospecting, Processing and Applications. Society for Geology Applied to Mineral Deposits, Berlin (DE), pp. 359–370.

Raslan, M.F., 2009. Mineralogical and minerallurgical characteristics of Samarskite-Y, columbite and zircon from stream sediments of the ras baroud area, Central Eastern Desert, Egypt. Studia i Materialy 128 (36), 179–194.

Rosenblum, S., Brownfield, I.K., 1999. Magnetic Susceptibilities of Minerals – Report for US Geological Survey, pp. 1–33.

Roy, S., 2011. Recovery improvement of fine magnetic particles by floc magnetic separation. Mineral Processing and Extractive Metallurgy Review 33 (3), 170–179.

Svoboda, J., Fujita, T., 2003. Recent developments in magnetic methods of material separation. Minerals Engineering 16 (9), 785–792.

Waters, K.E., Rowson, N.A., Greenwood, R.W., Williams, A.J., 2007. Characterising the effect of microwave radiation on the magnetic properties of pyrite. Separation and Purification Technology 56, 9–17.

Yang, J., Matsui, M., Kawa, M., Ohta, H., Michioka, C., Dong, C., Wang, H., Yuan, H., Fang, M., Yoshimura, K., 2009. Magnetic and Superconducting Properties of Single Crystals of $Fe_{1+\delta}$ Te_{1-x} Sex System. arXiv, Preprint arXiv: 0911.4758.

Zhang, J., Edwards, C., 2012. A Review of Rare Earth Mineral Processing Technology. In: 44th Annual Meeting of The Canadian Mineral Processors, CIM, Ottawa, pp. 79–102.